creative commons
COMMONS DEED

저작자표시 2.0 대한민국

이용자는 아래의 조건을 따르는 경우에 한하여 자유롭게

- 이 저작물을 복제, 배포, 전송, 전시, 공연 및 방송할 수 있습니다.
- 이차적 저작물을 작성할 수 있습니다.
- 이 저작물을 영리 목적으로 이용할 수 있습니다.

다음과 같은 조건을 따라야 합니다:

저작자표시. 귀하는 원저작자를 표시하여야 합니다.

- 귀하는, 이 저작물의 재이용이나 배포의 경우, 이 저작물에 적용된 이용허락조건을 명확하게 나타내어야 합니다.
- 저작권자로부터 별도의 허가를 받으면 이러한 조건들은 적용되지 않습니다.

저작권법에 따른 이용자의 권리는 위의 내용에 의하여 영향을 받지 않습니다.

이것은 이용허락규약(Legal Code)을 이해하기 쉽게 요약한 것입니다.

Disclaimer

dCollection

공학석사 학위논문

Experimental Investigation of Flow Characteristics in a Confluent Channel with Bed Elevation Difference

하상고 차이가 있는 합류수로에서의 흐름특성에 대한 실험적 연구

2013년 8월

서울대학교 대학원

건설환경공학부

이 주 하

Experimental Investigation of Flow Characteristics in a Confluent Channel with Bed Elevation Difference

하상고 차이가 있는 합류수로에서의
흐름특성에 대한 실험적 연구

지도교수 서 일 원

이 논문을 공학석사 학위논문으로 제출함
2013 년 4 월

서울대학교 대학원
건설환경공학부
이 주 하

최수웅의 석사 학위논문을 인준함
2013 년 6 월

위 원 장 서경덕 (인)
부위원장 徐一源 (인)
위 원 Van Thinh Nguyen (인)

Abstract

Experimental Investigation of Flow Characteristics in a Confluent Channel with Bed Elevation Difference

Joo Ha Lee

Department of Civil and Environmental Engineering

The Graduate School

Seoul National University

Changes of the river morphology at the river confluence became a big issue nowadays. The large-scale dredging at the main streams as a part of the Four Major River Restoration Project led to the bed elevation difference between the tributary and main streams. This may induce headward erosion and the stronger secondary flow motion at the confluence. Dredging to secure water induces headward erosion and sudden increase of the tributary discharge takes the detention at the confluence. The most previous studies of experiments were performed without considering the bed elevation difference between main and tributary channels. The purpose of this study is to investigate confluent flow by analyzing flow mechanism at junction with bed elevation difference. Velocity components at confluence with bed elevation difference were measured in the hydraulic model experiment. The confluent channel was designed with data from the Nakdong River in Korea. In this experiment, three dimensional velocity components were measured using micro-ADV, and they were analyzed in depth to reveal flow and turbulent characteristics at the confluence.

The measured u-v vector fields show the flow characteristics of the confluence near surface. Comparing the u-v vector fields with the discharge ratio, the bed elevation difference and the confluent angle, the lateral momentum of the tributary flow entity was found to be an important factor to induce the separation zone. As the lateral momentum of the tributary flow entity is greater, the entity angle is larger and the separation zone is wider. By analyzing the v-w vector fields and the vorticity contours, how the surface water of the tributary affects the evolution of the secondary flow. Because of the bed elevation difference, the surface momentum of the tributary flow force to rotate the upper part water of the main channel. The surface water of the tributary is approaching the right side wall of the main channel and the clockwise circulation starts. This flow mechanism can be defined as the down flow. The down flow results in the evolution of the secondary flow.

The turbulent kinetic energy (TKE) and the Reynolds shear stress were calculated at confluence. Both the turbulent kinetic energy and the Reynolds shear stress developed at the confluence and dissipated at the downstream. The analysis of the turbulent kinetic energy and the Reynolds shear stress at the confluence showed that, the region of turbulent motion is bigger with the greater discharge ratio and the increased bed elevation difference.

The regression analysis of the relative turbulent kinetic energy revealed that, among many hydraulic and geometric parameters, both the confluence angle and velocity ratio were main factors to the TKE. As these factors increase, then TKE increase monotomically.

Keywords: confluence channel, hydraulic experiments, bed elevation difference , down flow, secondary current, separation zone, turbulent kinetic energy

Student Number: 2011-23399

Contents

Chapter 1 Introduction 1
1.1 Research Backgounrds and Necessities 1
1.2 Objectives and Methodology 8

Chapter 2 Theoretical Backgrounds.....9
2.1 Secondary Currents in Confluence 9
2.2 Separation zone.....12

Chapter 3 Hydraulic Experiments.....18
3.1 Physical Models and Similitude.....18
3.1.1 Theory of Similitude..... 18
3.1.2 Distorted Model 21
3.2 Experimental Facilities 24
3.2.1 Confluent Channel and Water Supply..... 24
3.2.2 Auto Traverse System..... 36
3.2.3 Micro-ADV..... 37
3.3 Experimental Cases.....41
3.3.1 Object Region 41
3.3.2 Conditions of Discharge and Water Level 42
3.3.3 Conditions of Confluent Channel with Bed elevation difference 44

Chapter 4 Experimental Results.....48
4.1 Separation Zone 48
4.2 Secondary Flow 53

4.2.1 Flow Field 53
4.2.2 Vorticity 57
4.2.3 Turbulent Kinetic Energy 60
4.2.4 Reynolds Shear Stress 66
4.2.5 Relative Turbulent Kinetic Energy 70

Chapter 5 Conclusion and Future Study 74
5.1 Summary and Conclusion 74
5.2 Future Study 77

Reference 78

Abstract in Korean 82

Appendix 85
A.1 Experimental Results 87
A.2 The Matlab Code 274
A.2.1 Averaging the instantaneous velocity data 274
A.2.2 Plotting the time averaged velocities 274

List of Tables

Table 3.1 Dimensions of confluent flow. 25
Table 3.2 Dimensions of the confluent channel 30
Table 3.3 Experimental conditions 45

List of Figures

Figure 2.1 Secondary currents in Confluent channel for $Q_m/(Q_m+Q_t)=0.25$ (Webber et al., 2001) 16
Figure 2.2 Scheme of down flow 17
Figure 3.1 Scheme of the confluent channel. 29
Figure 3.2 Front view of the main channel 31
Figure 3.3 Side view of the tributary channel 31
Figure 3.4 Confluence with bed elevation difference 32
Figure 3.5 Head box of the main channell 32
Figure 3.6 Uniforming flow filter in main channel head box..... 33
Figure 3.7 Pump of main channel and valve for discharge control..... 33
Figure 3.8 Pump of tributary channel and valve for discharge control . 34
Figure 3.9 Electronic flowmeters 34
Figure 3.10 Manual tailgate 35
Figure 3.11 Water supply reservoir 35
Figure 3.12 Scheme of automatic measurement system for micro-ADV 39
Figure 3.13 Auto traverse system and micro-ADV..... 40
Figure 4.1 (AR205) Streamwise velocity characteristics near surface..... 52
Figure 4.2 (AR205) *v*, *w* vector fields 56
Figure 4.3 (AR205) Vorticity contours..... 59
Figure 4.4 (AR203) Turbulent Kinetic Energy contours..... 63
Figure 4.5 Turbulent Kinetic Energy contours with discharge ratio change.... 64
Figure 4.6 Turbulent Kinetic Energy contours with step height change 64
Figure 4.7 Turbulent Kinetic Energy contours with confluent angle change... 65
Figure 4.8 (AR203) Reynolds shear stress contours 67
Figure 4.9 Reynolds shear stress contours with discharge ratio change..... 68
Figure 4.10 Reynolds shear stress contours with step height change..... 68
Figure 4.11 Reynolds shear stress contours with confluent angle change..... 69

Figure 4.12 The regression analysis of relative turbulent kinetic energy at X = 0 m 73

LIST OF SYMBOLS

Latin Uppercase

A_r	Cross section scale of prototype to model
B_m	Width of main channel
B_t	Width of tributary channel
C_s	Velocity of acoustic wave
D	Averaged diameter of bed material
F_c	Change in frequency at a probe
F_t	Frequency of initial wave from a probe
Fr	Froude number
Fr_d	Tailwater Froude number
Fr_M	Froude number of model
Fr_P	Froude number of prototype
L	Dimension of length
L_r	Length ratio of prototype to model
L_s	Length of separation zone
Q	Discharge of straight channel
Q_m	Discharge of main channel
Q_t	Discharge of tributary channel

Q_s	Sediment discharge
R_r	Ratio of hydraulic radius
Re	Reynolds number
S	Bed slope
S_r	Slope scale
U_r	Velocity ratio of tributary channel to main channel
V_r	Relative velocity between a transmitter probe and a sampling volume
V	Flow velocity
V_M	Flow velocity of model
V_P	Flow velocity of prototype
V_r	Velocity ratio of prototype to model
V_r	Flow velocity ratio of prototype to model
X_r	Horizontal scale
Y_r	Vertical scale

Latin Lowercase

b_s	Width of separation zone
g	Gravity acceleration

g_M	Gravity acceleration of model
g_P	Gravity acceleration of prototype
h	Downstream water depth
h_s	Bed elevation difference
n_r	Ratio of Manning roughness coefficient
q^*	Discharge ratio of prototype to model
t_r	Time ratio
u	Stream wise velocity component
u'	Fluctuating velocity components of stream wise
$\overline{u'}$	Averaged fluctuating velocity components of stream wise
u^*	Non-dimensional *u* velocity component
v	Horizontal direction velocity component
v'	Fluctuating velocity components of horizontal direction
$\overline{v'}$	Averaged fluctuating velocity components of horizontal direction
v^*	Non-dimensional *v* velocity component
w	Vertical direction velocity component
w'	Fluctuating velocity components of vertical direction
$\overline{w'}$	Averaged fluctuating velocity components of vertical direction
w^*	Non-dimensional *w* velocity component

GreekLowercase

α	Junction angle
β	Energy correction coefficient
τ	Reynolds shear stress

Chapter 1. Introduction

1.1 Research Backgrounds

Management of the river environment is very important to protect future water resources. Change of river topography should be especially considered as an important part of hydraulic engineering, because it may change soil and vegetation environments. Among problems of river management, river confluence (or junction) was focused on nowadays. For instance, the confluence of the Nakdong River and the Geum River has the problem of sediment deposition at separation zone. The separation zone is the region where stagnant flow occurs. The shoal has been made due to stagnant flow of the separation zone. The shoal or sandbank is linear landform within or extending into water. There are the shoal near the confluence of the Nakdong River and the Hwang River. Another example is the confluence of the Nakdong River and the Gam Stream. Headward erosion has occurred due to difference between bed elevations at the mouth of tributary. Considering the examples, understanding confluent flow is

necessary.

Confluence of open channel is a major element of natural and man-made waterways, and their systematic hydraulic treatment was not considered carefully. Because there are the separation zone and secondary flow at the downstream of confluence, confluent flow is very complicated. Although there have been many former studies for confluent flow characteristics, only limited research with non-bed elevation difference confluent channel has been conducted. River confluence with the bed elevation difference where the main channel has lower bed than the tributary induces headward erosion or head cut. Headward erosion depends on down flow. A research of the down flow generated from the bed elevation difference of the tributary is required.

There are several former studies of confluent flow. Previous studies have conducted experimental research to find the flow characteristic at junction. Taylor (1944) presented the first study on confluent flow, with combined angles between the tributary and the main channel (45° and 135°). Anwar (1955) conducted experiments at a trapezoidal junction structure. Junction angles were 22.5°, 45°, 67.5° and 90°. He found that a separation

wall stars at the junction point and extends into the junction. Such a separation wall was recommended for the trapezoidal cross section of junction and found unnecessary for the sharp edged junction with rectangular cross sections. Webber and Greated (1966) focused on the flow characteristics of back water effect with momentum equation. They defined a theoretical flow characteristic at a confluent region by using the conformal mapping method. They showed the stagnation point at the upstream corner of the channel junction and explained the separation zone specifically. Joy (1981) presented a study on the velocity patterns, shear stress distribution, and energy correction coefficients, β, for a 90° confluence. Modi (1981) also used the method of conformal mapping to determine the flow patter at confluence. Best and Reid (1984) focused on separation zone. They found that the shape of separation zone changes with the discharge ratio between main and tributary channel. Gurram et al. (1997) presented many characteristics of confluent flow. They proposed empirical relationship to determine width or length of separation. These equations were used to validate simulated result or to find separation zone size near the water surface.

In 21th century, researchers developed the theory of confluent flow from previous studies. Webber et al. (2001) measured water depth and velocities using a point gauge and acoustic Doppler velocimeter over a grid throughout the junction region. The average velocity components and turbulent intensity were calculated from a measurement. Separation zone and secondary currents were presented plotting non-dimensional velocity components. 2D mapping of water surface, velocity and turbulent intensity were used for the presentation of characteristics at right angle confluence. Barkdoll (2003) studied a secondary current involved in non-uniform vertical velocity profile. The non-uniform vertical velocity profile induces three-dimensionality into these flow features and the secondary vortex appears in the main channel downstream of the side channel. Thanh et al. (2010) characterized one separation zone or recirculation zone arising at the downstream of the confluence in the inner bank side and one contracted flow region in the outer bank side. Biswal et al. (2012) compared the confluent flow of compound channel to the simple confluent channel. They measured the flow velocities, bed stress and Reynolds stress of the each confluent channel. The flow field at a compound channel junction was different from

that of simple channel junction.

Many field studies and moveable bed experiments of river confluence were conducted recently. Rhoads and Sukhodolov (2004) focused on the shear layer developing at the interface between converging flows. They examined the spatial and temporal characteristics of turbulence and coherent turbulent structures within a shear layer. Boyer et al. (2006) examined the relations between flow and sediment transport at a confluence. They measured near-bed turbulence, bed load transport rates and changes at bed morphology with eight flow conditions at a sand bed discordant confluence. They found that low mean flow velocities have the highest values of Reynolds shear stresses and turbulence is associated with intense upward movements of the flow. At the shear layer region, high sediment transport rates were observed. These patterns match changes in turbulent characteristics along the shear layer. Ghobadian and Shafai (2007) focused on a scour hole developed just downstream of the river confluence. General non-dimensional equations of scour hole were developed under different hydraulic conditions. Ghobadian (2012) developed his previous research of scour hole to penetration of scour hole. Nédélec and Gay (2008) presented

an experimental study of a junction between a closed conduit and an open channel. Transitions between free-surface and pressurized pipe flow appeared to be strongly dependent on the longitudinal slope of the pipe. Yang et al. (2009) developed the theory of separation zone. They found that separation zone differs with variations of distance to the flume bottom.

Choi et al. (2003a) studied erosion and deposition rate at a junction by changing discharge ratio between the main channel and the tributary. Tributary discharge increases, erosion depth and length of sediment transport. However, deposition is constant when the ratio is higher than 0.4. Choi et al. (2003b) focused on confluent angle. Changing confluent angle, they measured velocity magnitudes. They presented that confluent angle increases flow velocity. And they found that the length of separation zone increases with the confluent angle. Chung et al. (2006) studied the flow mechanism of river junction with sewerage outlet. They suggested a guide line for minimizing the disturbance by various conditions (discharge, sewerage outlet projecting part, sewerage outlet direction and position).

Natural river confluence changes big effects to sediment transport, bank erosion and topography change, by secondary current occurring in confluence.

Webber et al. (2001) showed secondary currents near the junction. However, there is no the confluent flow study considering bed elevation difference. Therefore, it is necessary to analyze down flow quantitatively. This is a footnote example.

1.2 Objectives and Methodology

Objectives of this research were to analyze down flow, secondary flow, and separation zone near the river confluence with the bed elevation difference. In order to find how down flow and secondary flow affect a separation zone, a comprehensive experimental study was conducted using a confluent channel in the laboratory. Both main and tributary channels with the section were prepared with adjustable step height to represent the bed elevation differences. Down flow, secondary flow, and separation zone are measured using the micro-ADV. The shape of separation zone and secondary current (and down flow) was examined by analyzing measured data with various methods. By analyzing separation zone quantitatively, empirical equation for separation width and length near water surface was presented and compared to the previous equation (Gurram et al., 1997). The down flow and the secondary flow were measured from junction to downstream of main channel. Relationship between headward erosion and down flow was studied by analyzing turbulent characteristics.

Chapter 2. Theoretical Backgrounds

2.1 Secondary Currents in the Confluence Channels

Secondary currents are one of the most complicated mechanisms in rivers. The secondary flow is a relatively small flow superimposed on the primary flow. The secondary flow takes the spiral motion by which the water in the upper part of the channel is driven outward and the water near the bottom is driven inward. The centrifugal force applied to the water, the bottom friction, and pressure gradient due to the decline of the water surface creates the secondary flow (Henderson, 1966).

In case of secondary flows at a confluence, flow momentum from the tributary induces secondary flows in main channel with separation zone. Webber et al. (2001) measured secondary currents and presented the flow structure near the junction. Figure 2.1 shows a schematic of presented flow structure for the case. At the downstream of the junction the surface water approaches to the junction-opposite wall but not going into the wall. This flow mechanism is evolved by the two flows from the main and the tributary

channel. As Figure 2.1 presented, the form of shear plane is distorted and skewed. This is due to the effects of the relative magnitudes of the combined flows and the non-uniform vertical velocity profile (Song and Seo, 2011). Barkdoll (2003) presented that non-uniform vertical velocity profile leads three dimensional flow features. The secondary vortex appearing in the main channel downstream rotates counter clockwise looking upstream. A similar secondary vortex rotates against the secondary current of tributary channel and forms along the other side of the main channel as well. Song and Seo (2011) also presented decay of secondary currents. Both vortices dissipate in downstream direction, mainly due to fluid viscosity. Webber et al. (2001) showed the dissipation of secondary vortexes with v^*-w^* vector field illustrating secondary currents for $Q_m/(Q_m+Q_t)=0.25$. Where v^* is non-dimensional velocity components of horizontal direction, w^* is non-dimensional velocity components of vertical direction, Q_m is the discharge of main channel and Q_t is the discharge of tributary channel.

Down flow from the tributary channel induces the secondary flow. Down flow can be generated from the bed elevation difference . Meeting the bed elevation difference , water falls down. Figure 2.2 illustrates a schematic

of the down flow. The change of water surface induces the erosion of the stream channel. Because the flow responds to the knick point created by the surface change, turbulence in the water undercuts substrate material resulting in collapse of the upper level. This under-cut-collapse process advances up the stream channel. The flow of tributary meets the main channel and falling water from the tributary generates the momentum to rotate the water at the stream channel.

2.2 Separation zone

A separation zone or a recirculation zone is important for river management. Flow separation occurs at the inner bank of the downstream where flow of the tributary cannot remain attached to the channel wall. Sediment deposits due to low velocity where the flow recirculates. Thus the sediment is concentrated along a distinct pathway and is carried into this zone. Within asymmetrical confluences morphology is dominated by avalanche slopes, a central scour, and a bar formed below the inner bank of downstream junction where the large-scale separation zone exists (Best and Reid, 1984). Retention of pollutant can be another problem. When some pollutant comes from a tributary or from a sewer system, understanding separation zone is very important to predict mixing zone.

To define the separation zone at the confluence quantitatively, Gurram et al. (1997) tried to express separation size as length and width and proposed the equations to determine the length L_s and width b_s of separation. The equations are expressed by using width of main channel, B_m, the tail water Froude number, Fr_d, and junction angle, α as

$$\frac{b_s}{B_m} = \frac{1}{2}\left(Fr_d - \frac{2}{3} \right)^2 + 0.45\left(\frac{Q_t}{Q_m + Q_t} \right)^{1/2} \left(\frac{\alpha}{90°} \right) \tag{2.1}$$

$$\frac{L_s}{B_m} = 3.8 \sin^3 \alpha \left(1 - \frac{1}{2} Fr_d \right) \left(\frac{Q_t}{Q_m + Q_t} \right)^{1/2} \quad \text{for } Fr_d < 1 \tag{2.2}$$

$$\frac{L_s}{B_m} = 0.26\left(1 + \frac{3\alpha}{90°} \right) \left(\frac{Q_t}{Q_m + Q_t} \right)^{1/2} \quad \text{for } Fr_d = 1 \tag{2.3}$$

Webber et al. (2001) showed the streamwise velocities to present the flow characteristics near the separation zone. Surface flow enters at a larger angle than near bed flow. This results in that separation size is narrower near bed than near surface. Change of the shape of a separation zone is related to the secondary current. The reduced channel constriction coupled with the downstream deflection of the near bed branch flow results in the concentration of high velocities near the bed. Yang et al. (2009) presented a change of separation zone with vertical direction due to bed resistance. To determine the size of separation zone, the streamline method was compared to the isoline velocity method. Because the isoline velocity method can show a region where velocity is lower than zero, but the streamline method cannot, the isoline velocity method is better to determine

the size of separation zone. Using experimental results from Webber et al. (2001), they presented that the geometry of the separation zone has different forms with variations of distance to the channel bottom. Separation zone is compressed by secondary flow or even disappears near bed due to bed resistance. Variation of separation zone with streamwise direction is due to secondary flow. Relationship between secondary flow and separation zone is important in river confluence.

The equation for the separation size will be presented including the term of the bed elevation difference in this study. The width of the separation zone can be expressed as

$$b_s = f\left(Fr_d, \mathrm{Re}, q^*, \alpha, h_s, h, S, B_m, B_t\right) \tag{2.4}$$

Where, Fr_d is Froude number of downstream, Re is Reynolds number, q^* is discharge ratio of tributary discharge to total discharge, h_s is bed elevation difference , h is water depth of downstream, S is bed slope, B_m is width of main channel and B_t is width of tributary channel. If flow is turbulence, flow doesn't change with Reynolds numbers. The term of Reynolds number, Re was dropped. Gurram et al. (1997) presented that bed slope doesn't affect confluent flow at subcritical flow. The term of bed

slope, S was dropped. The channel widths are fixed on this study.

The equation (2.4) can be arranged as

$$\frac{b_s}{B_m} = f\left(Fr_d, q^*, \alpha, \frac{h_s}{h} \right) \tag{2.5}$$

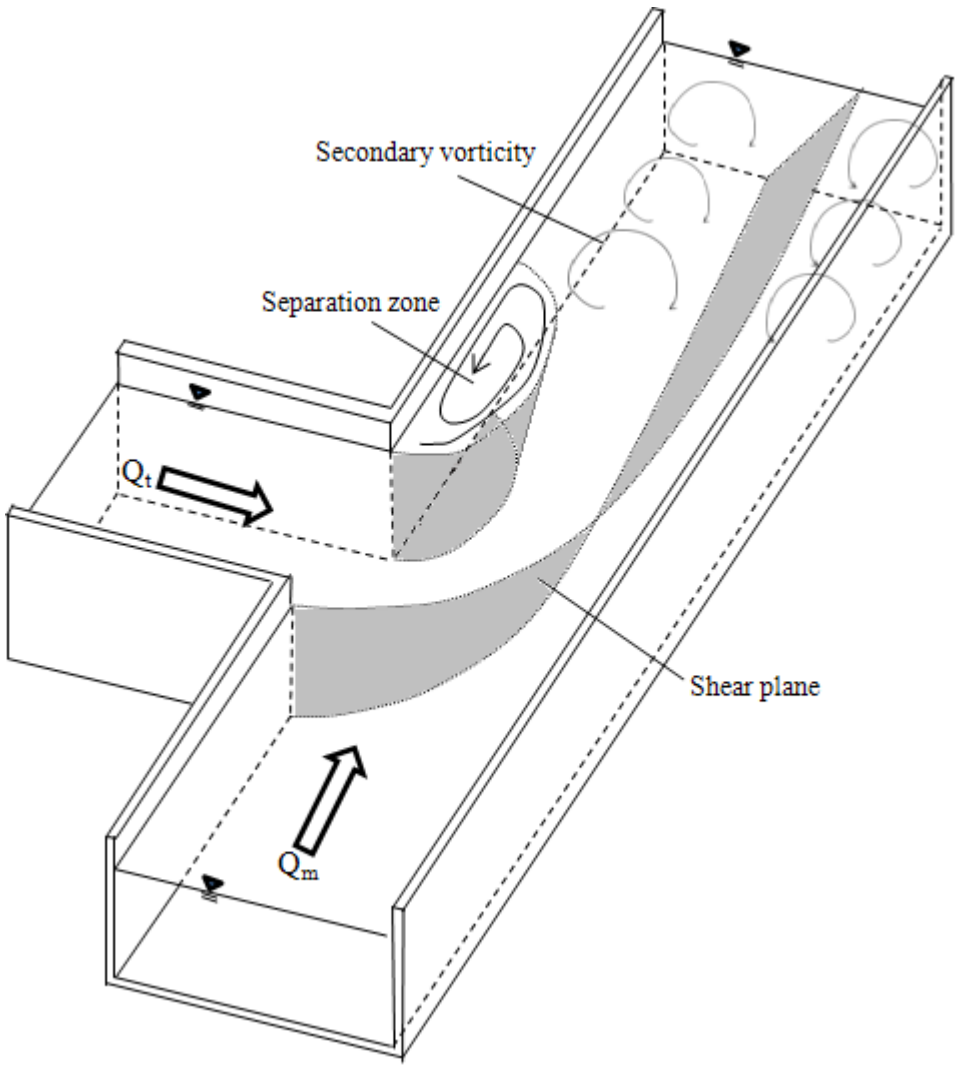

Figure 2.1 Secondary currents in the confluent channel for $Q_m/(Q_m+Q_t)=0.25$ (After Webber et al., 2001)

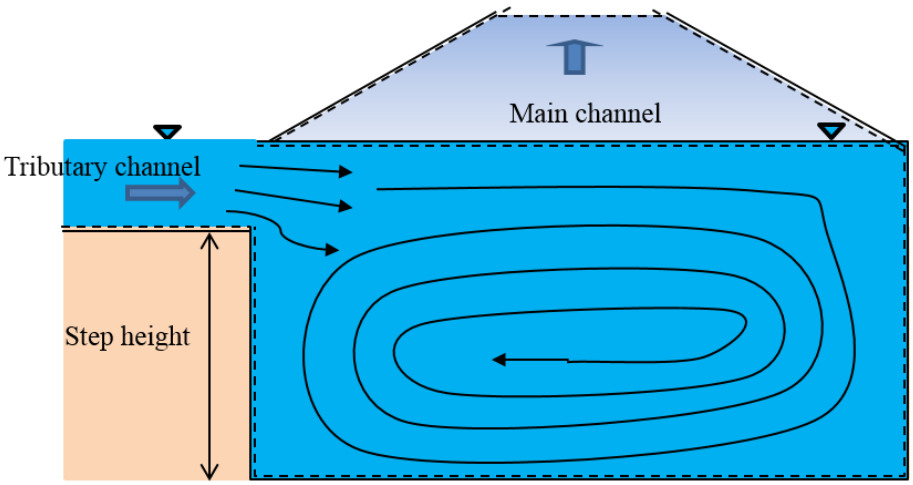

Figure 2.2 Scheme of the evolution of the secondary flow

Chapter 3. Experimental Research

3.1 Physical models and similitude

3.1.1 Theory of similitude

A confluent channel was designed considering law of similitude. However, it is impossible to have perfect similitude due to the scale effect and costs.

Components of force from fluid movement are inertia force, pressure force, gravitational force, viscous force and surface tension. When the ratio between forces of prototypes and models is a constant, dynamic similitude is valid. But some components of fluid force are negligible and it is enough to consider one component of fluid force in real fluid motion. Determination of the dominant force and law should be considered to design physical models. Reynolds similitude is for the case of viscous force, Froude similitude for gravity force, Webber similitude for surface tension and Cauchy similitude for elastic force. Two dominant forces should be considered at moveable bed experiment.

In this research, Froude similitude should be considered, because inertia force and gravity are dominant. Froude similitude between prototype and model is:

$$F_{r_P} = F_{r_M} \tag{3.1}$$

Where F_r is Froude number, $F_r = \frac{V}{\sqrt{gL}}$. V is flow velocity, g is gravity acceleration, and L is dimension of length. So,

$$\frac{V_P}{\sqrt{g_P L_P}} = \frac{V_M}{\sqrt{g_M L_M}} \tag{3.2}$$

$$V_r = \frac{V_P}{V_M} = L_r^{1/2} \tag{3.3}$$

From continuity equation, derived ratio of discharge Q_r is:

$$Q_r = A_r V_r = \left(L_r\right)^2 \cdot L_r^{1/2} = L_r^{5/2} \tag{3.4}$$

$$t_r = \frac{L_r}{V_r} = L_r^{1/2} \tag{3.5}$$

Where A_r is scale of cross sections and t_r is time ratio.

Primary interests are velocity distribution, change of water surface or energy slope in fixed bed experiment. So effects of bed roughness are very important for fixed bed experiment. Because roughness is determined with Manning's equation, fluid viscous force keeps similitude law. Important restriction is that flow of model holds turbulence. This law of similitude is expressed as

$$V_r = \frac{1}{n_r} R_r^{2/3} S_r^{1/2} \tag{3.6}$$

Where n_r is ratio of Manning roughness coefficient, $S_r = \left(y / L \right)$ is slope scale, R_r is ratio of hydraulic radius and *y* is depression head of length *L*.

If model is normal model and width of model is wide, $S_r = 1$ and $R_r = L_r$. At the moment, Manning's equation can be arranged as

$$V_r = \frac{1}{n_r} L_r^{2/3} \tag{3.7}$$

Substituting Froude similitude law into Equation (3.7), roughness ratio of model can be derived as

$$n_r = L_r^{1/6} \tag{3.8}$$

3.1.2 Distorted model

In case of small scale model, it is difficult to measure exact value of velocity and maintain flow state of prototype and similitude, due to low flow velocity in model. In this case, using distorted model having larger vertical scale Y_r than horizontal scale X_r, is a method to solve the problem. Slope ratio of distorted model is $S_r = Y_r / X_r$. Substituting the equation of this relation into Manning's equation is:

$$V_r = \frac{1}{n_r} R_r^{2/3} \left(\frac{Y_r}{X_r} \right)^{1/2} \tag{3.9}$$

Velocity is determined by gravitational acceleration in distorted model, Y_r is used instead of L_r in Froude similitude law

$$V_r = Y_r^{1/2} \tag{3.10}$$

From Equation (3.9) and (3.10), roughness ratio of model is:

$$n_r = \frac{R_r^{2/3}}{X_r^{1/2}} \tag{3.11}$$

Discharge ratio in a distorted model is expressed as

$$Q_r = A_r V_r = X_r Y_r^{3/2} \tag{3.12}$$

Ettema (2000) encouraged that scope of distortion is better to be controlled from 2 to 10.If distortion ratio is excessively big, there would be seriously distortion of flow velocity and pressure distribution in curved flow like shear flow.

There is also a need to use distorted model in this research. Flow field and boundary geometry of model and of prototype have same shape and ratios of corresponding lengths in model and prototype are same for geometry similarity. Although the confluent channel was designed to model the confluences along the Nakdong River with bed elevation difference in this research, this channel cannot represent all the prototypes perfectly. To determine experimental condition (flow rate, water depth etc.) of the confluent channel, a concept of the distorted model was used.

3.2 Experimental Facilities

3.2.1 The confluent channel and water supply

Understanding the confluent channel in previous research is necessary to design new confluent channel. Gurram et al. (1997) conducted the experiment when confluent angles are 30°, 60° and 90°. The cross sections were rectangular. The widths of tributary channels were changed to use dimensionless width ratio for empirical equations of separation zone. The experimental condition was determined as changing the discharge ratio, Froude number of downstream and confluent angle. Webber et al. (2001) presented the confluent flow characteristics at a right junction angle. The cross sections were also rectangular. The width of tributary channel was same as the width of main channel. The experimental condition was determined, changing discharge conditions. These conditions were not from prototypes. The conditions of the confluent channels of the previous studies are shown in Table 3.1.There are width ratio of main channel width to tributary channel width, confluent angle and bed elevation difference in this table. As Table 3.1 shows, previous studies didn't involve bed elevation

Table 3.1 Dimensions of the confluent channels

Confluent channel	Width ratio	Confluent angle	Bed elevation difference	Note
Gurram et al. (1997)	1	30°, 60°, 90°	-	Experiment
Webber et al. (2001)	1	90°	-	Experiment
Choi et al. (2003a)	0.8	90°	-	Experiment
Choi et al. (2003b)	0.8	30°, 60°, 90°		Experiment
Ghobadian and Bajestan (2007)	1	60°, 75°, 90°	-	Experiment
Bejestan and Hemmati (2008)	0.714, 1	60°	-	Experiment
Yang et al. (2009)	0.5	90°	-	Experiment
Mignot et al. (2011)	1	90°	-	Experiment
Ghobadian (2012)	0.428, 0.714, 1	60°, 75°, 90°	-	Experiment
This study	0.33	30°, 60°, 90°	0.1m, 0.16m, 0.22m	Experiment

difference.

To disclose real confluence, the confluent channel was produced with adjustable bed elevation difference . To determine dimensions of the confluent channel, data of the Nakdong River basin was used. The rivers have stream orders as 1 and 2. Angles are from 60° to 90° and ratio of main channel width to tributary channel width is from 2 to 4. Thus, Angles are 60° and 90°and width ratio is 3. Considering space of the lab, widths of main and tributary channel are determined to be 0.3 m, 0.1 m and lengths of main and tributary are 3.6m, 1m respectively. The uniforming flow filters were set in the head box of main channel. Picture of the uniforming flow filters is shown on Figure 3.6. Because Gurram et al. (1997) presented that bed slope isn't major influence to confluent flow at subcritical flow, type of bed elevation difference is edge. Because of viscous effect, water depth of tributary is at least 5 cm. Bed elevation difference is at least 0.16 m due to measurement space. Thus, water depth of main channel is higher than 0.21 m. Bed elevation difference conditions are 0.16 m, 0.19 m and 0.22 m as moving tributary channel vertically. These channel dimensions are arranged on Table 3.2.

Frames of the confluent channel are stainless steel. To attach and detach the tributary channel safely, wall of the main channel was made acrylic at junction. Surface of tributary channel is also made of acrylic to make lightly. The scheme of the confluent channel is shown on Figure 3.1.The front view is shown on Figure 3.2. The confluent channel has two pumps for each branch channel. The pump for main channel can supply the max discharge, 0.43 m^3/s, and the other pump for tributary channel can supply the max discharge, 0.23 m^3/s. The pumps are located near each channel and connected to each electronic flowmeter. Pictures of each pump are on Figure 3.7 and Figure 3.8. Picture of the electronic flowmeters is on Figure 3.9. Measurement capacity of the electronic flowmeters is from 6.7ℓ/min to 420 ℓ/min. Picture of the tail gate is Figure 3.10. The comparison to the discharge from the continuity equation was used as the verification of the electronic flowmeter. The velocity to calculate the continuity equation was measured by micro-ADV. Water depth of main channel can be changed by controlling the manual tail gate. Considering the conditions of bed elevation difference , setting water depth of main channel is important because high water depth of main channel attributes to overflow of water in tributary channel. Picture of the reservoir is Figure 3.12. The reservoir is located at the end of the main channel. Water discharge is

controlled by each valve located at main and tributary channel. The reservoir can store the volume of water, 1 m^3.

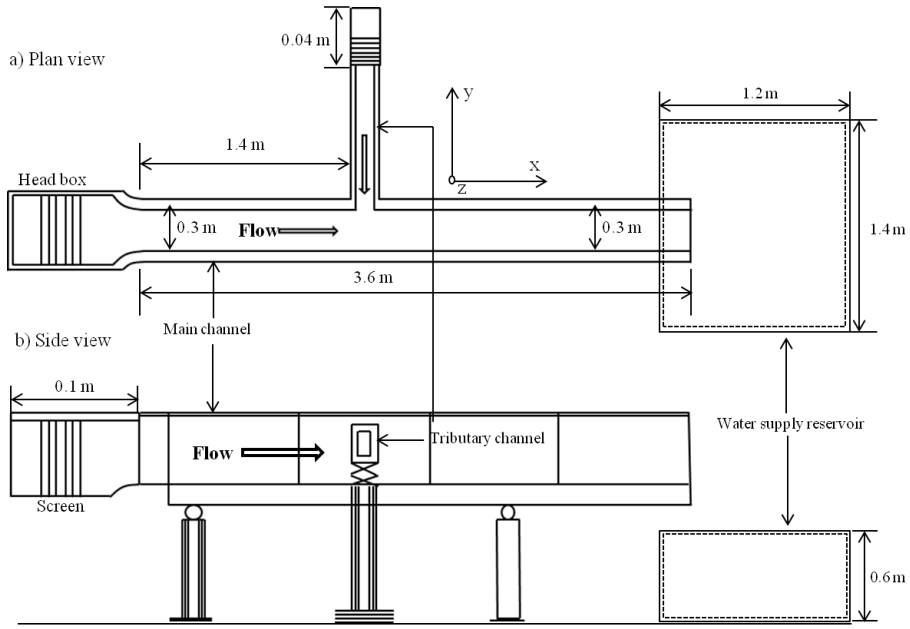

Figure 3.1 Scheme of the confluent channel

Table 3.2 Dimensions of the confluent channel

Channel component		Dimension
Main channel	Width (*W*)	0.3 m
	Height	0.5 m
	Length	3.6 m
Tributary channel	Width (*W*)	0.1 m
	Height	0.1 m
	Length	1 m
Confluent angle		30°, 60°, 90 °
Step height		0.10 m, 0.16 m, 0.22 m

Figure 3.2Front view of the main channel

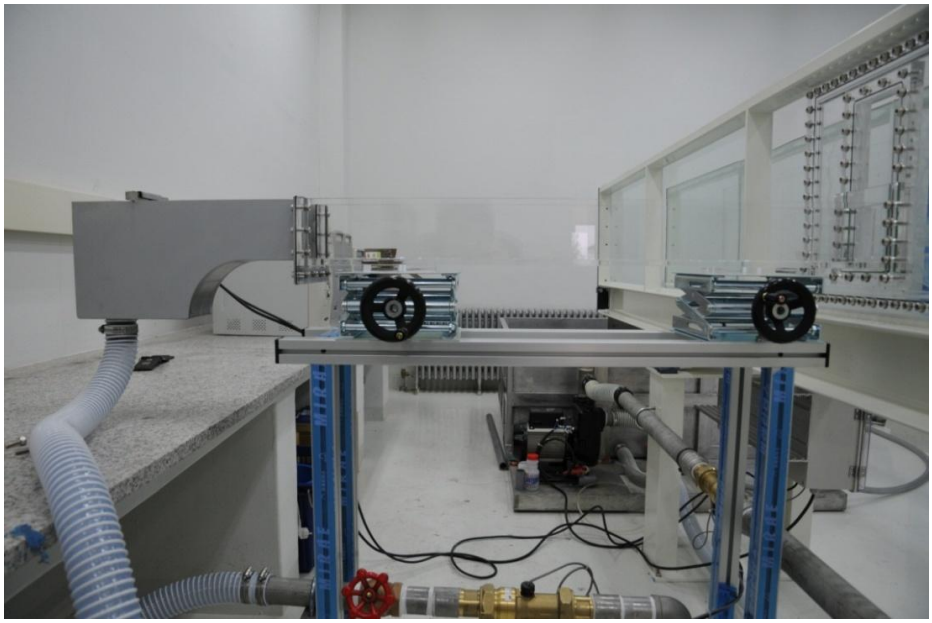

Figure 3.3 Side view of the tributary channel

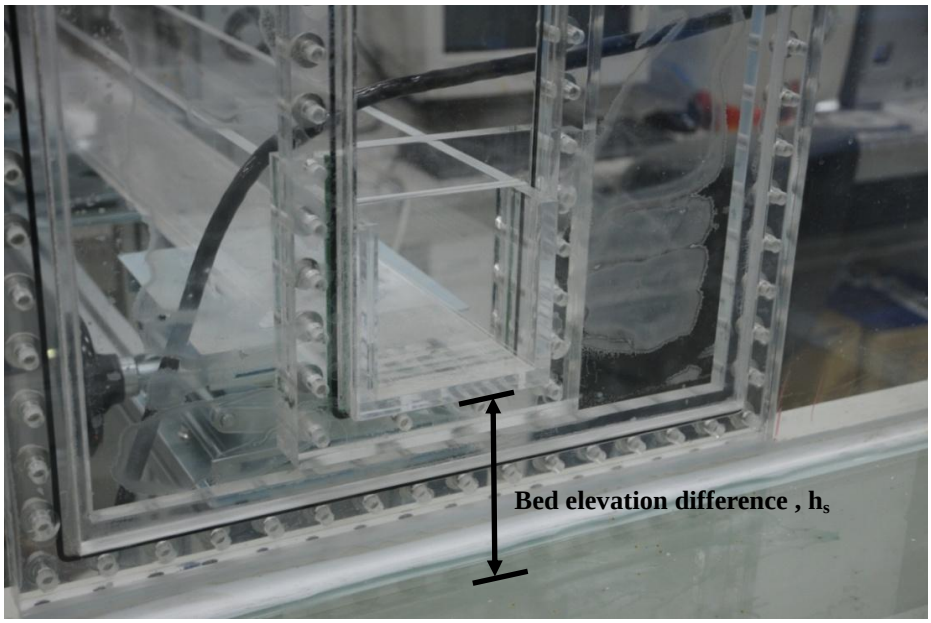

Figure 3.4 Confluence with bed elevation difference

Figure 3.5 Head box of the main channel

Figure 3.6 Uniforming flow filter in main channel head box

Figure 3.7 Pump of the main channel and valve for discharge control

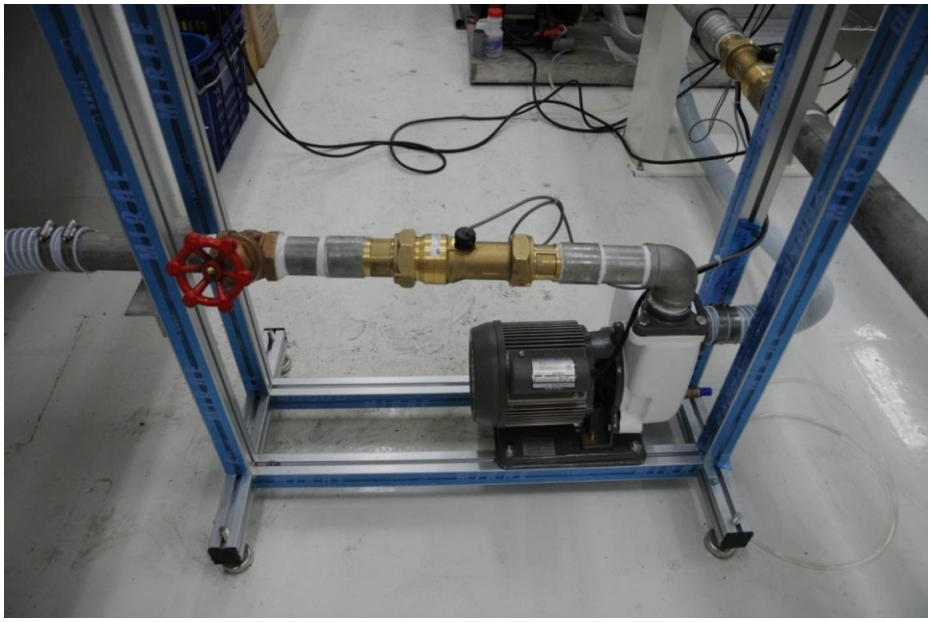

Figure 3.8 Pump of tributary channel and valve for discharge control

Figure 3.9 Electronic flowmeters

Figure 3.10 Manual tailgate

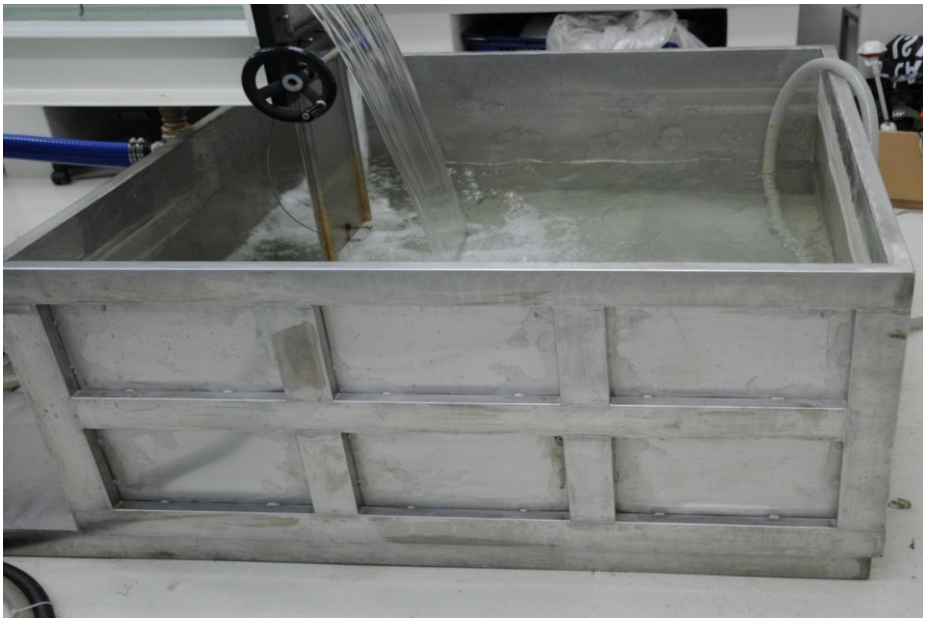

.Figure 3.11 Water supply reservoir

3.2.2 Auto traverse system

The measurement device, micro-ADV (Acoustic Doppler Velocimeter), is an intrusive measurement. Velocity components are measured at one point from probes. In order to measure velocity at a observed region, micro-ADV should be moved. To move micro-ADV exactly and stably, auto traverse system is necessary. Auto traverse system was designed to move *y*-*z* sections (*x*-axis is for streamwise direction, *y*-axis is for horizontal direction and *z*-axis is for vertical direction). Commanding movement on the computer, the control box converts digital signal to analog signal. Then auto traverse system can move as commanded. The auto traverse system can move the maximum vertical distance, 50 cm, and the maximum horizontal distance, 40 cm. The auto traverse system is installed on the carriage. Carriage can move along x-axis by hand, and it can be tied up with special wheels. Rails are attached at both side of the main channel and the carriage can move on the rails. The combined form between the carriage and auto traverse system is as schematic diagram on Figure 3.12.The picture of auto traverse system and micro-ADV is shown on Figure 3.13.

3.2.3 Micro-ADV

To measure the exact velocity field, three-dimensional micro-ADV (Acoustic Doppler Velocimeter) is used. ADV is made by Sontek Co. in USA. Making a precise measurement of turbulence is feasible and performance is more excellent than general ADV. Sampling volume decreases to 0.09cc and measuring range of velocity increases to 0.1~250 cm/s. It can measure fifty samples per second. Measuring velocity is possible if it is positioned 5 cm away from a transmitter probe. According to direction of measurement, micro-ADV is classified to side looking and down looking micro-ADV. Side looking micro-ADV can measure in water but not near bed. Down looking micro-ADV can measure near bed but not near wall. Side looking micro-ADV will be used to define separation zone near surface. Down looking micro-ADV will be used when measuring down flow and secondary flow.

Principle of micro-ADV is the Doppler shift. The device sends out a beam of acoustic waves a fixed frequency from a transmitter probe. These waves bounce off of moving particulate matter in the water and three

receiving probes take for the change in frequency of the returned waves. Then the device calculates velocity components with the equation. (Lee and Seo, 2006)

$$F_c = -2F_t\left(U_r - C_s\right) \tag{3.13}$$

Where, U_r is relative velocity between a transmitter probe and a sampling volume, C_s is velocity of acoustic wave, F_c is change in frequency at a probe and F_t is frequency of initial wave from a probe. To verify the micro-ADV, the comparison to the electronic flowmeter was used. Measuring the velocities by one point method, the discharge from the continuity equation was compared to the discharge of the electronic flowmeter.

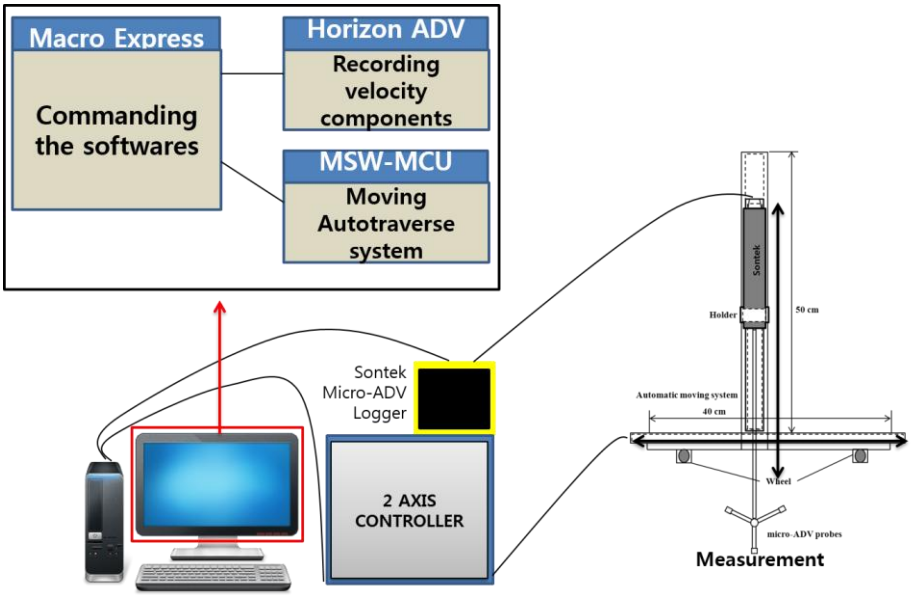

(a) Scheme of measurement system

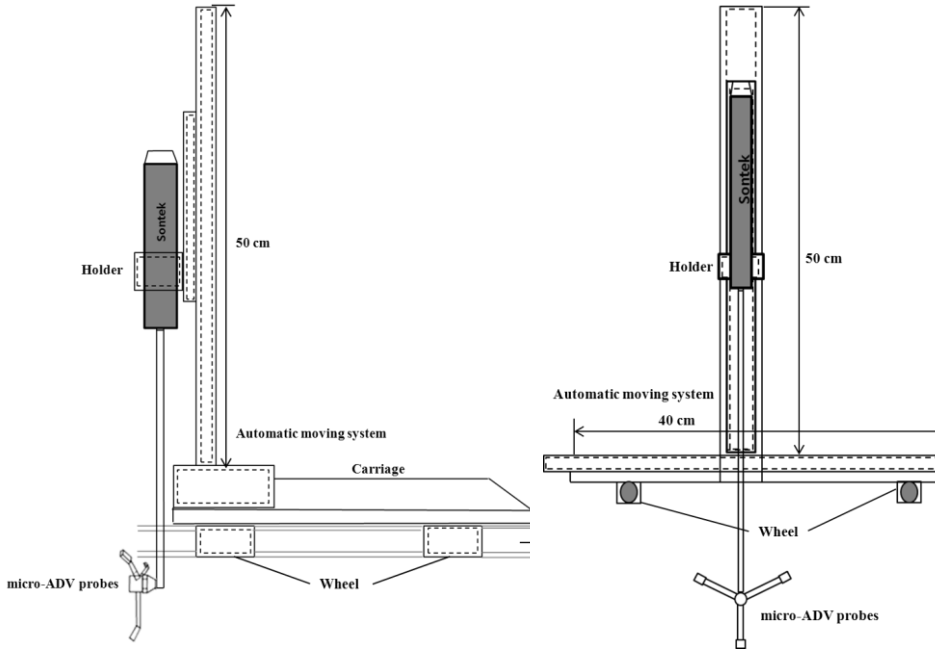

Carriage and micro-ADV: (b) Side view (c) Front view

Figure 3.12 Scheme of automatic measurement system for micro-ADV

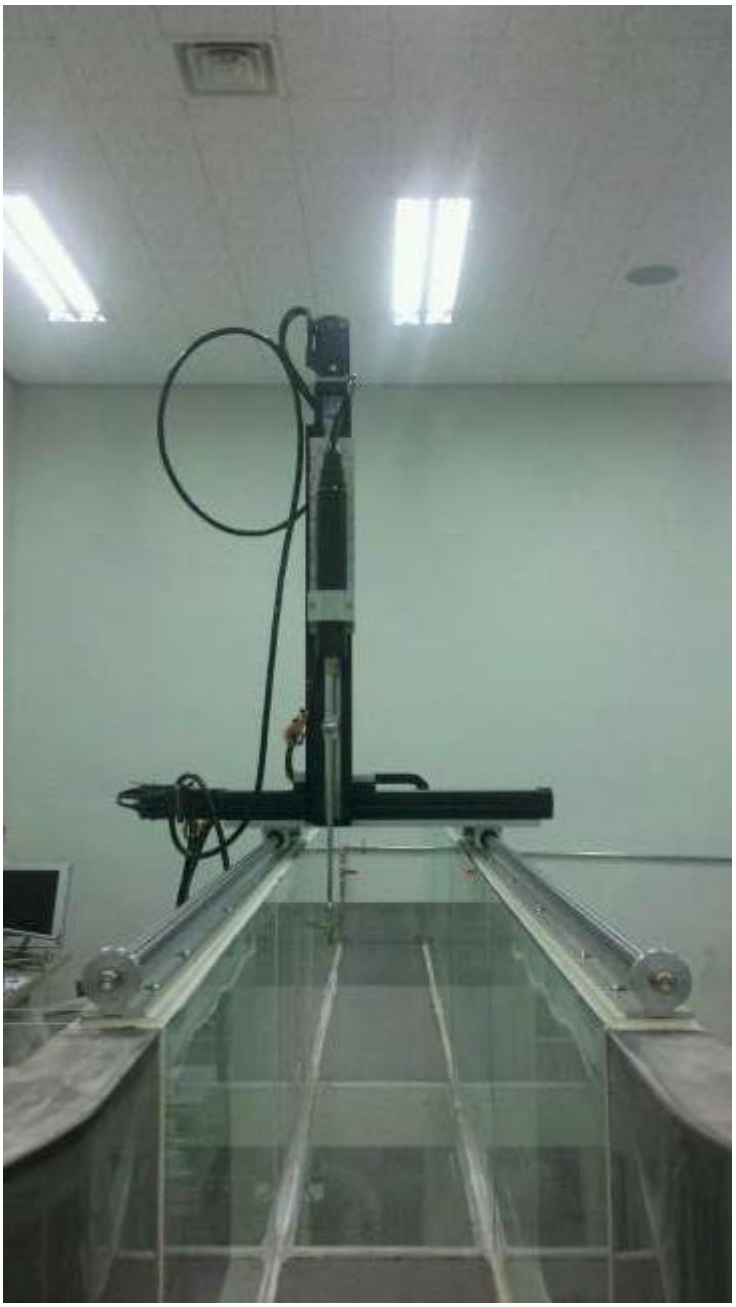

Figure 3.13 Auto traverse system and micro ADV

3.3 Experimental Cases

3.3.1 Object Region

The huge construction project called ‘the Four Major River Restoration Project’ was over recently in Korea. Main purposes of the project are securing sufficient water, improvement of water quality and flood protection. During the construction, dredging main rivers and building weirs were performed during the project to retain sufficient water in the rivers. After the project, some problems were on the rise. Different bed elevation between main and tributary channel leads headward erosion due to dredging. Headward erosion can induce collapse of levee and flood damage.

Among the four river basins (the Han River basin, the Geum River basin, the Youngsan River basin and the Nakdong River basin), the Nakdong River basin is the object region for the research. The river is the longest river in South Korea and the river confluences (the Gam Stream confluence and the Geumho River confluence etc.) are being magnified. Therefore, the river confluences between two branches having stream orders, 1 and 2, are considered as prototypes.

3.3.2 Conditions of Discharge and Water Level

The experimental conditions were determined based on similitude law and distorted model. At this fixed bed experiment, inertia force and gravity are dominant. Water viscosity and surface tension have less of an effect on this experiment. Thus, the similitude law is Froude similitude law. Determining experimental conditions is difficult due to small size of the model. Natural rivers have small water depth compared to its channel width. If the small size model is normal model, viscosity effect is very big. So the theorem of distorted model is necessary.

Water depth was determined with the theorem of distorted model. Because the confluent channel has bed elevation difference, water surface elevations of main and tributary channel are same but water depths are not. Considering an effect of water viscosity, water depth of tributary channel was determined to 0.5 m. Widths of the channels are fixed. Then, the horizontal scales, X_r and the vertical scales, Y_r were calculated from the prototypes. From the horizontal scales and the vertical scales, experimental conditions of tributary discharge could be determined using Equation (3.12).

Although discharge of main channel is normally larger than tributary discharge, the reverse is the case of flood season. Discharge conditions of main channel were determined by ratio to discharge of tributary to study how confluent flow change with discharge ratio. The experimental conditions are shown on Table 3.3.

3.3.3 Conditions of Confluent Channel with Bed elevation difference

Because the experimental study is a fixed bed experiment, bed elevation should be changed directly to study flow characteristics of confluence with bed elevation difference. The bed elevation difference of the channel can be controlled moving tributary channel vertically. Type of bed elevation difference is edge type due to small region of experimental channel. And Gurram et al. (1997) presented that bed slope isn't an important factor for confluent flow. So there is no slope for the tributary channel and bed elevation difference is edge type. Considering measurement space, minimum bed elevation difference, h_s is 0.10 m. The other conditions of bed elevation difference are 0.16 m and 0.22 m. Water depths at downstream, h_d are 0.15 m, 0.21 m and 0.27 m for each bed elevation difference condition to keep the water depth of tributary channel 0.5 m.

Table 3.3 Experimental conditions

Series		Q_m **(l/sec)**	Q_t **(l/sec)**	q^*	h_s **(m)**	h_d **(m)**
AR ($\alpha = 90^\circ$)	101	2	0.5	0.20	0.10	0.15
	102	2.75		0.154		
	103	3.5		0.125		
	104	4.25		0.105		
	105	5		0.09		
	201	2	0.5	0.20	0.16	0.21
	202	2.75		0.154		
	203	3.5		0.125		
	204	4.25		0.105		
	205	5		0.09		
	301	2	0.5	0.20	0.22	0.27
	302	2.75		0.154		
	303	3.5		0.125		
	304	4.25		0.105		
	305	5		0.09		

Table 3.3 Experimental conditions (Cont.)

Series		Q_m **(l/sec)**	Q_t **(l/sec)**	q^*	h_s **(m)**	h_d **(m)**
AM ($\alpha = 60^\circ$)	101	2	0.5	0.20	0.10	0.15
	102	2.75		0.154		
	103	3.5		0.125		
	104	4.25		0.105		
	105	5		0.09		
	201	2	0.5	0.20	0.16	0.21
	202	2.75		0.154		
	203	3.5		0.125		
	204	4.25		0.105		
	205	5		0.09		
	301	2	0.5	0.20	0.22	0.27
	302	2.75		0.154		
	303	3.5		0.125		
	304	4.25		0.105		
	305	5		0.09		

Table 3.3 Experimental conditions (Cont.)

Series		Q_m **(l/sec)**	Q_t **(l/sec)**	q^*	h_s **(m)**	h_d **(m)**
AS ($\alpha = 30^\circ$)	101	2	0.5	0.2	0.10	0.15
	102	2.75		0.154		
	103	3.5		0.125		
	104	4.25		0.105		
	105	5		0.09		
	201	2	0.5	0.2	0.16	0.21
	202	2.75		0.154		
	203	3.5		0.125		
	204	4.25		0.105		
	205	5		0.09		
	301	2	0.5	0.2	0.22	0.27
	302	2.75		0.154		
	303	3.5		0.125		
	304	4.25		0.105		
	305	5		0.09		

Chapter 4. Experimental Results

4.1 Separation zone

To study separation zone near surface, *u*, *v* flow fields were used. Using the micro-ADV, velocity components in 19 cross sections were measured. The velocity measurements were taken for 45 seconds near junction and 25 seconds at the remainder at the sampling rate of 50 Hz. The 40 seconds or 20 seconds were calculated as the time average. The averaged values of velocity were used to analyze *u*, *v* vector fields and *u* contours.

Webber et al. (2001) and Yang et al. (2009) presented that the streamwise flow patterns are very different at the bed and the surface. But the separation zone near surface was focused on because the trashes have damaged the weirs due to the reverse flow near surface. The figures from figure 4.1 to figure 4.7 show the results of 2D surface flow at the each experimental conditions.

As the discharge ratio, q^* increases when α is 90°, the width of the separation zone is wider due to the momentum of the tributary flow. The entering tributary flow near surface is significantly skewed toward the streamwise direction of the main channel. Comparing the angle of entry with

that of the surface flow, surface flow enters at a larger angle to the main channel with the larger discharge ratio, q^*. The smaller angle of the entry of the tributary results in the decrease of the discharge ratio, q^*. The difference in width of the separation zone is also clearly evident when comparing the each separation zone as the change of the discharge ratio, q^*.

When q^* is fixed and α is 90°, the width of the separation zone is wider with the higher bed elevation difference . The conditions of the bed elevation difference s are 0.1 m, 0.16 m and 0.22 m. Although the water elevations of the main and tributary channels are same, the water depths are different due to the bed elevation difference . Comparing the angle of the tributary entry with the confluent angle, surface flow is entering at a smaller angle to the main channel as the smaller bed elevation difference . The larger angle of entry results in the increase of the bed elevation difference . If the conditions of the discharge and the confluent angle are fixed, the larger angle of entry is taken by the lower momentum due to the increase of the bed elevation difference .

The separation zones were observed only when the confluent angle is 90° . The conditions of the confluent angle are 30°, 60° and 90°. The smaller angle of entry results in the decrease of the confluent angle. The separation zone where reverse flow occurs was not observed when the

confluent angles were 30° and 60°. That means that the closer angle of the branch entry to zero takes less effects to the flow of the main channel.

Several relationships were observed between the streamwise velocity components (u and v) and the flow characteristics of confluence (discharge ratio, bed elevation difference and confluent angle) through examination of the u-v vector fields and the u contours. First, the entrance angle of the tributary flow is less for the conditions of high q^*, low h_s and low α. Second, the velocity vectors in the main channel show that less deflection toward the outer wall through the confluence occurs for higher Q_r, lower h_s and lower α.

The results of the u-v vector fields shows the angles of the tributary entity at the confluence as the change of the experimental conditions (the discharge ratio, the bed elevation difference and the confluent angle). It is apparent that the increased momentum of the main channel provides the less effects of the tributary channel. This momentum change of the main channel causes variance in the deflection toward the longitudinal direction of the main channel. As a result of this change in flow momentum, direction of the tributary flow, the streamwise flow characteristics and separation zone are significantly different as the confluence conditions (discharge ratio, bed elevation difference , confluent angle).

The empirical equation for the width of the separation zone including the term of the bed elevation difference was developed. When the confluent angles are 30° and 60°, the separation zone was not observed. The term of the confluent angle, α, should be dropped on the equation (2.5). After performing the multiple regression analysis, the empirical equation for the width of the separation zone can be expressed as

$$\frac{b_s}{B_m} = 0.5995 \exp\left(\frac{h_s}{h}\right) + 9.8981 q^{*2} - 0.0099 Fr_d^{\,2} - 0.9691 \qquad (4.1)$$

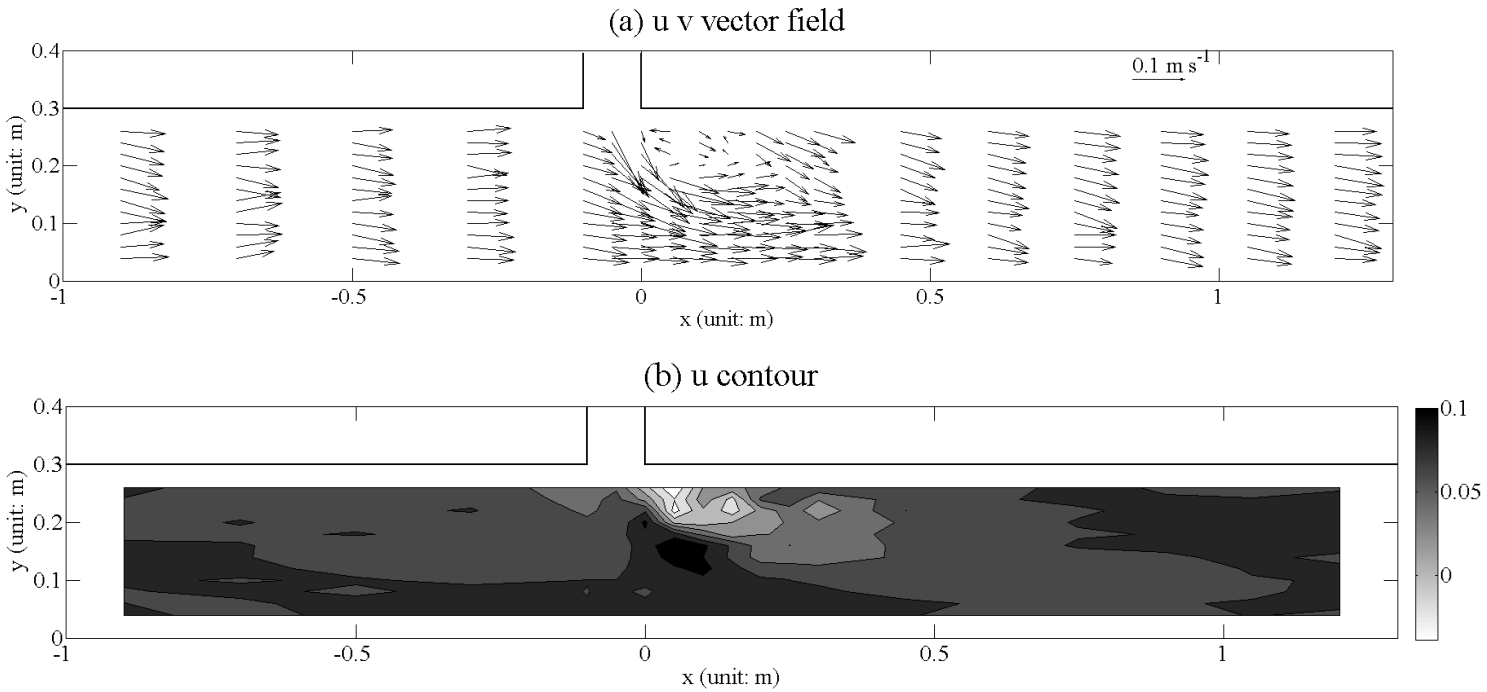

Figure 4.1 (AR205) Streamwise velocity characteristics near surface

4.2 Secondary flow

4.2.1 Flow Field

Although the 3D nature of the open-channel confluence flow problem has been widely addressed in many previous works, there has been few studies about the confluence flow with different bed elevation. To be a true model of the river confluence, 3D flow characteristics should be considered and secondary flows are an important factor of the confluent flow. For this study, the 3D time averaged velocity data has been made by benchmarking the data type for 3D numerical models and Webber et al. (2001). The figures from figure 4.8 to figure 4.14 show the results of the secondary flow fields at the each experimental condition. All these figures show the evolution from down flow to secondary flow due to the bed elevation difference. The down flows were observed at the confluence where the tributary flow meets the flow of the main channel. The flow at X = -0.05 m shows that the surface water is approaching the right side wall of the main channel and the clockwise circulation starts. This flow mechanism can be defined as the down flow. As a result of the down flow, the lateral momentum near surface is greater than near bed. As propagating from the down flow to the secondary flow, the lateral momentum near bed is greater

than near surface.

Figure 4.8, 4.9 and 4.10 shows the difference of the evolutions from the down flow to the secondary flow as the discharge ratio, Q_r. Comparing the variance of the velocity values at Figure 4.8, 4.9 and 4.10, the momentum of the secondary flow at the left wall is greater than at the right wall with the larger discharge ratio, Q_r. Webber et al. (2001) presented that the surface water of the tributary is deflected slightly downstream by the flow of the main channel. This motion creates a secondary flow. As the main channel flow is more dominant, the deflection of the surface water is weaker. This weaker surface water circulates at closer left side wall.

Figure 4.9, 4.11 and 4.12 were used to present the effects of the bed elevation difference, h_s to the secondary flow. The conditions of the bed elevation difference s are related to the water depth of the main channel. If the other experimental conditions are fixed and the condition of the bed elevation difference is only changed, the velocity value of the main channel is lower as the bed elevation difference and the water depth increase. Comparing the different evolution of the secondary flow at Figure 4.9, 4.11 and 4.12, the momentum of the surface water from the tributary is lesser with the higher bed elevation difference. As the bed elevation difference increases, the momentum of the secondary flow at the left wall is greater

than at the right wall due to the less lateral flow momentum from the tributary.

Figure 4.9, 4.13 and 4.14 were used to present the change of the evolution with the confluent angle, α. The smaller confluent angle takes the less effects to the flow travel of the main channel. When the confluent angle is 30°, the down flow was not observed at the confluence. The entity angle of the tributary flow is smaller at 30° (Figure 4.7), the effects of the flow deflection is also smaller. Merging two flows with the small deflection effects make the combined secondary flow at the confluence.

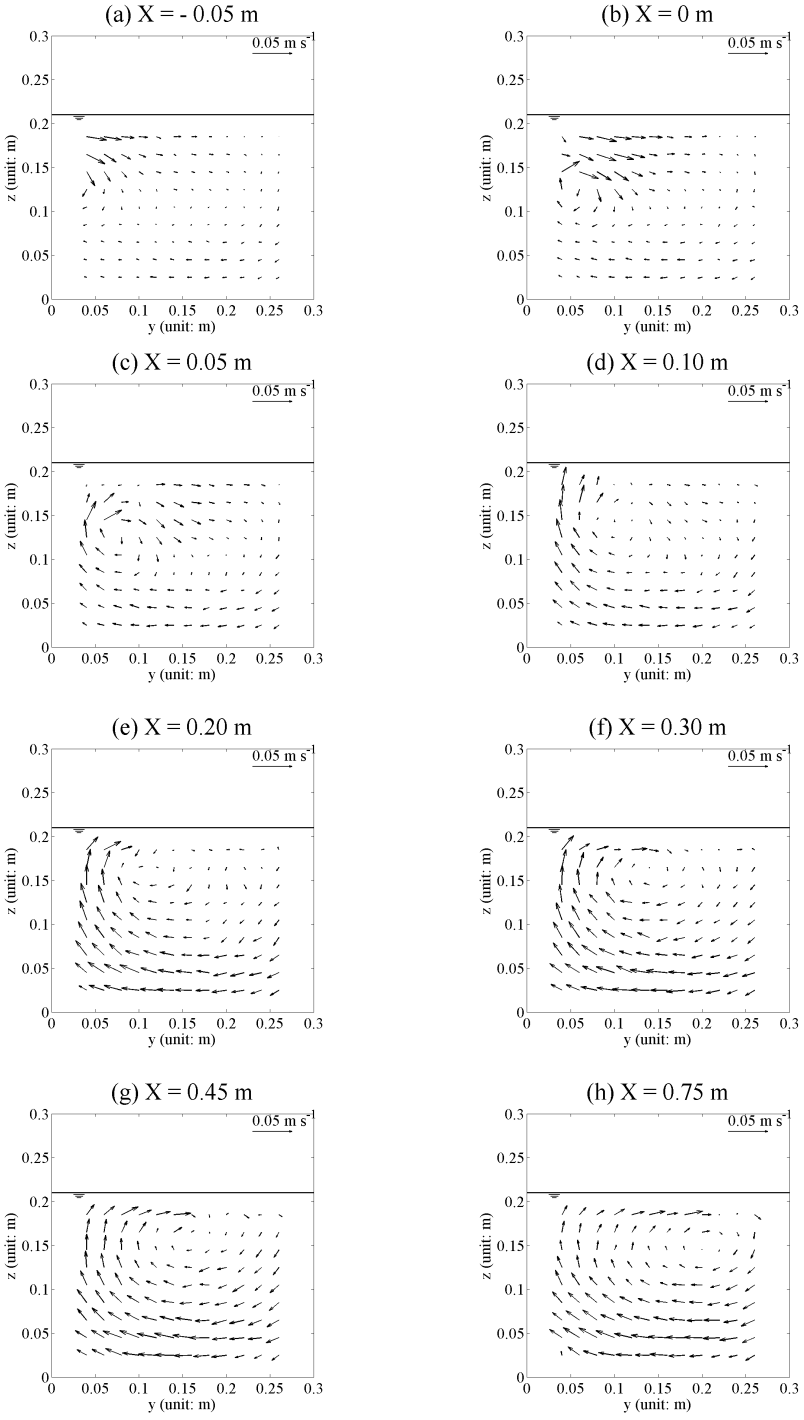

Figure 4.2 (AR205) *v*-*w* vector fields

4.2.2 Vorticity

To study the secondary flow more detailed, the vorticity at whole sections were performed. Vorticity is the standard defining how turbulence is rotational. To analyze how the secondary flow develops, the vorticity values were calculated.

$$\vec{\omega} = \frac{\partial w}{\partial y} - \frac{\partial v}{\partial z} \tag{4.1}$$

When confluent angle is 90°, there is the maximum value of the vorticity at X=0 m (Figure 4.15, 4.16 and 4.17). As going the downstream of the main channel, the values of the vorticity decrease. That means the secondary flows dissipate as going to the downstream. When confluent angle is 60°, the region having the maximum vorticity was observed at X = 0.5 m or X = 0.10 m. All the maximum values of the vorticity were observed where the down flow develops. Because there is no down flow at 30°, the variance of the vorticity is much less than at 60° and 90°. After the surface entity of

the tributary flow meets the upper part of the flow of the main channel, the ongoing flows starts the rotation with the greater later momentum.

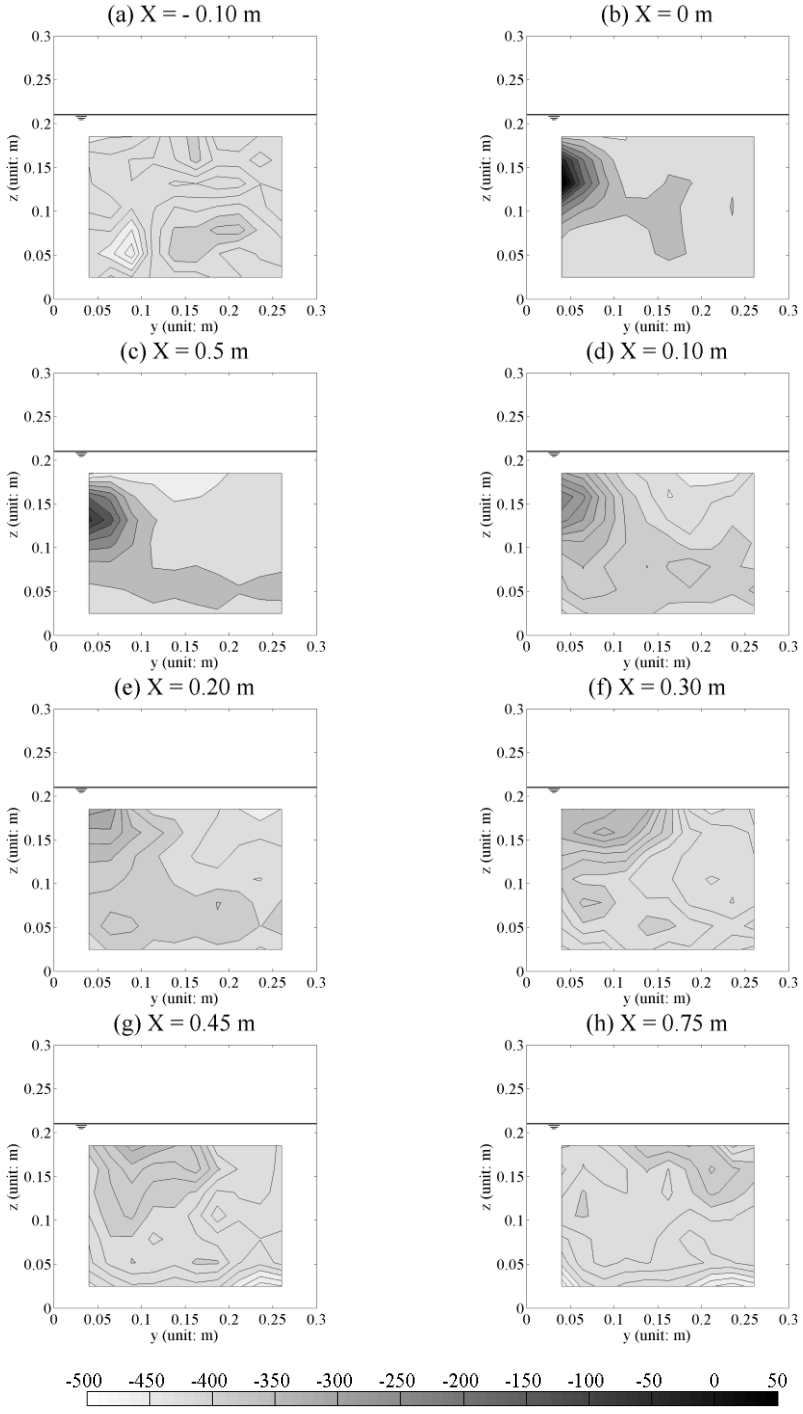

Figure 4.3 (AR205) Vorticity contours

4.2.3 Turbulent Kinetic Energy

The measurements at one point consisted of 40 seconds (Near junction) or 20 seconds of instantaneous velocities collected at 50 Hz. The mean velocities from each individual location were calculated. From the all analyzed velocity fluctuations, the turbulence kinetic energy k was calculated as

$$k = \frac{1}{2}\left[\left(u'\right)^2 + \left(v'\right)^2 + \left(w'\right)^2\right] \tag{4.2}$$

$$k = \frac{1}{2}\left[\left(v'\right)^2 + \left(w'\right)^2\right] \tag{4.3}$$

To study the relationship between the secondary flow and the effects to the bed, Equation 4.3 was used. Figure 4.22 shows that the turbulent kinetic energy was observed right after junction. The values of the turbulent kinetic energy decrease and dissipate with the longitudinal direction of the main channel in the all experimental conditions (Appendix). That is related to the development and the dissipation for the secondary flow. Because the greater values of the turbulent kinetic energy were observed at

X = 0 m, the distribution of the turbulent kinetic energy at X = 0 m was compared with the discharge ratio, the bed elevation difference and the confluent angle.

Figure 4.23 shows the comparison of the turbulent kinetic energy contours with the discharge ratio change. As the discharge ratio q^* decreases, the maximum turbulent kinetic energy values are higher and the region where the turbulent kinetic energy develops is smaller. That is related to the lateral momentum of the entity flow. As the later momentum of the tributary entity flow is greater, the tributary flow is closer to the opposite side of the main channel. The region of the turbulent kinetic energy is bigger with the greater lateral momentum of the entity flow. The maximum value of the turbulent kinetic energy is less due to the lower flow velocity of the main channel.

Comparing the turbulent kinetic energy contours with the bed elevation difference change, Figure 4.24 was used. As discussed in the previous sections, when the other experimental conditions are fixed, the velocity of the main channel is lower with the increase of the bed elevation difference. The lateral momentum of the tributary entity is greater due to the lower velocity of the main channel with the increased bed elevation difference. Figure 4.24 shows that the region where the turbulent kinetic

energy develops is bigger with the increased bed elevation difference and the water depth.

Figure 4.25 was used to compare the contours of the turbulent kinetic energy with the confluent angle change. The tributary flow enters better and the turbulent kinetic energy is less at the smaller confluent angle. When the confluent angle is 30°, the values of the turbulent kinetic energy is much less than at 60°, 90°.

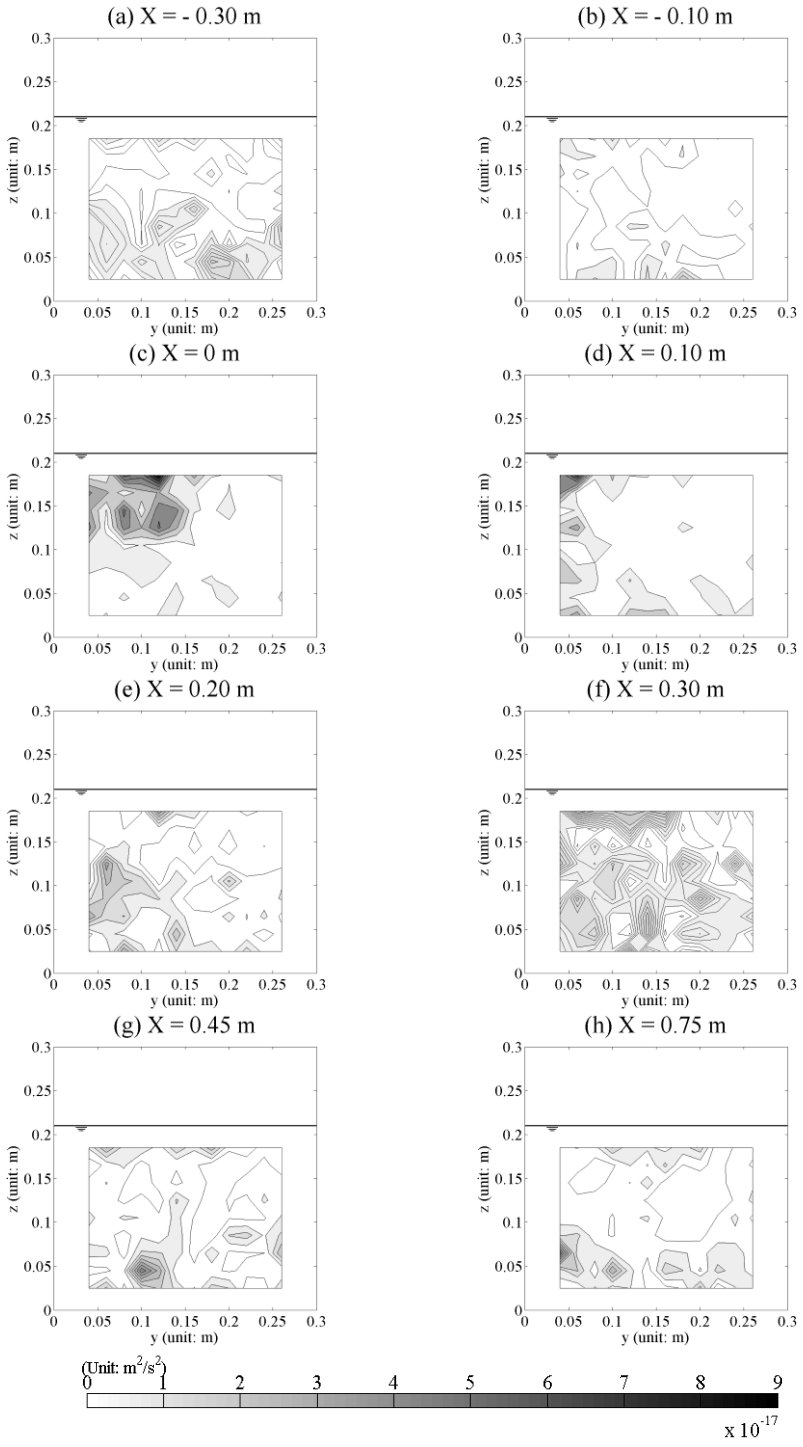

Figure 4.4 (AR203) Turbulent Kinetic Energy contours

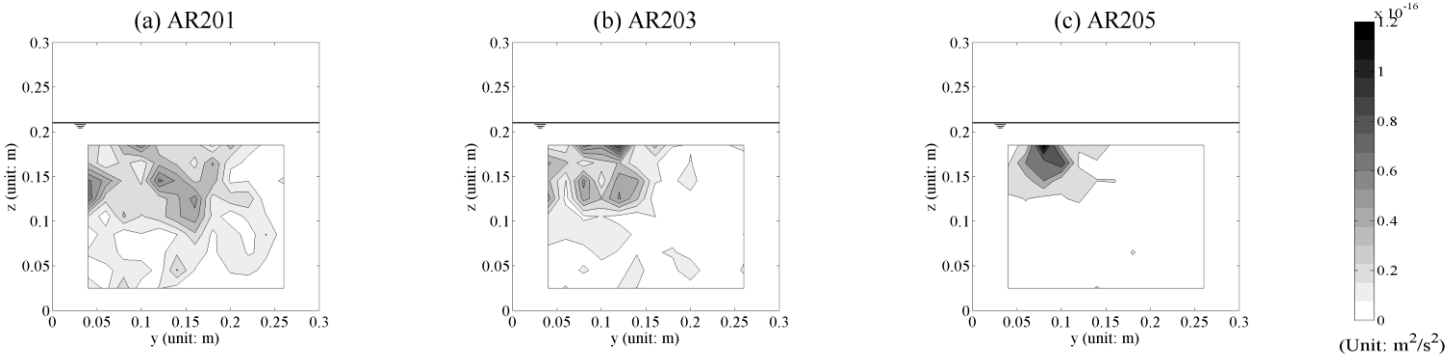

Figure 4.5 Turbulent Kinetic Energy contours with discharge ratio change (At X = 0 m)

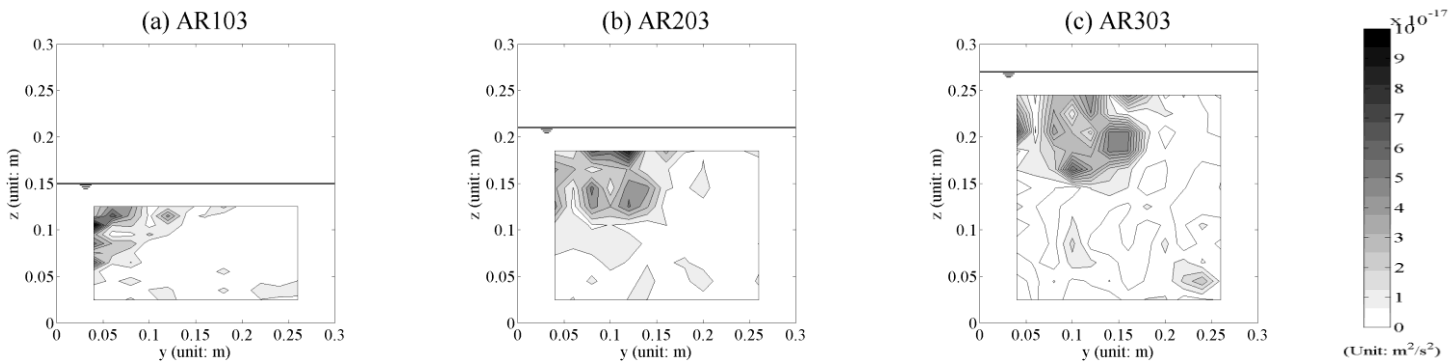

Figure 4.6 Turbulent Kinetic Energy contours with bed elevation difference change (At X = 0 m)

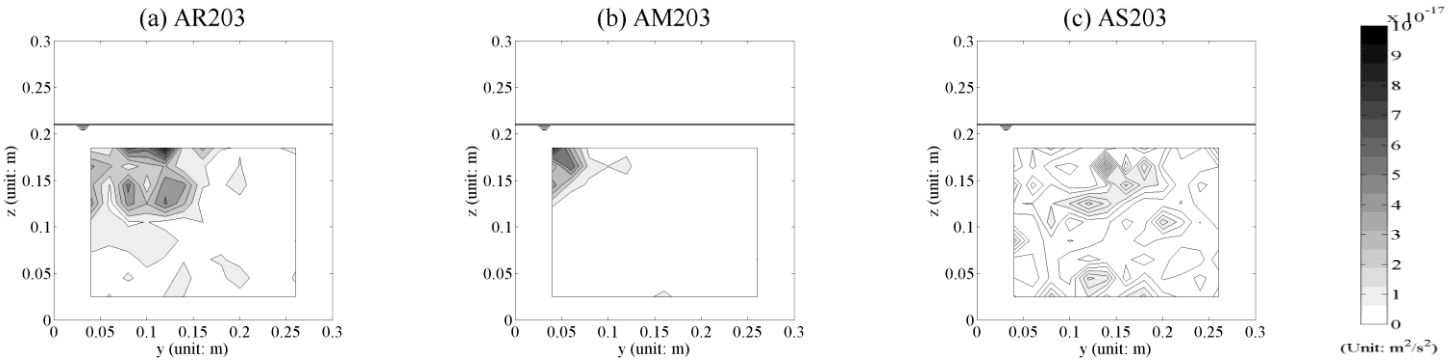

Figure 4.7 Turbulent Kinetic Energy contours with confluence angle change

4.2.4 Reynolds Shear Stress

Among the Rerynolds shear stress, $-\rho\overline{v'w'}$ is related to the secondary flow. Because the averaged velocity fluctuation, v' and w' were used to calculate the Reynolds shear stress, the tendency of the result is similar to the turbulent kinetic energy result. The degree of the Reynolds shear stress is MPa and ρ is the water density (9800 N/m^3). Figure 4.26 shows the evolution of the Reynolds shear stress. Figure 4.27, 4.28 and 4.29 are the comparison of the Reynolds shear stress at X = 0 m with the experimental conditions (discharge ratio, bed elevation difference and confluent angle). As discussed the distribution of the fluctuated velocity components in the previous section, the Reynolds shear stress is greater in which down flow or secondary flow develop well.

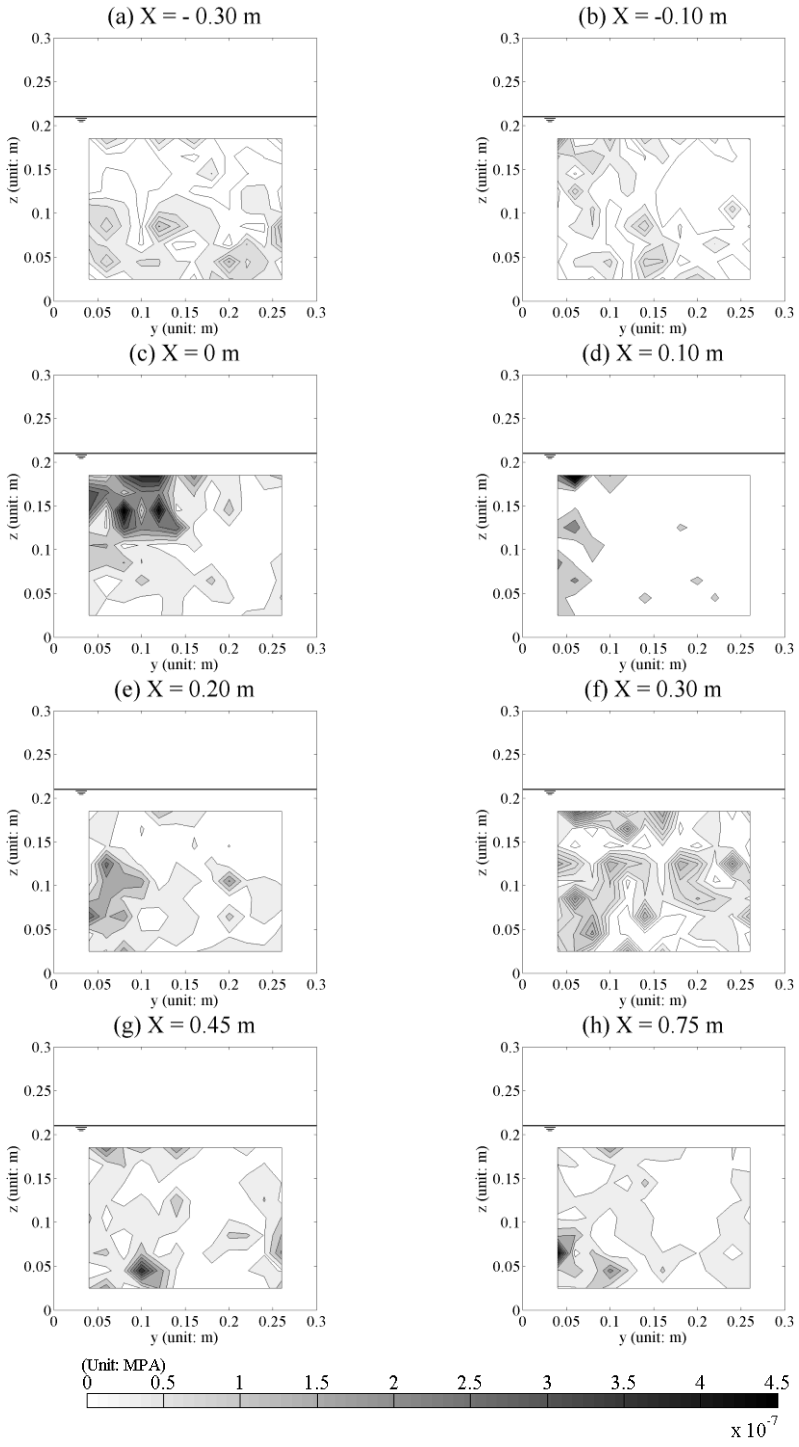

Figure 4.8 (AR203) Reynolds shear stress contours

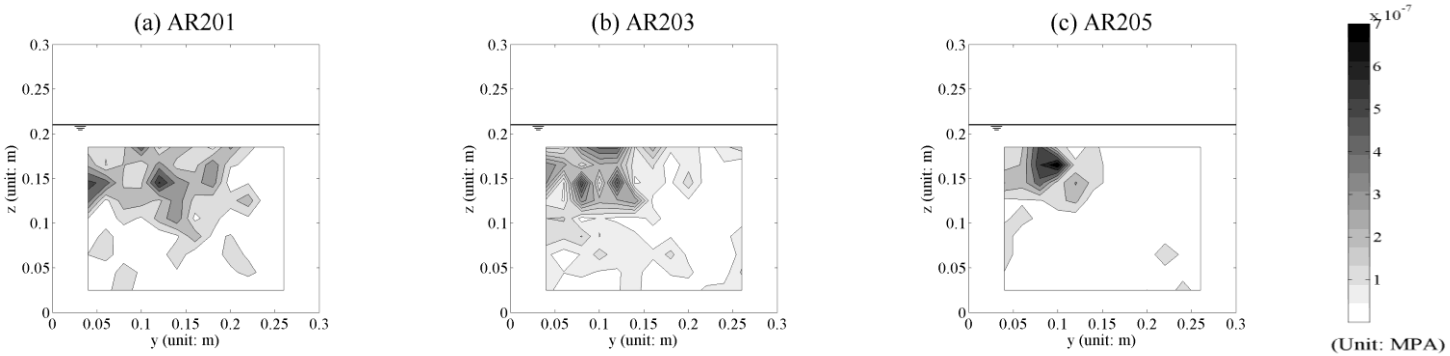

Figure 4.9 Reynolds shear stress contours with discharge ratio change

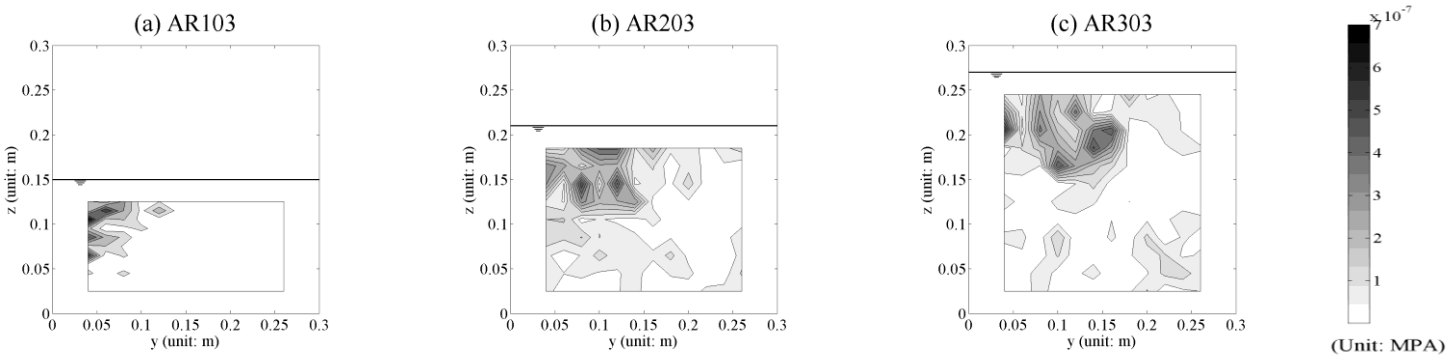

Figure 4.10 Reynolds shear stress contours with bed elevation difference change

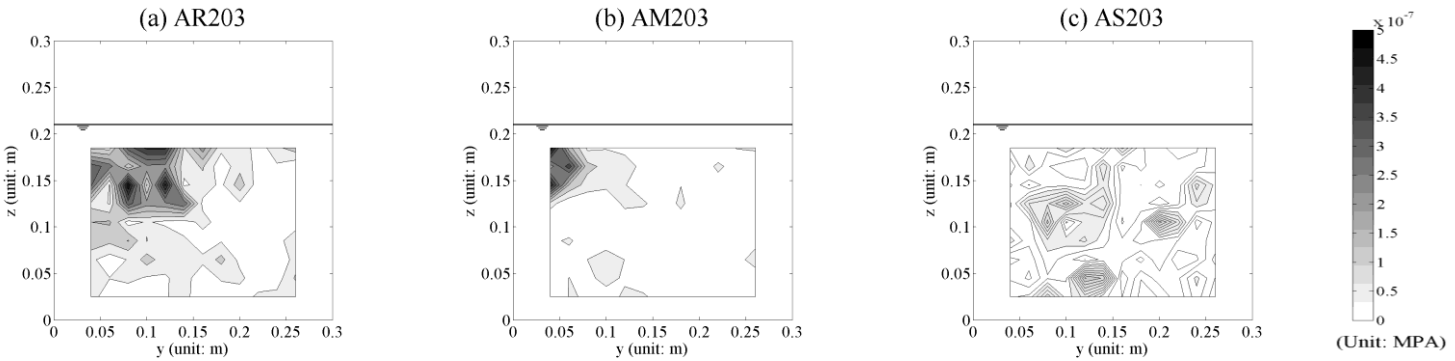

Figure 4.11 Reynolds shear stress contours with confluent angle change

4.2.5 Relative turbulent kinetic energy

The relative turbulent kinetic energy was used to predict the headward erosion at a confluence with bed elevation difference. Hoffmans et al. (1994) presented the local scour can be predicted by the value of the relative turbulent kinetic energy. He described that the local scour occurs due to the flow at the straight channel with bed elevation difference . And the local scour depth can be calculated from the value of the relative turbulent kinetic energy. The equation (4.4) is for the calculation of local scour depth and the equation (4.6) is for relative turbulence intensity.

$$\frac{y_m}{h_0} = \frac{wU_0 - U_c}{U_c} \tag{4.4}$$

$$w = 1 + 3r \tag{4.5}$$

$$r = \frac{\frac{1}{h}\int_0^h \sqrt{TKE}\,dz}{U_0} \tag{4.6}$$

Where, y is local scour depth (m), h_0 is upstream water depth (m), U_c is critical mean velocity (m/s) , U_0 is the mean velocity (m/s),

Q is discharge (m^3/s), A is cross section (m^2), r_0 is relative turbulent kinetic energy, TKE is turbulent kinetic energy.

As Hoffman et al. (1994) presented, relative turbulent kinetic energy is necessary to predict headward erosion. Because the distribution of turbulent kinetic energy with horizontal direction is important at a confluence, the values of the turbulent kinetic energy are averaged with the area. The regression analysis was performed at each cross section.

$$r_0 = \frac{\frac{1}{A}\int_0^A \sqrt{TKE}\,dA}{U_0} \tag{4.7}$$

The lateral momentum of the tributary entity is the highest at the right after junction (Section 4.2.4). The regression analysis for the relative turbulent kinetic energy was performed at X = 0 m. Figure 4.30 shows the regression analysis of the relative turbulent kinetic energy at X = 0 m. As the velocity ratio U_r increases, the relative turbulent kinetic energy is higher. The velocity ratio, U_r means the effectiveness of the tributary flow to the main channel. The effectiveness of the tributary flow to the main channel increases, the value of the relative turbulent kinetic energy also increases. Because the lateral momentum of the entity flow increases, the relative

turbulent kinetic energy is higher with the confluent angle.

The degree of headward erosion at the confluence was predicted by the relative turbulent kinetic energy. Because the velocity ratio, U_r means the effectiveness of the tributary flow to the main channel, the regression analysis of the relative turbulent kinetic energy was performed with U_r. The relative turbulent kinetic energy is higher with U_r. When the discharge ratio, the bed elevation difference and the confluent angle increase, the velocity ratio increases in the study. Although all three variables (discharge ratio, bed elevation difference and confluent angle) induce the relative turbulent kinetic energy at the confluence, the bed elevation difference affects the relative turbulent kinetic energy most right after junction. The bed elevation difference is the most important factor for the headward erosion at the confluence.

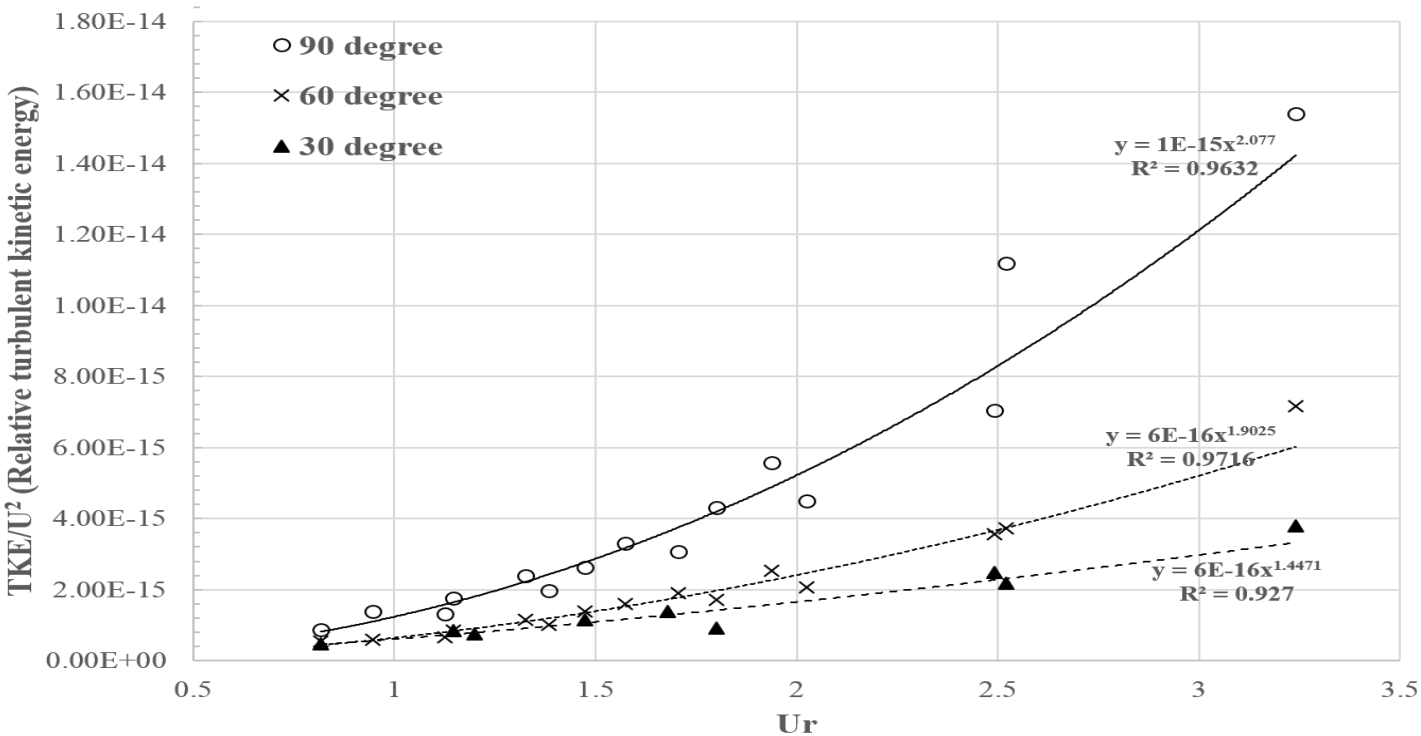

Figure 4.12 The regression analysis of relative turbulent kinetic energy at X = 0 m

Chapter 5. Conclusion and Future Study

5.1 Summary and Conclusion

To study the flow characteristics at the confluence, three dimensional velocity components were measured and analyzed with the five conditions of discharge ratio, the three conditions of bed elevation difference and confluent angle. Using micro-ADV, the instantaneous velocity components were measured at each one point and these measured velocities were averaged.

The u-v vector fields show the flow characteristics of the confluence near surface. Comparing the u-v vector fields with the discharge ratio, the bed elevation difference and the confluent angle, the lateral momentum of the tributary flow entity is the important factor to induce the separation zone. As the lateral momentum of the tributary flow entity is greater, the entity angle is larger and the separation zone is wider.

The mechanism of the confluence is the 3D flow characteristics. Analyzing the v-w vector fields and the vorticity contours, how the surface water of the tributary affects the evolution of the secondary flow. Because of the bed elevation difference, the surface momentum of the tributary flow

force to rotate the upper part water of the main channel. The surface water of the tributary is approaching the right side wall of the main channel and the clockwise circulation starts. This flow mechanism can be defined as the down flow. The down flow results in the evolution to the secondary flow. Considering the discharge ratio, Q_r, as Q_r decreases, the deflection of the surface water is weaker. This weaker surface water circulates at closer left side wall. Comparing the evolution of the secondary flow with the bed elevation difference , h_s, as the bed elevation difference increases, the momentum of the secondary flow at the left wall is greater than at the right wall due to the less later flow momentum from the tributary. For the confluent angle, α, the entity angle of the tributary flow is smaller with at the smaller confluent angle, the effects of the flow deflection is also smaller. Merging two flows with the smaller deflection effects make the combined secondary flow at the confluence.

To study the turbulent characteristics for the confluent flow, the turbulent kinetic energy and the Reynolds shear stress were calculated. Both the values of the turbulent kinetic energy and the Reynolds shear stress is greater at the confluence than at the downstream. Both of them develop at the confluence and dissipate at the downstream. Comparing the turbulent kinetic energy and the Reynolds shear stress at X = 0 m with the

experimental conditions, the region where they develops is bigger with the greater discharge ratio and the increased bed elevation difference. When the confluent angle is 30°, the values of the turbulent kinetic energy and the Reynolds shear stress is much less than at 60°, 90°.

The regression analysis for the relative turbulent kinetic energy was performed to predict the degree of the headward erosion. Because the velocity ratio, U_r means the effect of the tributary flow to the main channel, the relationship between the relative turbulent kinetic energy and the velocity ratio was analyzed. Although the velocity ratio increases with the discharge ratio, the bed elevation difference and the confluent angle, the confluent angle affects the relative turbulent kinetic energy most at right after junction. The bed elevation difference is the most important factor to induce the headward erosion at the confluence.

The confluent flow is the 3D flow mechanism due to the entity flow of the tributary. The lateral momentum of the tributary forces to rotate the upper body of the main channel water and induces the down flow due to the bed elevation difference. The momentum of the tributary entity induces greater with the less discharge ratio, the higher bed elevation difference and the larger confluent angle. That means the tributary flow enters better with these conditions.

5.2 Future Study

In the confluent channel, the movable experiment can be performed. The headward erosion is the significant problem of the river management due to the bed elevation difference. To understand the mechanism of the headward erosion, the movable experiment is necessary. The results from this study can be used to understand the flow inducing the sediment transport at the confluence.

Although the and 90°velocity components were measured in the confluent channel with bed elevation difference for this study, an entity of pollutants can be studied in the future. Because the confluence is the basic hydraulic structure, sewerage systems discharge chemical or biochemical pollutants to rivers. The general sewerage system has the bed elevation difference. So this confluent channel having the bed elevation difference can be useful for the study of the physical pollutant movement.

The hydraulic experiment was only performed on this study. If the result from this study is compared to the result of numerical models, the application to the real rivers is possible. Investigating the flow mechanism, managing the river environments and using the natural river construction method are also possible with the models.

Reference

Anwar, H. (1955). StrömungsverhältnissebeiFlussvereinigungen. PhD thesis, Technical University of Karlsruhe, Karlsruhe, Germany

Barkdoll, B. D. (2003). “Discussion of ‘experiments on flow at a 90° open-channel junction’ by Weber et al.” J. *Hydraul. Engrg.*,129(2), 167-168

Best, J. L. and Reid, I. (1984). “Separation zone at open-channel junctions.”*J. Hydr. Engrg.*, 110(11), 1588-1594.

Biswal, S.K., Mohapatra, P.K., and Muralidhar, K. (2012).“A comparison study of flow fields at open channel junction.”*Proc., 10th Can. Hydroscience& Engineering Conf.*

Boer, C., Roy, A.G., and Best. J. L. (2006). “Dynamics of a river channel confluence with discordant beds: flow turbulence, bed load sediment transport, and bed morphology.”*J. Geophysical Research*, Vol. 111, F04007

Choi, G. W., Kim, Y. K., and Yun, Y. J. (2003a).“Changing of channel bed through discharge ratio at junction.*” Proc., Can. KSCE Journal of Civil Engineering Conf.*, 2439-2442

Choi. G. W., Park, Y. S., and Han, M. S. (2003b). “The change of flow

depending upon the discharge and approaching angle at channel junctions.”*Proc., Can. KSCE Journal of Civil Engineering Conf.,* 2835-2840

Chung, Y. J., Choi, G. W., Kim, Y. K., and Cho, S. W. (2006).“Analysis of water depth and velocity through discharge condition from sewerage outlet at near channel junction.”*J. Korean Society of Hazard Mitigation*, 6(4), 49-56

Ghobadian, R. and Shafai, M. B. (2007). “Investigation of sediment patterns at river confluence.”*J. Applied Sciences,* 7(10), 1372-1380

Ghobadian, R. (2012). “Predictoin of progressive penetration of scour hole into the tributary channel in laboratory channel confluences.*” J. Applied Sciences*, ISSN 1812-5654

Gurram, S. K., Kariki, K. S., and Hager, W.H. (1997).“Subcritical junction flow.”*J. Hydraul. Engrg., 123(5), 447-455.*

Henderson (1966). *Open channel flow*. Macmillian Publishing Company, New York.

Joy, D. M. and Townsend, R. D. (1981). “Improved flow characteristics at a 90° channel confluence.”*Proc., 5th Can. Hydrotechnical Conf.*

Lawrence, P. (2003). Bank Erosion and Sediment Transport in a Microscale

Straight River.Ph.D thesis, University of Paris 7 – Denis Diderot, 167p

Lee, K. H. and Seo, I. W. (2006). Experimental Investigation of Flow Characteristics in Meandering Channels. Master Thesis, Seoul National University, Seoul

Modi, P.N., Dandekar, M. M., and Ariel, P. D. (1981).“Conformal mapping for channel junction flow.”*J. Hydr. Div.,* 107(12), 1713-1733

Nédélec, Y., and Gay, B. (2008).“Experimental study of a right-angled end junction between a pipe and an open channel.”*J. Hydrual. Engrg*., 134:5(616), 616-625

Rhods, B. L., and Sukhodolov, A. N. (2004).“Spatial and temporal structure of shear layer turbulence at a stream confluence.”*J. Water Resources Research* Vol. 40, W06304

Shin, J., H. and Seo, I. W. (2012). Development of Transverse Velocity Profile Equation of Secondary Currents in Curved Channels by Numerical Simulation. Master Thesis, Seoul National University, Seoul

Song, C. G. and Seo, I. W. (2011). A Finite Element Model for Shallow Water Flow Incorporating Dispersion Stresses and Generalized BCs. Ph. D thesis, Seoul National University, Seoul, 16-23 and 123-134

Shumate, E. D. (1998). Experimental Description of Flow at an Open-channel Junctions. Master Thesis, University of Iowa, Iowa

Street, R. L., Watters. G. Z., Vennard. J. K.,(1997). Elmentary Fluid Mechanics. John Wiley & Sons,

Publishing Company, US

Taylor, E. H. (1944). "Flow characteristics at rectangular open-channel junctions."*J. Hydr. Engrg.*, 114(12), 1449-1460

Thanh, M. D., Kimura, I., Shimizu, Y., and Hosoda, T. (2010)."Depth-averaged 2D models with effects of secondary currents for computation of flow at a channel confluence."*Proc., River Flow 2010, 137-144*

Webber, L. J., Shumate, E. D., and Mawer, N. (2001)."Experiments on flow at a 90° open-channel junction."*J. Hydrual. Engrg.*, 127(5), 340-350

Webber, N. B., and Greated, C. A. (1966)."An investigation of flow behavior at the junction of rectangular channels."*Proc., Instn.of Civ. Engrs*., Vol. 34, Thomas Telford Ltd., London, 321-334.

Yang, Q. Y., Wang, X. Y., Lu. W. Z. and Wang. X. K. (2009). "Experimental study on characteristics of separation zone in confluence zones in rivers."*J. Hydrual. Engrg.*, 14:2(166), 166-171

초 록

하상고 차이가 있는 합류수로에서의 흐름특성에 대한 실험적 연구

서울대학교 대학원
건설환경공학부
이 주 하

지천 합류부에서 하천 지형이 급격히 변하는 문제가 발생하고 있다. 최근 4대강 사업이 완료됨에 따라서, 하천 정비사업으로 충분한 유량을 확보하기 위해 시행한 본류에서의 하천준설 공사는 지천 합류부에서 단차가 발생하는 문제를 발생시켰다. 이러한 지천 합류부에서의 하상고 차이는 침식을 야기시킬 수 있다. 그리고 홍수기에는 지류의 유량이 급격히 증가하여 합류부 부근의 사수역 (separation zone)에서의 퇴사가 문제가 되고 있다. 기존 합류부 실험은 지류와 본류의 바닥고가 같은 조건에 대해서 수행되었다. 국내 하천의 합류부가 본류와 지류의 바닥고 차이, 단차 (bed elevation difference) 가 존재하기 때문에 이러한 단차를 반영한 합류부 실험연구가 필요하다.

본 연구의 목적은 본류와 지류가 만나 형성되는 합류구간에서의 수리학적 거동을 분석하여 하상침식, 오염물 확산 등에 미치는 영향을 분석하는 것이다. 본 연구에서는 수리모형 실험을 수행하여 본류와 지류 하상고간의 단차에 따른 합류부에서의 유속 및 난류인자를 측정하고자 한다. 나아가서 지류 합류부 두부침식 문제나 오염물 확산에 영향을 미치는 사수역에 관한 경험식을 도출하고자 한다.

낙동강과 제 1지천에 대한 자료를 수집하여 합류수로를 제작하였고, 상사법칙과 왜곡모형 이론을 이용하여 실험 조건을 결정하였다. 유속측정은 직접 측정법인, Micro-ADV를 이용하여 측정할 것이다. Micro-ADV를 통해 취득한 유속자료를 분석하였다.

u-v 벡터장은 수표면 근처에서의 흐름특성을 보여준다. 유량비, 단차 그리고 합류각도에 따른 u-v 벡터장을 비교하면, 지류유입으로 인한 모멘텀은 사수역에 영향을 주는 중요한 요소이다. 지류유입의 모멘텀이 커짐에 따라, 흐름의 유입각도가 커지고, 사수역의 너비가 넓어진다. v-w 벡터장과 와도 컨투어를 분석하여, 지류의 수표면 유입이 이차류의 발달과정에 영향을 미친다. 단차로 인해서, 지류의 수표면 모멘텀은 본류의 윗 부분에 힘을 가해 회전시키기 시작한다. 지류의 흐름은 본류의 우안에 접근하면서, 시계방향 회전이 시작된다. 이 흐름 메커니즘을 하강류로 정의된다. 하강류는 이차류의 발달과정에 영향을 미친다. 합류흐름의 난류 특성에 대해 연구하기 위해, Turbulent Kinetic Energy와 난류 전단

력을 계산하여 분석하였다. 합류부에서 두 분석값이 매우 크며, 하류로 가면서 소산된다. 각 실험조건에 대한 X = 0 m 에서의 Turbulent Kinetic Energy 와 난류 전단력 값을 비교하면, 유량비가 커지고, 단차가 높아질수록 난류가 발달하는 영역은 점점 커진다. 합류부의 두부침식을 예측하기 위해서, 상대난류강도 이론을 사용하여 X = 0 m 구간에 대해서 회귀분석을 수행하였다. 그 결과, 유량비, 단차 그리고 합류각도가 증가할 경우 상대난류강도 값이 증가하였다. 그 중, 단차가 증가함에 따라 그 증가폭이 가장 커 두부침식에 영향을 주는 인자 중 단차의 영향이 가장 크다고 분석되었다.

합류흐름은 지류흐름으로 인한 3차원 흐름 메커니즘이다. 지류의 횡방향 모멘텀은 본류의 윗부분을 회전하는 힘을 가하고, 단차로 인한 하강류에 영향을 미친다. 유량비가 작아질수록, 단차가 높아질수록, 그리고 합류각도가 커질수록 지류 유입 모멘텀은 커지고, 이것은 지류의 흐름이 공학적으로 안정적으로 유입됨을 의미한다.

주요어: 지천 합류부, 수리실험, 단차, 이차류, 사수역, 난류에너지

학 번: 2011-23399

Appendix

This appendix chapter is to put the whole contents in this study. The whole results not in the body are shown in the appendix. The experimental methodology is also introduced in this chapter.

All results except for the results in the body are put in this chapter. The types of the results are also the u-v vector fields, the v-w vector fields, the vorticity contours, the turbulent kinetic energy contours and the Reynolds shear stress contours. These help readers understand the confluent flow with other experimental conditions. (From Figure A.2 to Figure A.172)

To measure the flow velocities, the measurement system having the auto traverse system and the micro-ADV was designed. The programs to command the auto traverse system and the micro-ADV are the MCU and the the Horizon ADV. These programs were controlled personally. Because the micro-ADV is the one point measurement method, measuring whole points are too laborious. The macro express is useful to command both the MCU and the Horizon ADV automatically. The computer commanded the measurement and the movement to the auto traverse system by the macro express. After measuring all points in the confluent channel, the Matlab was used to analyze the instantaneous velocities and to plot the all results. The

Matlab code is also put in the appendix chapter.

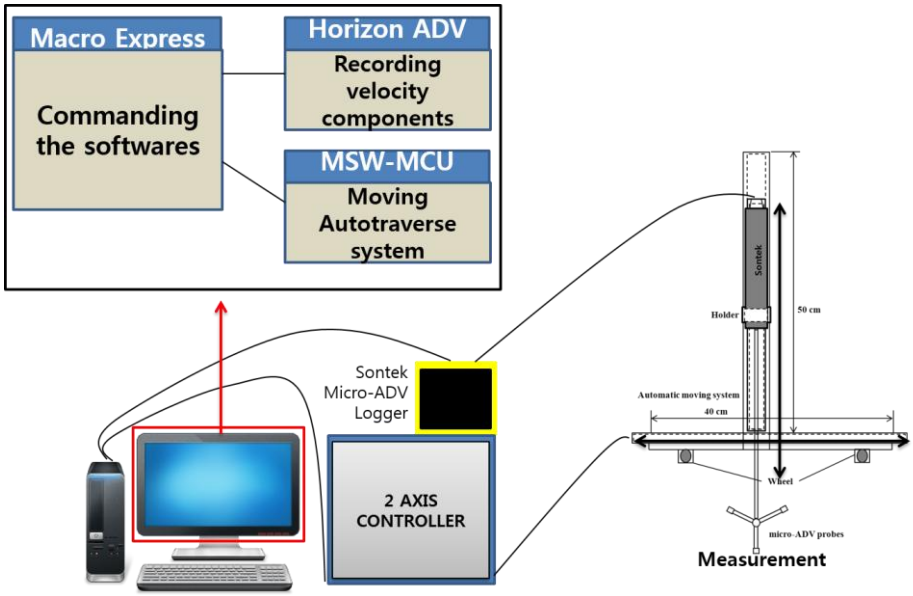

Figure A.1 The scheme of the measurement system

Appendix. 1. Experimental Results

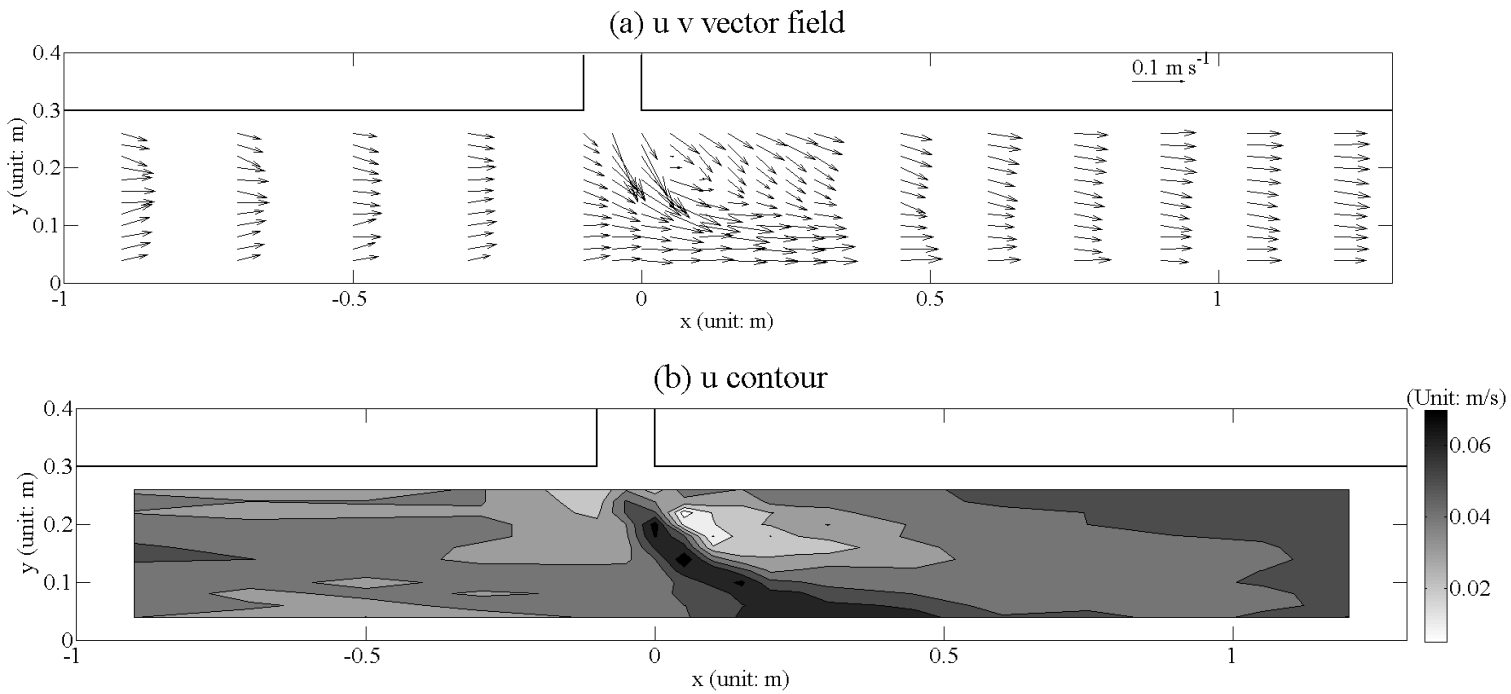

Figure A.2 (AR101) Streamwise velocity characteristics near surface

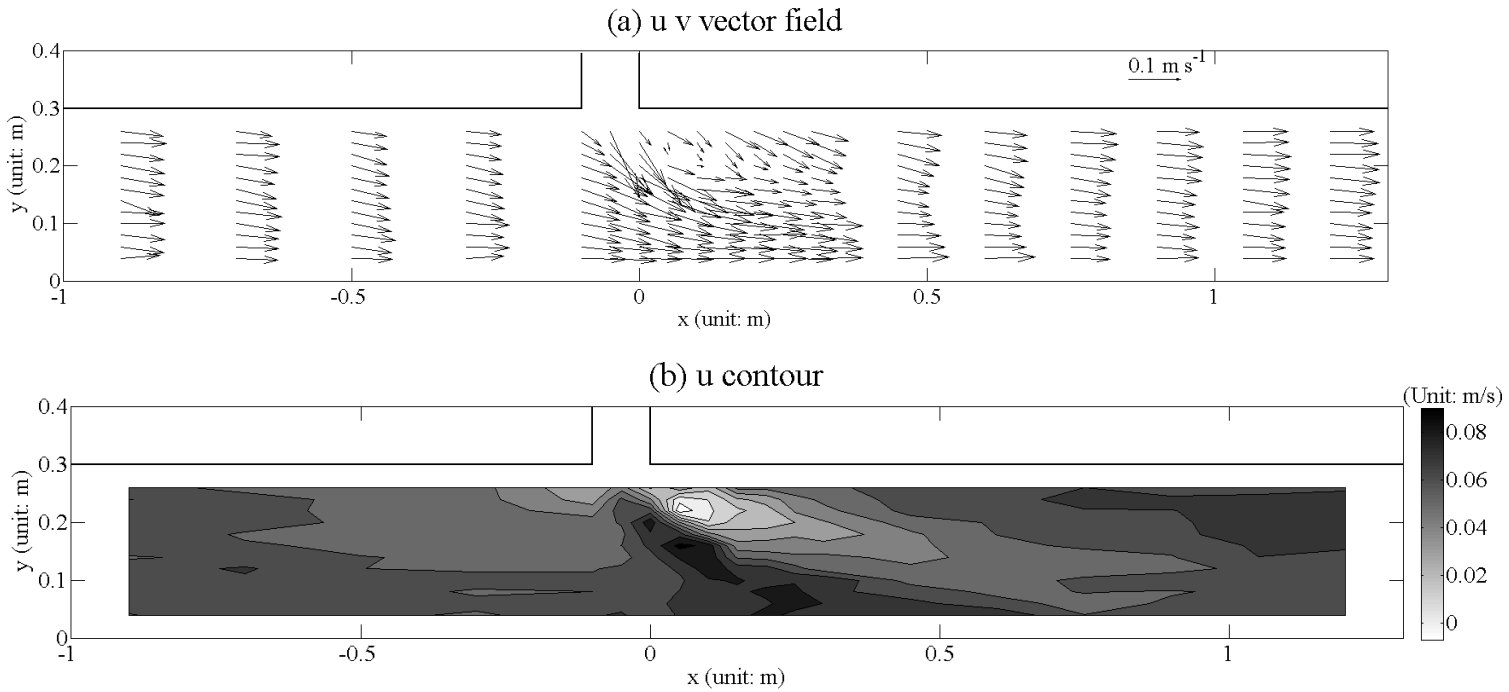

Figure A.3 (AR102) Streamwise velocity characteristics near surface

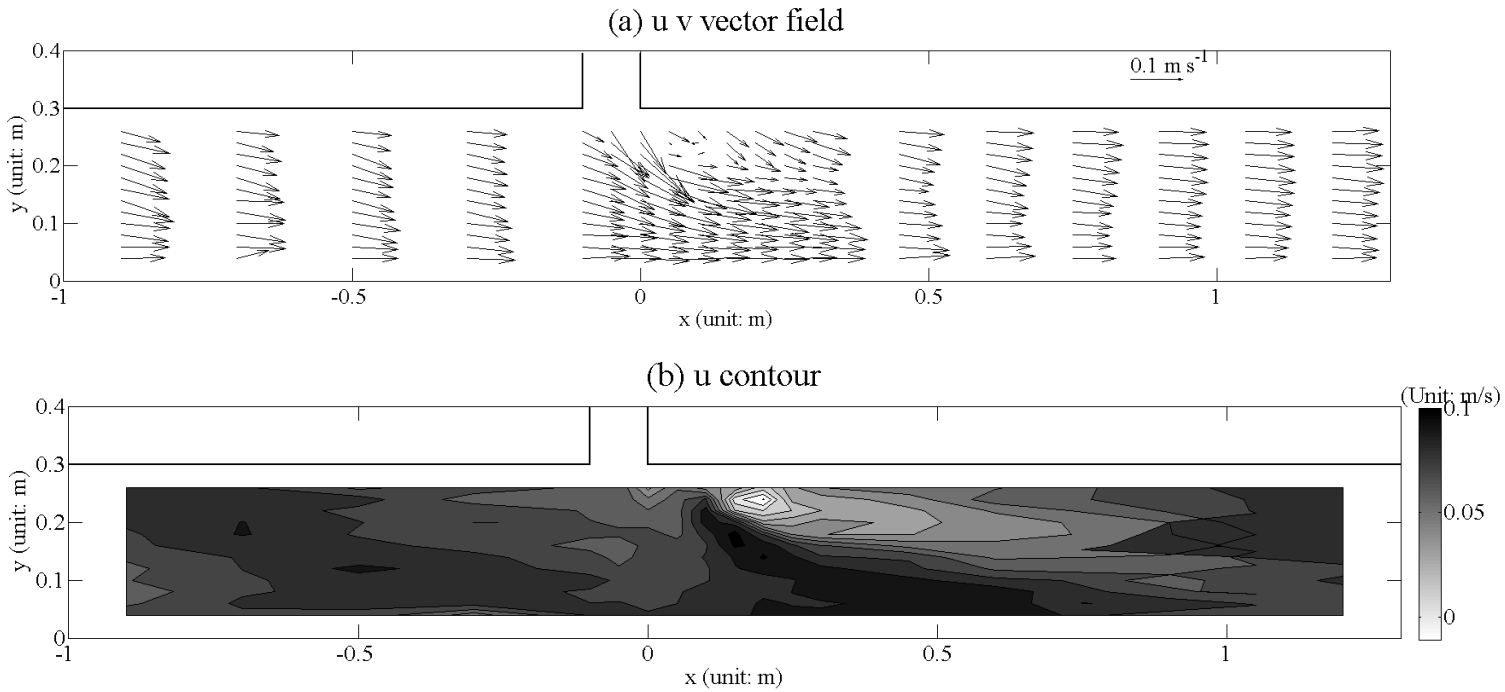

Figure A.4 (AR103) Streamwise velocity characteristics near surface

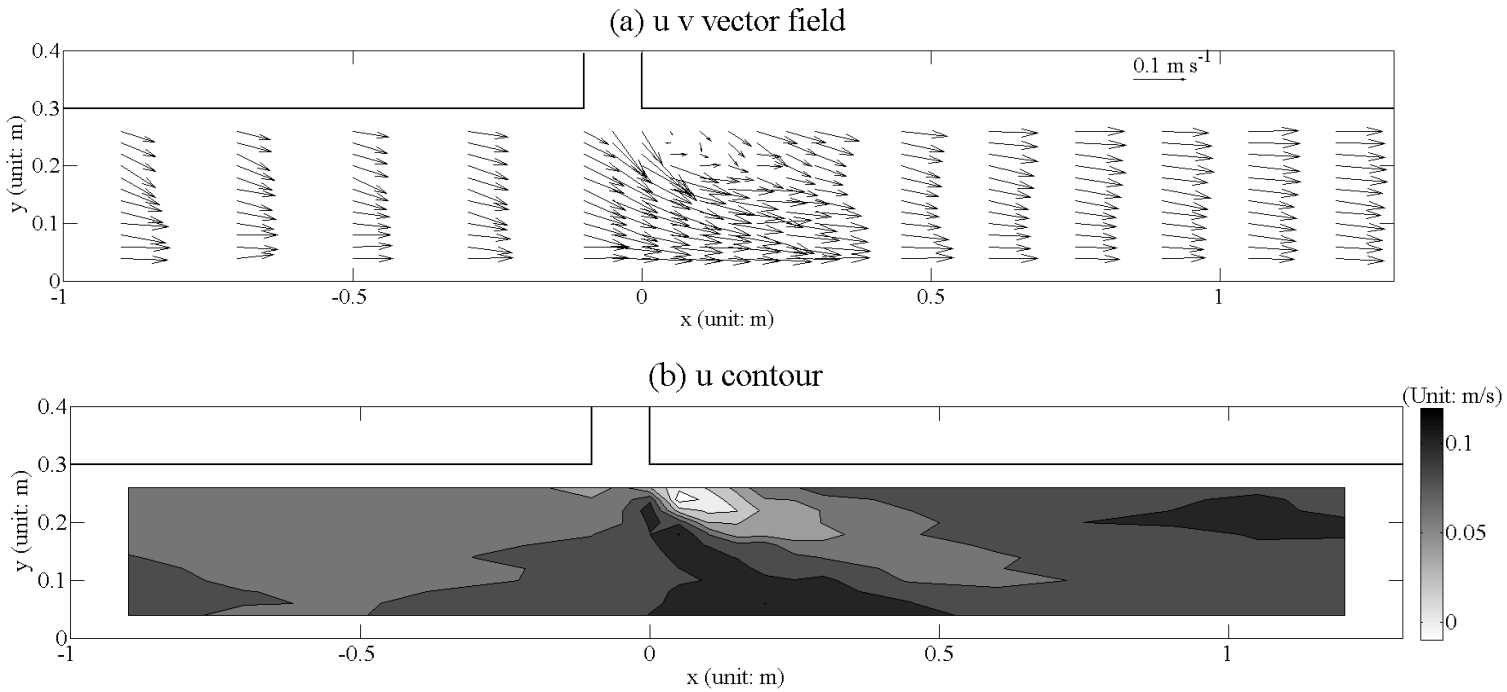

Figure A.5 (AR104) Streamwise velocity characteristics near surface

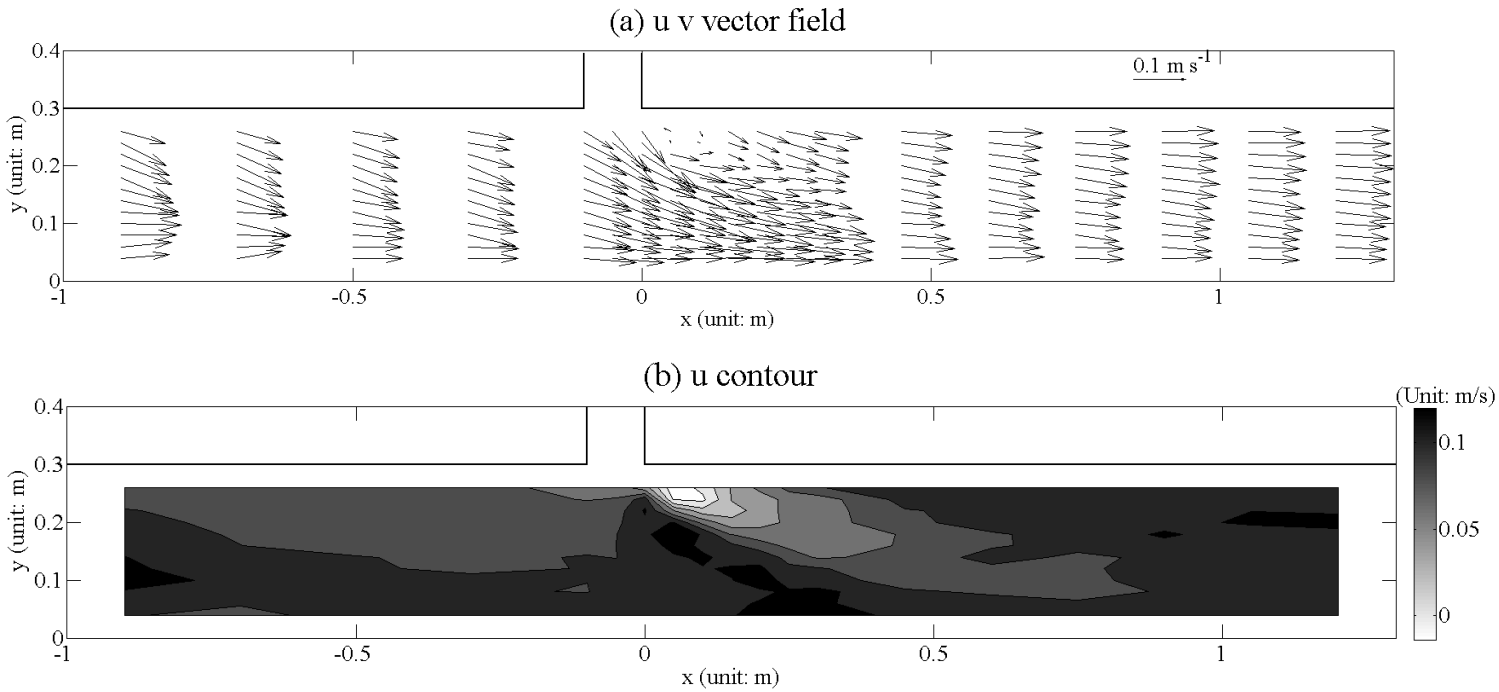

Figure A.6 (AR105) Streamwise velocity characteristics near surface

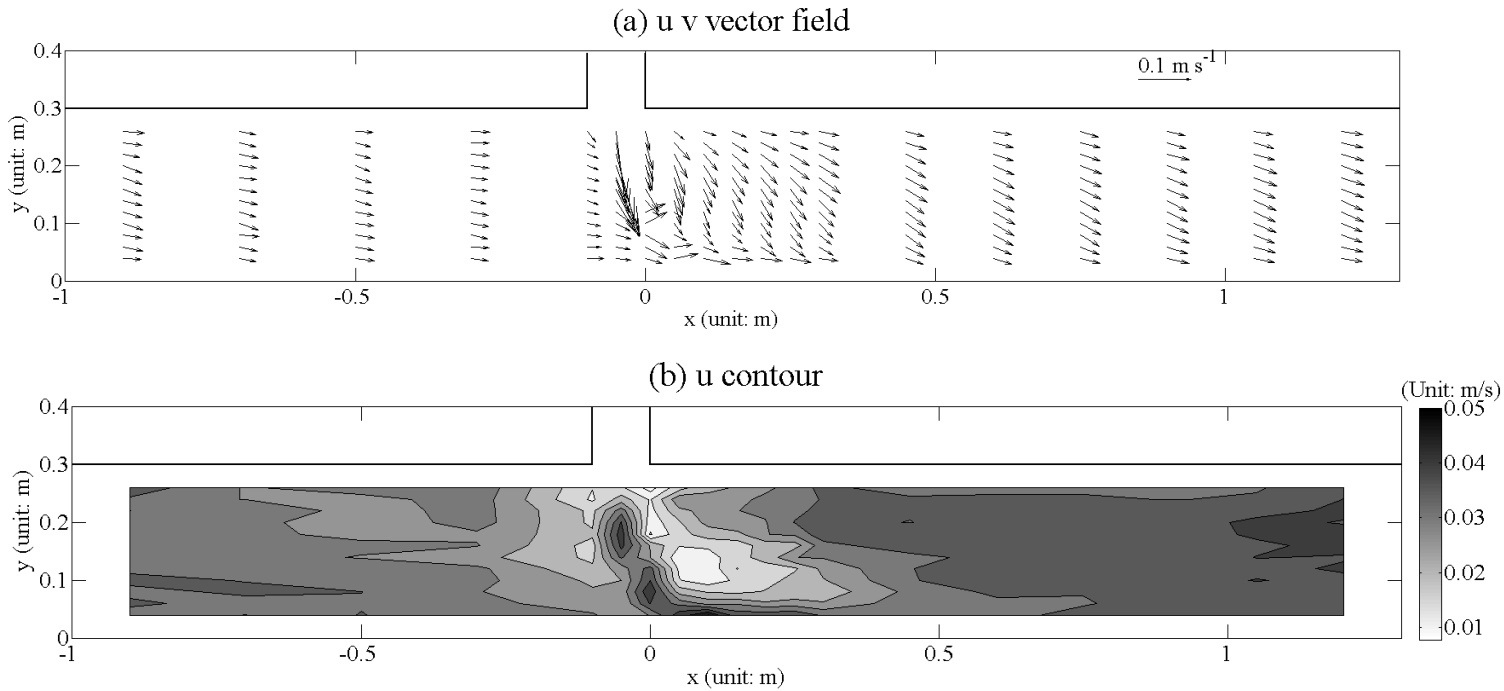

Figure A.7 (AR201) Streamwise velocity characteristics near surface

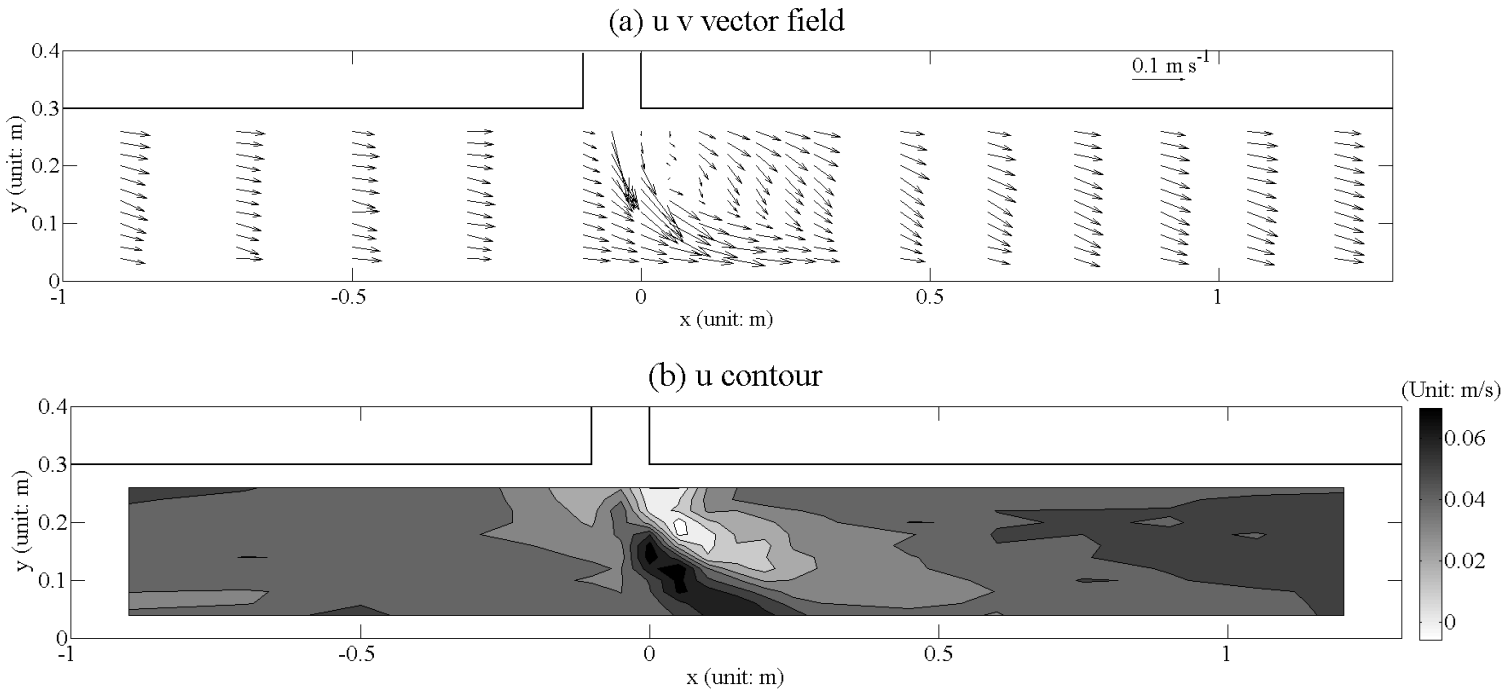

Figure A.8 (AR202) Streamwise velocity characteristics near surface

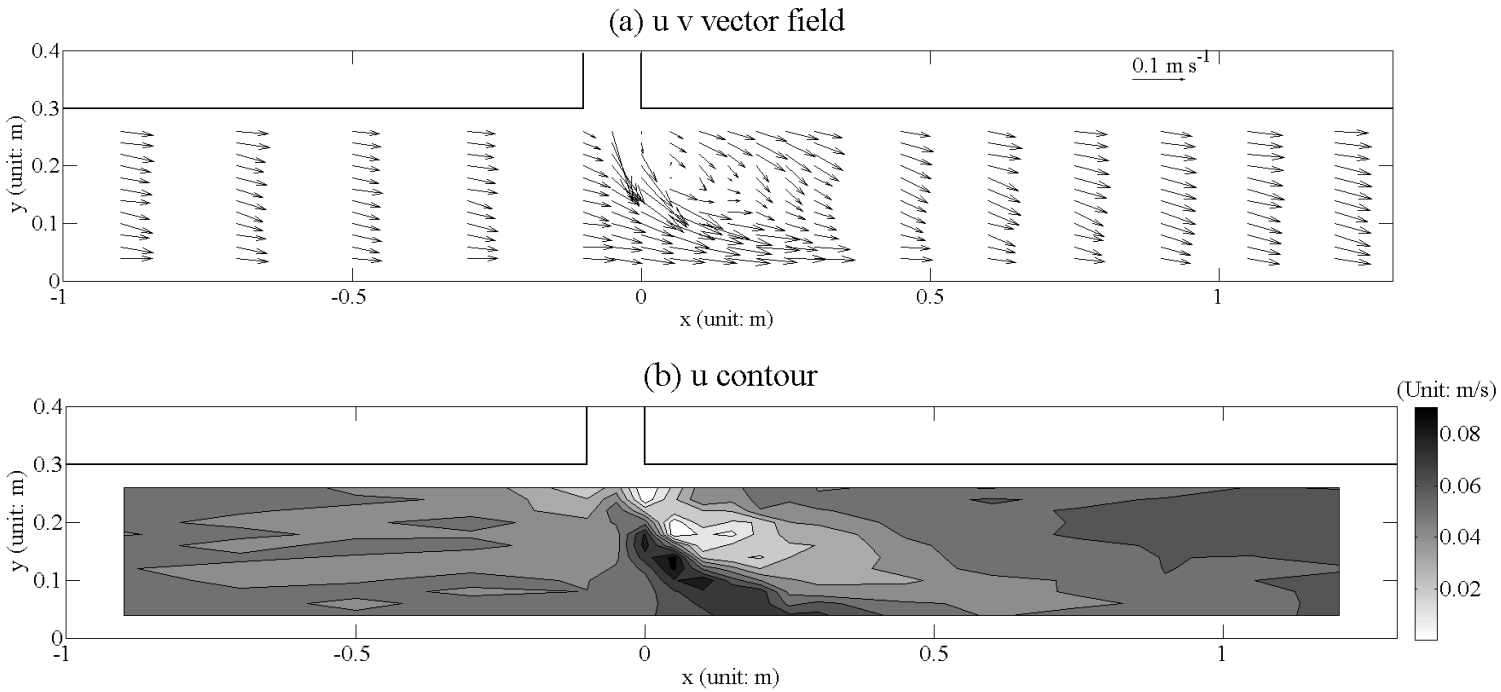

Figure A.9 (AR203) Streamwise velocity characteristics near surface

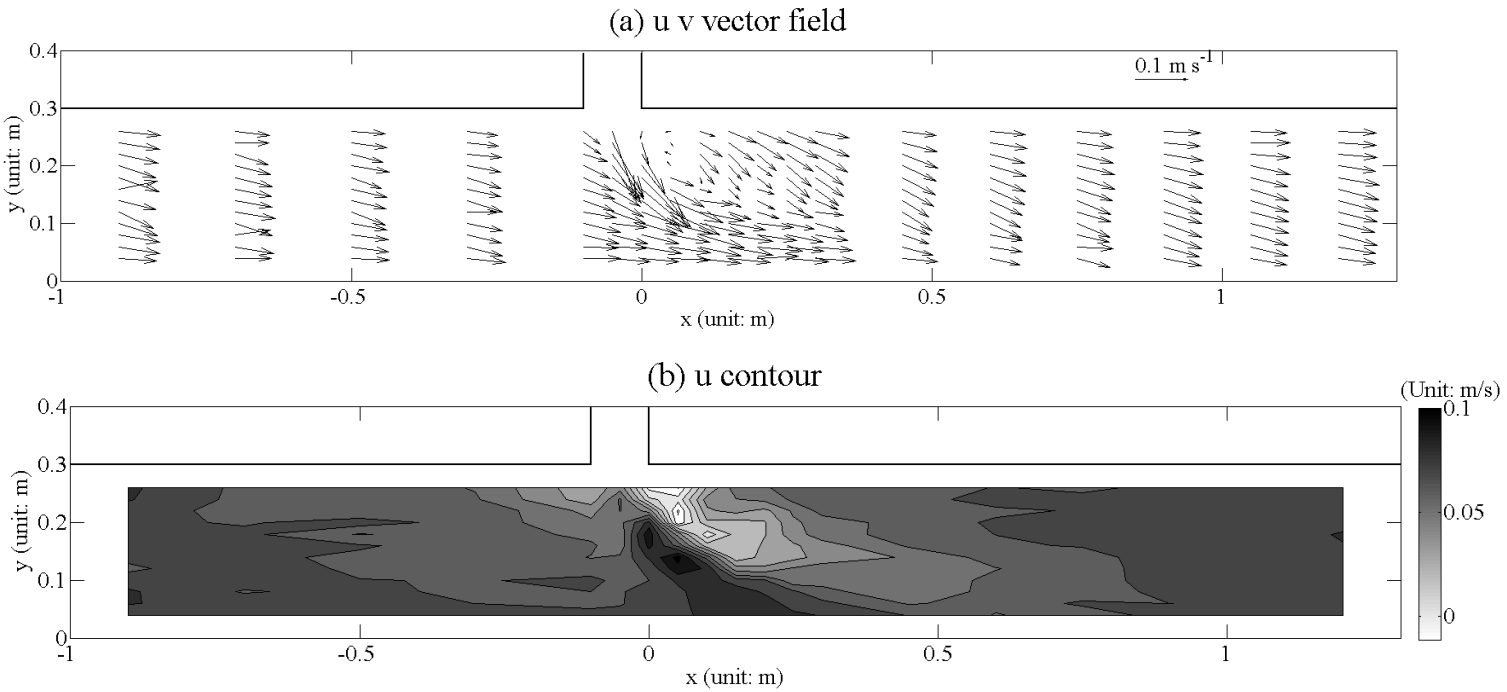

Figure A.10 (AR204) Streamwise velocity characteristics near surface

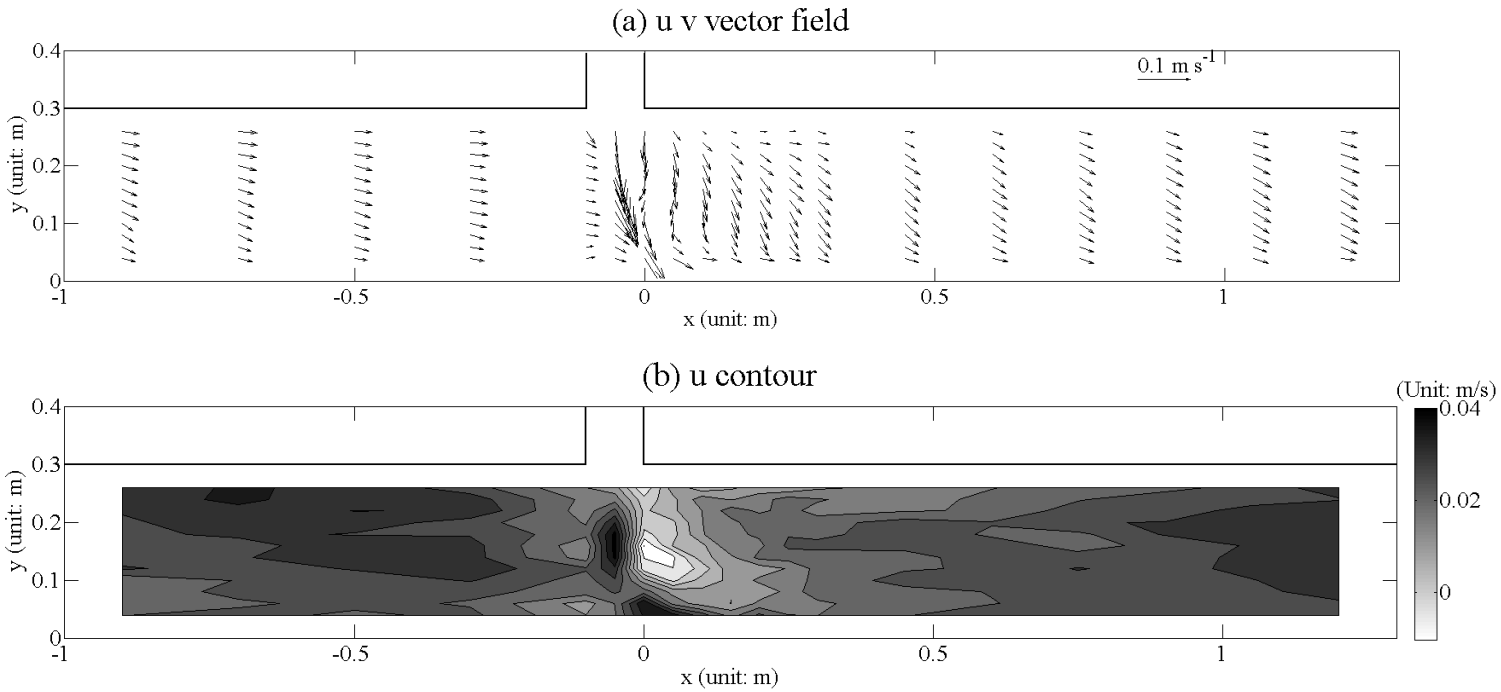

Figure A.11 (AR301) Streamwise velocity characteristics near surface

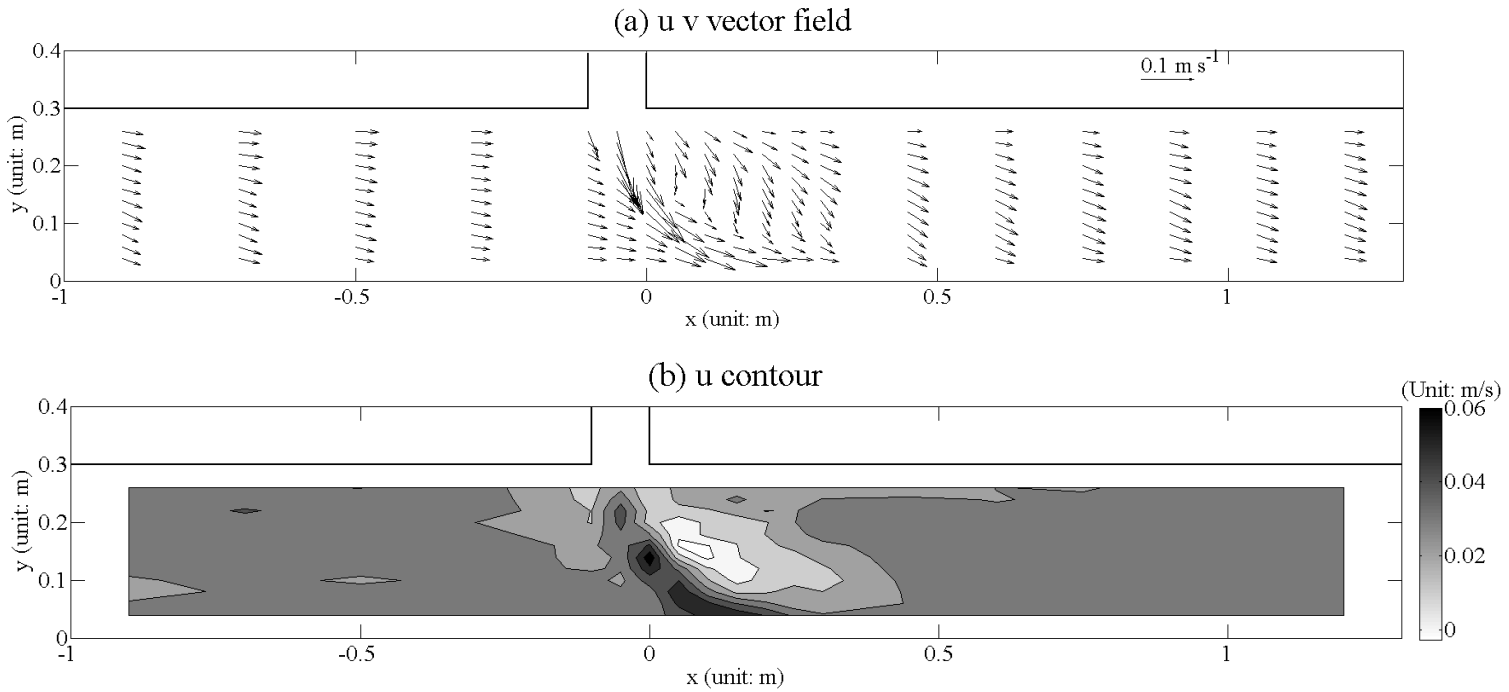

Figure A.12 (AR302) Streamwise velocity characteristics near surface

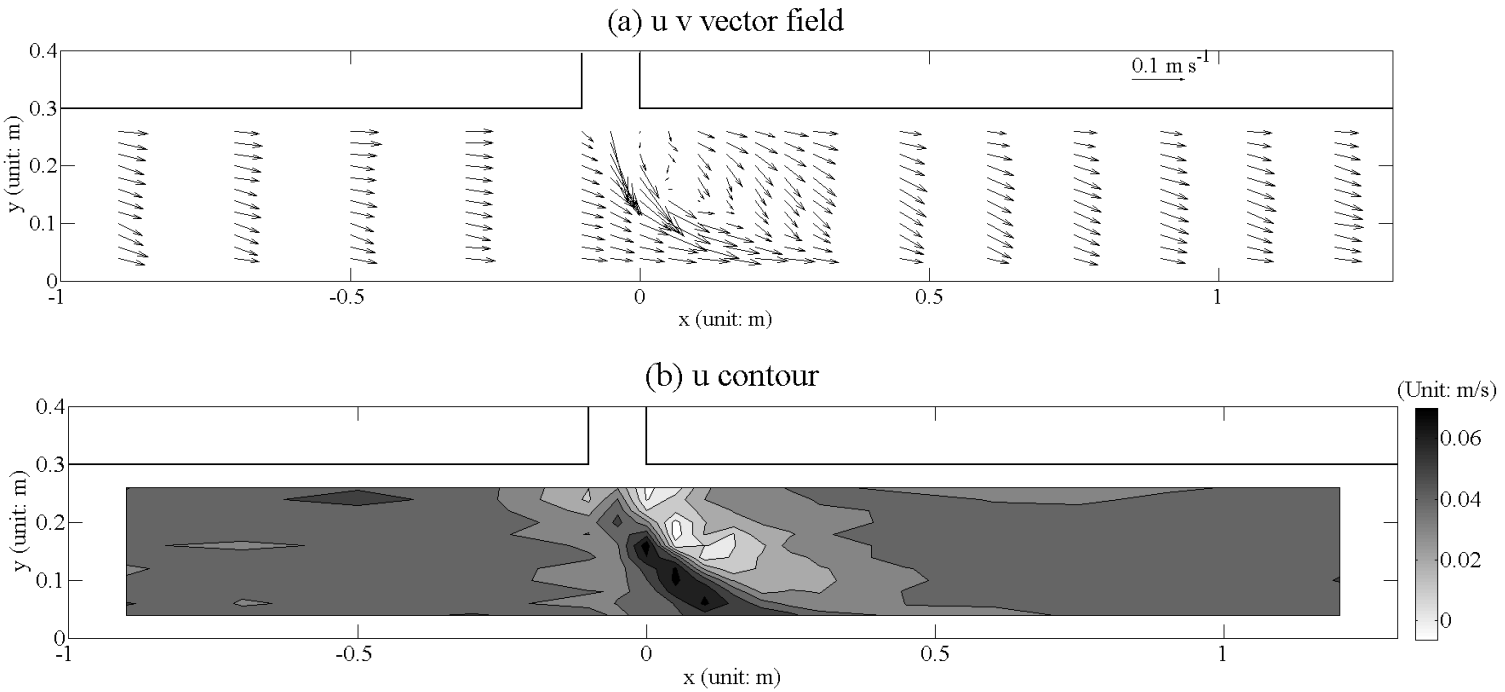

Figure A.13 (AR303) Streamwise velocity characteristics near surface

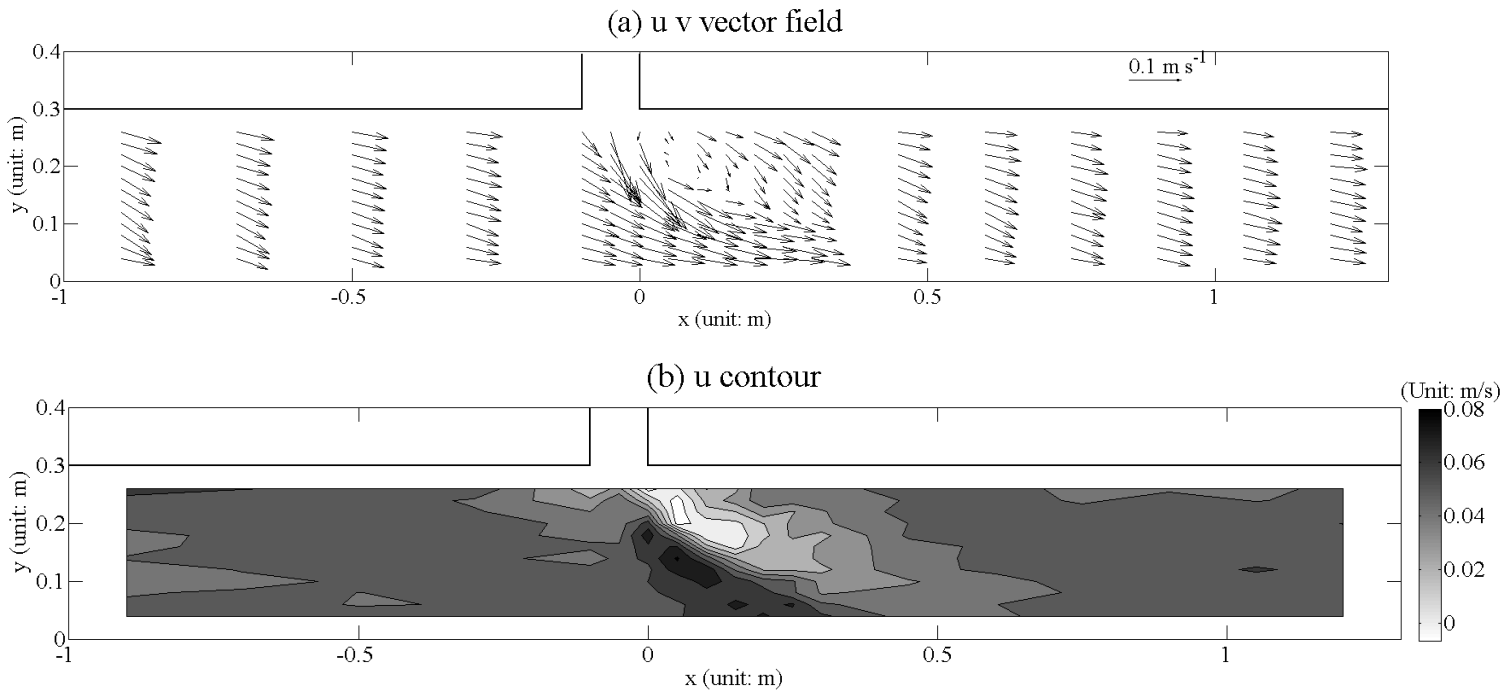

Figure A.14 (AR304) Streamwise velocity characteristics near surface

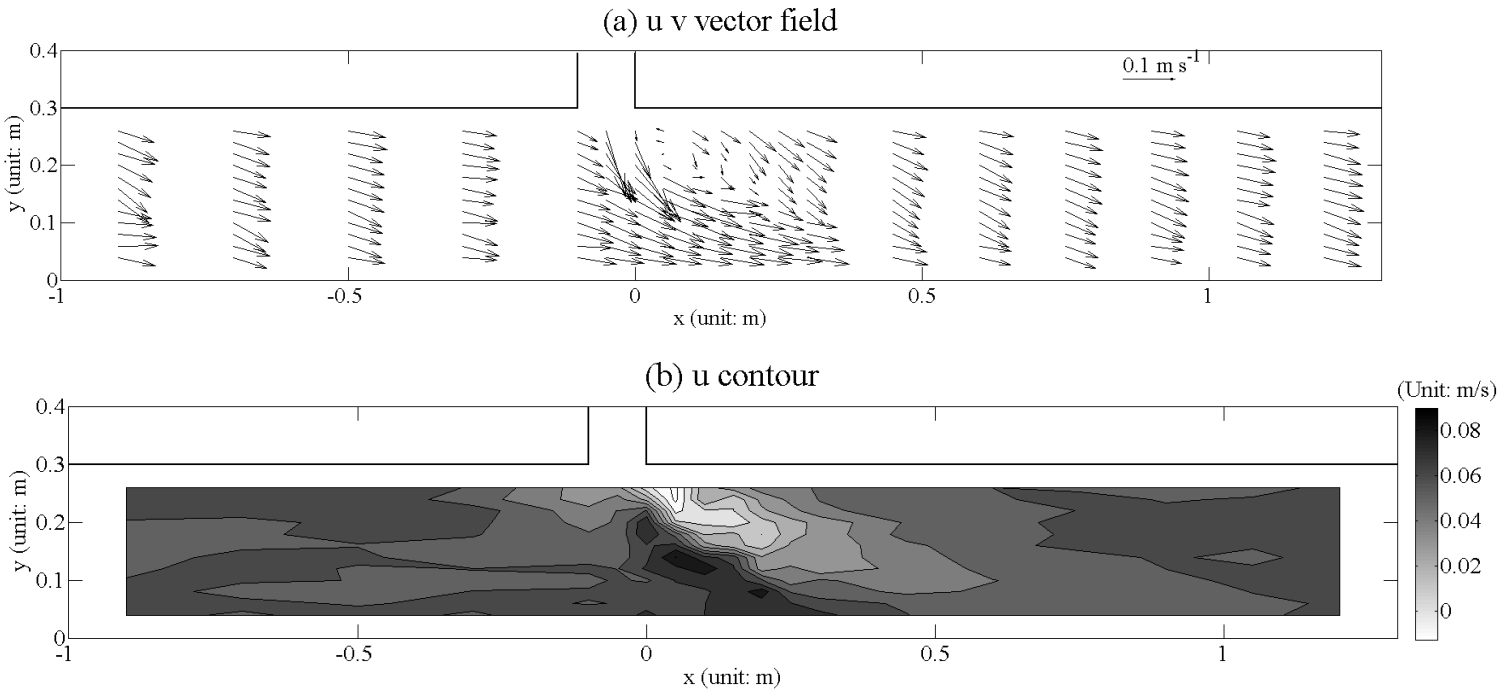

Figure A.15 (AR305) Streamwise velocity characteristics near surface

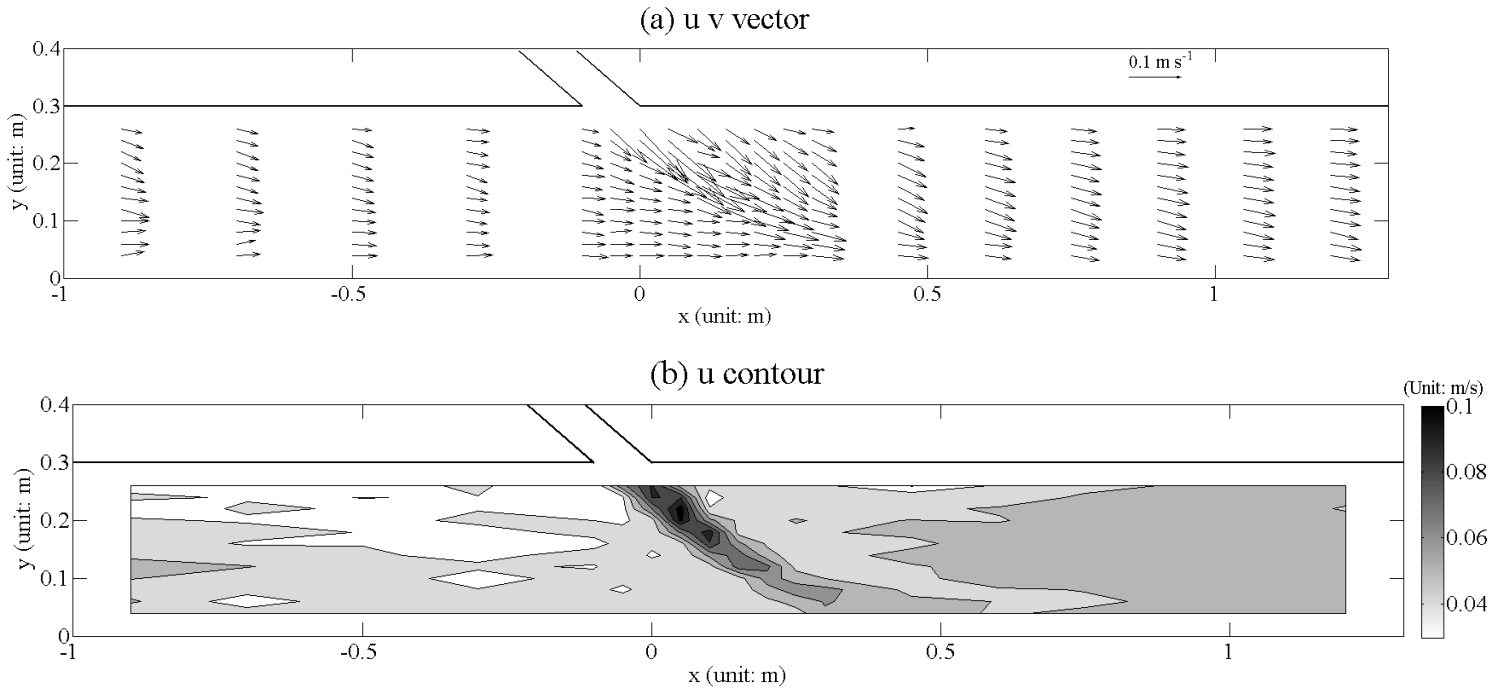

Figure A.16 (AM101) Streamwise velocity characteristics near surface

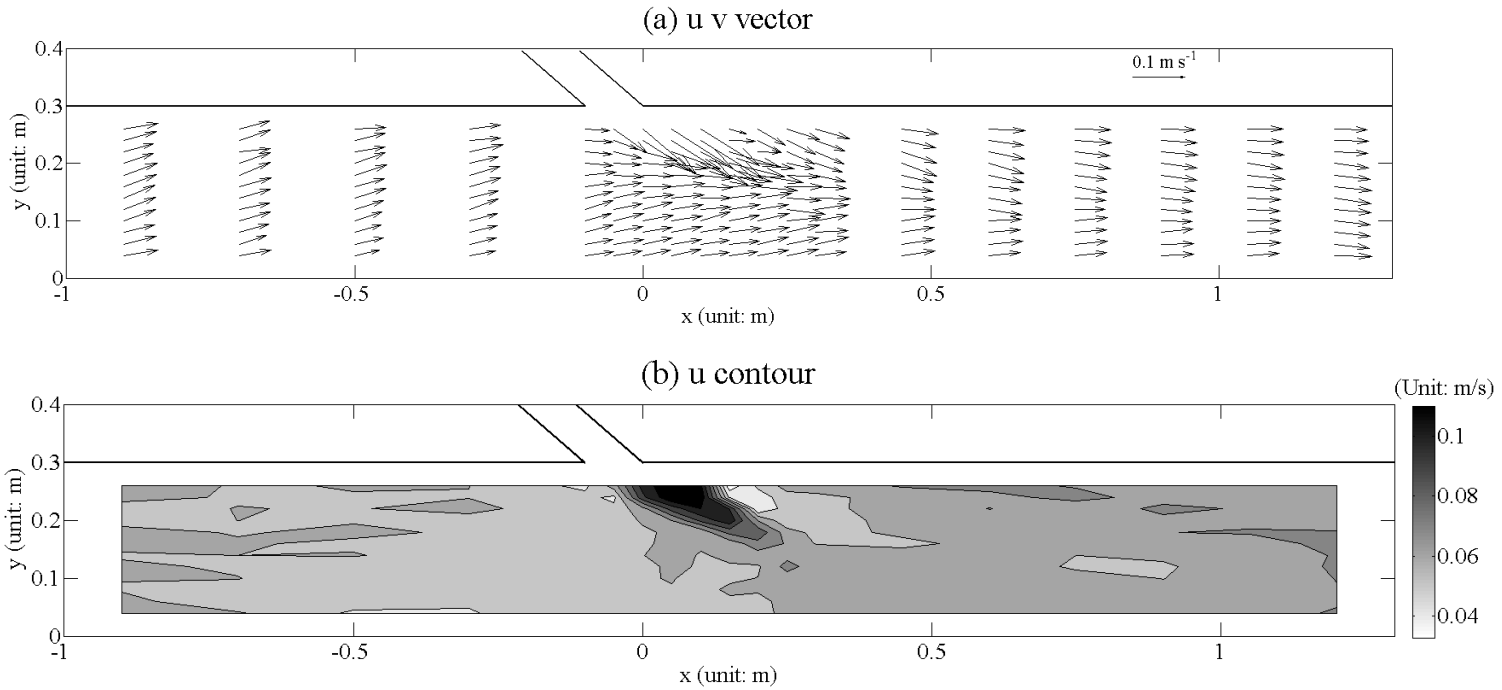

Figure A.17 (AM102) Streamwise velocity characteristics near surface

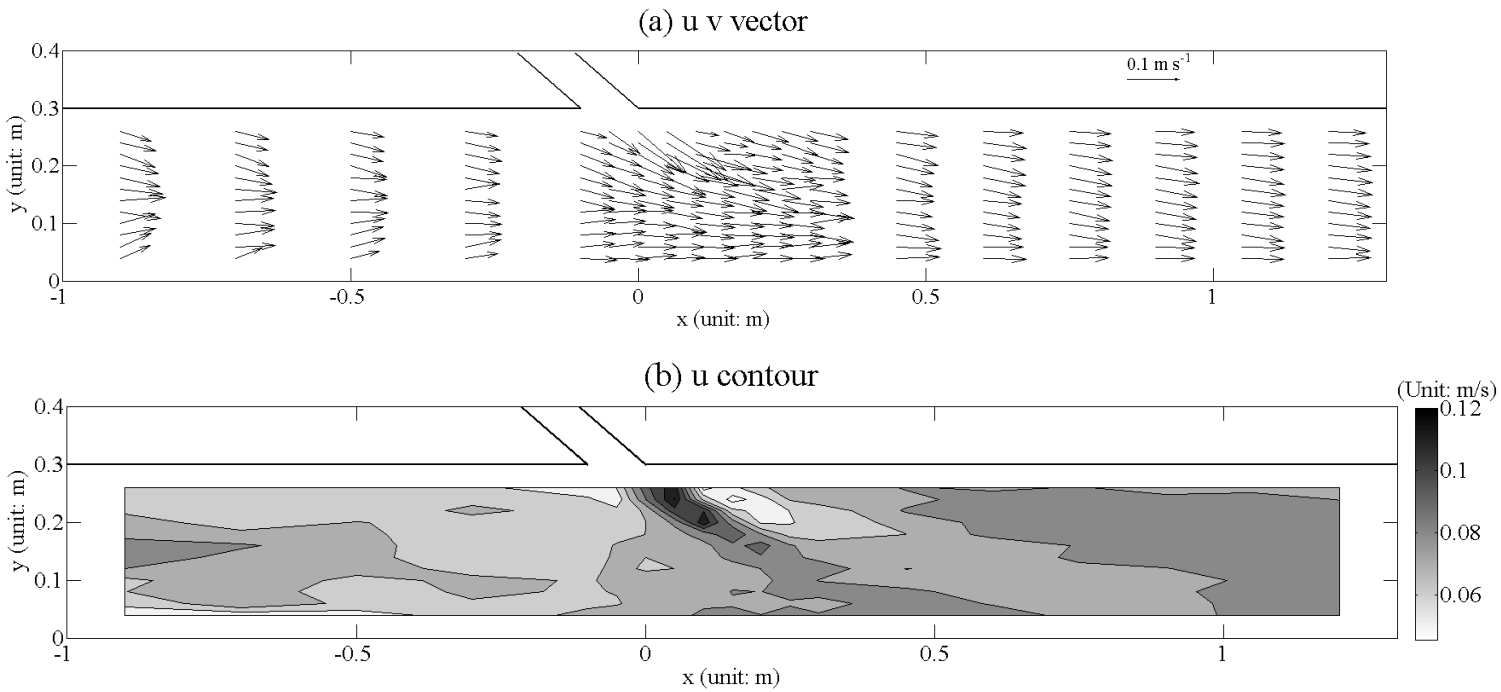

Figure A.18 (AM103) Streamwise velocity characteristics near surface

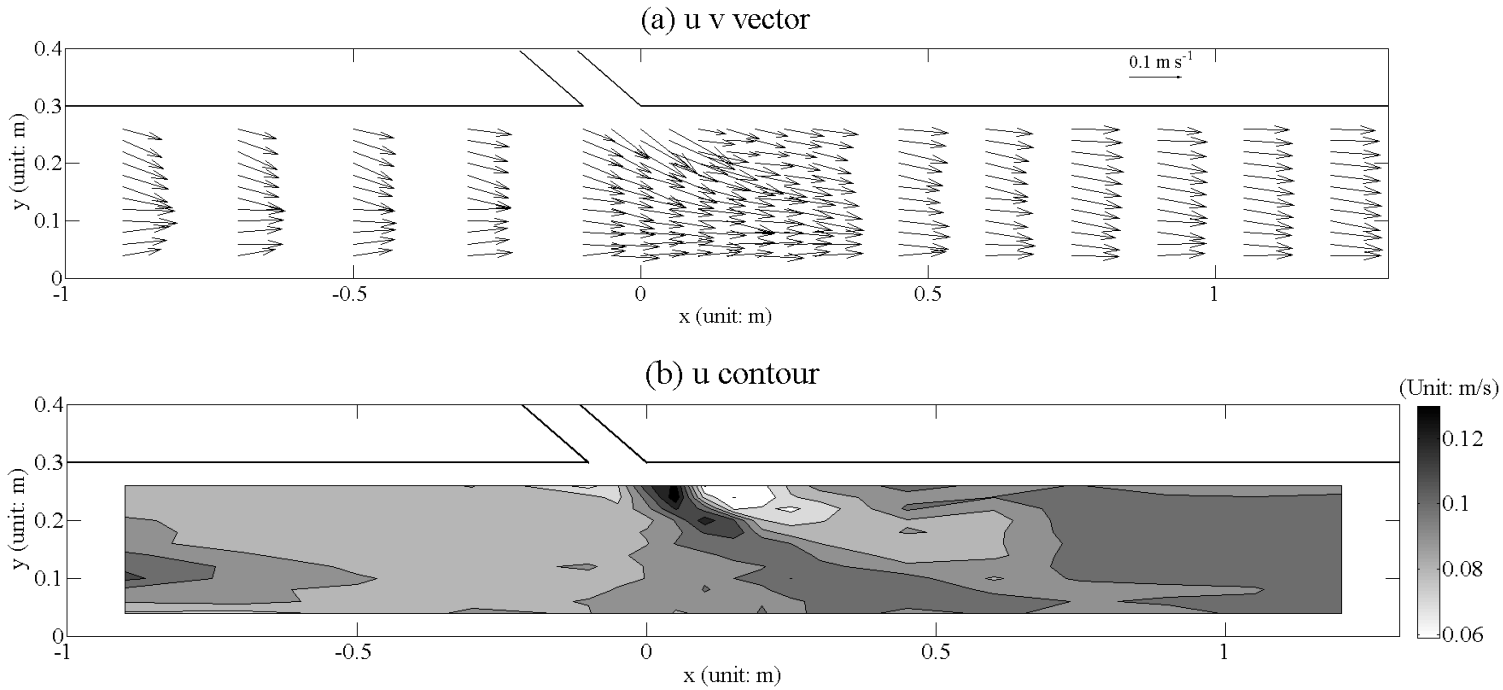

Figure A.19 (AM104) Streamwise velocity characteristics near surface

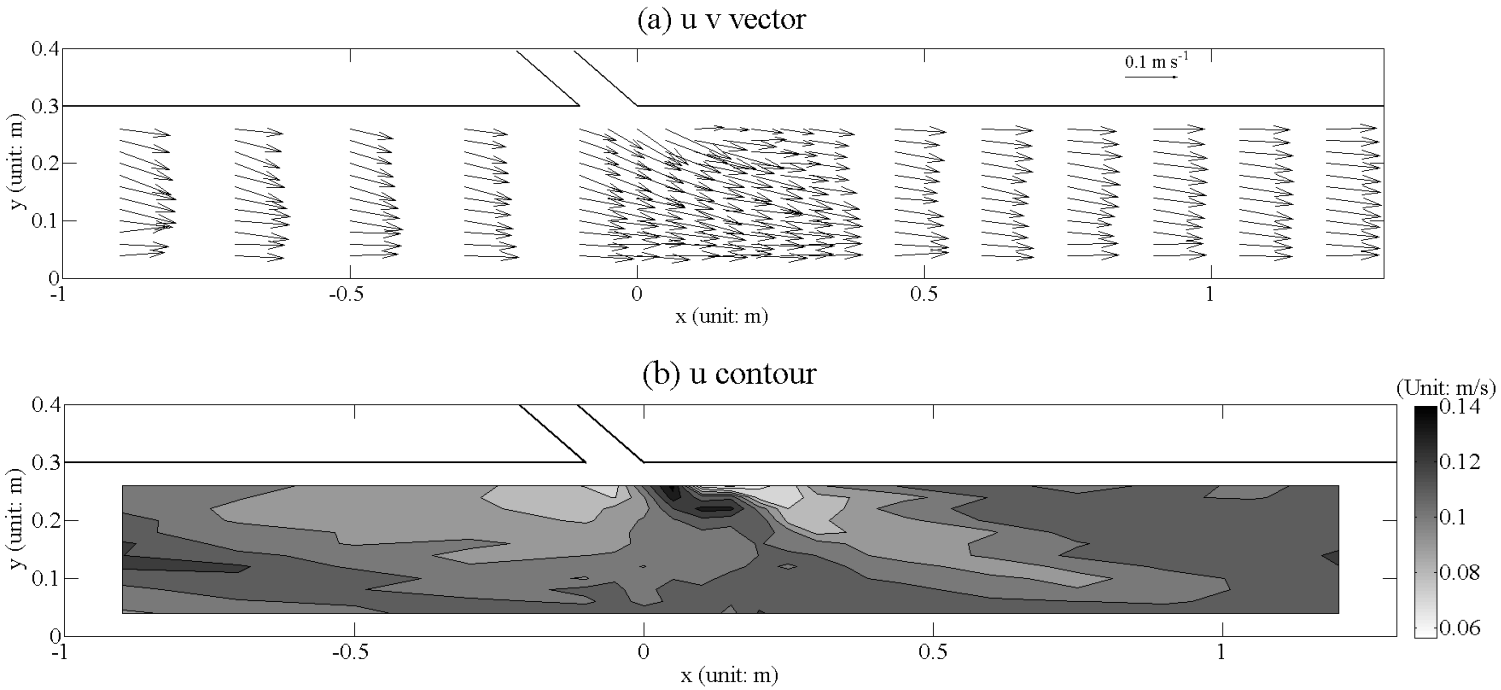

Figure A.20 (AM105) Streamwise velocity characteristics near surface

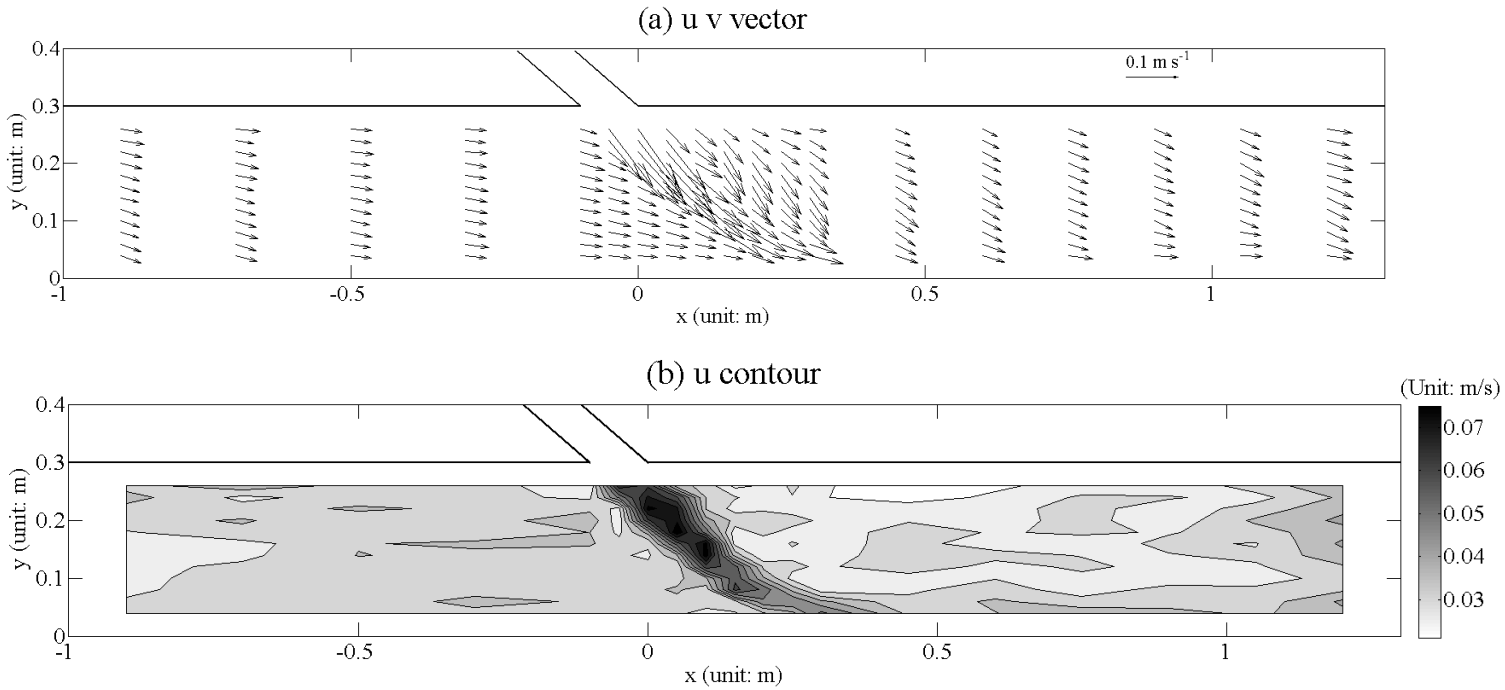

Figure A.21 (AM201) Streamwise velocity characteristics near surface

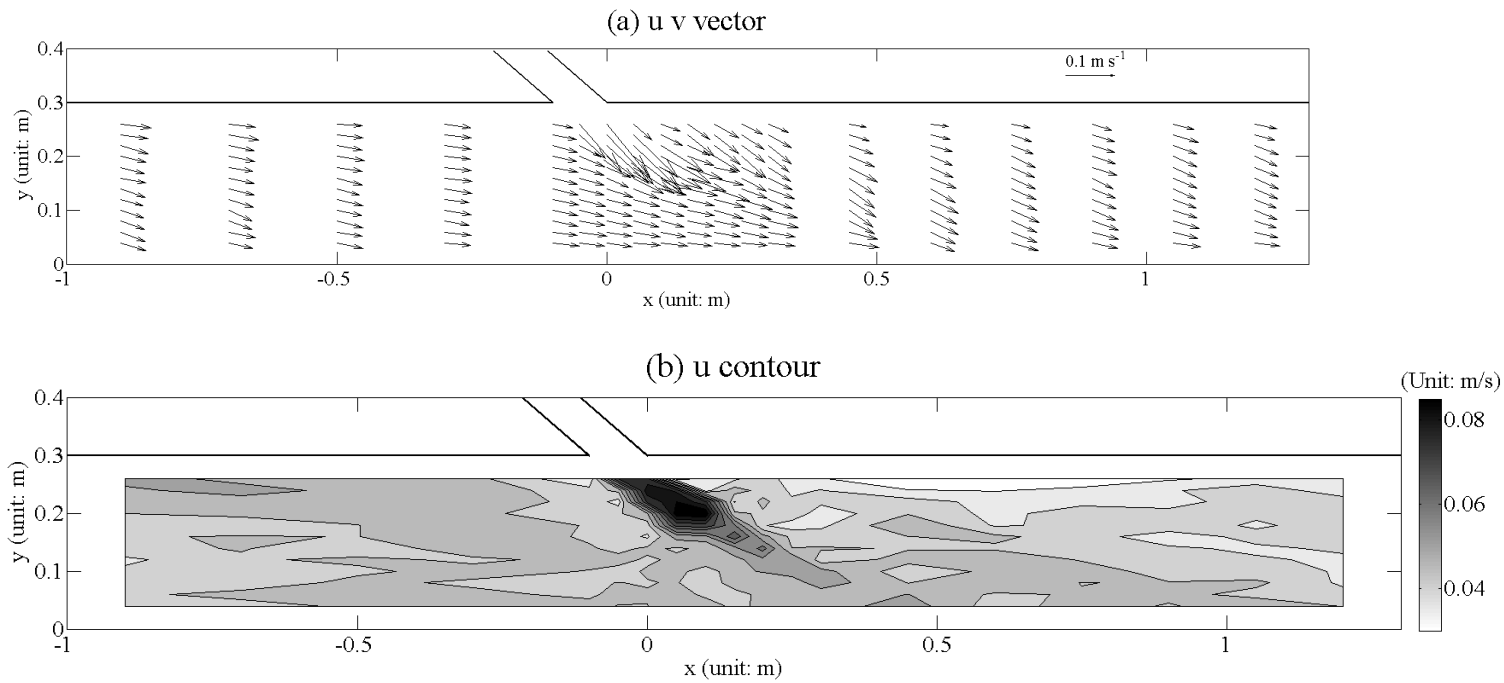

Figure A.22 (AM202) Streamwise velocity characteristics near surface

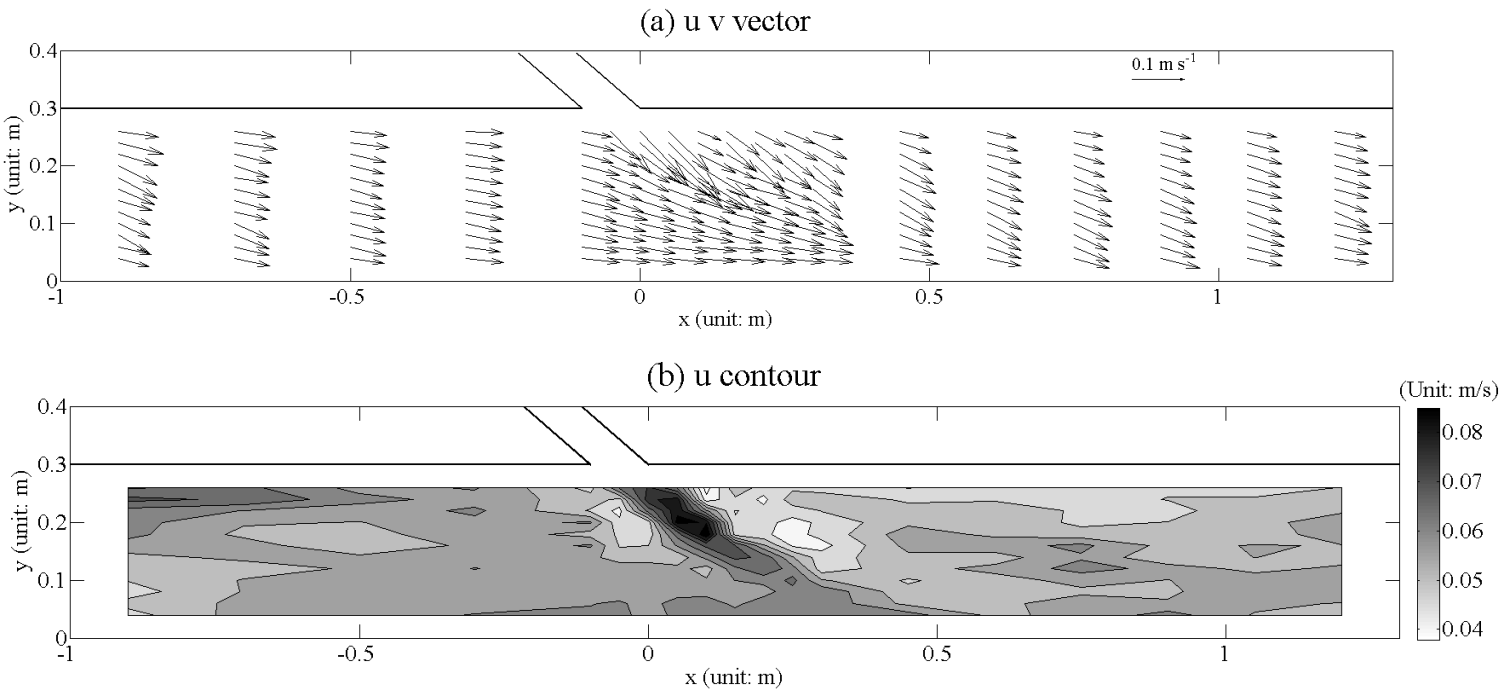

Figure A.23 (AM203) Streamwise velocity characteristics near surface

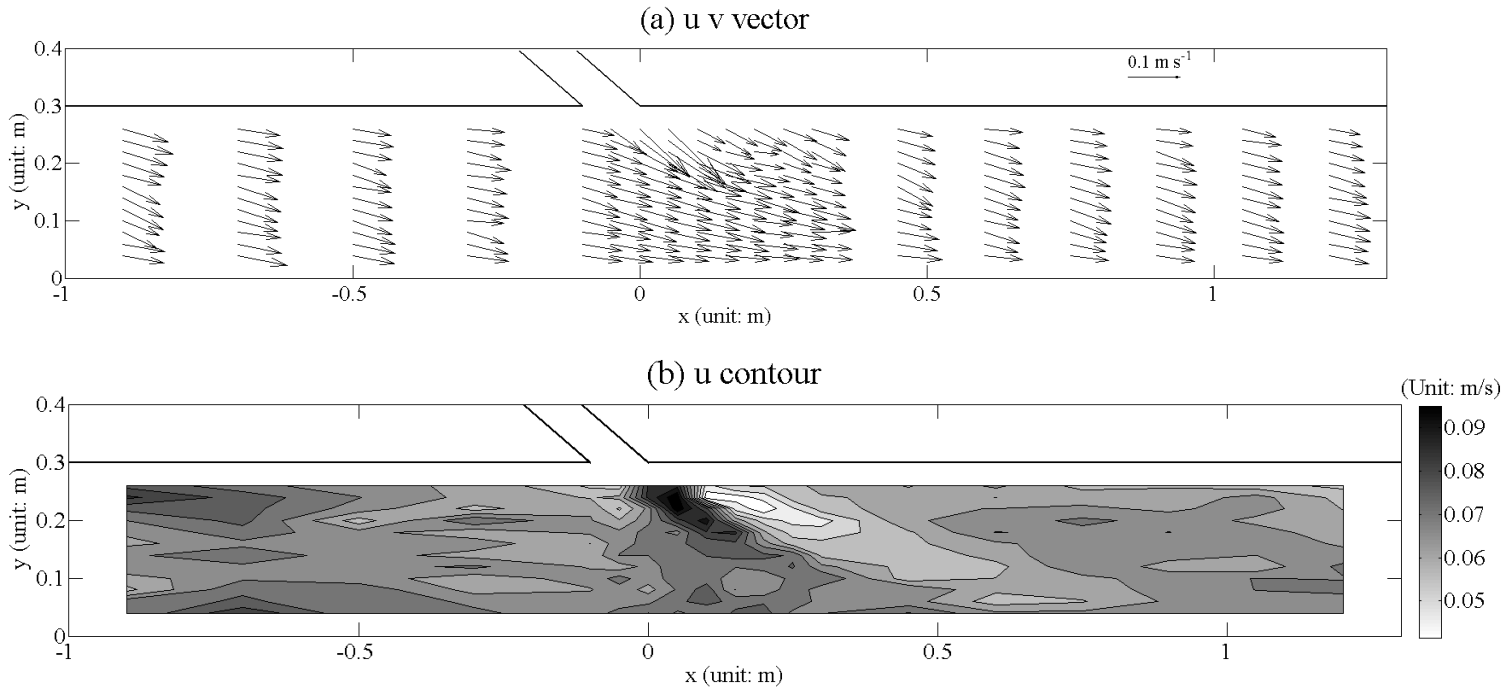

Figure A.24 (AM204) Streamwise velocity characteristics near surface

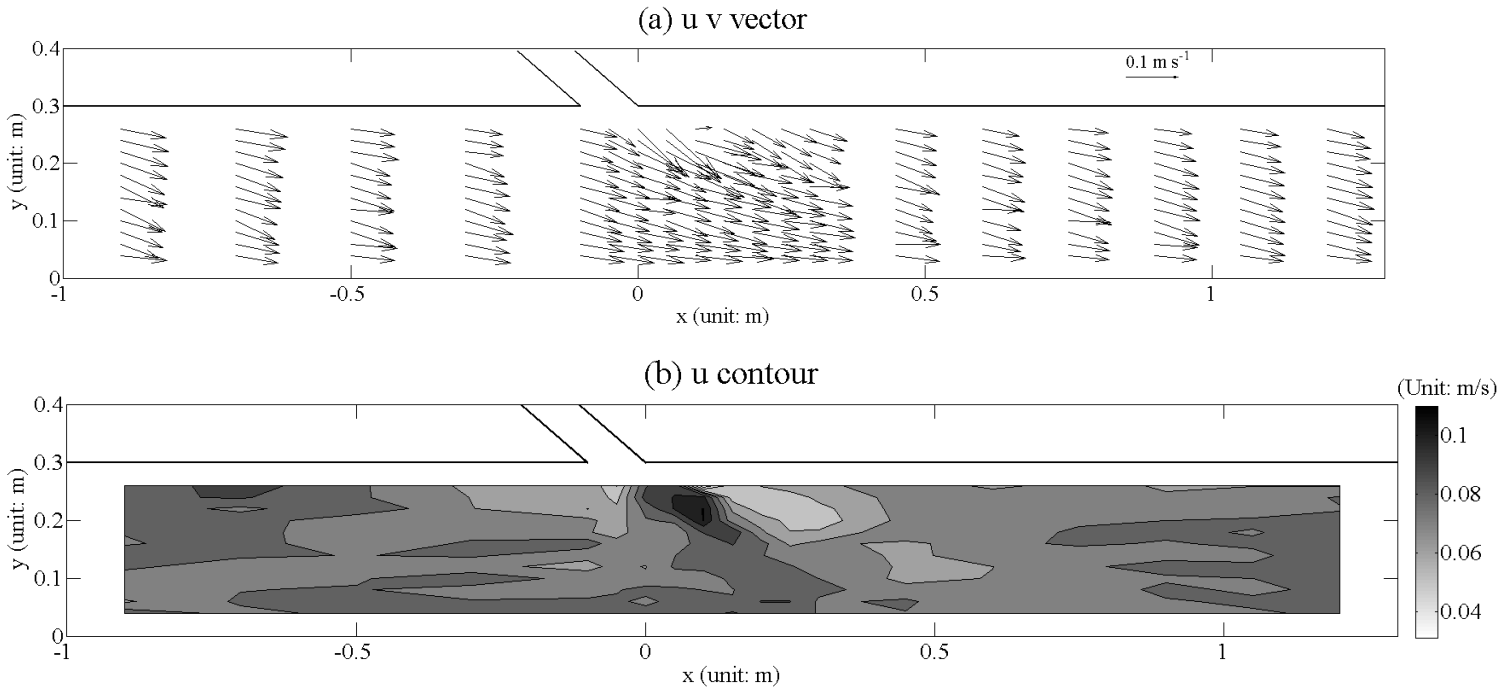

Figure A.25 (AM205) Streamwise velocity characteristics near surface

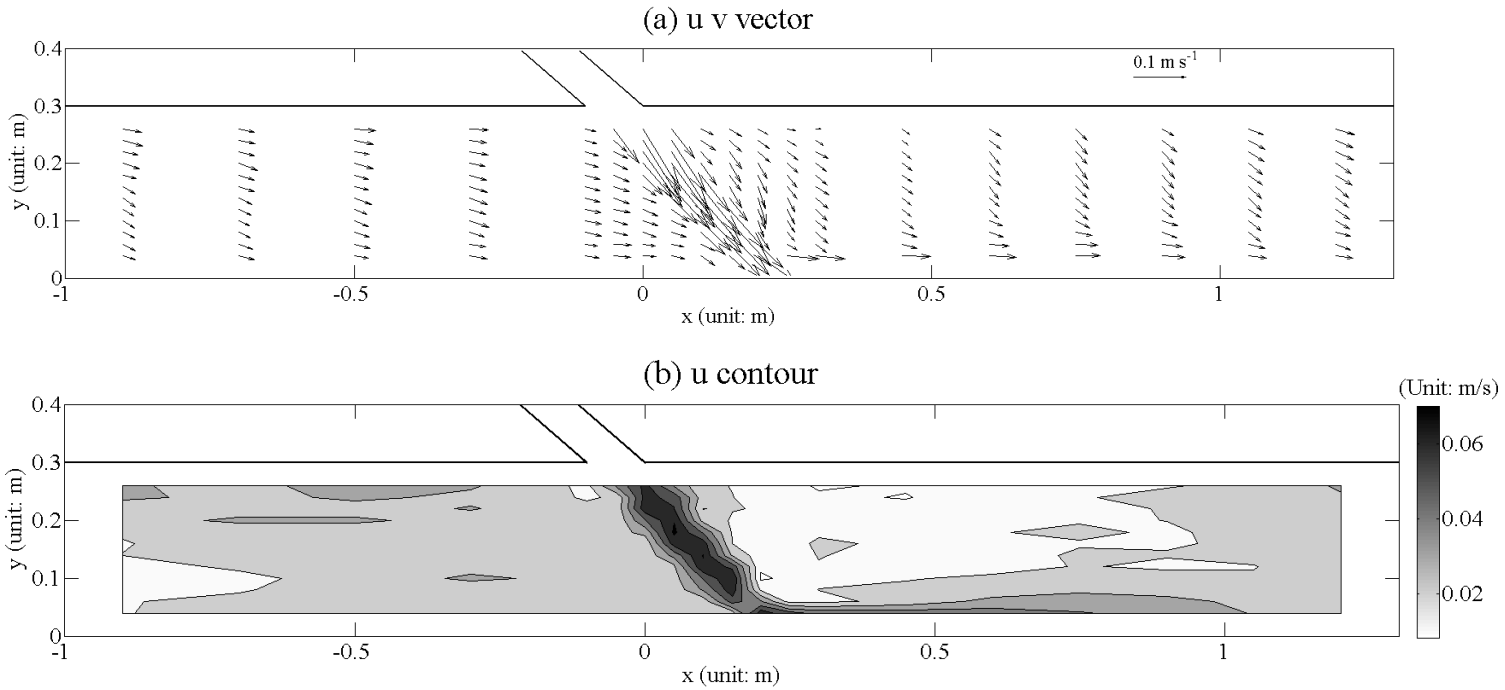

Figure A.26 (AM301) Streamwise velocity characteristics near surface

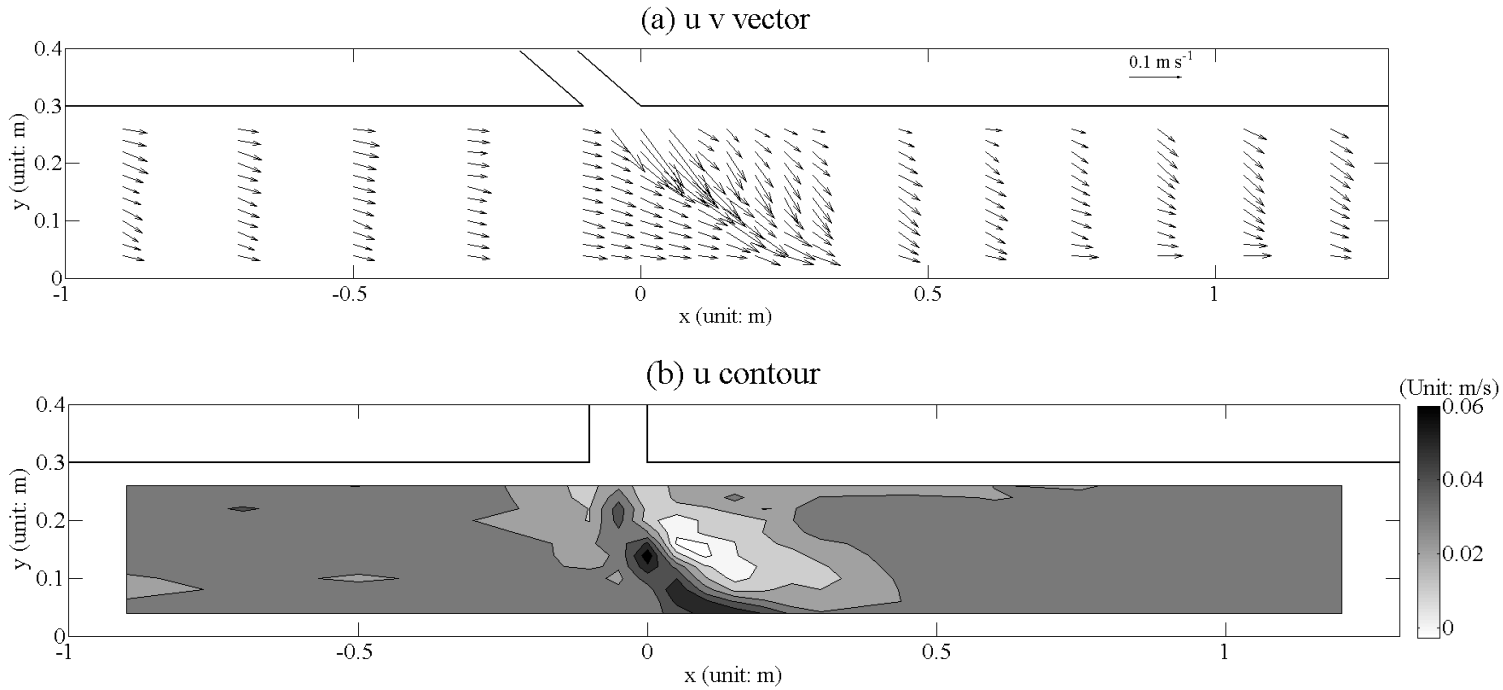

Figure A.27 (AM302) Streamwise velocity characteristics near surface

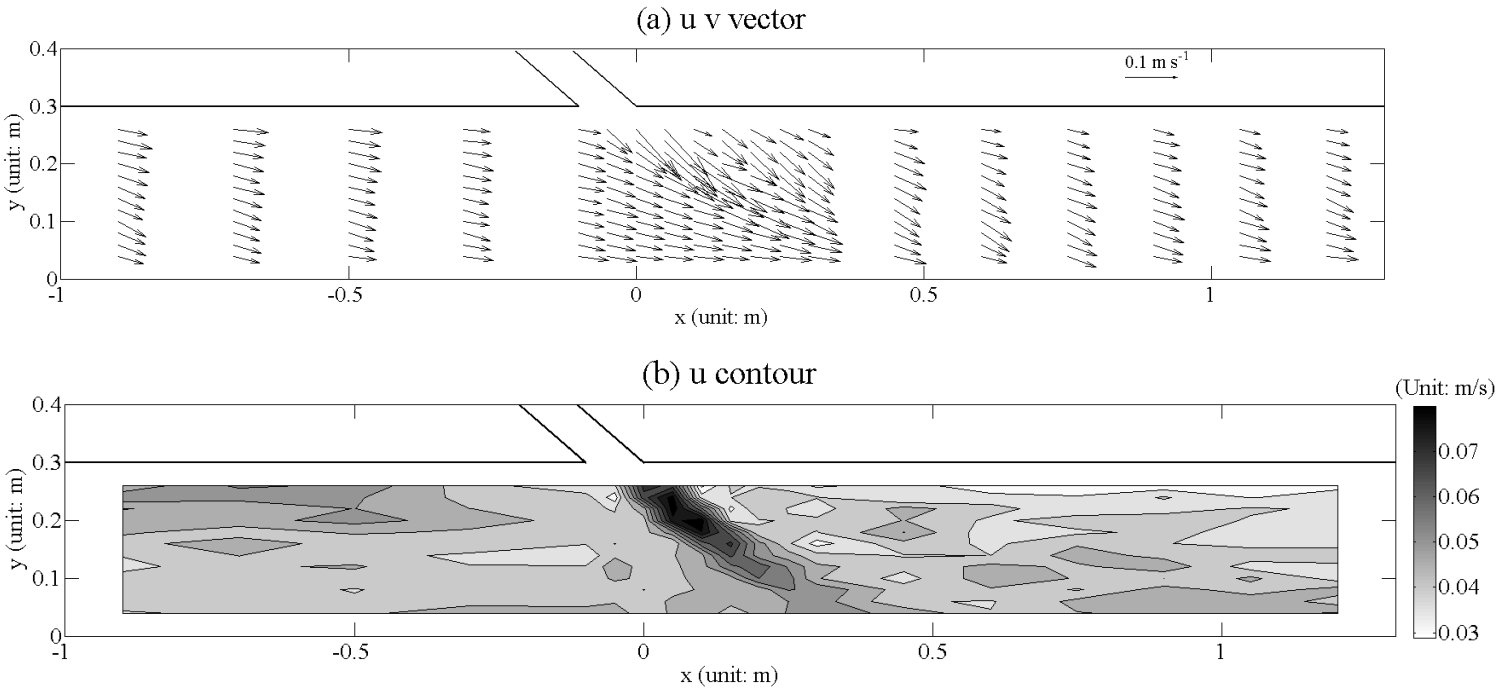

Figure A.28 (AM303) Streamwise velocity characteristics near surface

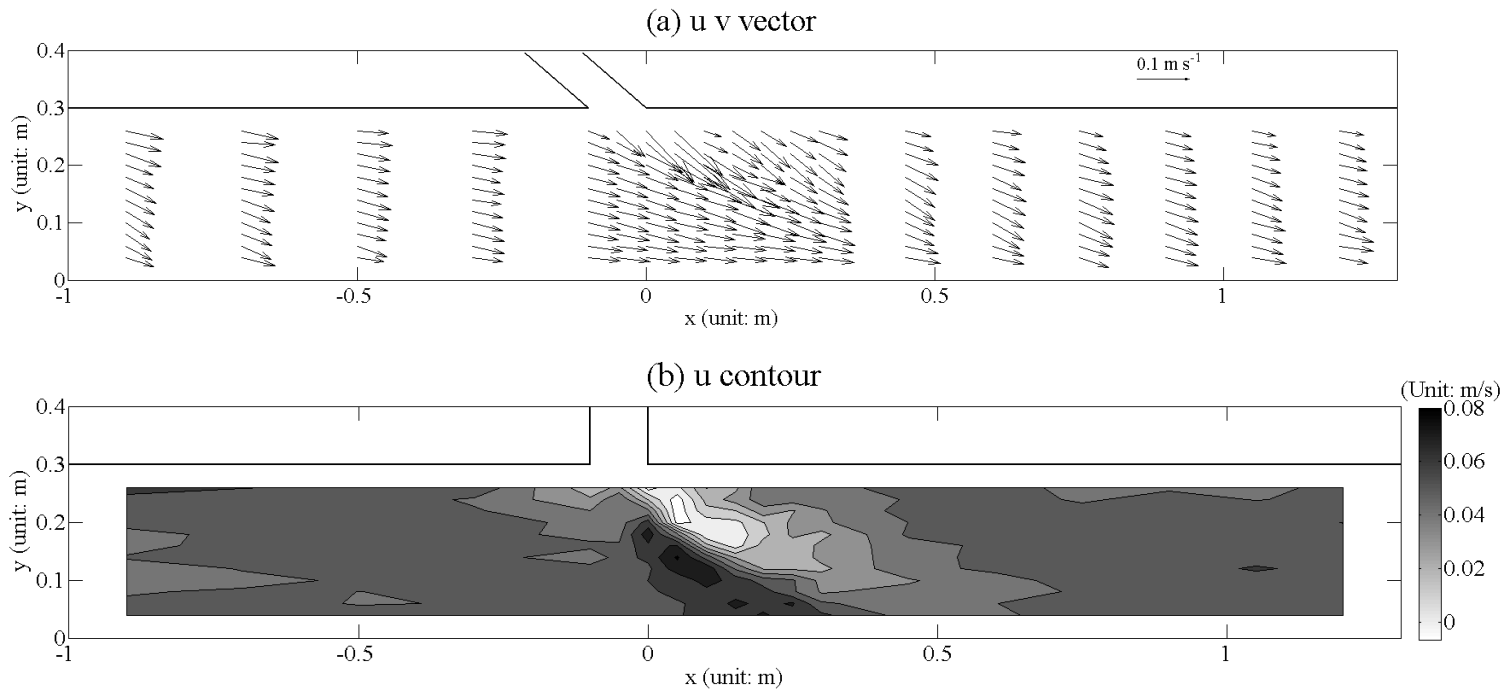

Figure A.29 (AM304) Streamwise velocity characteristics near surface

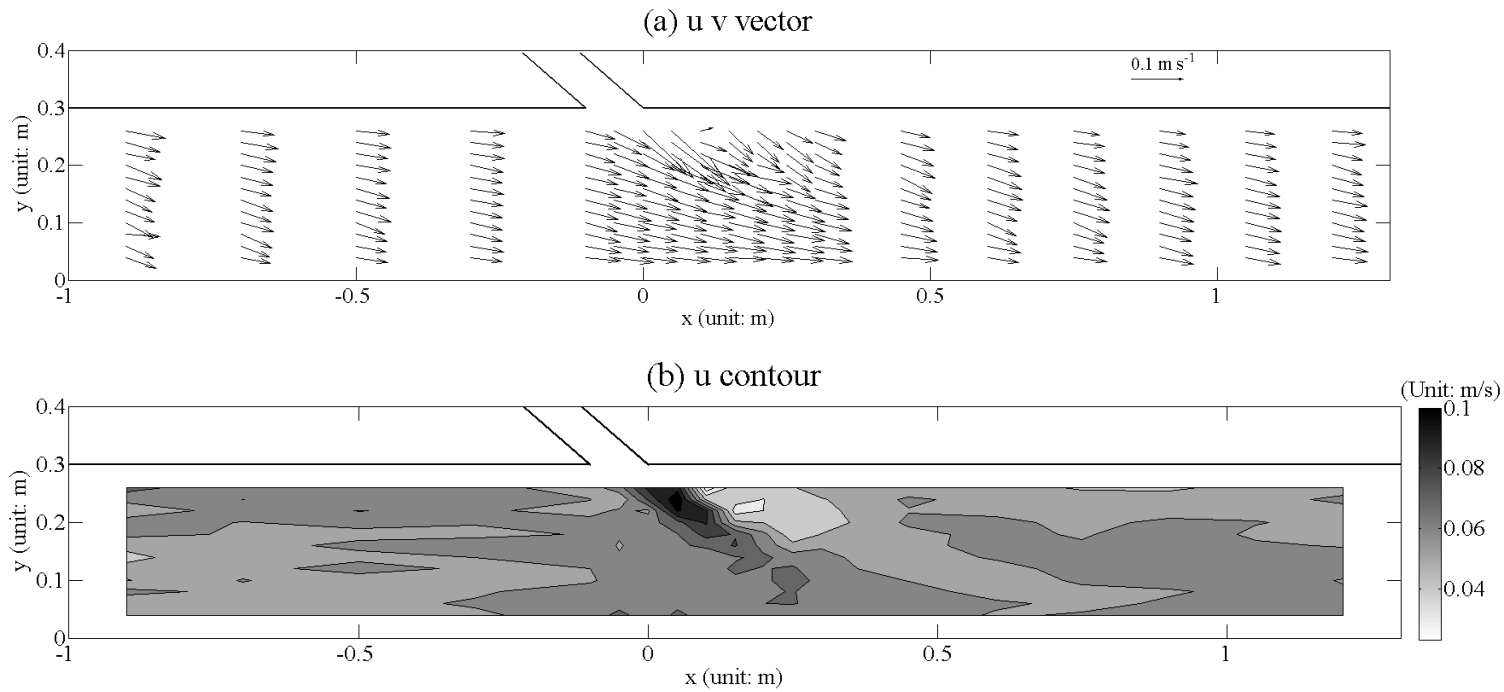

Figure A.30 (AM305) Streamwise velocity characteristics near surface

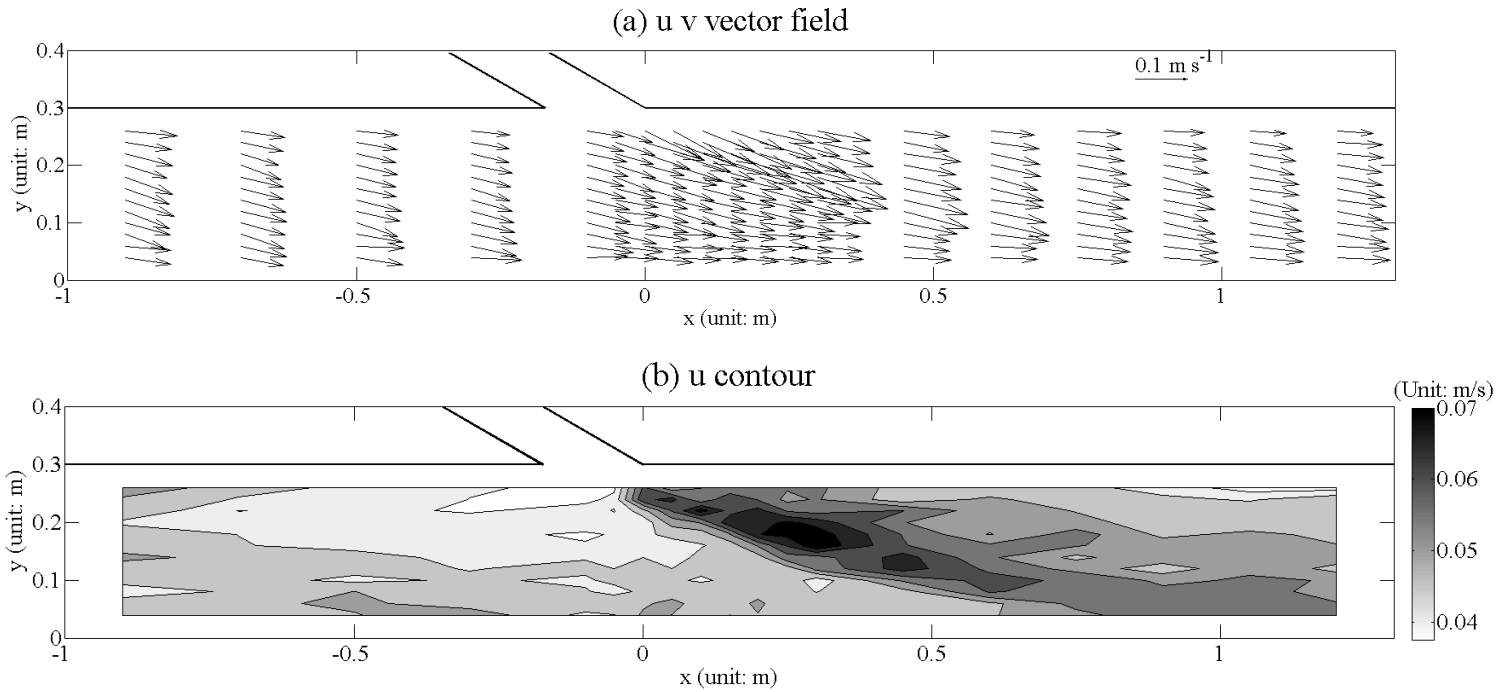

Figure A.31 (AS101) Streamwise velocity characteristics near surface

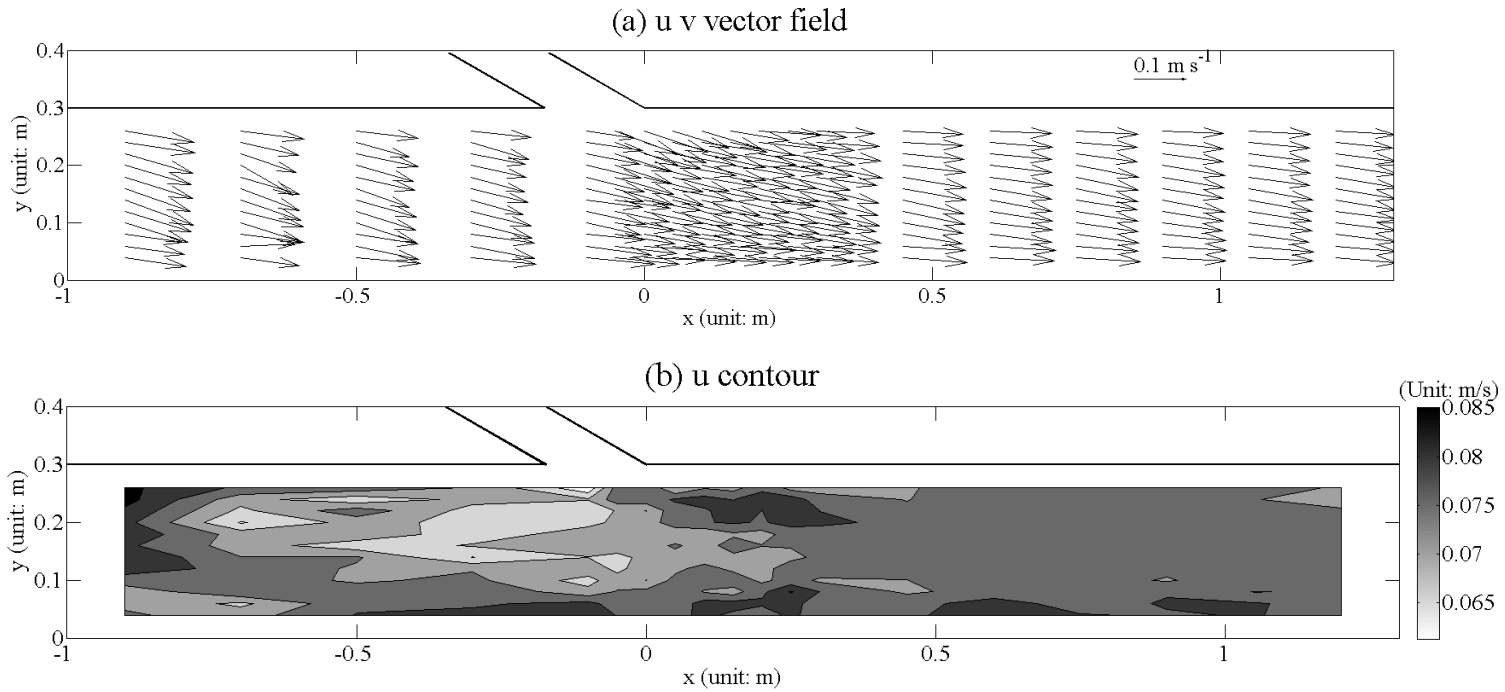

Figure A.32 (AS103) Streamwise velocity characteristics near surface

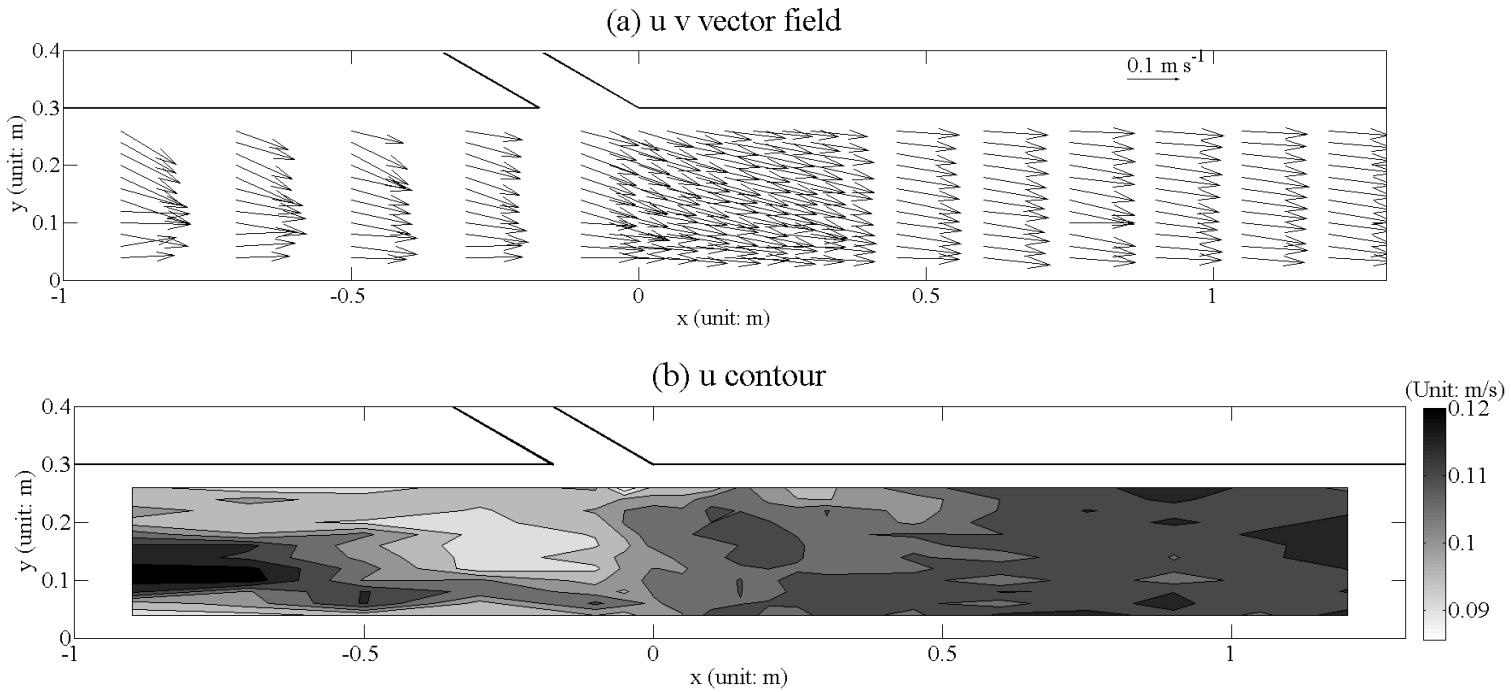

Figure A.33 (AS105) Streamwise velocity characteristics near surface

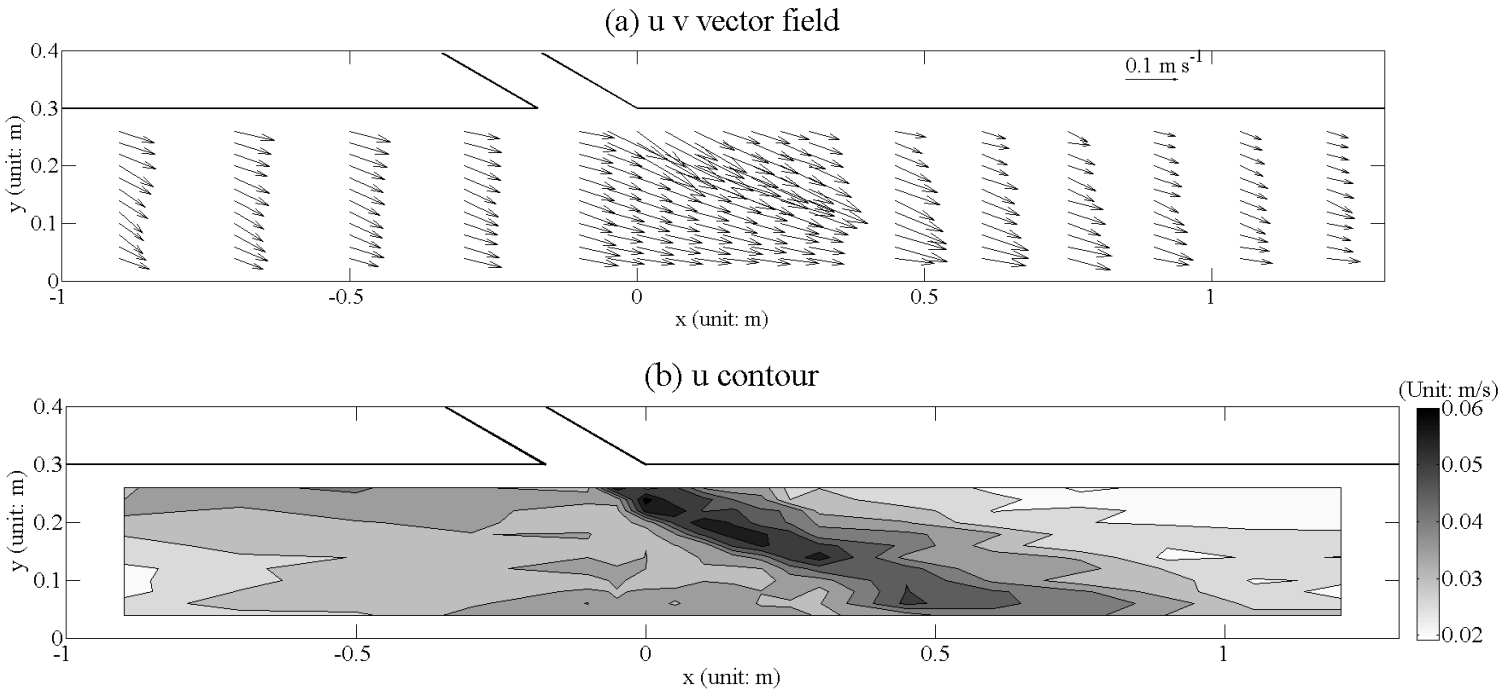

Figure A.34 (AS201) Streamwise velocity characteristics near surface

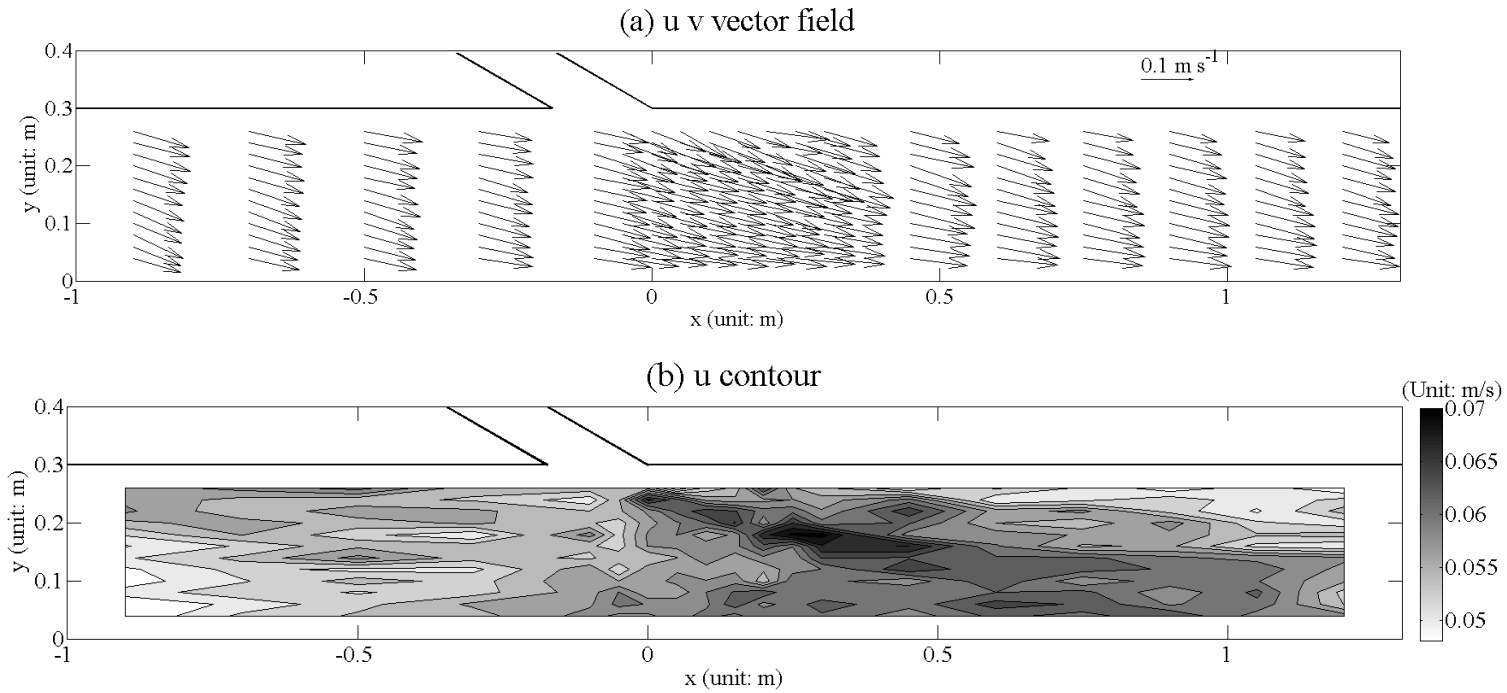

Figure A.35 (AS203) Streamwise velocity characteristics near surface

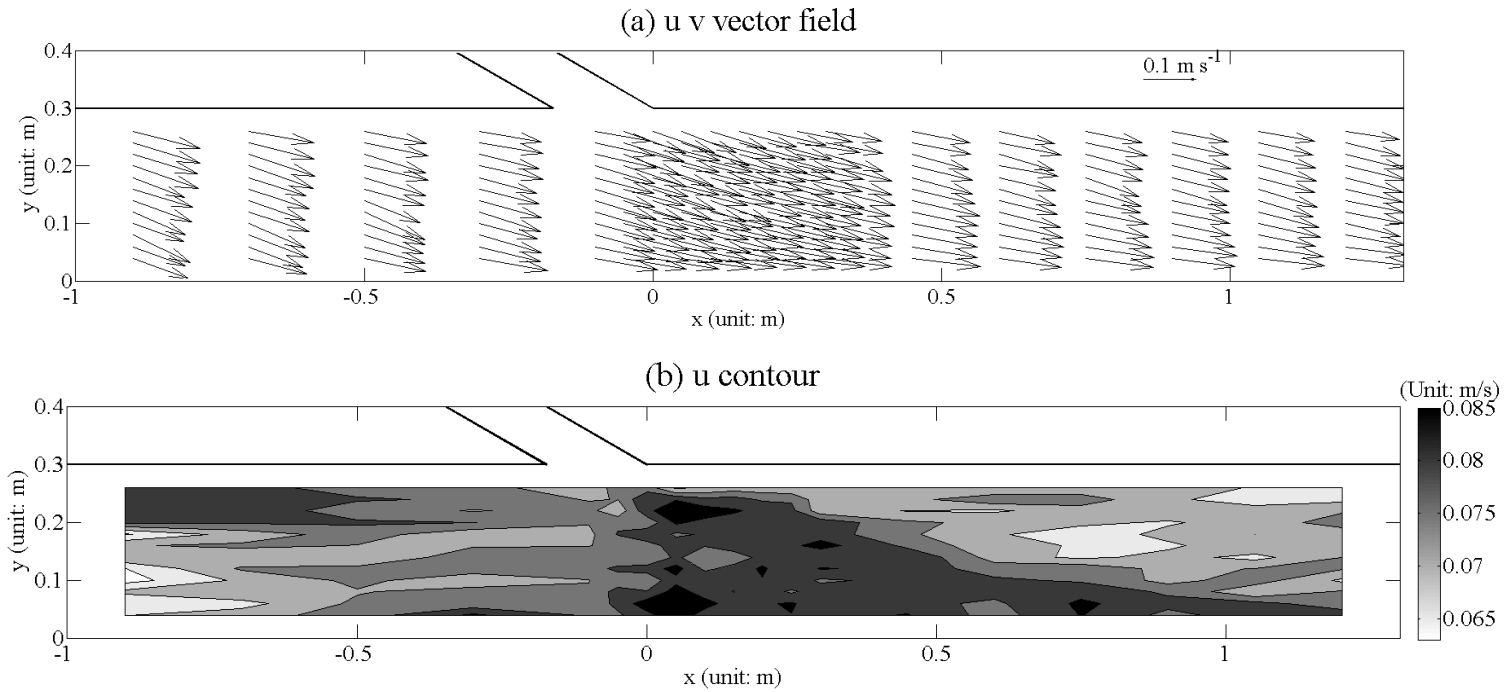

Figure A.36 (AS205) Streamwise velocity characteristics near surface

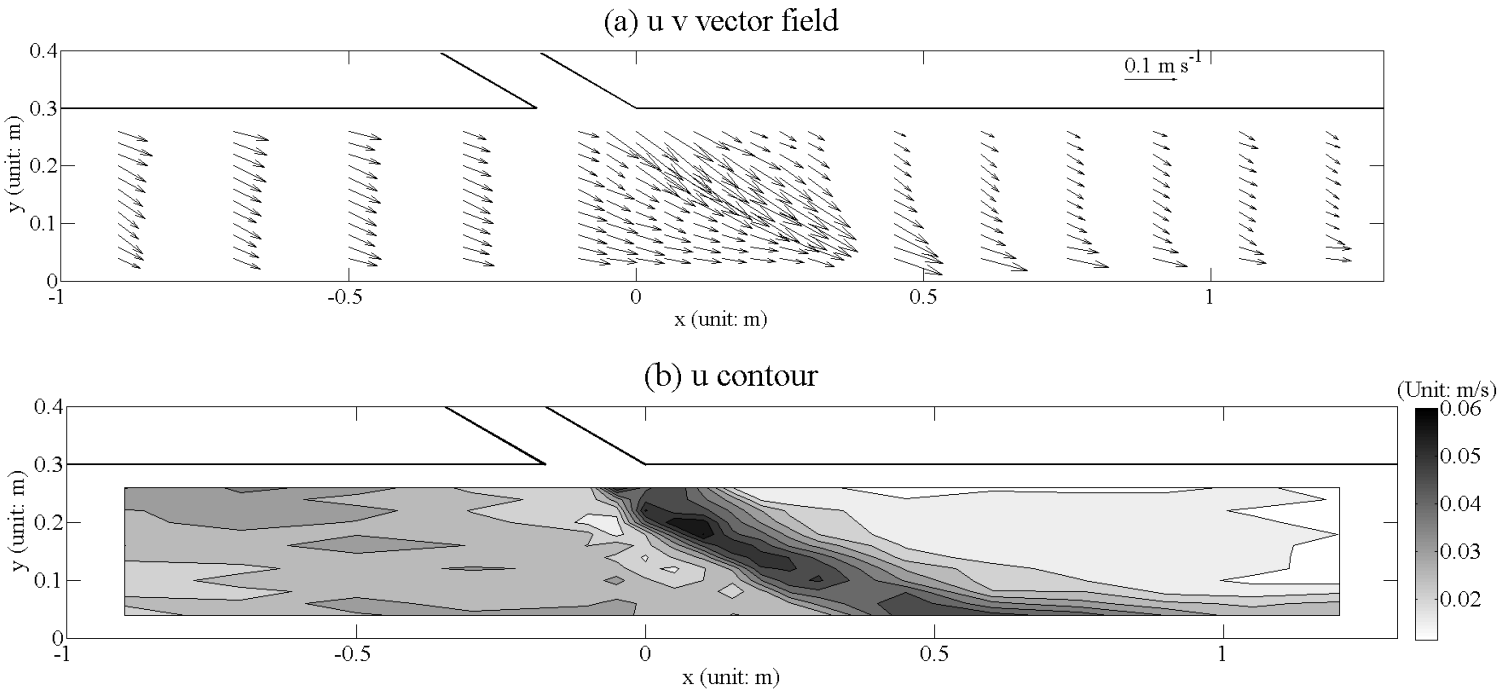

Figure A.37 (AS301) Streamwise velocity characteristics near surface

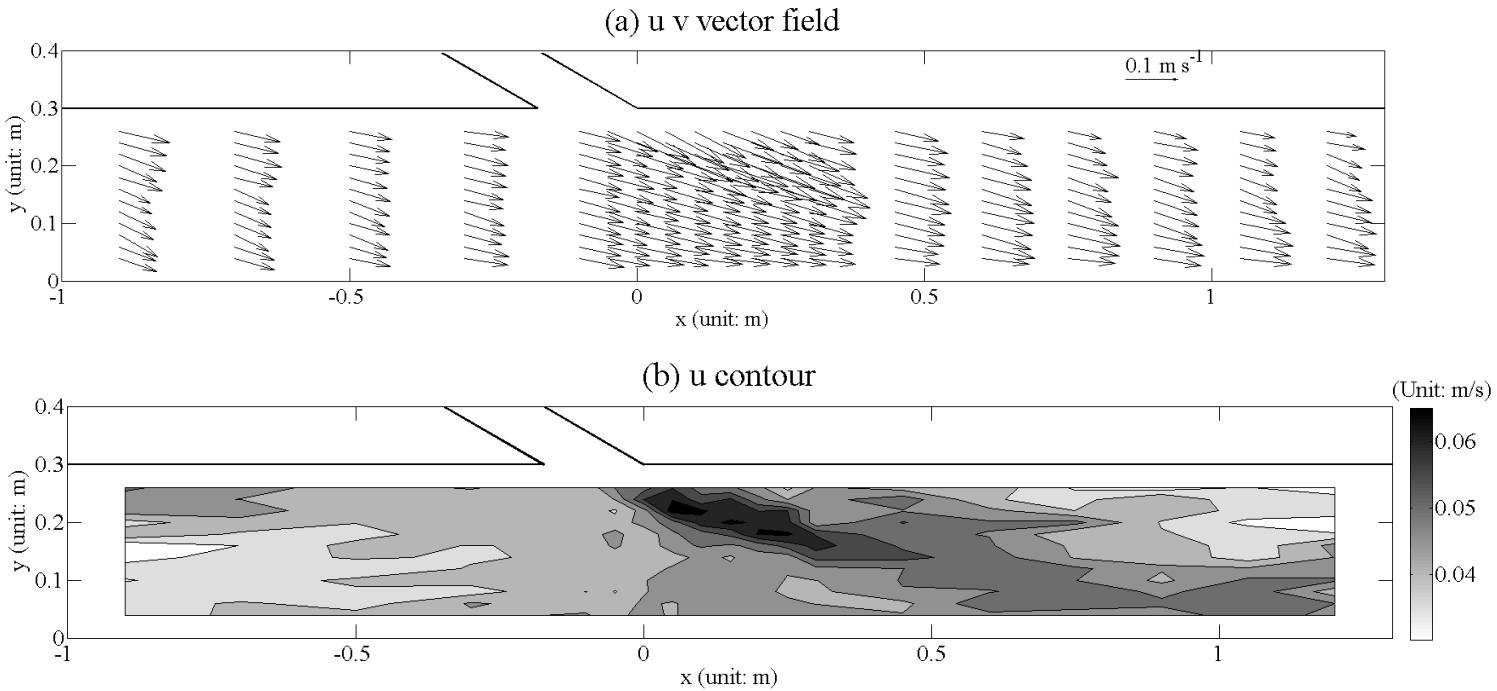

Figure A.38 (AS303) Streamwise velocity characteristics near surface

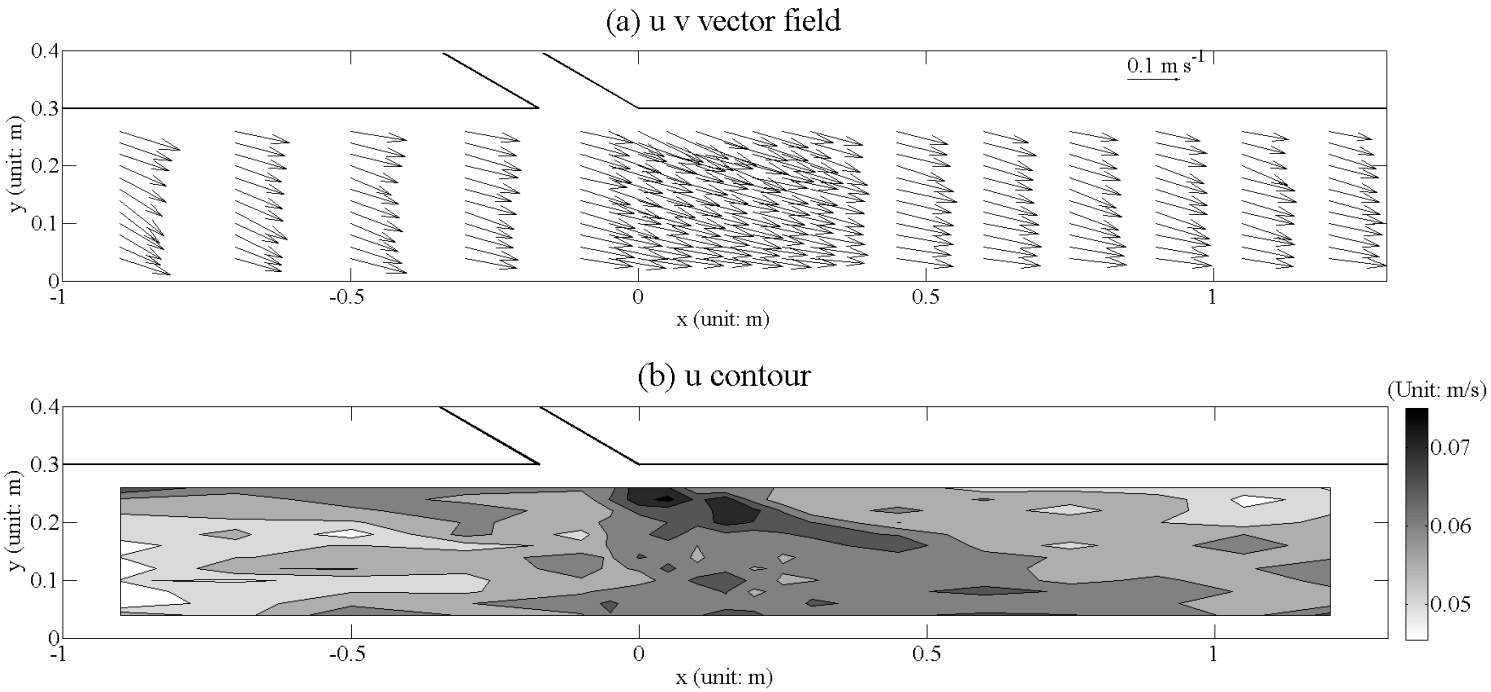

Figure A.39 (AS305) Streamwise velocity characteristics near surface

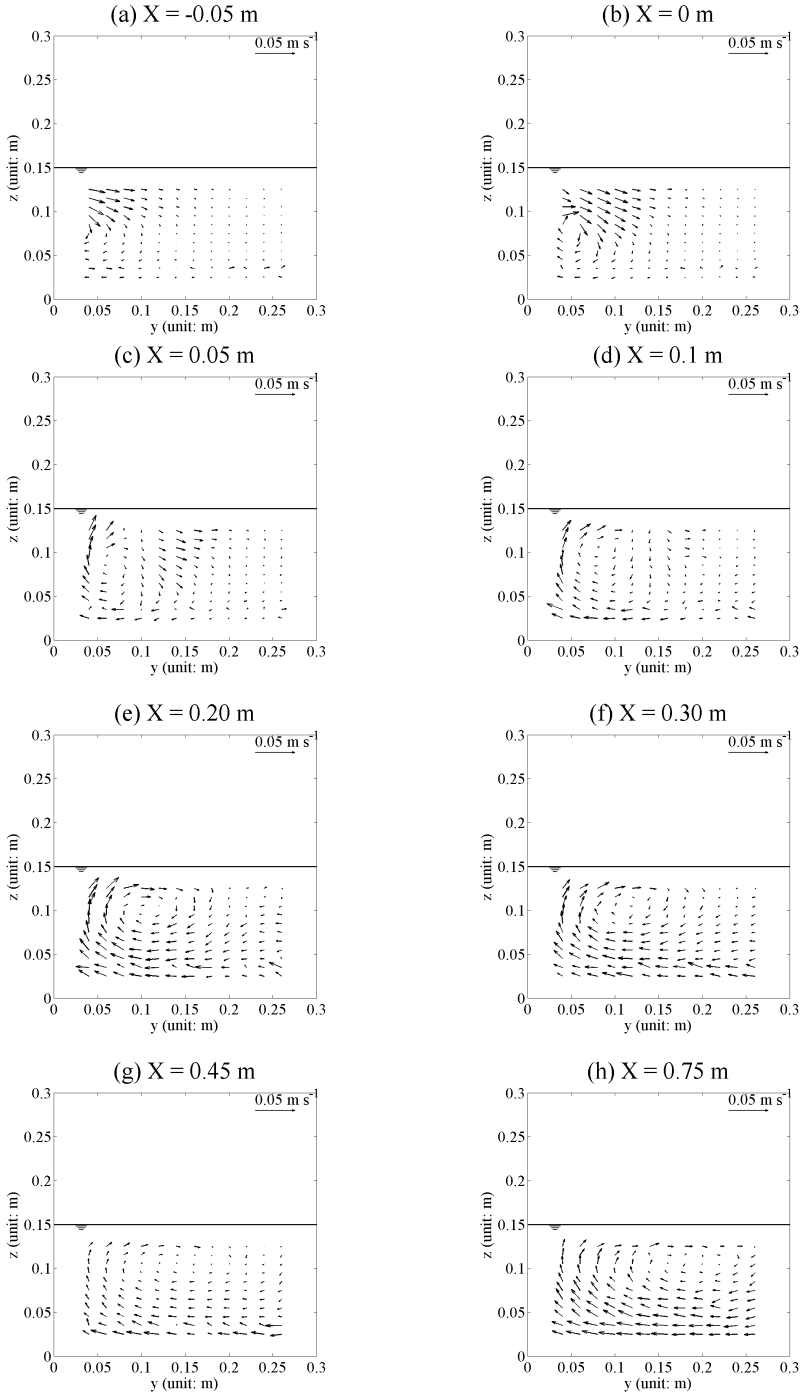

Figure A.40 (AR101) *v*, *w* vector fields

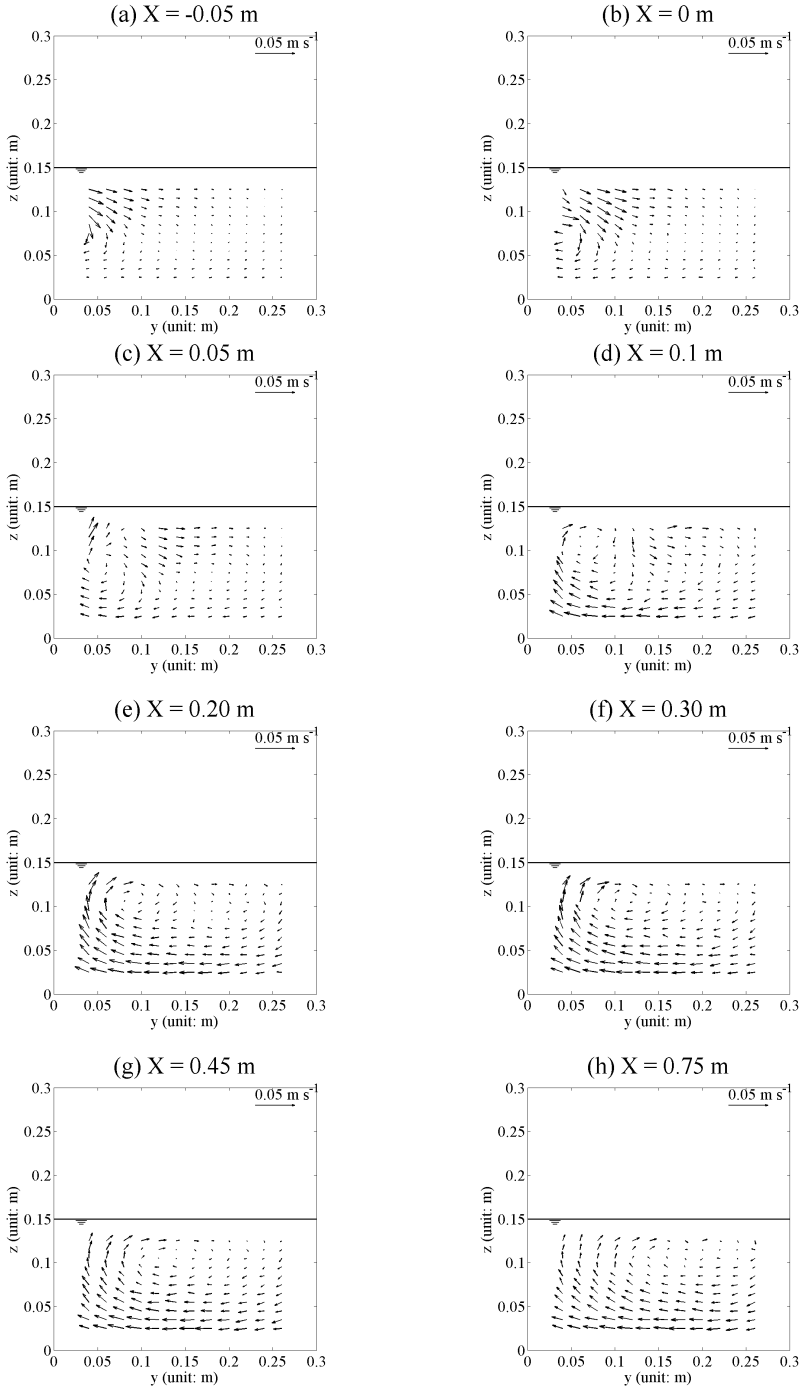

Figure A.41 (AR102) *v*, *w* vector fields

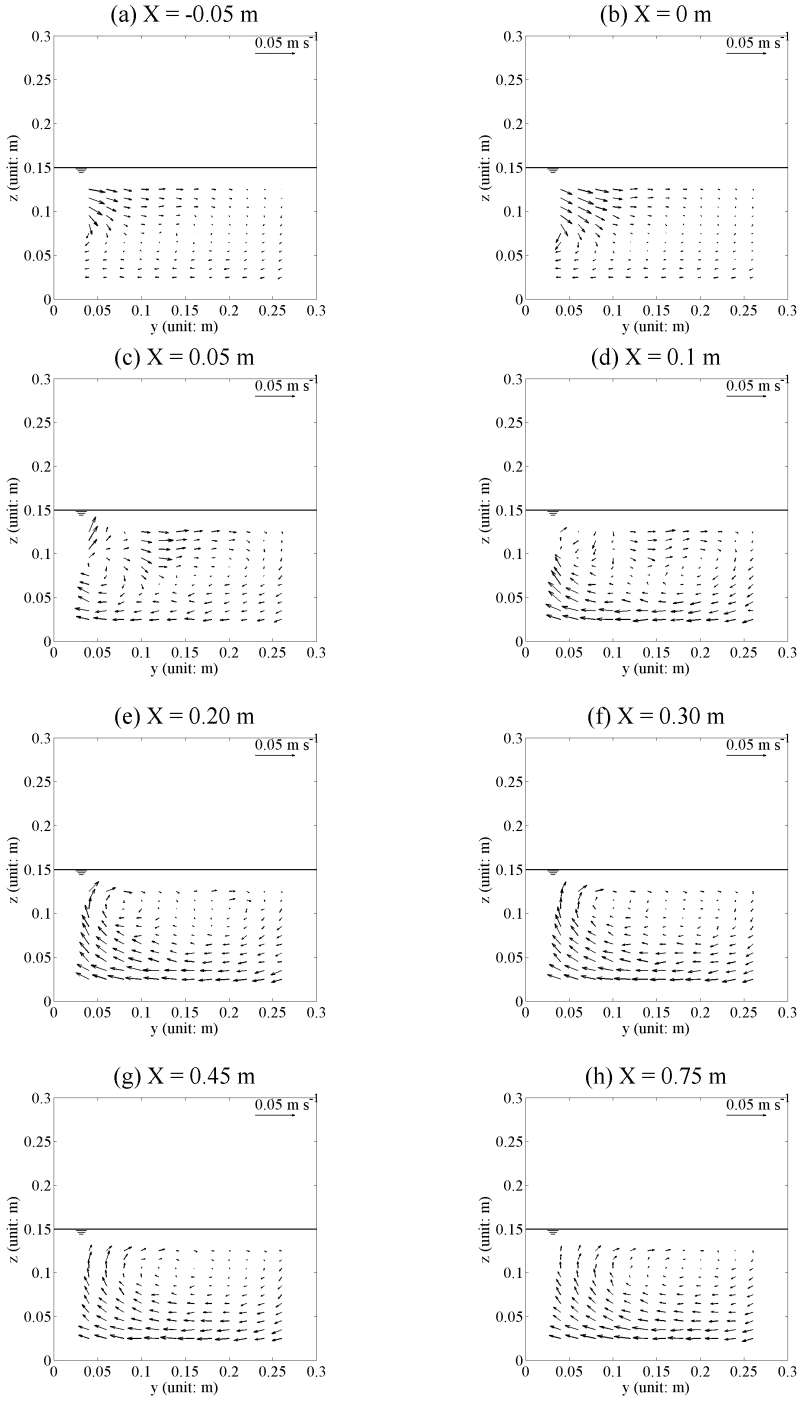

Figure 4.42 (AR103) *v*, *w* vector fields

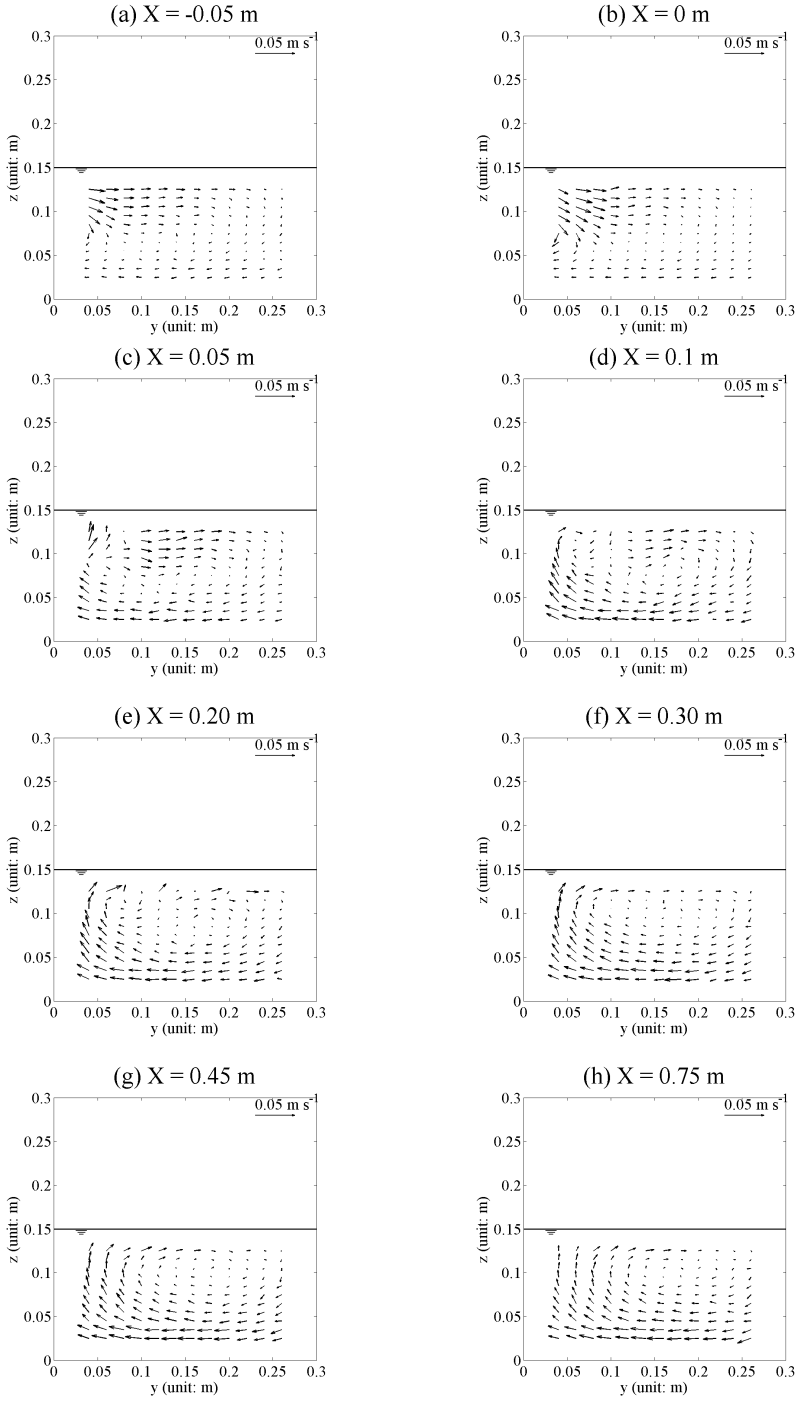

Figure A.43 (AR104) *v*, *w* vector fields

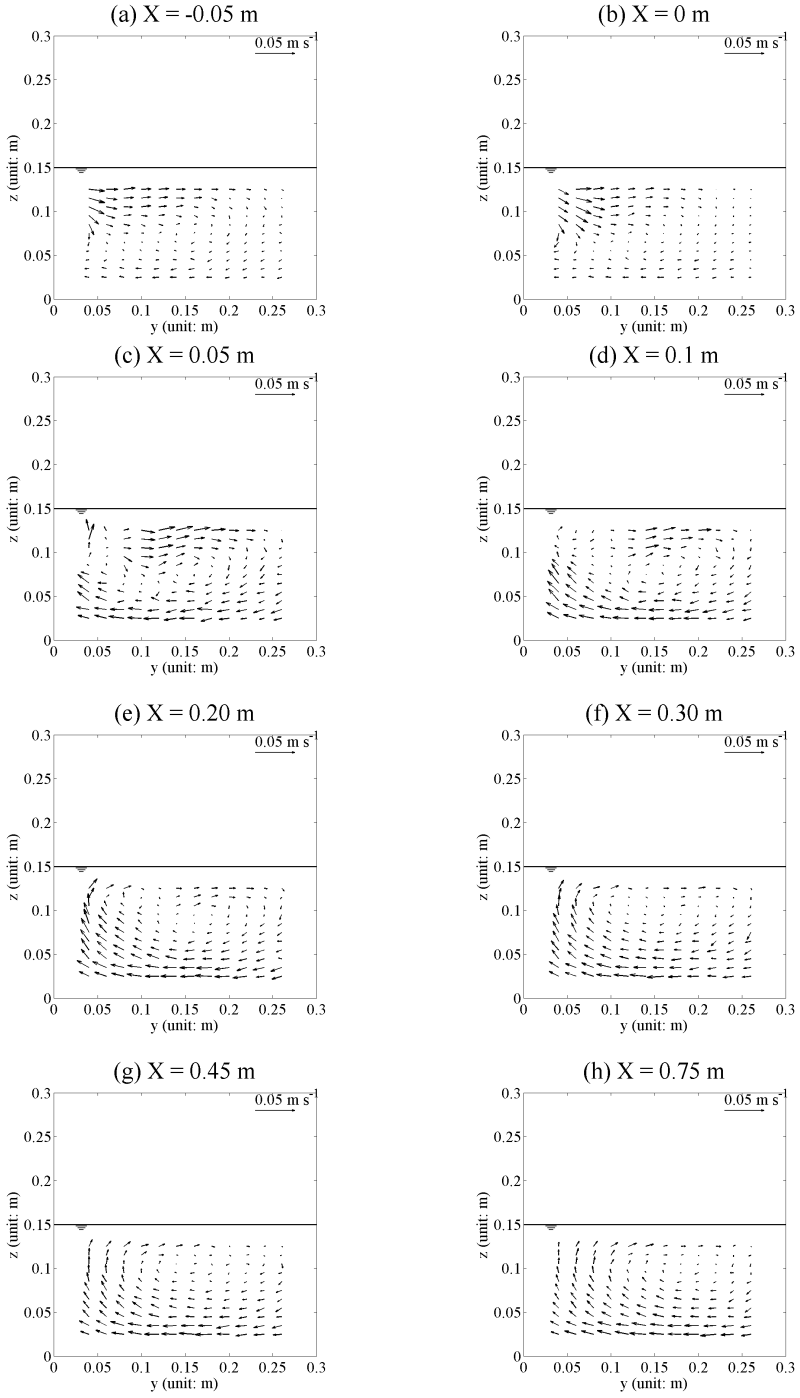

Figure A.44 (AR105) *v*, *w* vector fields

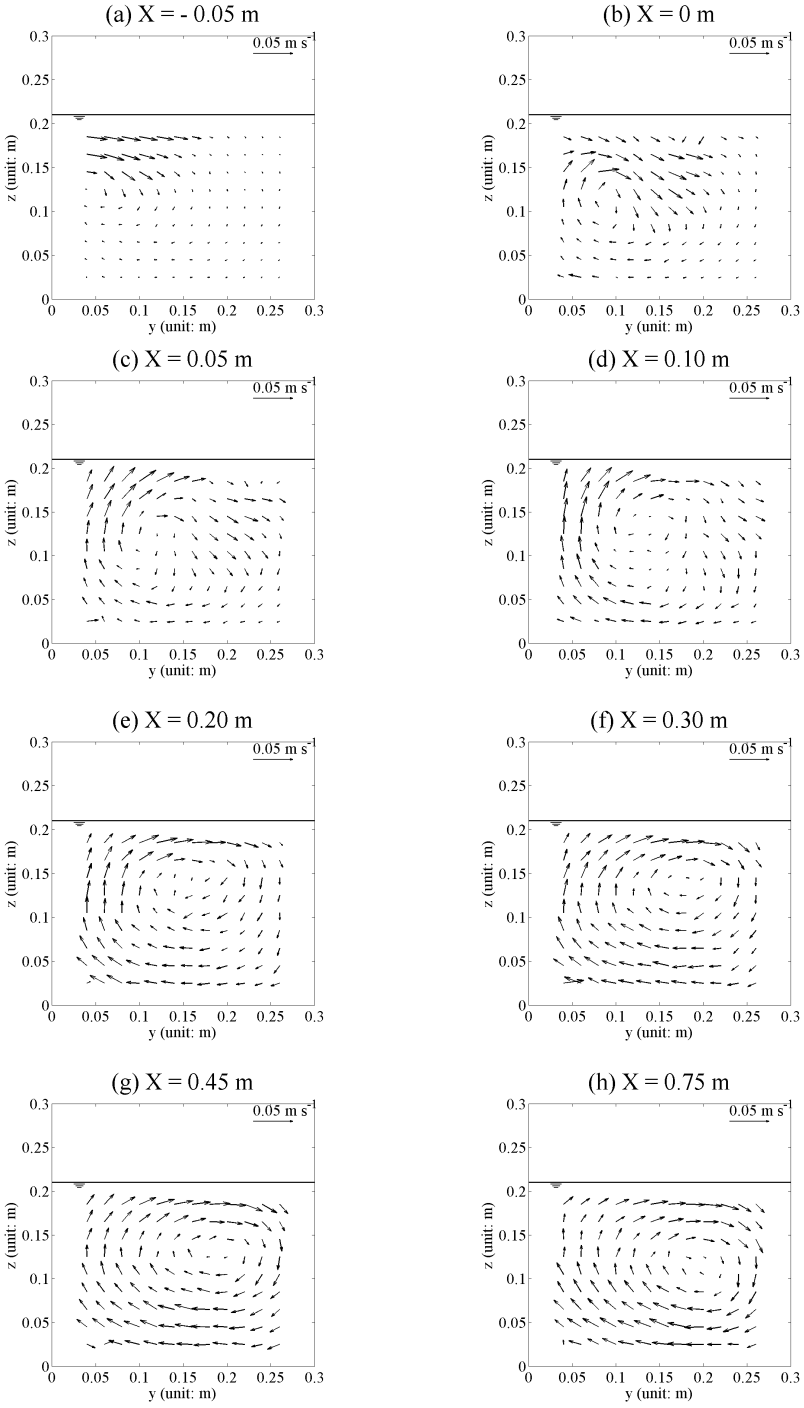

Figure A.45 (AR201) *v*, *w* vector fields

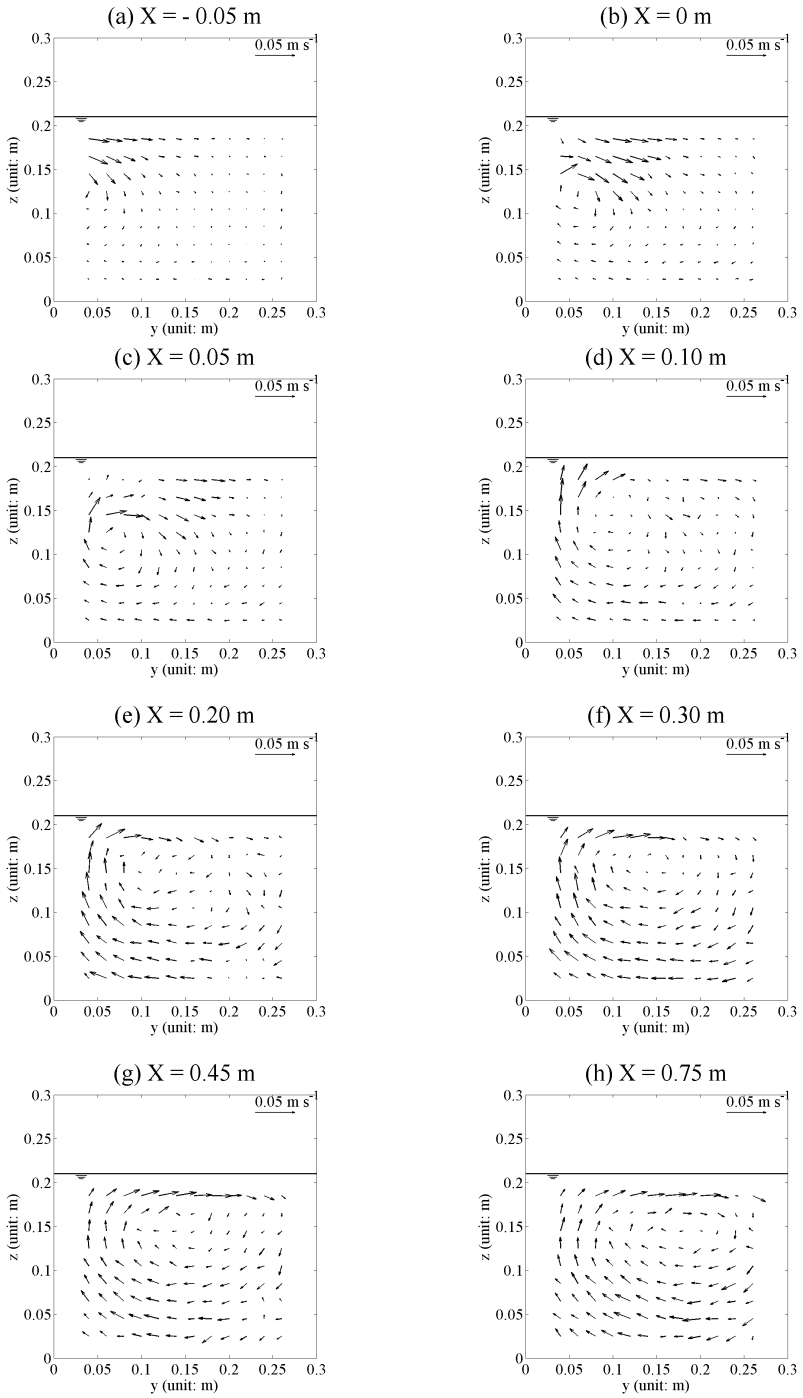

Figure A.46 (AR202) *v*, *w* vector fields

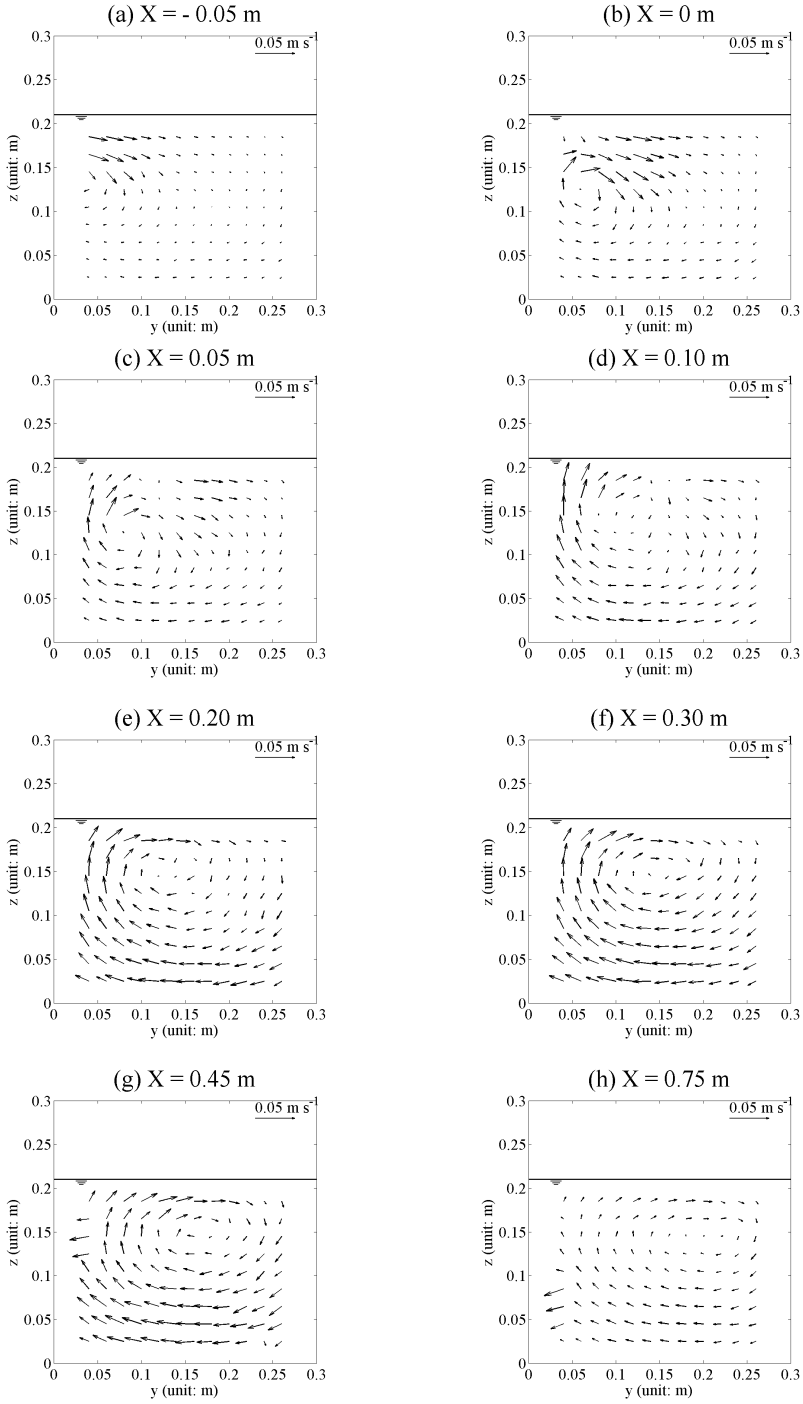

Figure 4.47 (AR203) *v*, *w* vector fields

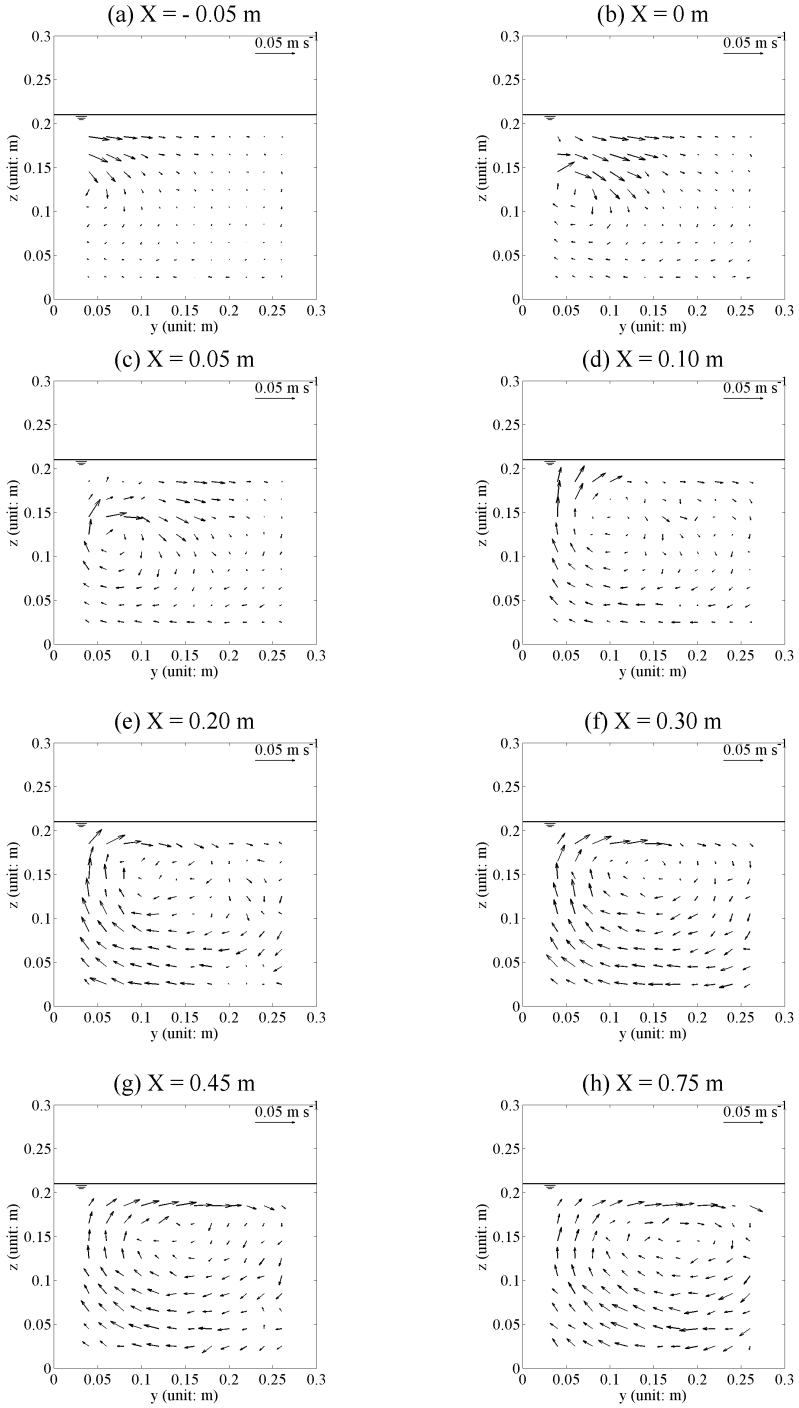

Figure A.48 (AR204) *v*, *w* vector fields

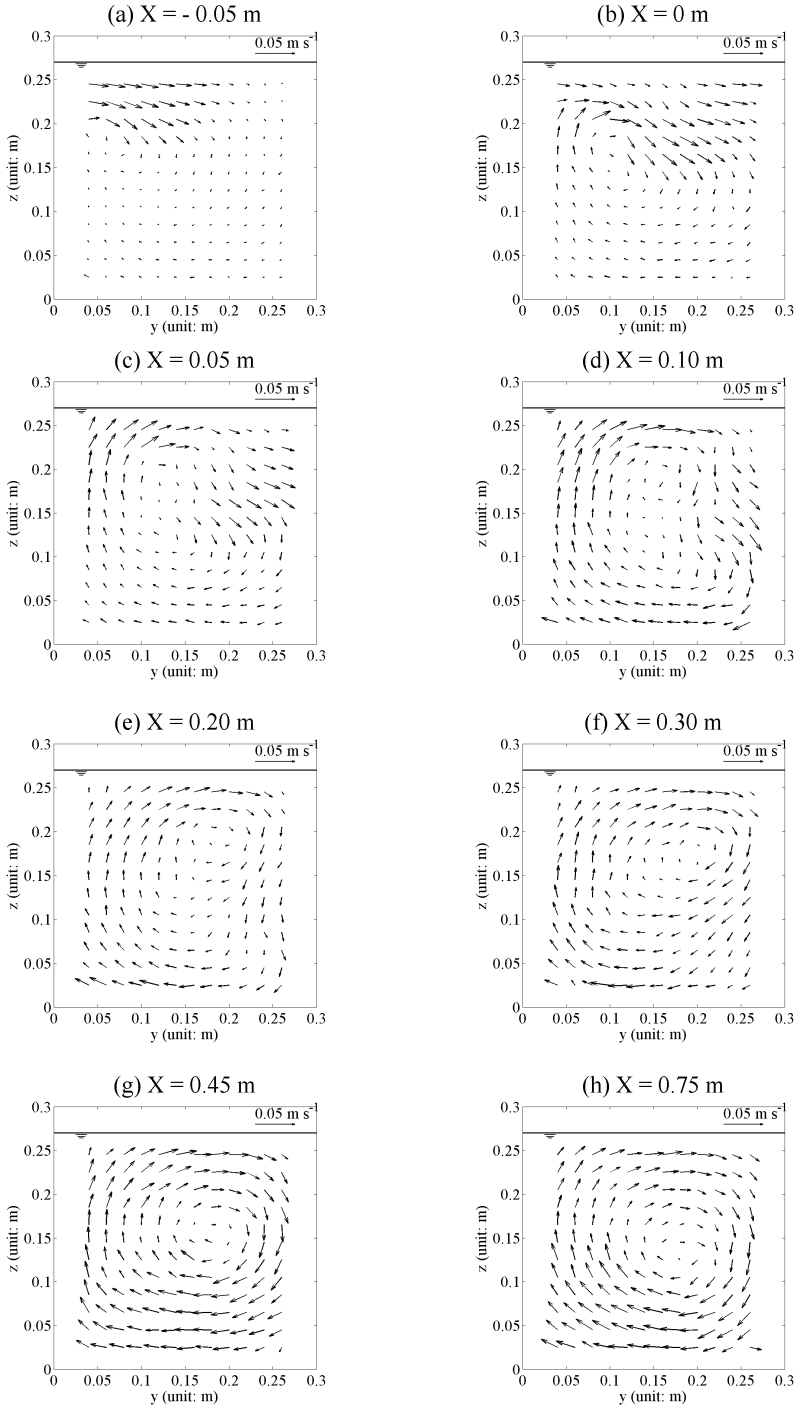

Figure A.49 (AR301) *v*, *w* vector fields

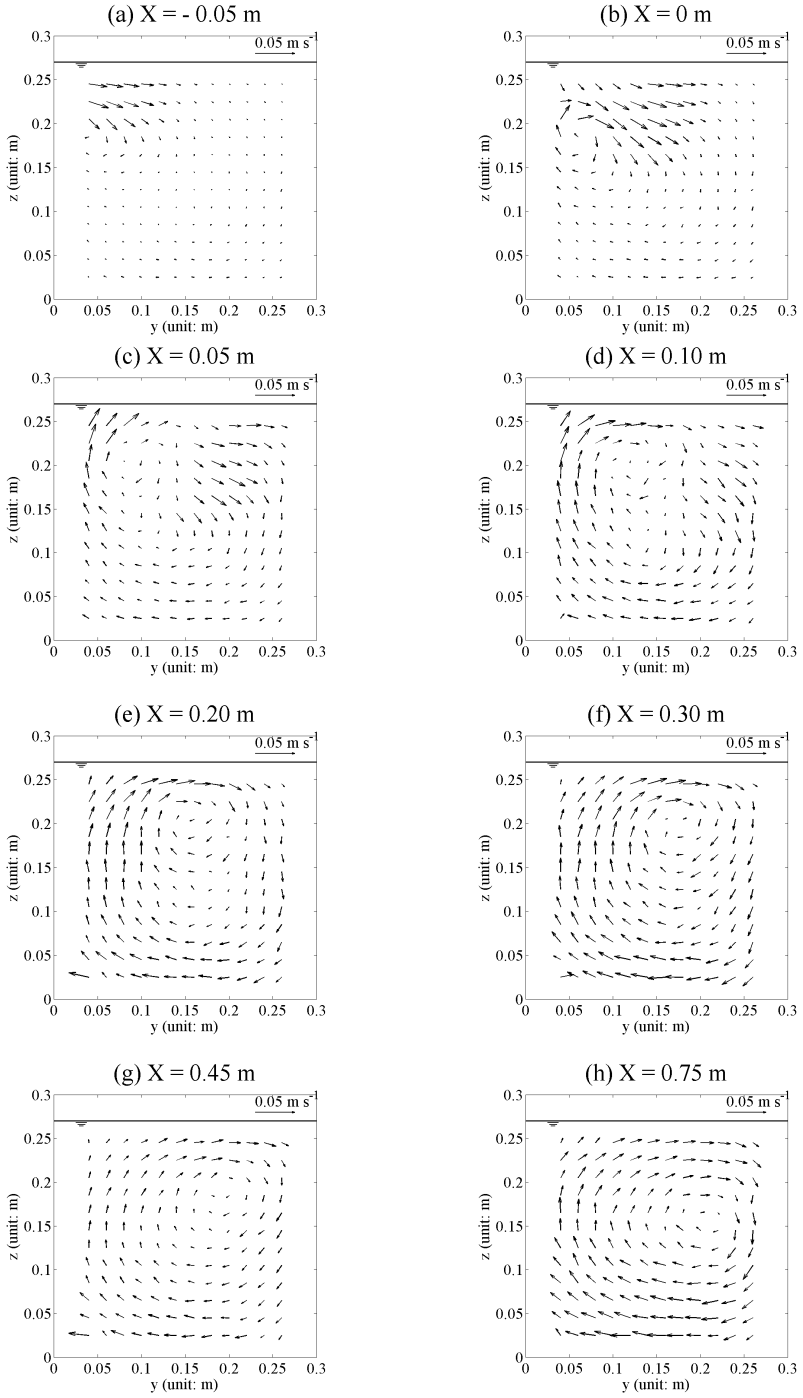

Figure A.50 (AR302) *v*, *w* vector fields

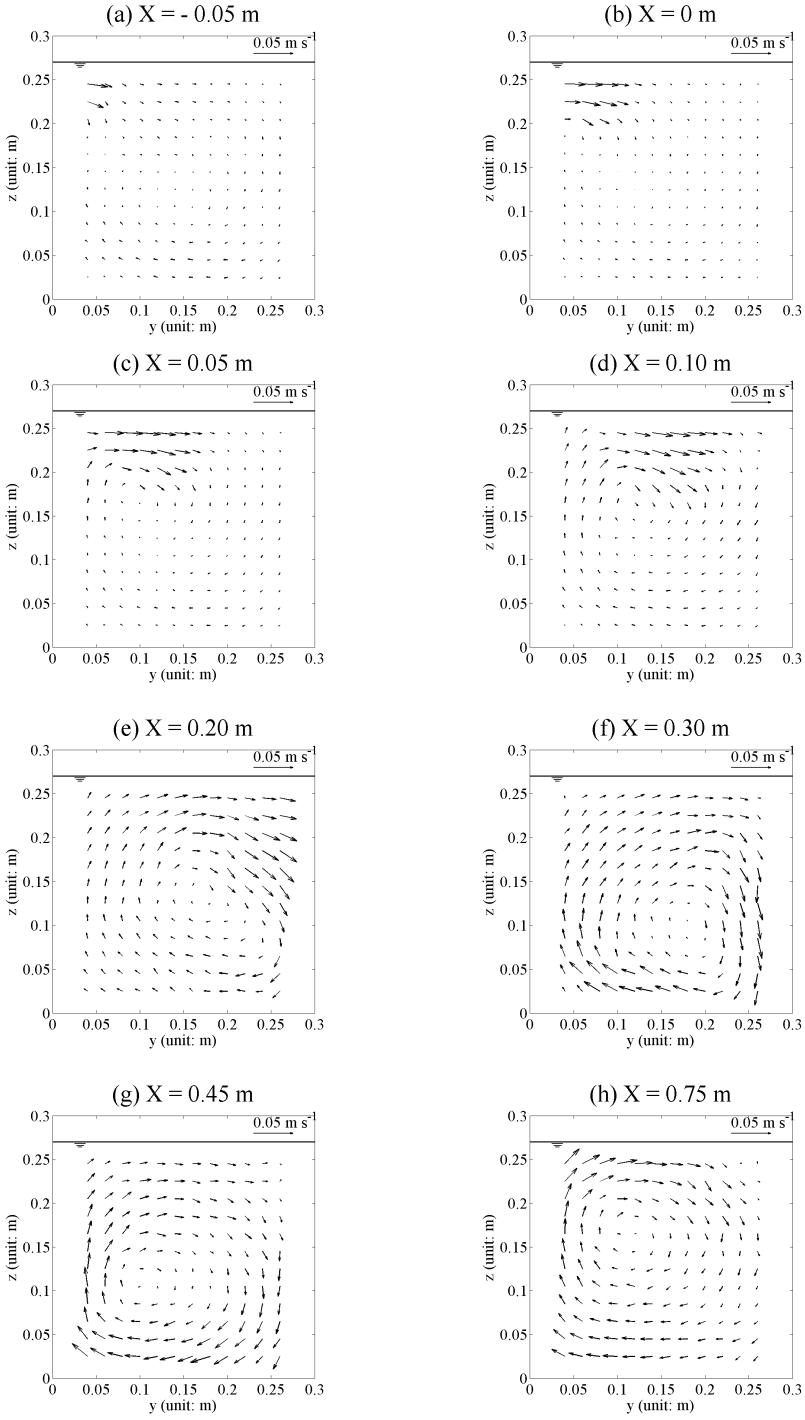

Figure 4.51 (AR303) *v*, *w* vector fields

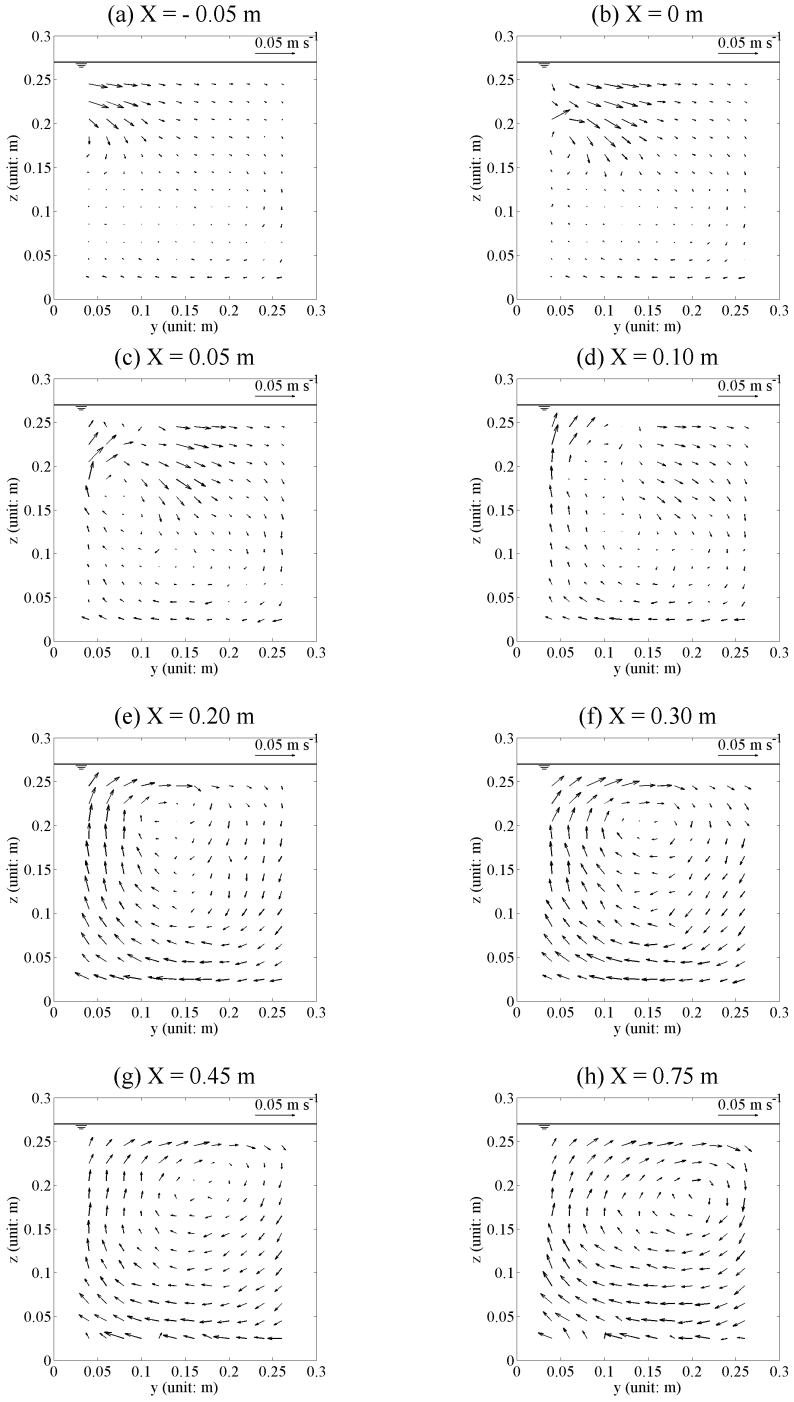

Figure A.52 (AR304) *v*, *w* vector fields

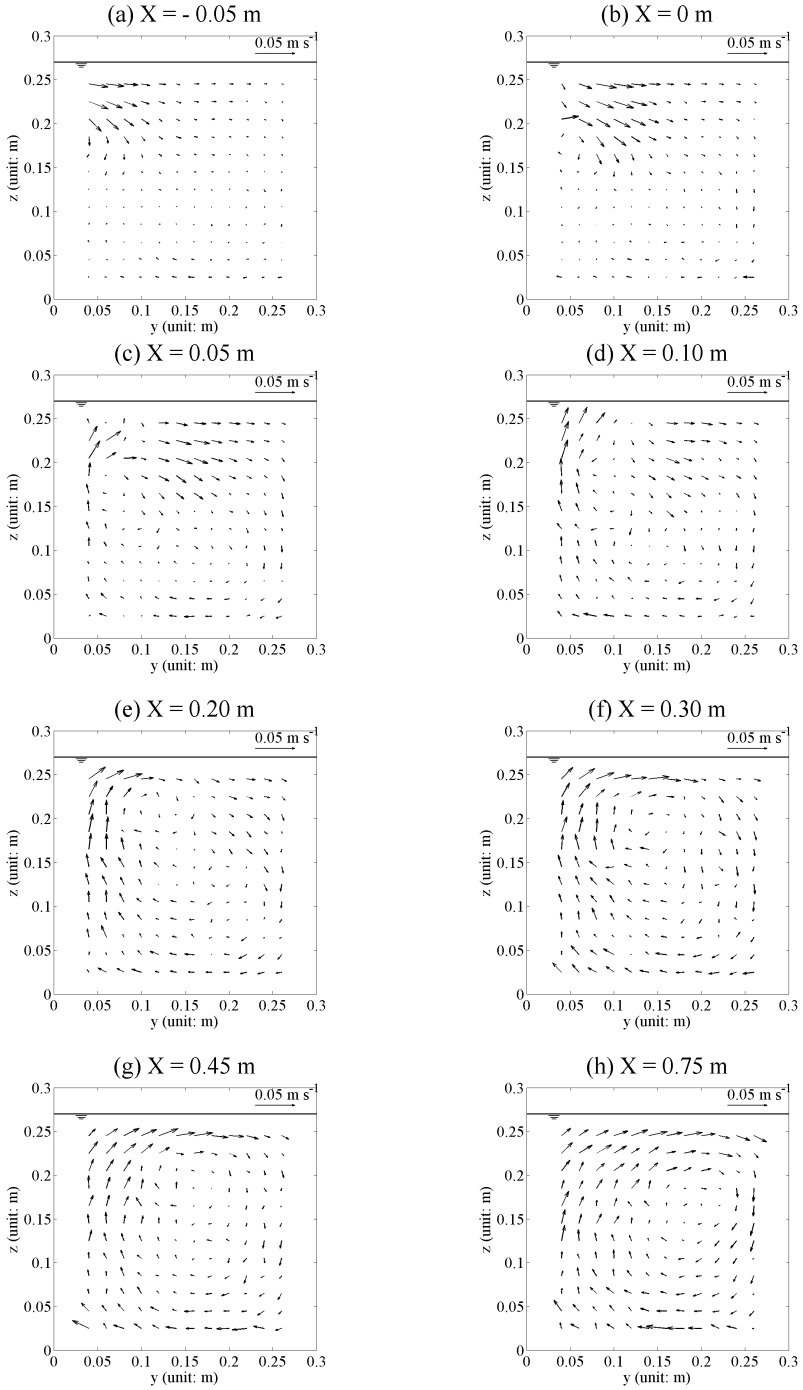

Figure A.53 (AR305) *v*, *w* vector fields

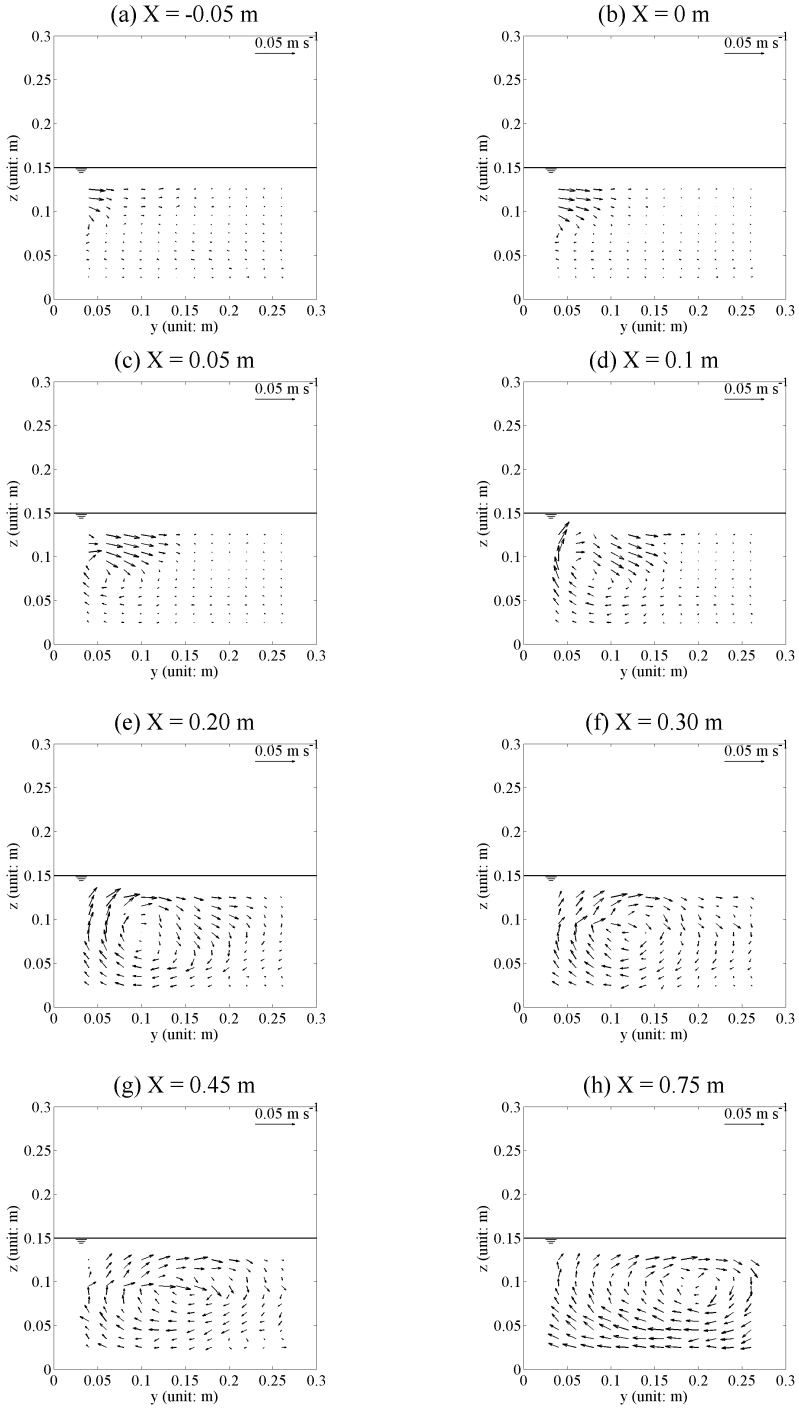

Figure A.54 (AM101) *v*, *w* vector fields

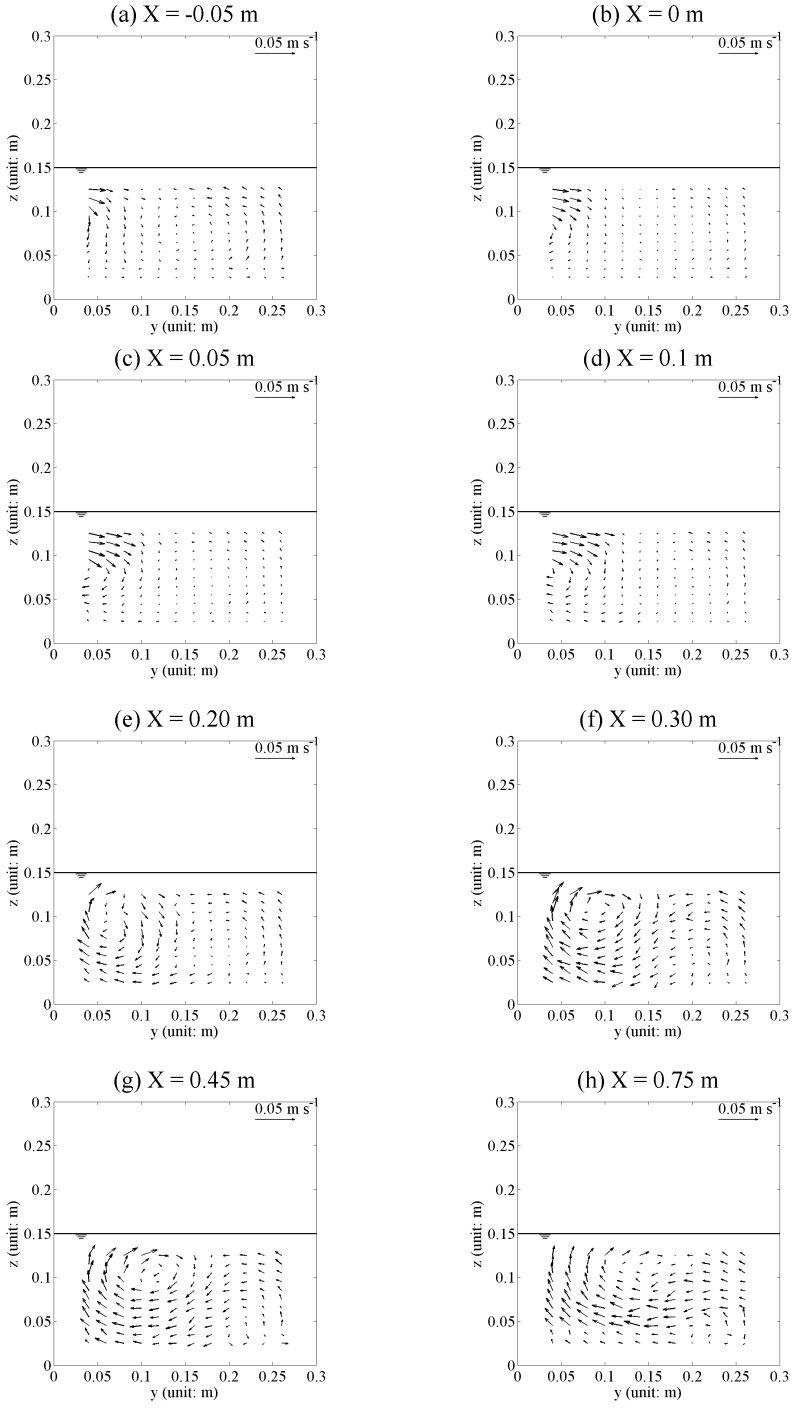

Figure A.55 (AM102) *v*, *w* vector fields

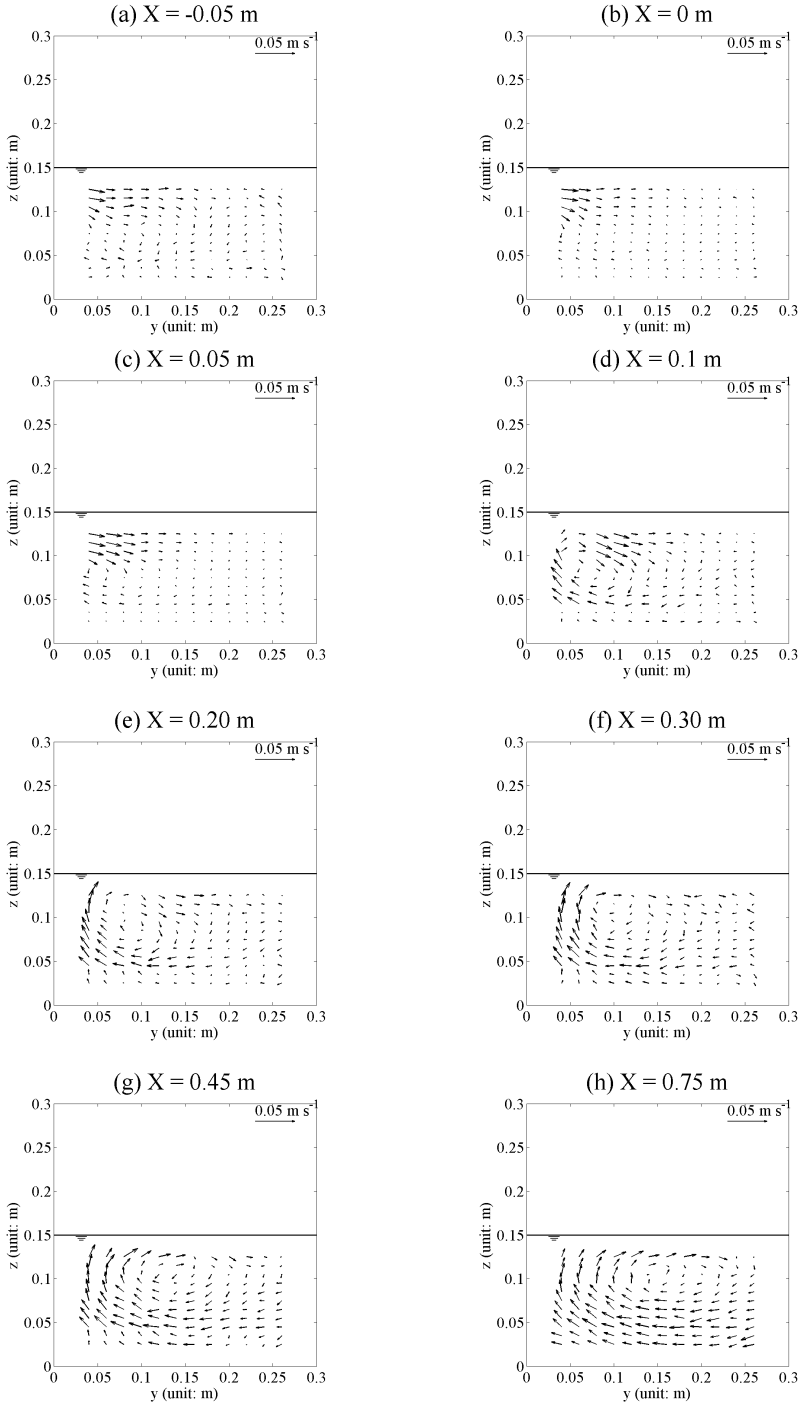

Figure A.56 (AM103) *v*, *w* vector fields

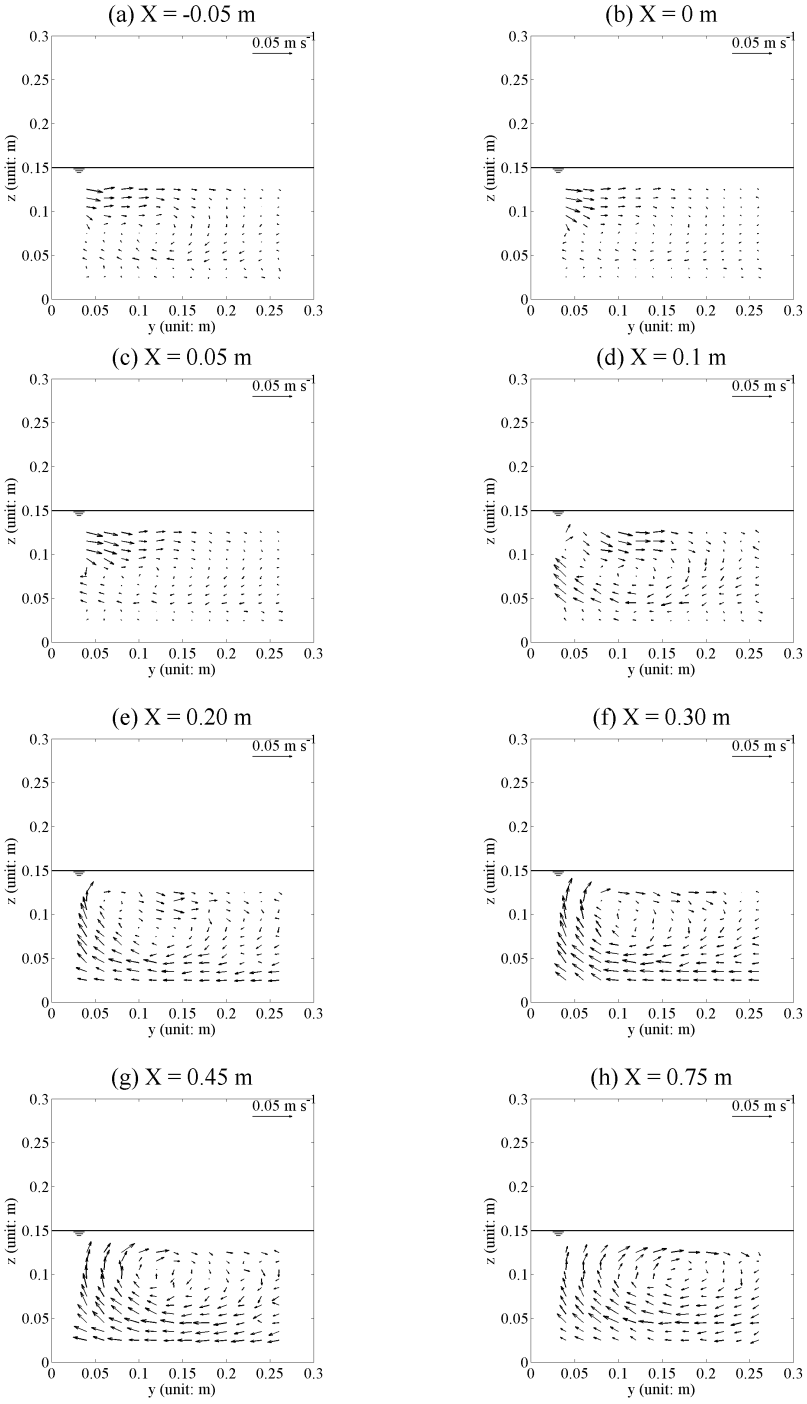

Figure A.57 (AM104) *v*, *w* vector fields

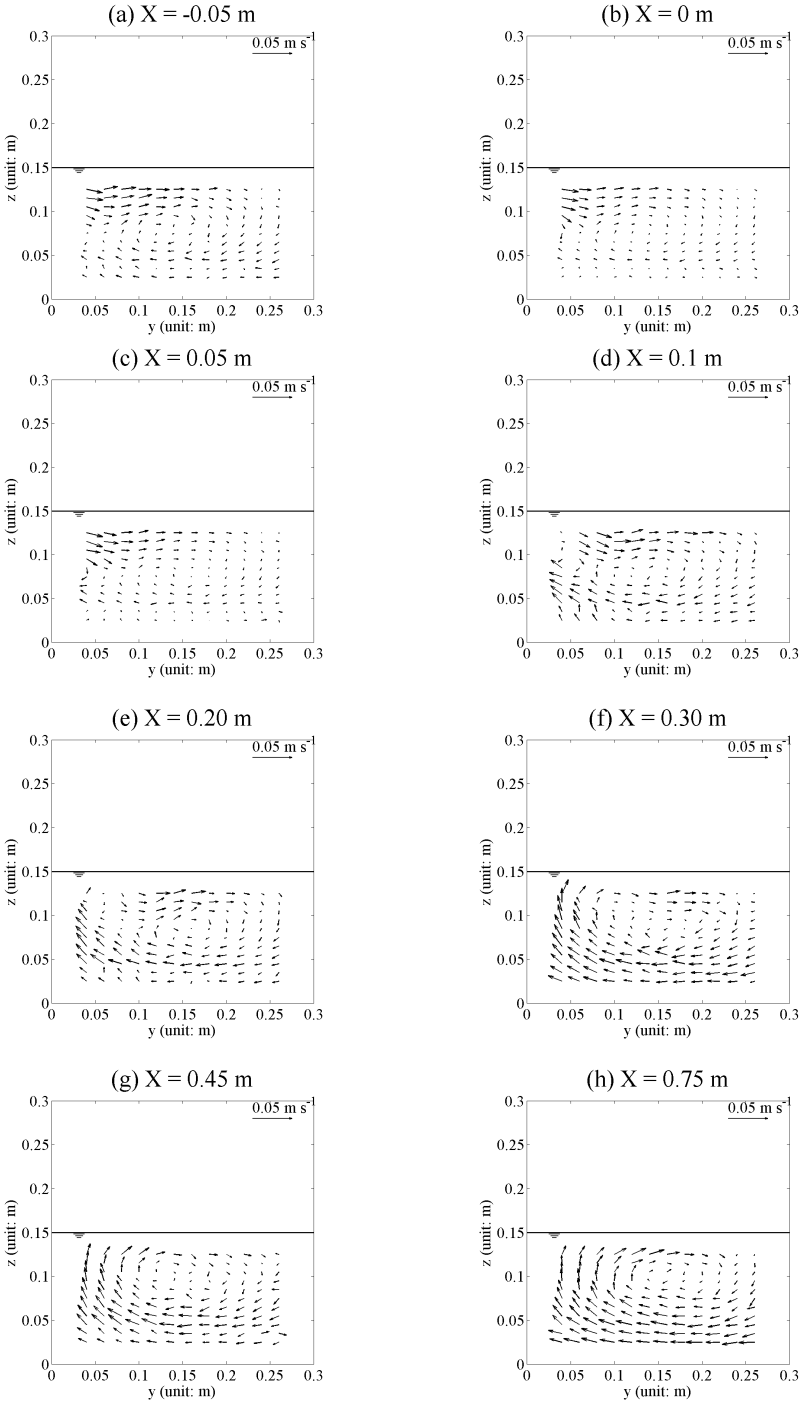

Figure A.58 (AM105) *v*, *w* vector fields

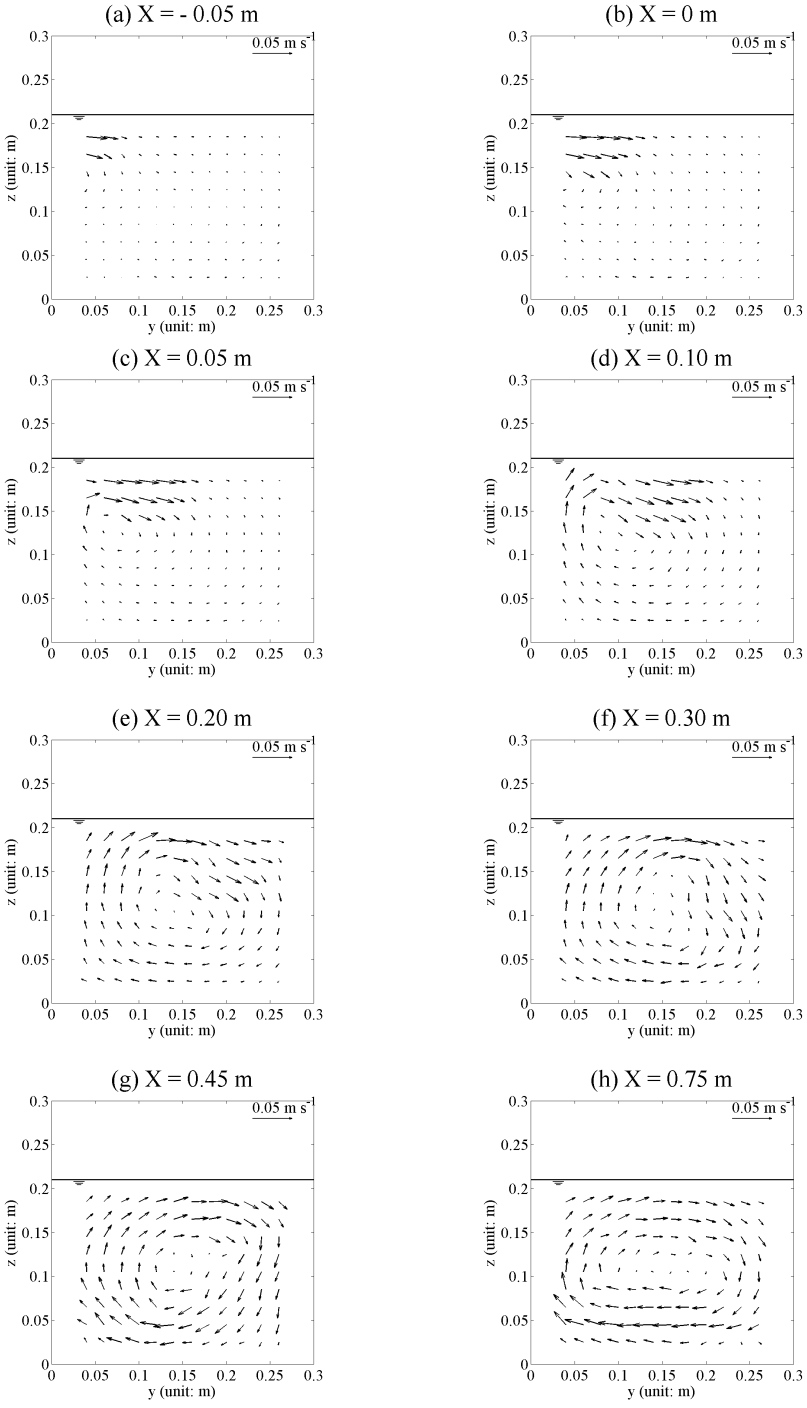

Figure A.59 (AM201) *v*, *w* vector fields

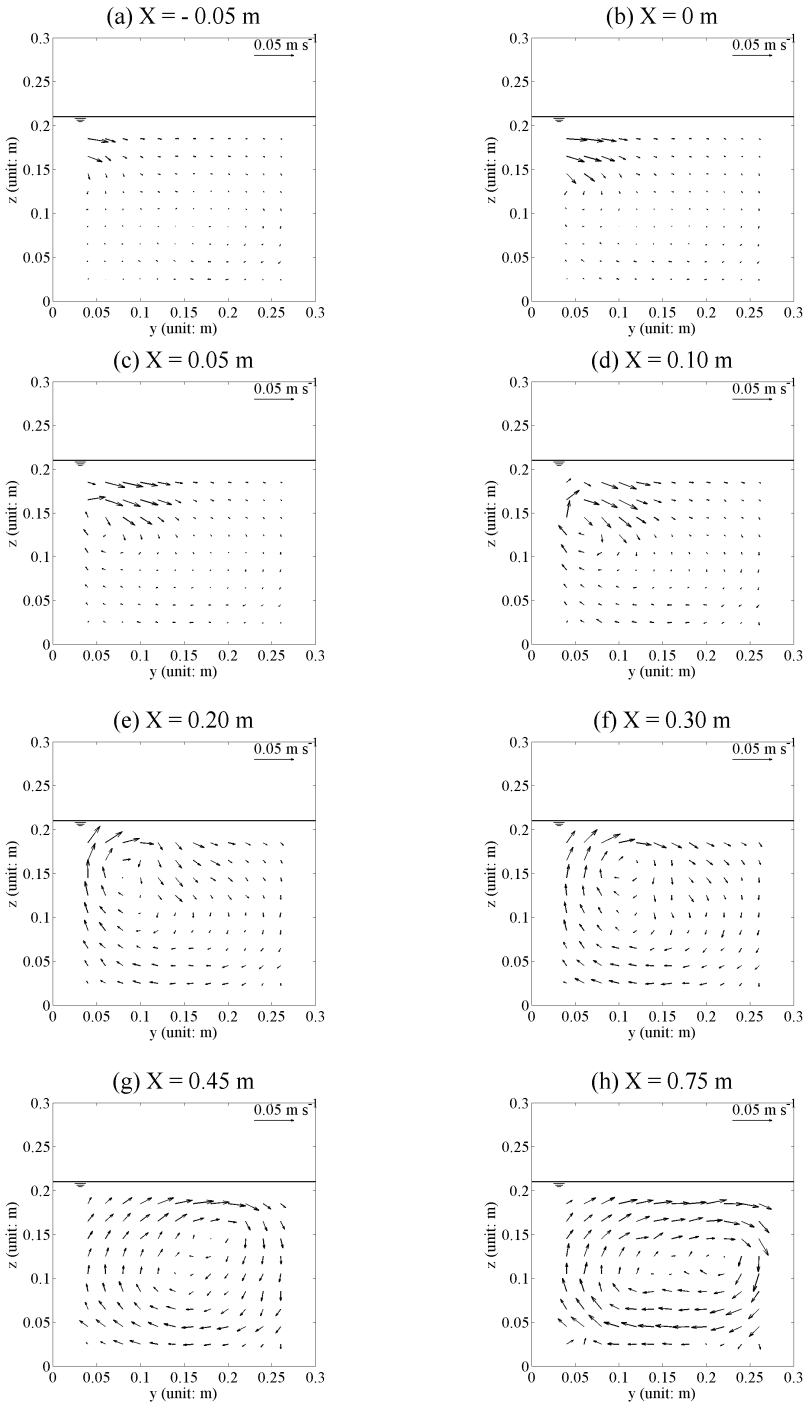

Figure A.60 (AM202) *v*, *w* vector fields

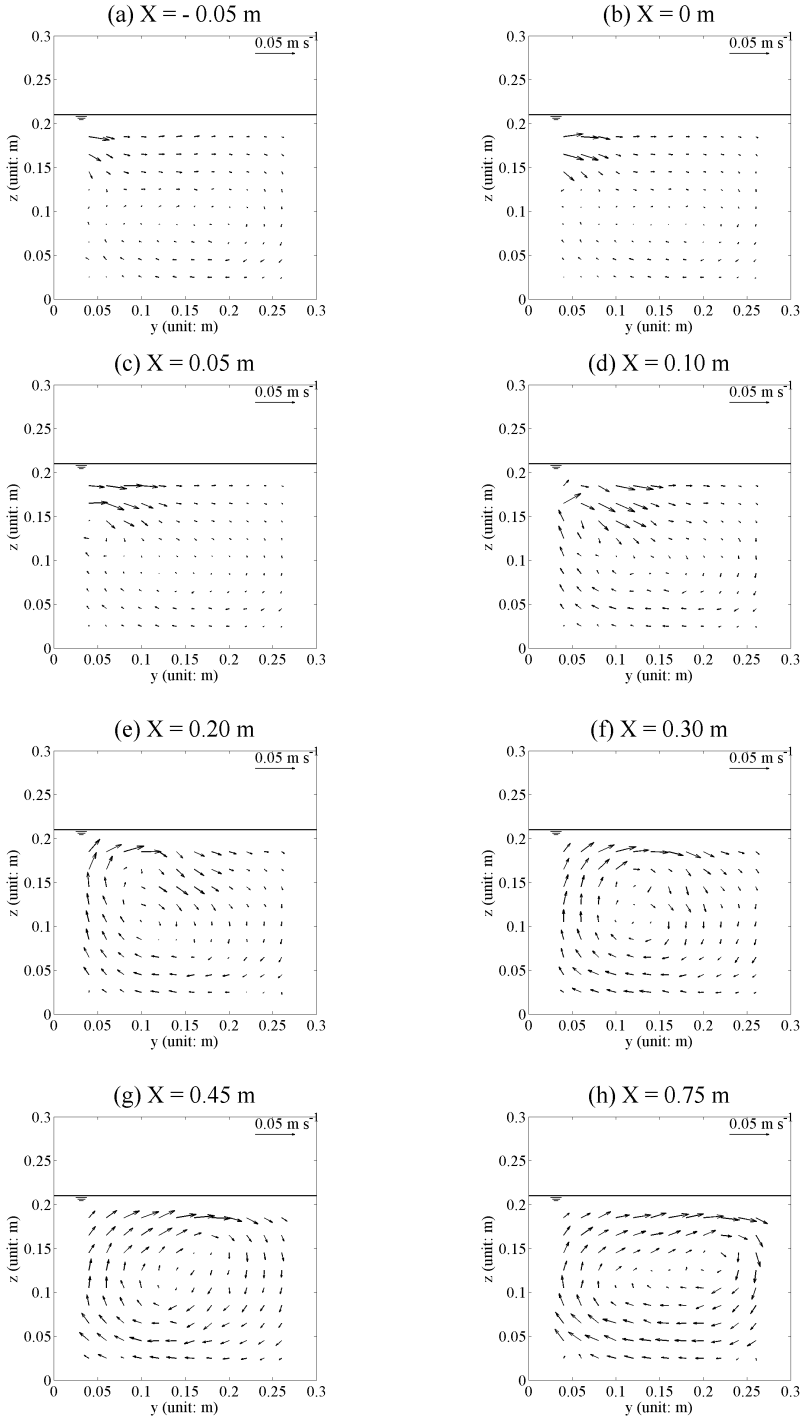

Figure A.61 (AM203) *v*, *w* vector fields

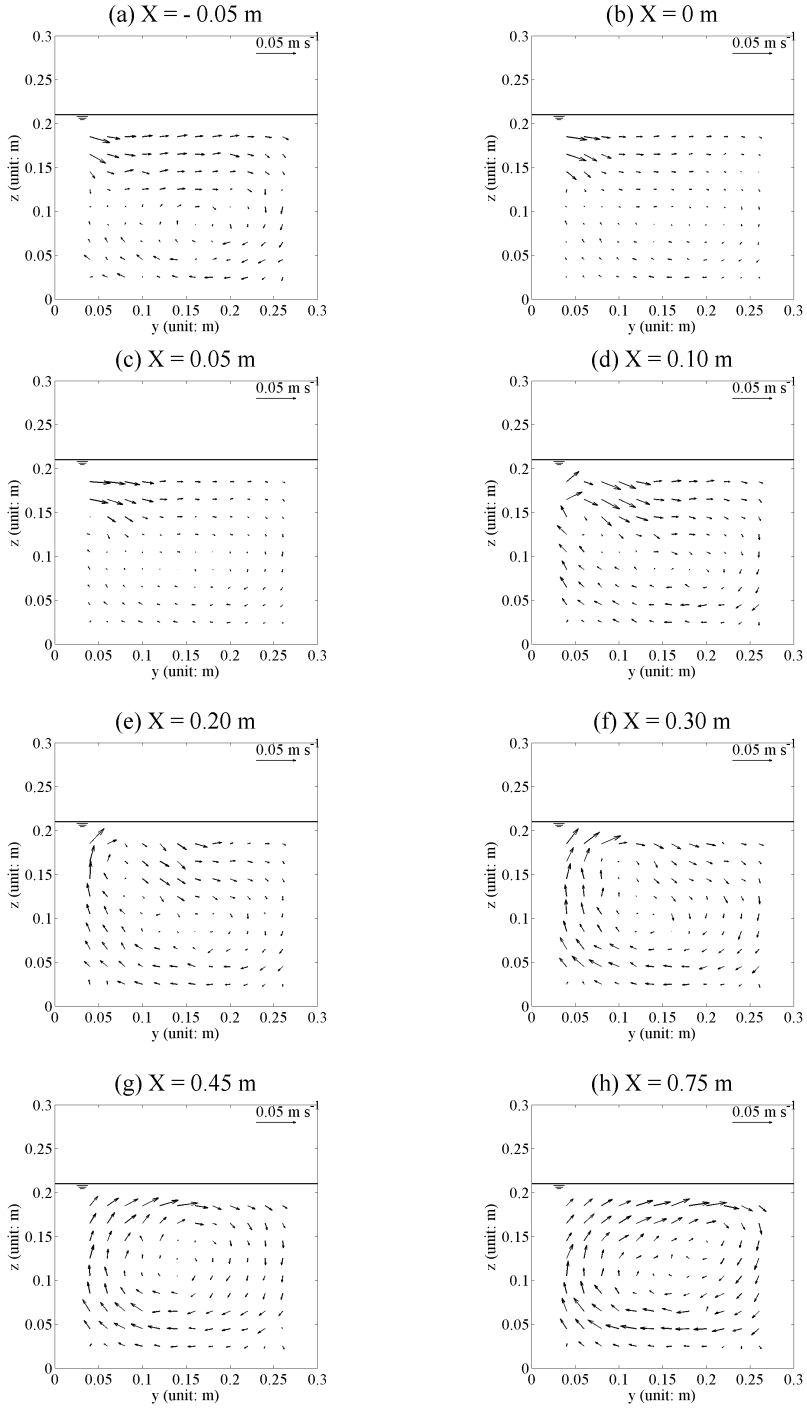

Figure A.62 (AM204) *v*, *w* vector fields

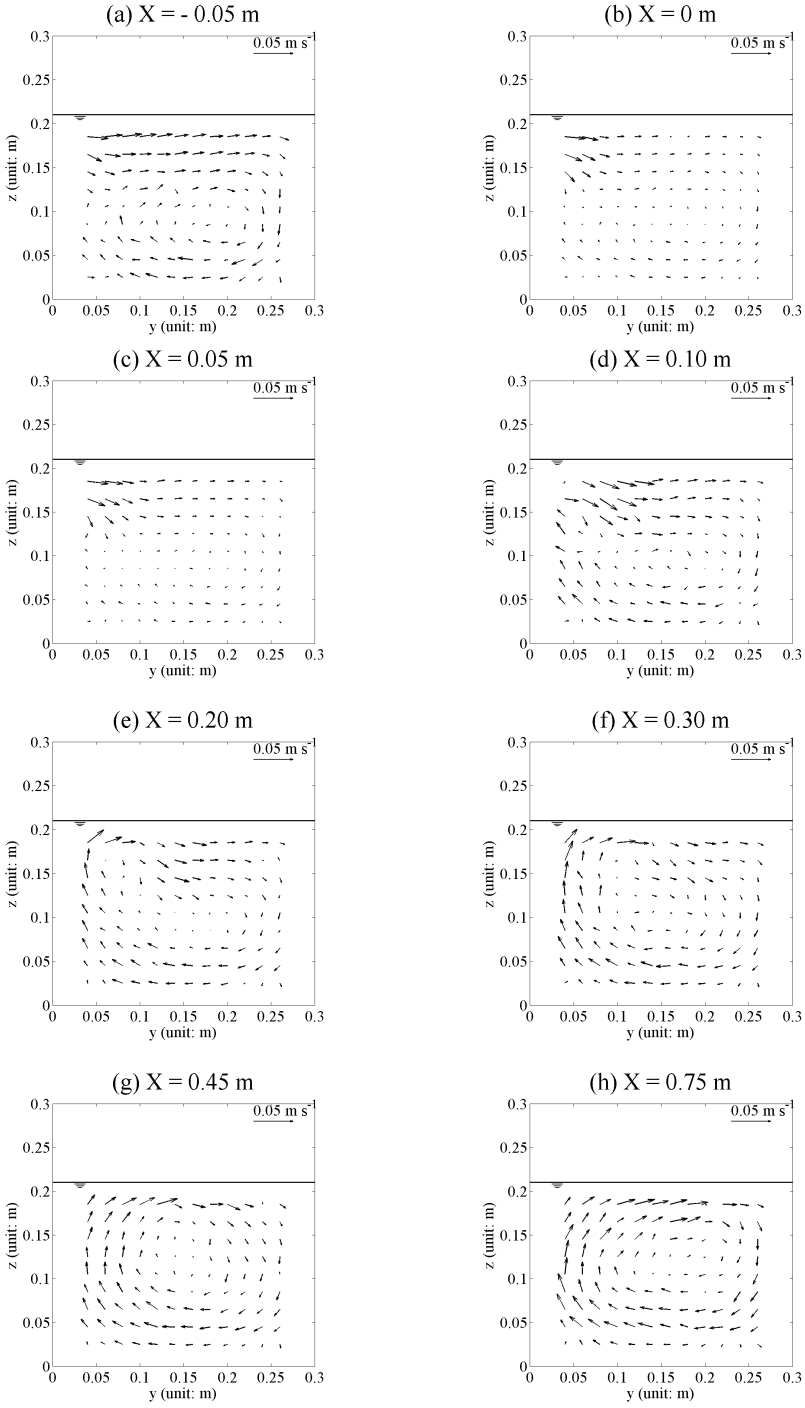

Figure A.63 (AM205) *v*, *w* vector fields

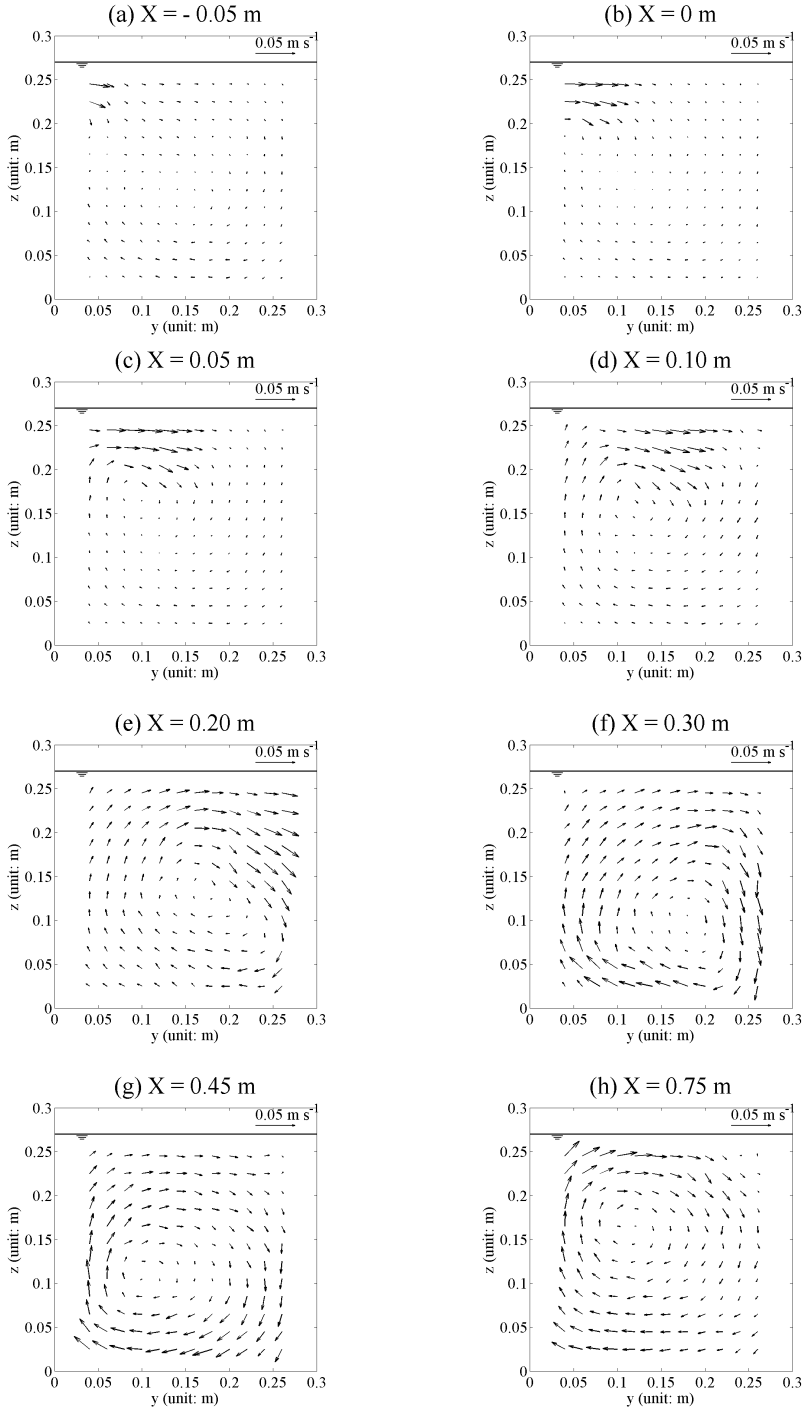

Figure A.64 (AM301) *v*, *w* vector fields

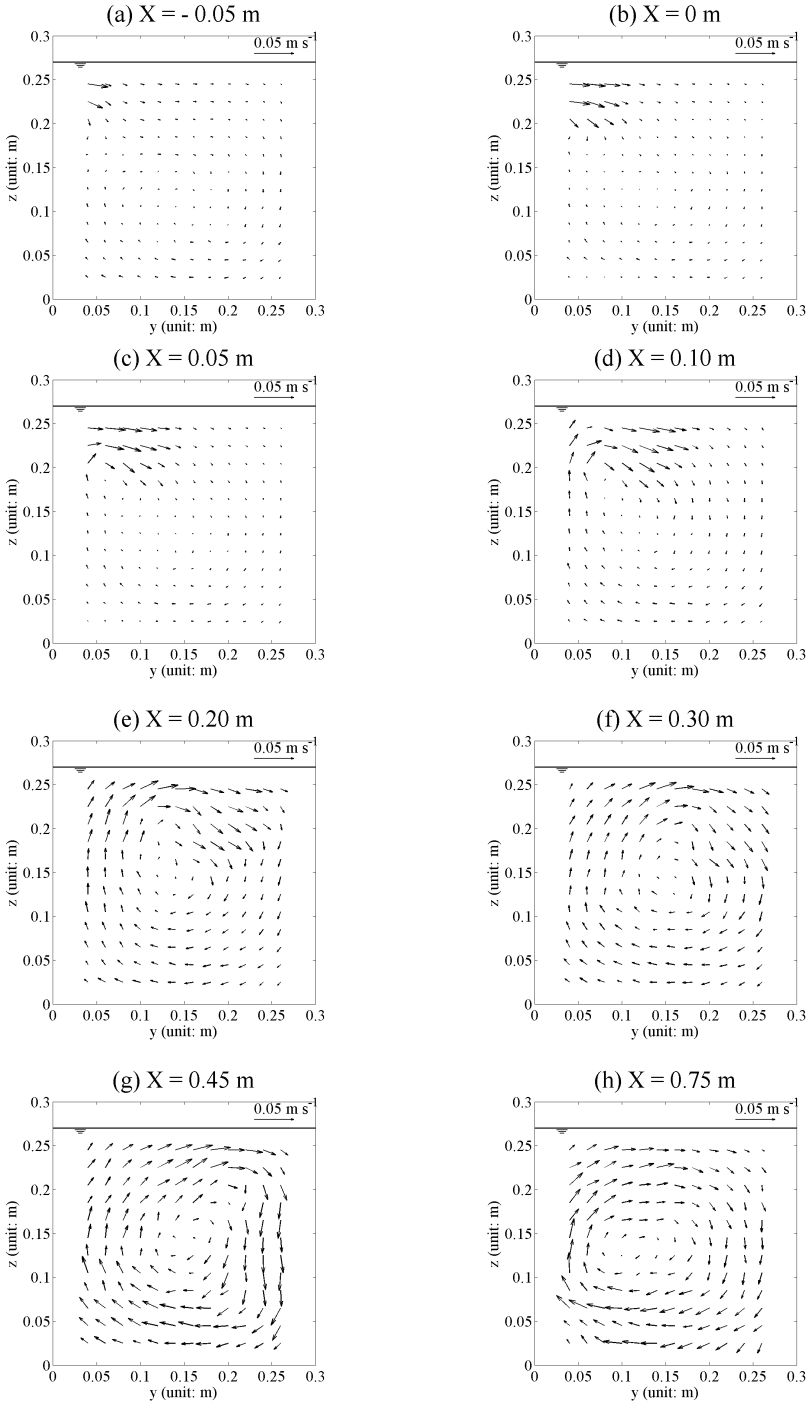

Figure A.65 (AM302) *v*, *w* vector fields

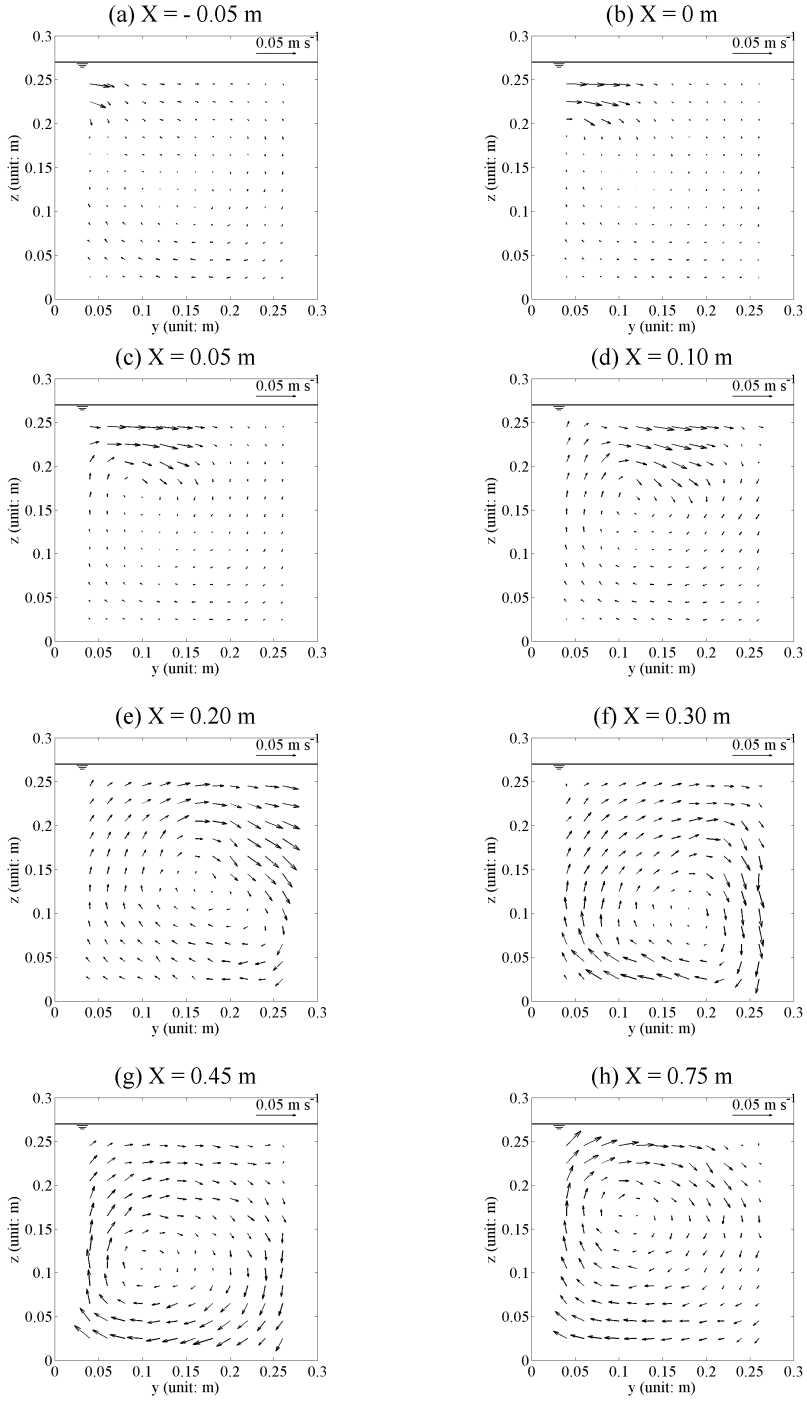

Figure A.66 (AM303) *v*, *w* vector fields

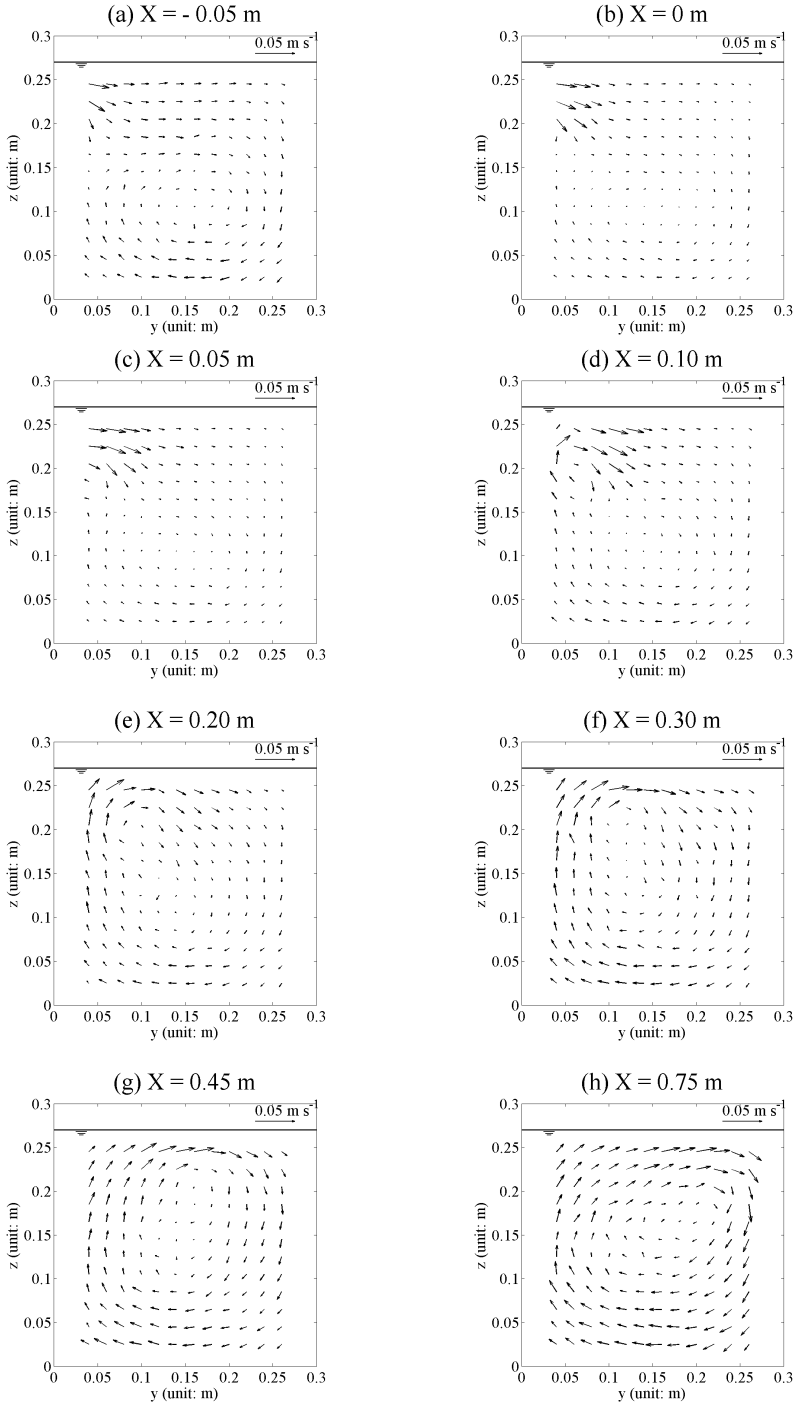

Figure A.67 (AM304) *v*, *w* vector fields

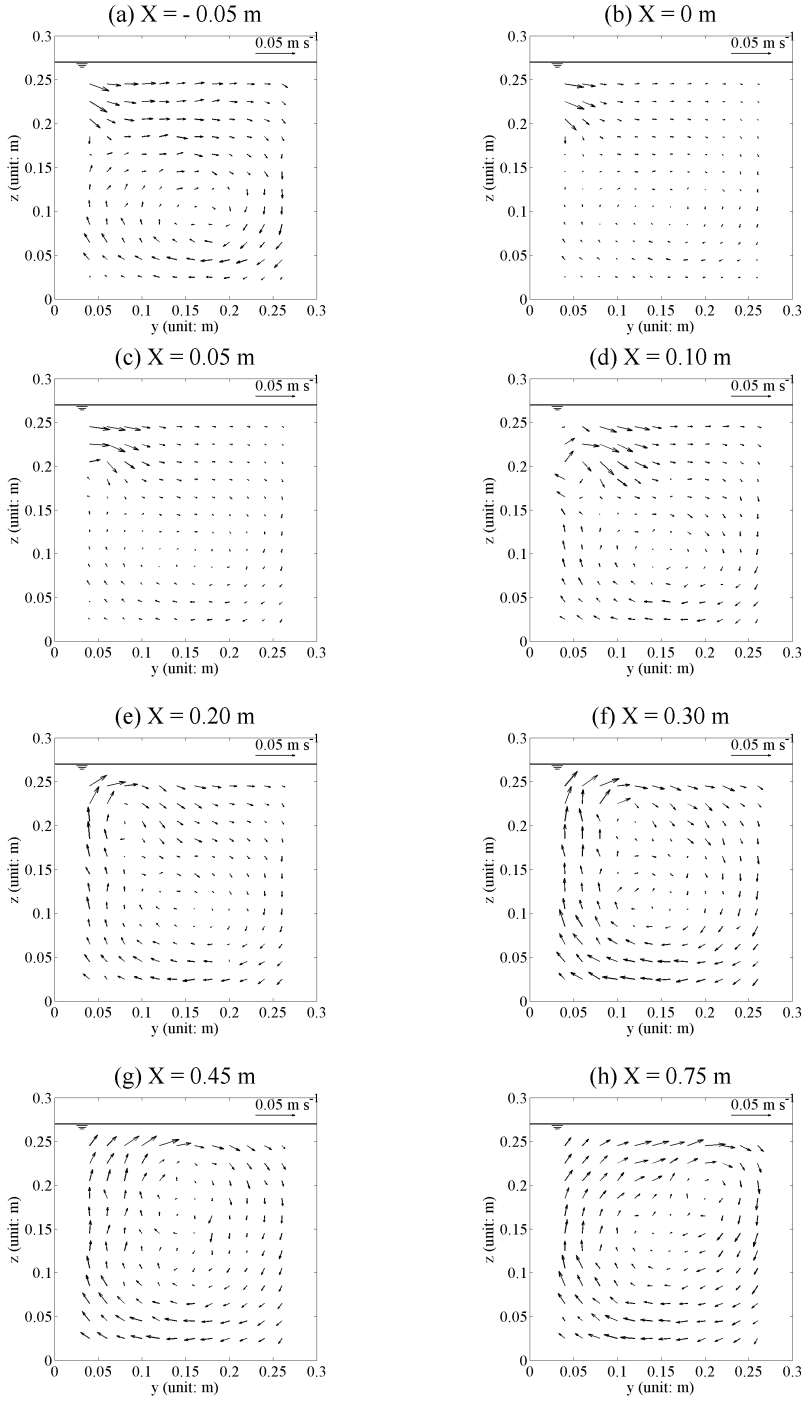

Figure A.68 (AM305) *v*, *w* vector fields

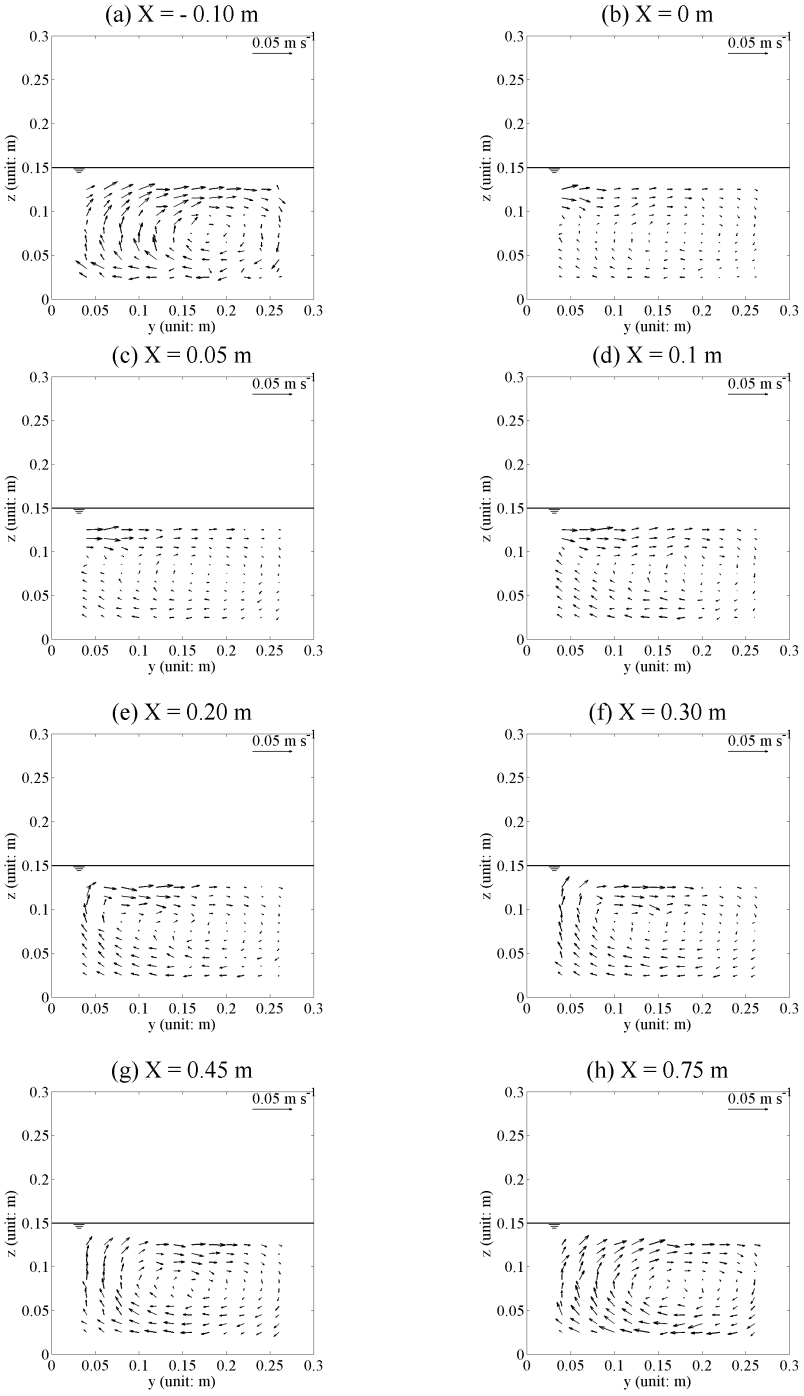

Figure A.69 (AS101) *v*, *w* vector fields

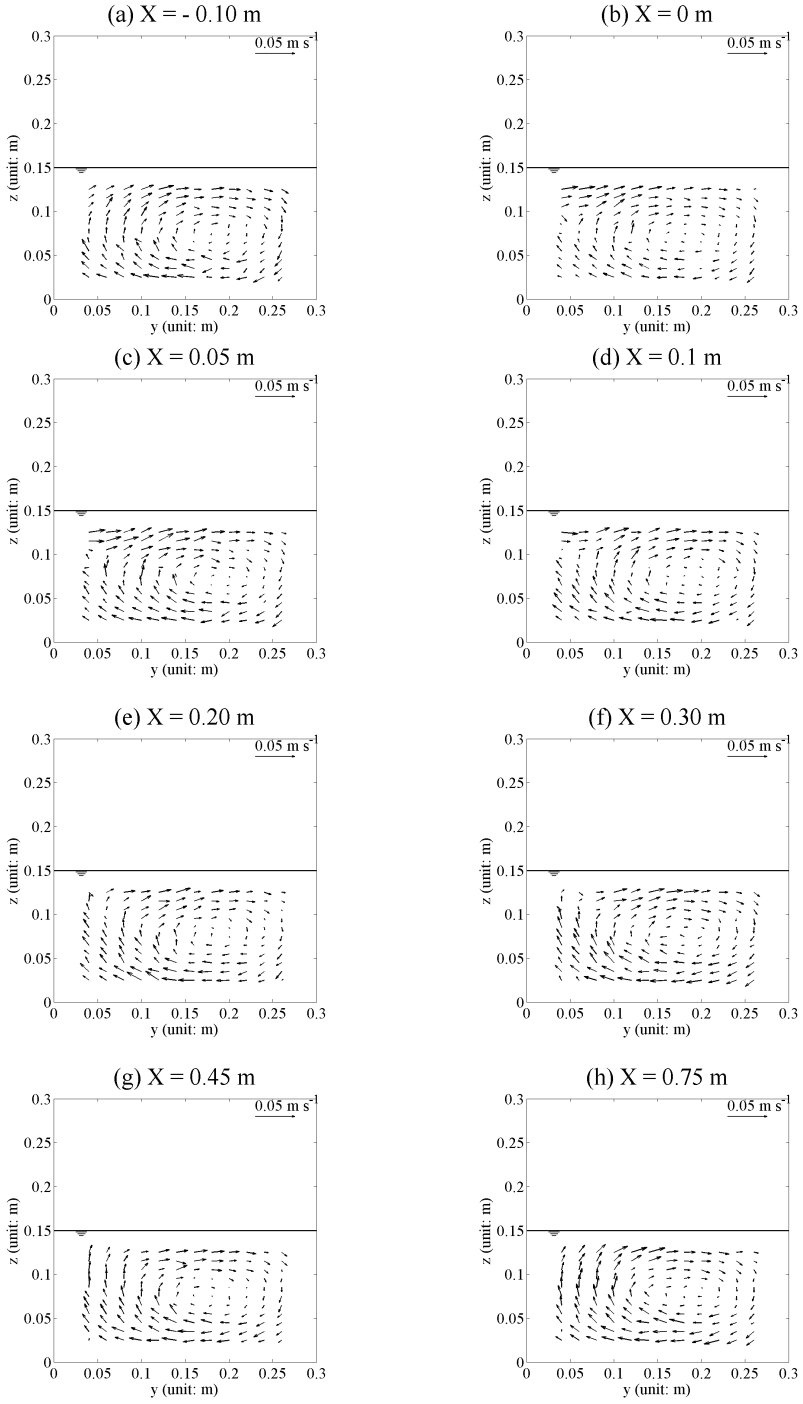

Figure A.70 (AS103) *v*, *w* vector fields

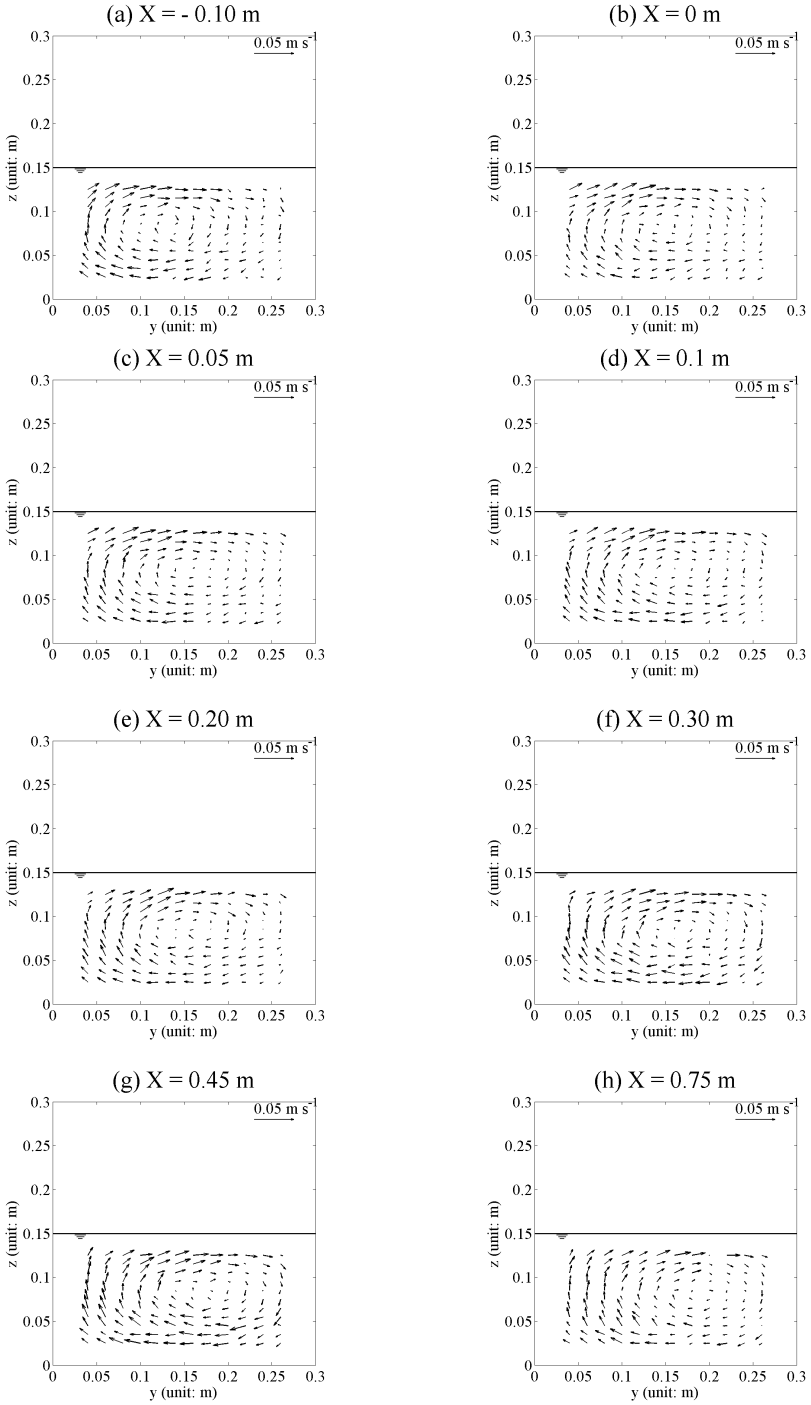

Figure A.71 (AS105) *v*, *w* vector fields

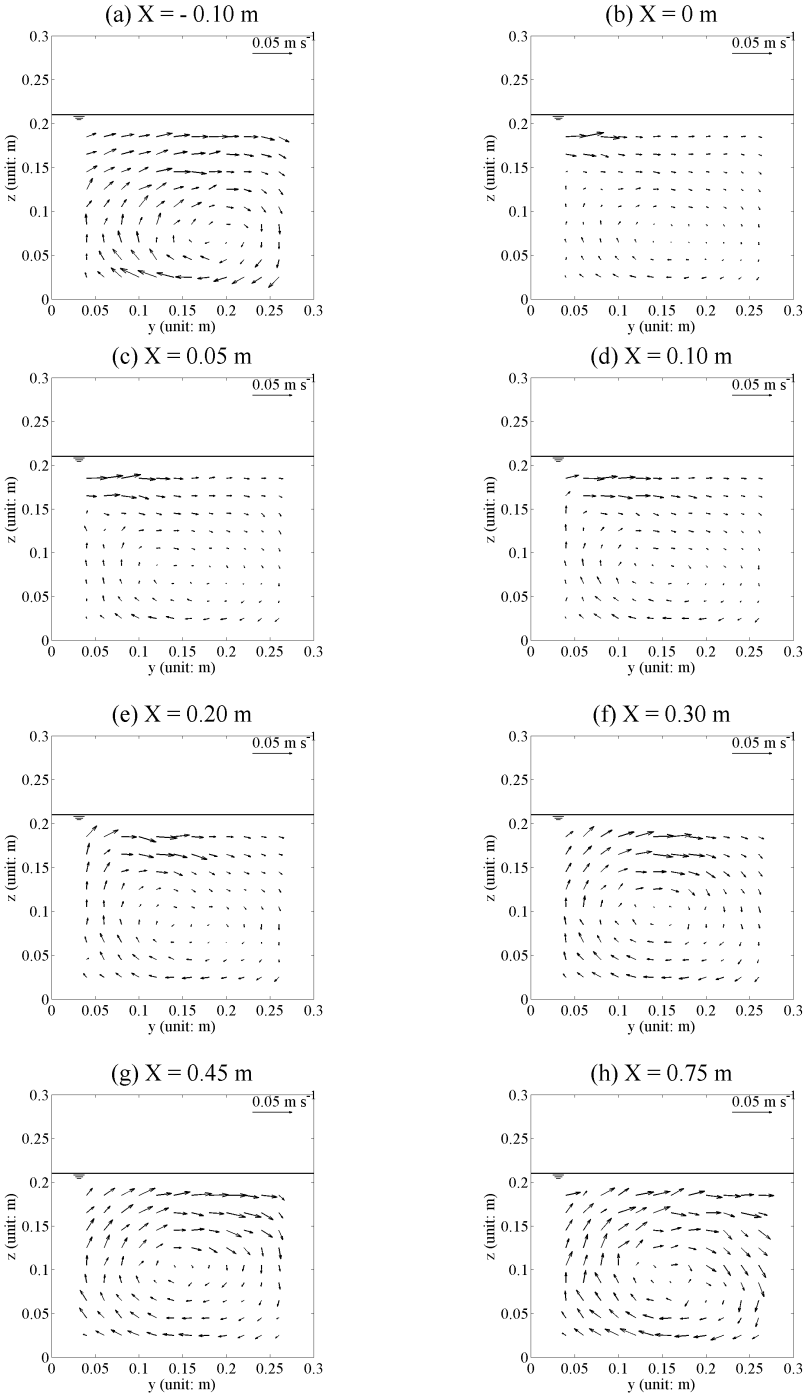

Figure A.72 (AS201) *v*, *w* vector fields

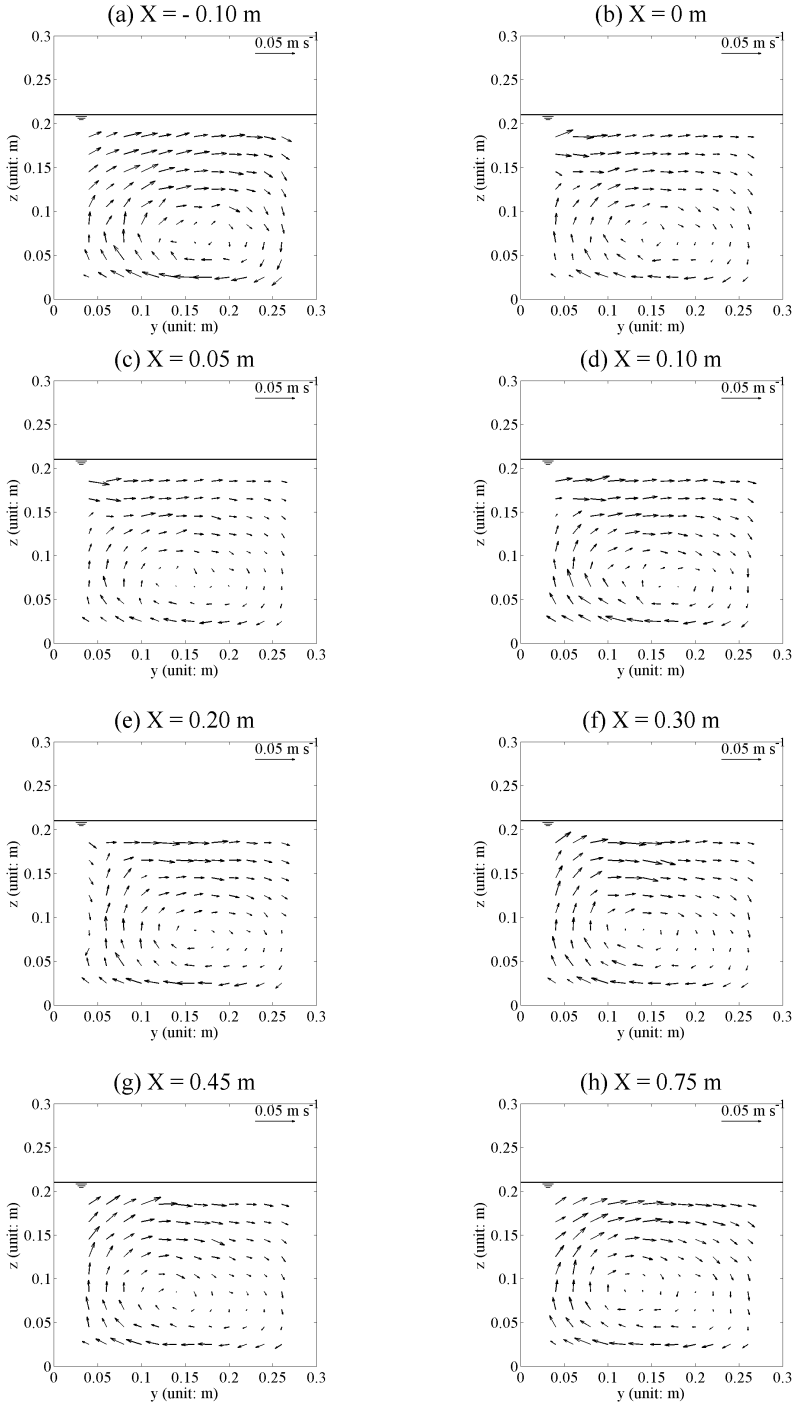

Figure A.73 (AS203) *v*, *w* vector fields

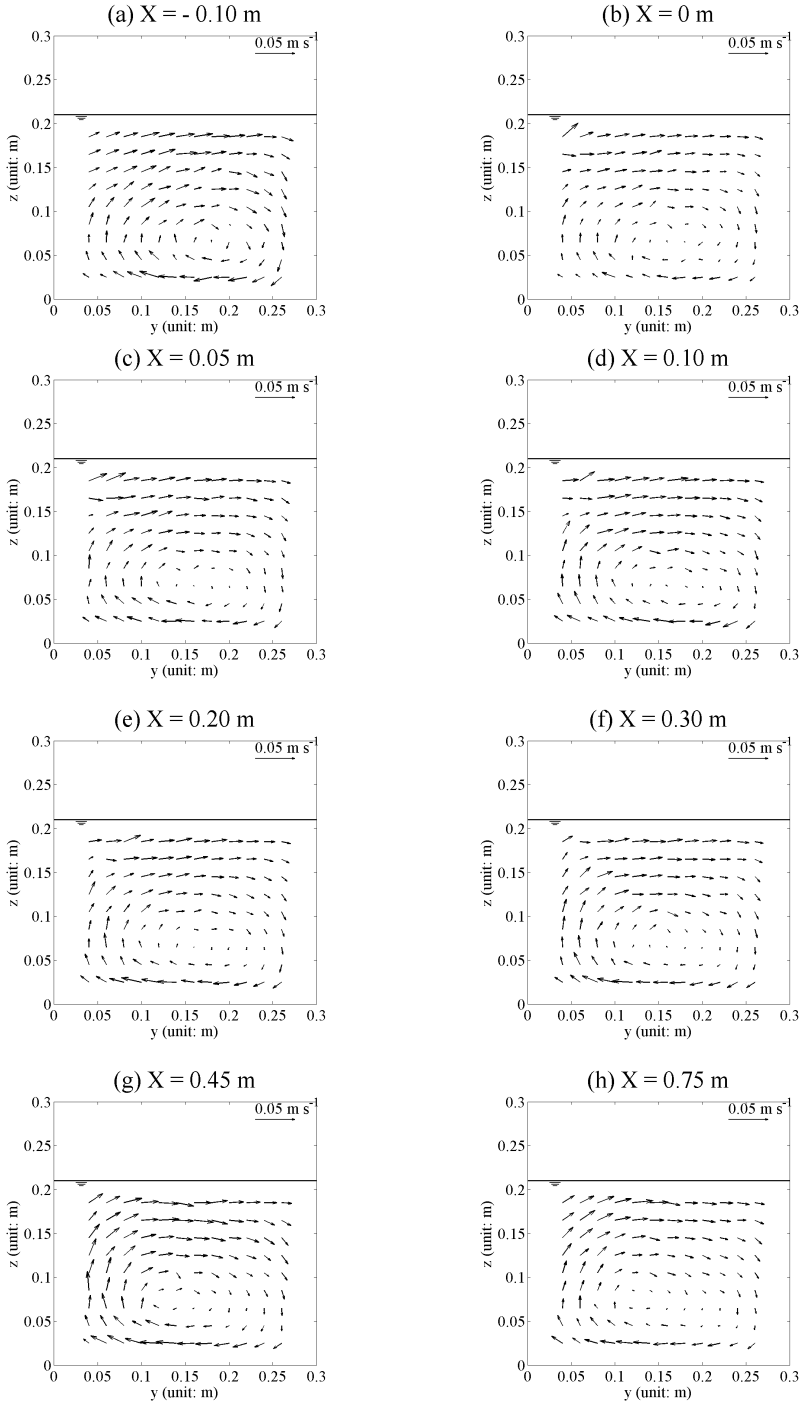

Figure A.74 (AS205) *v*, *w* vector fields

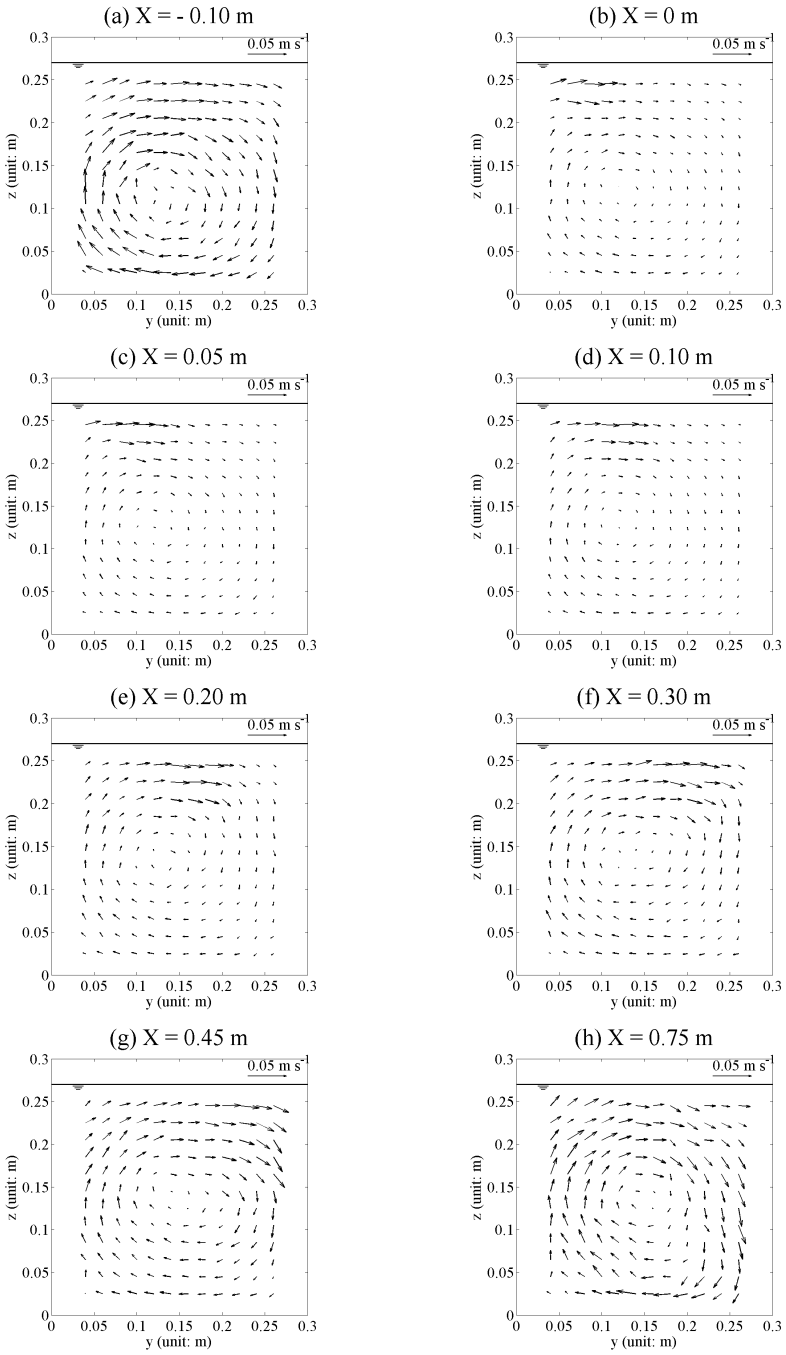

Figure A.75 (AS301) *v*, *w* vector fields

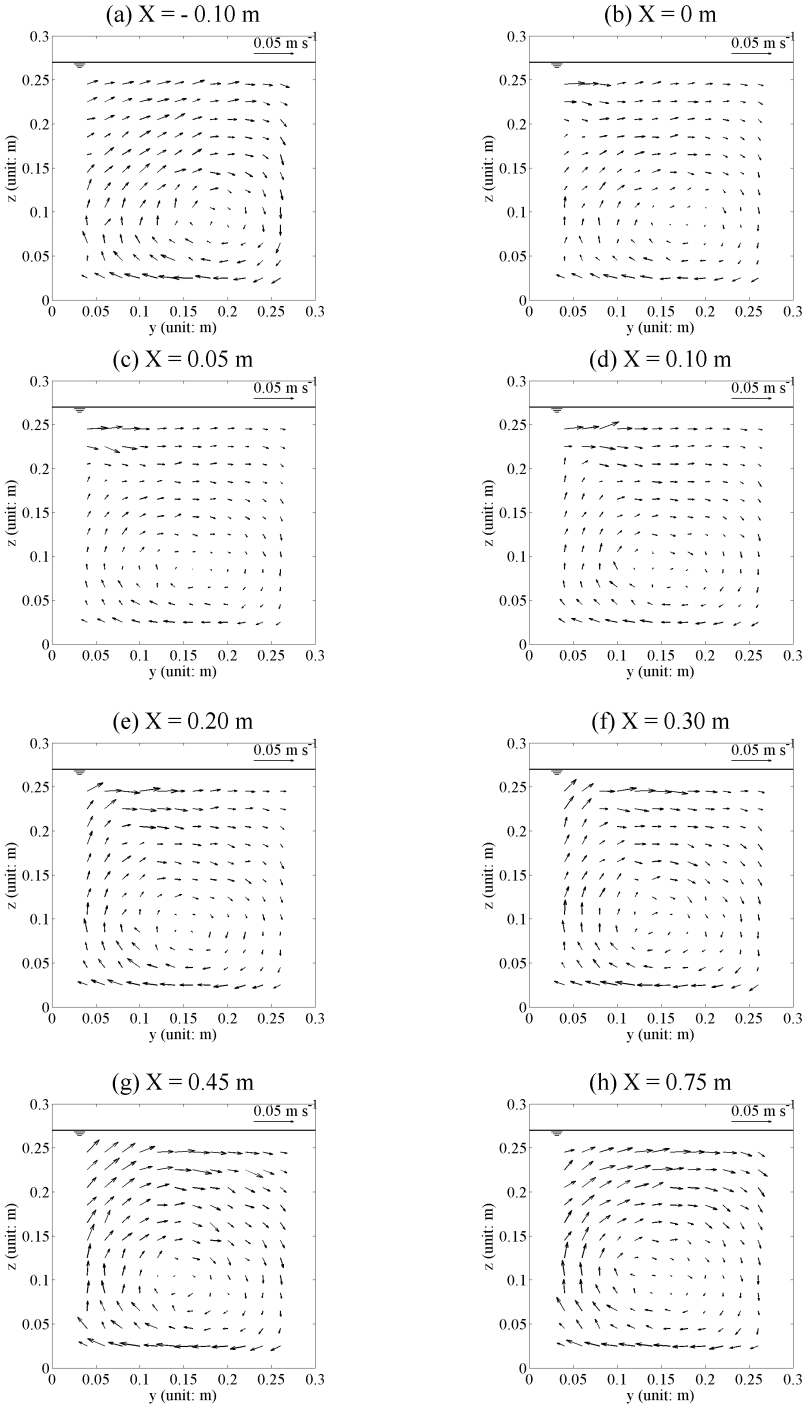

Figure A.76 (AS303) *v*, *w* vector fields

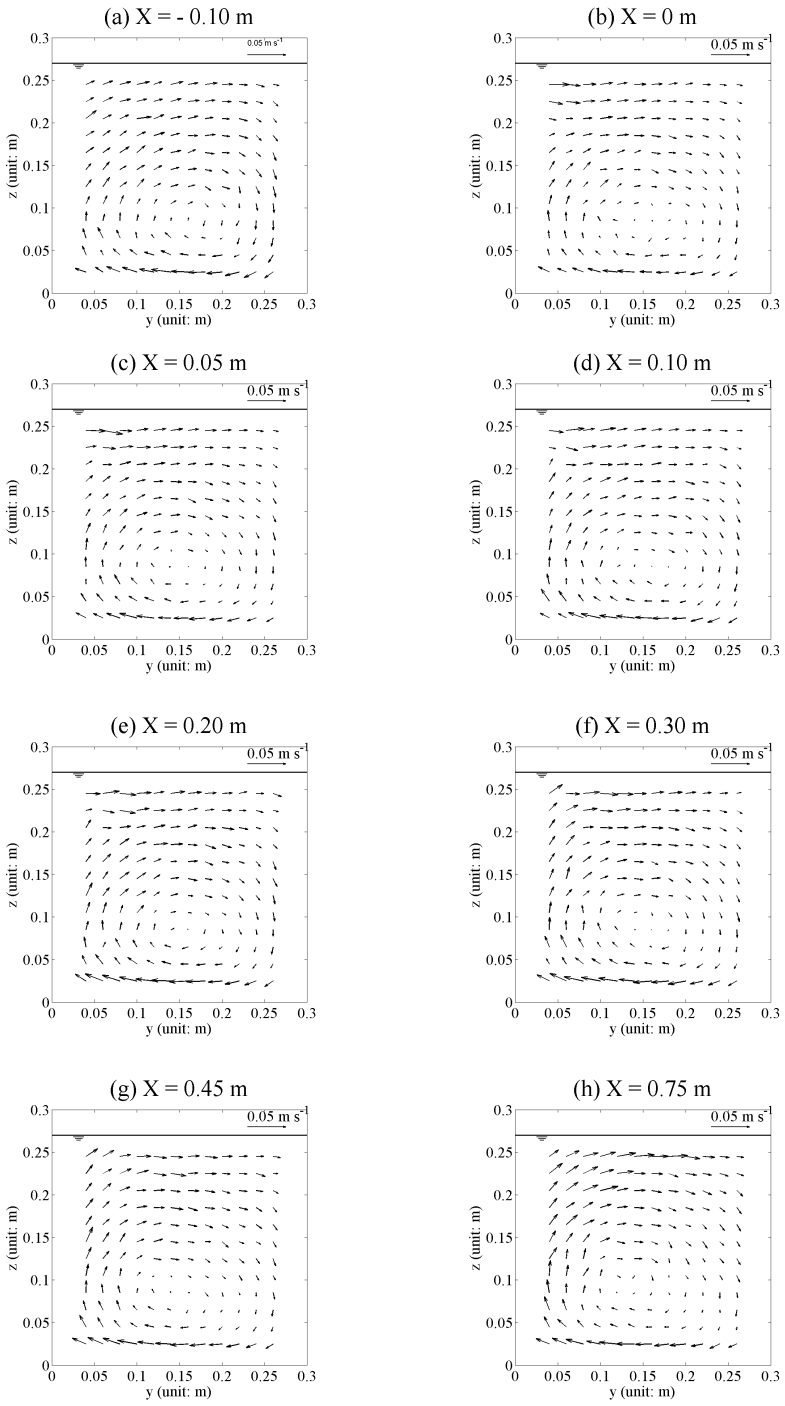

Figure A.77 (AS305) *v*, *w* vector fields

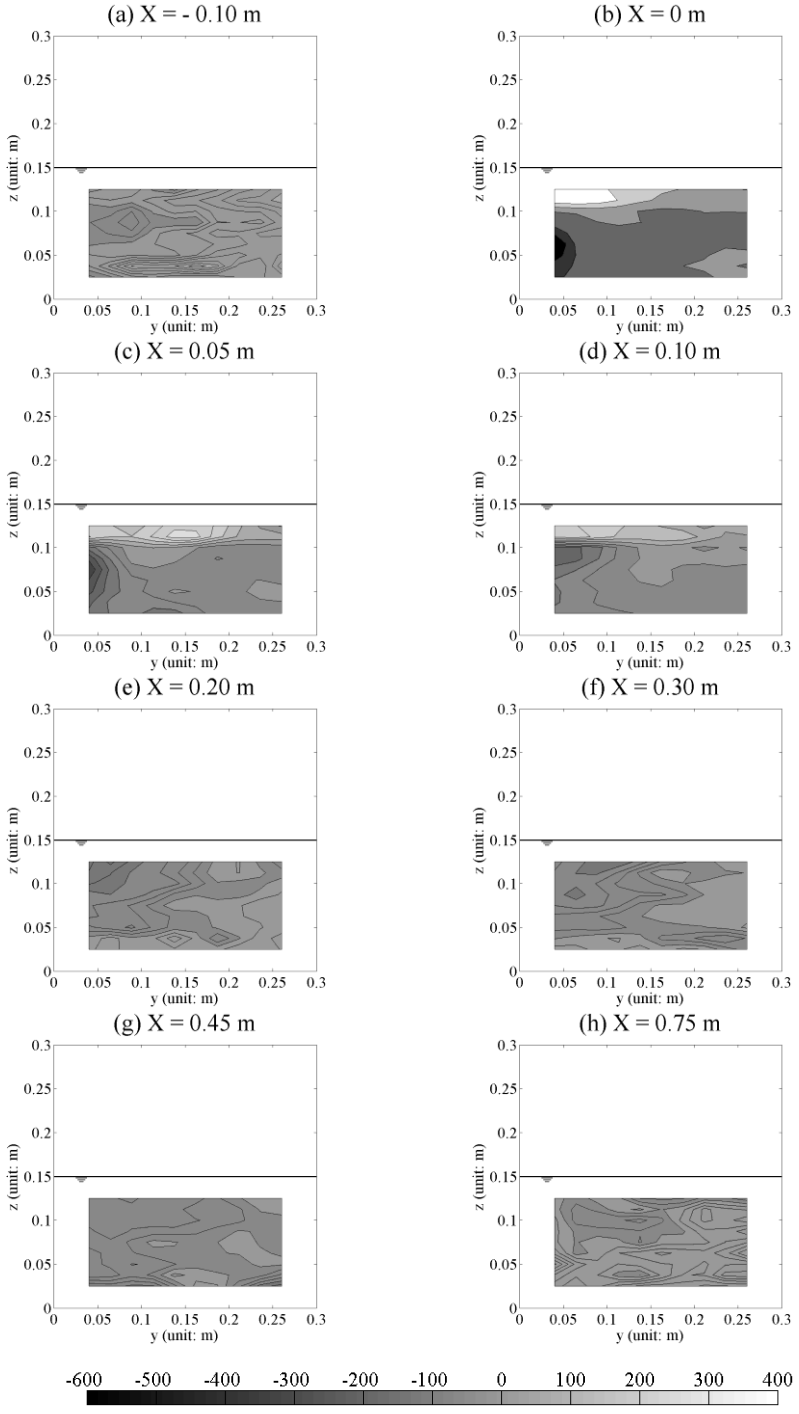

Figure A.78 (AR101) Vorticity contours

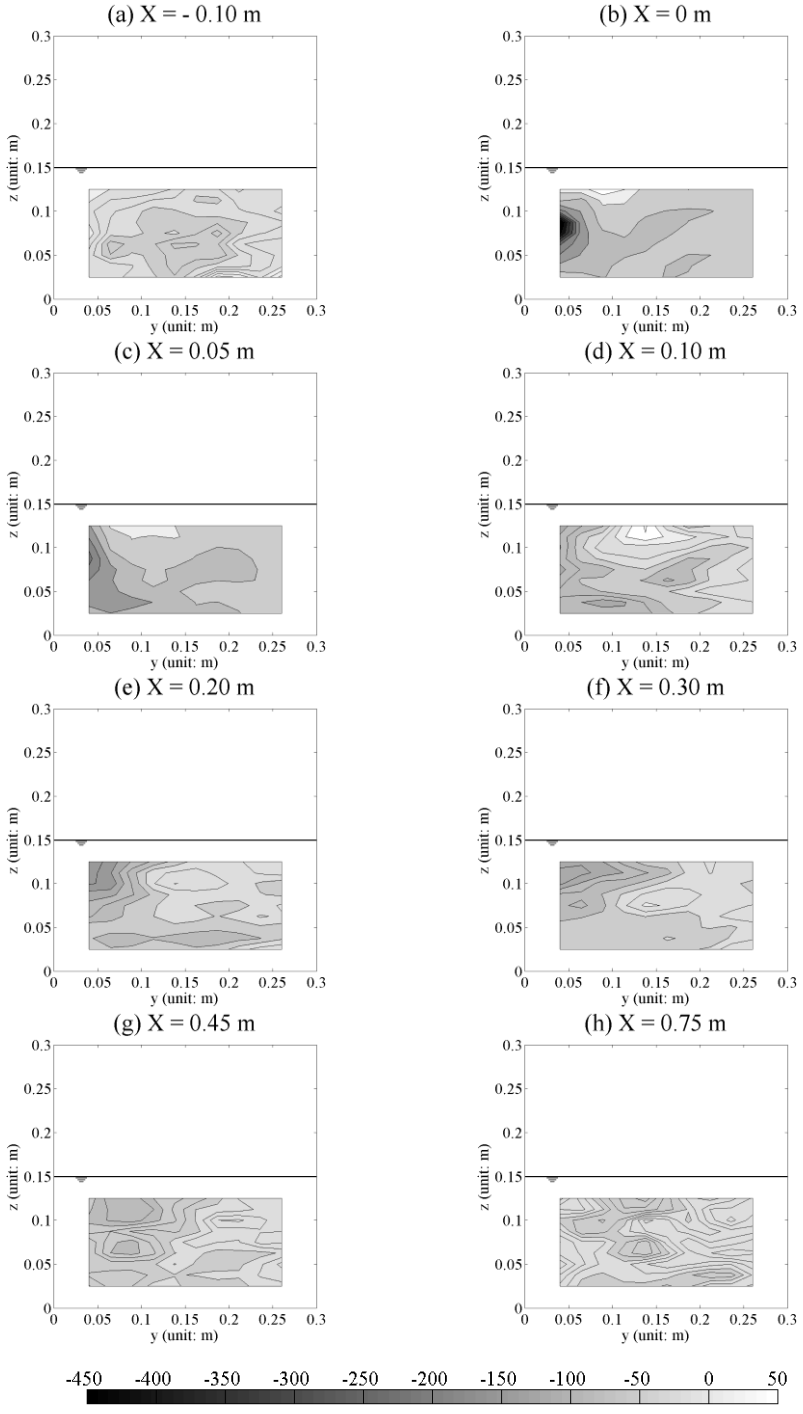

Figure A.79 (AR102) Vorticity contours

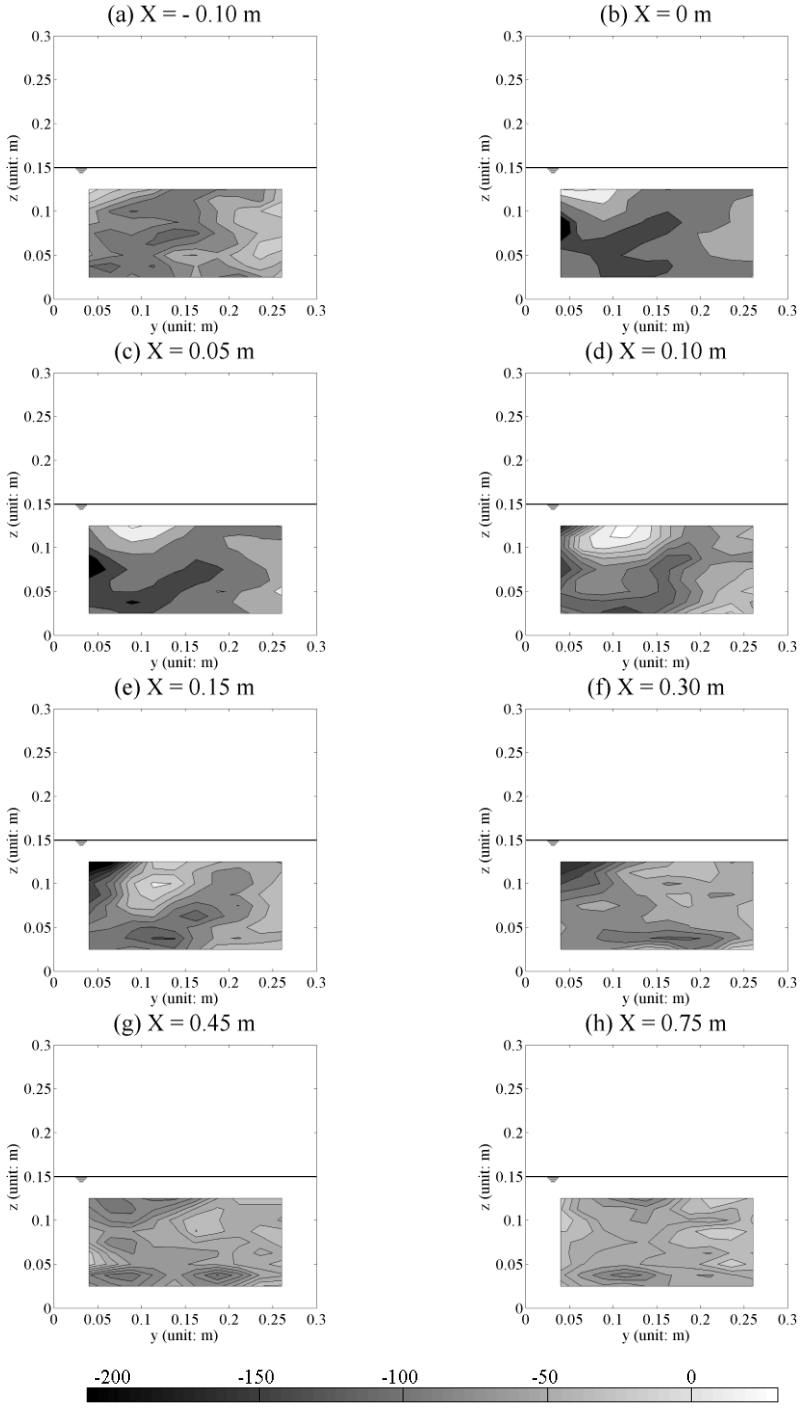

Figure A.80 (AR104) Vorticity contours

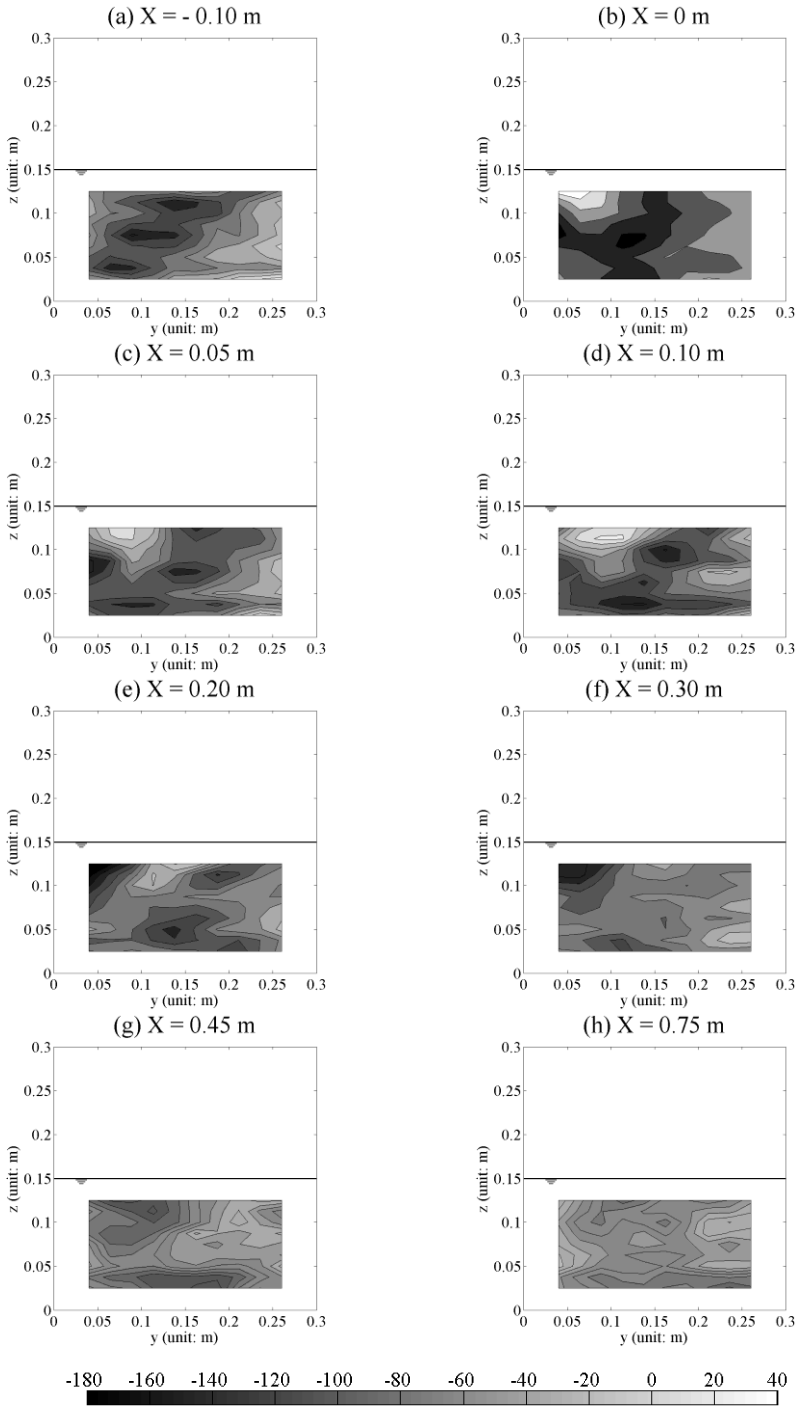

Figure A.81 (AR105) Vorticity contours

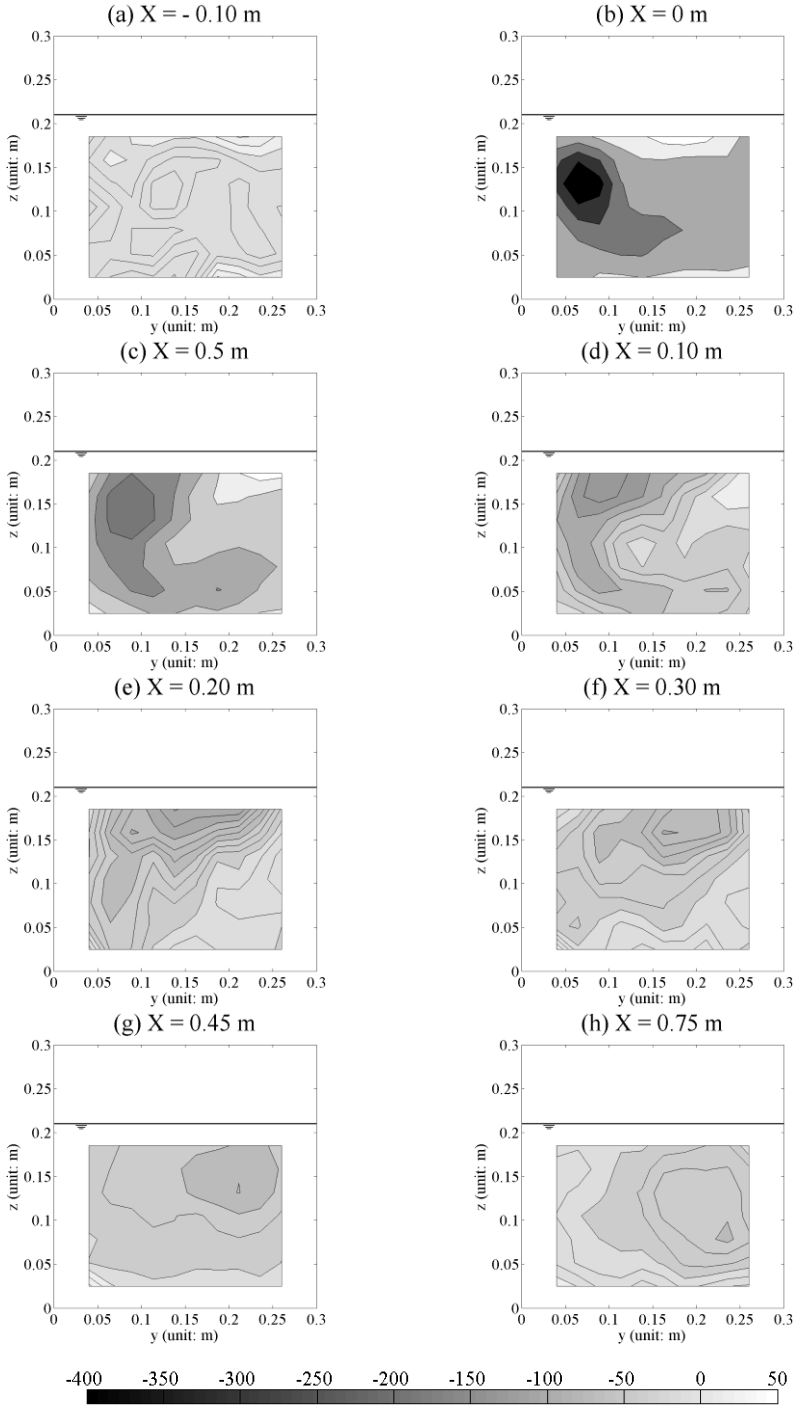

Figure A.82 (AR201) Vorticity contours

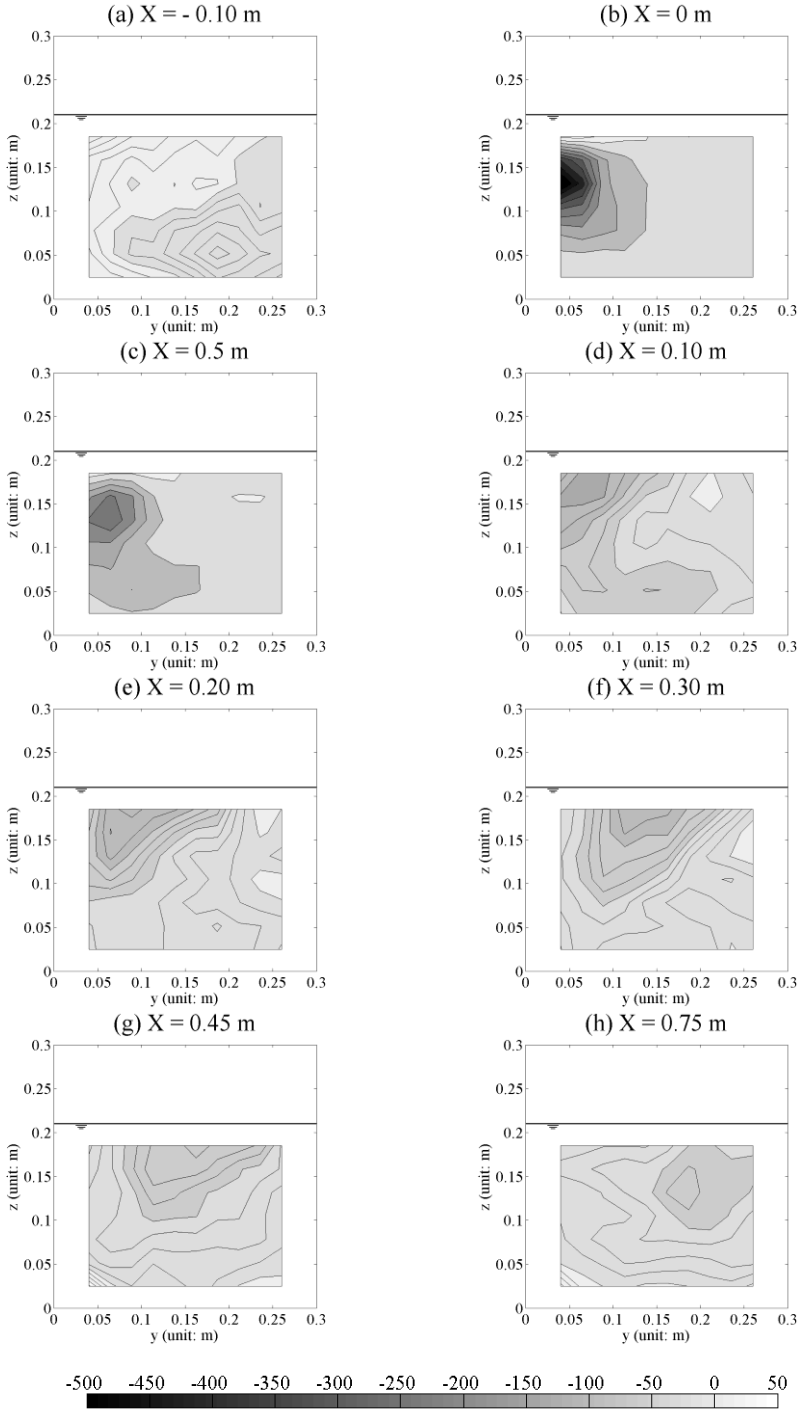

Figure A.83 (AR202) Vorticity contours

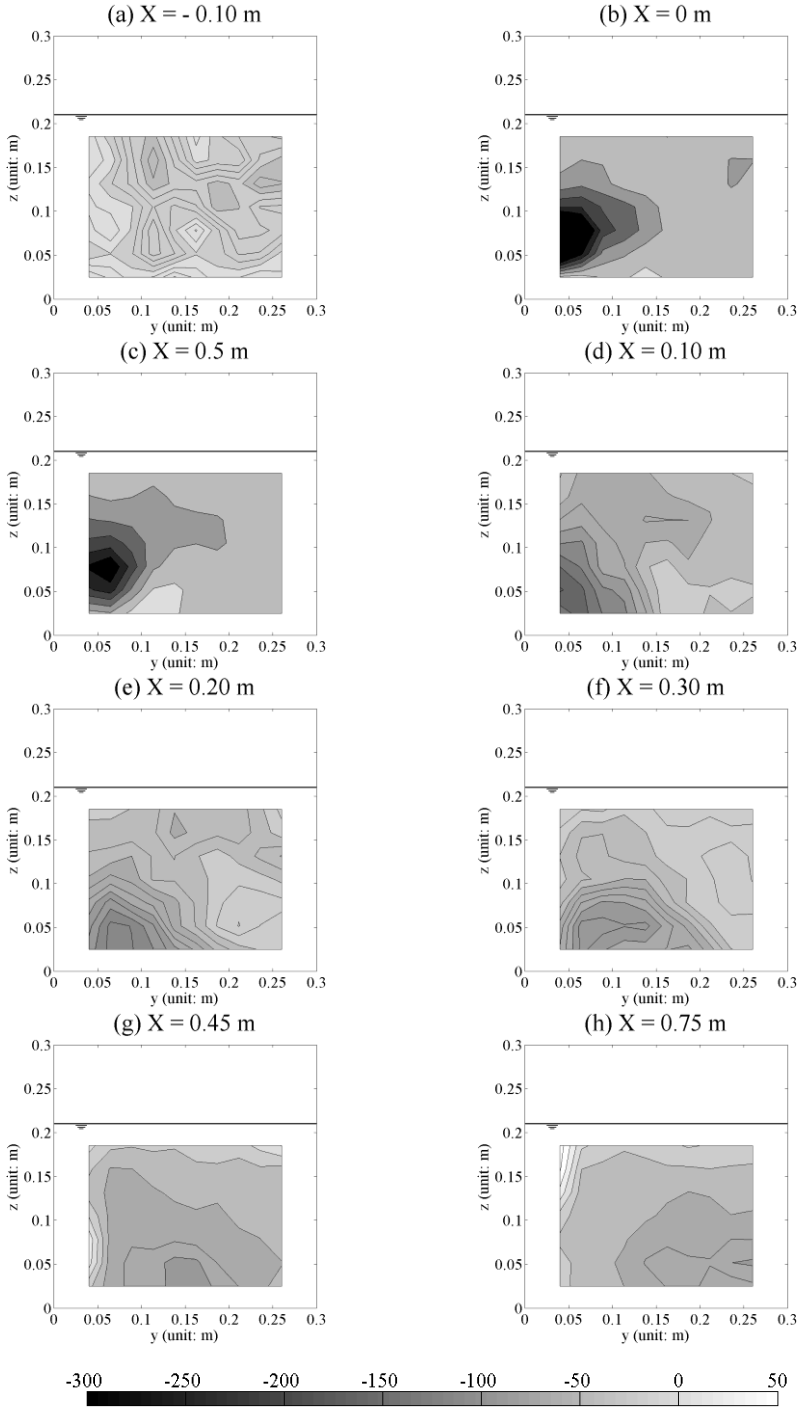

Figure A.84 (AR203) Vorticity contours

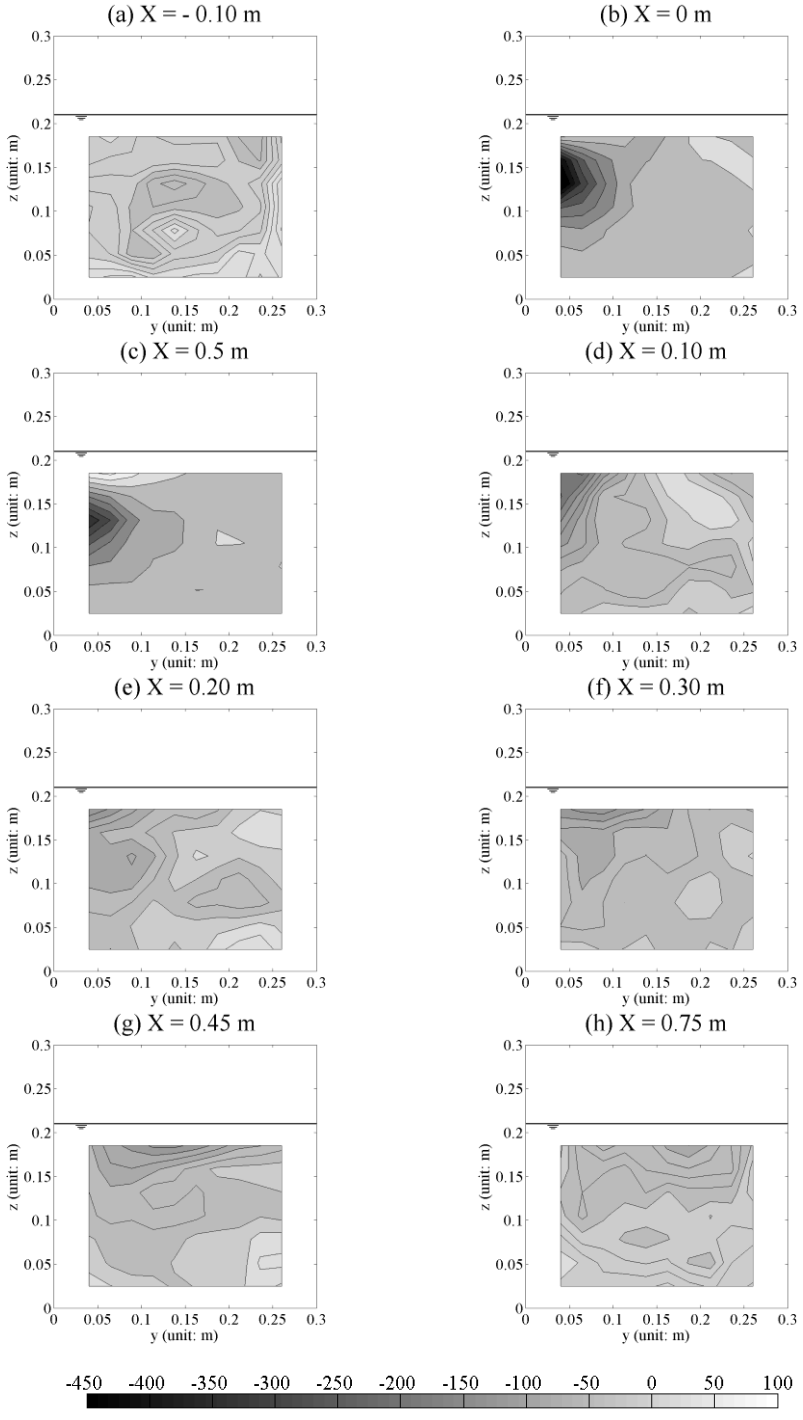

Figure A.85 (AR204) Vorticity contours

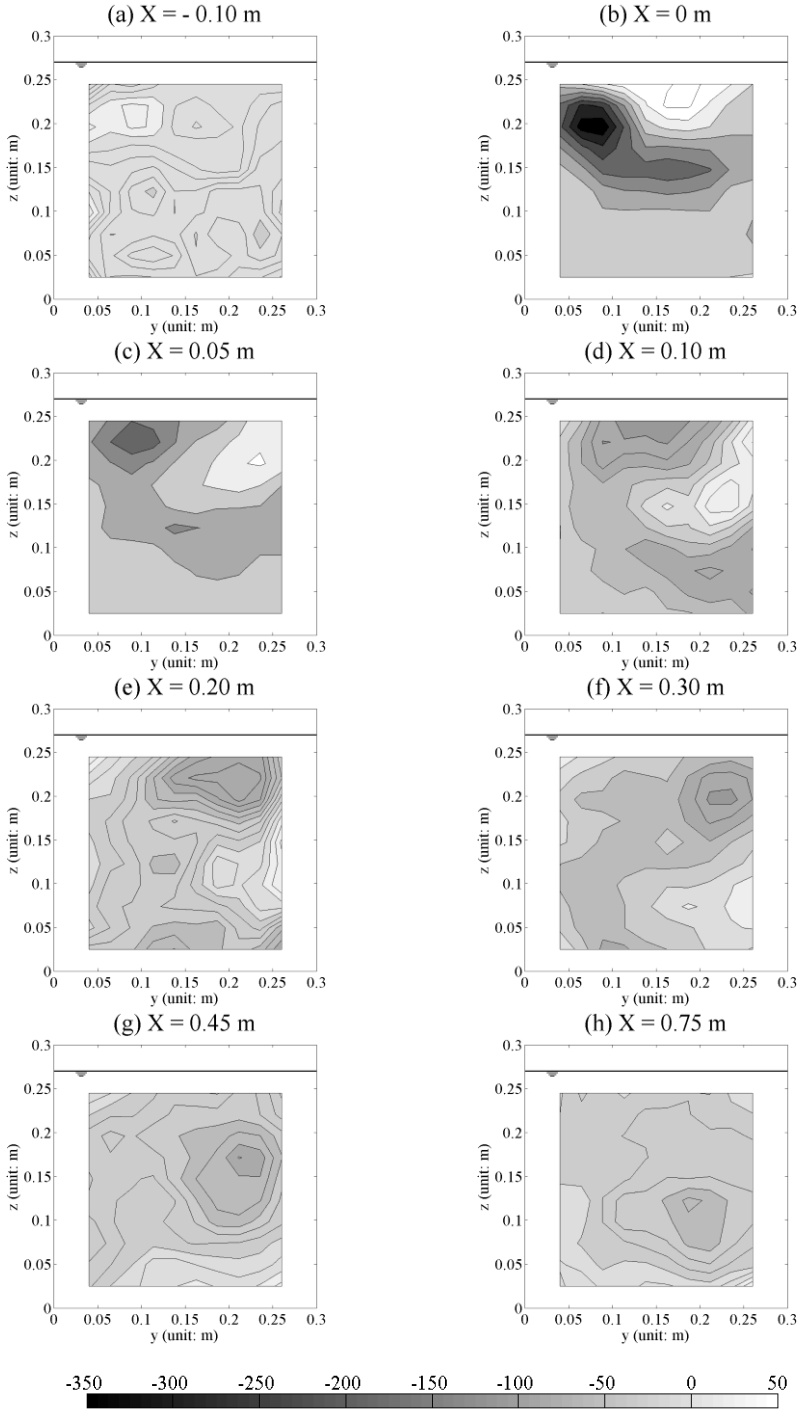

Figure A.86 (AR301) Vorticity contours

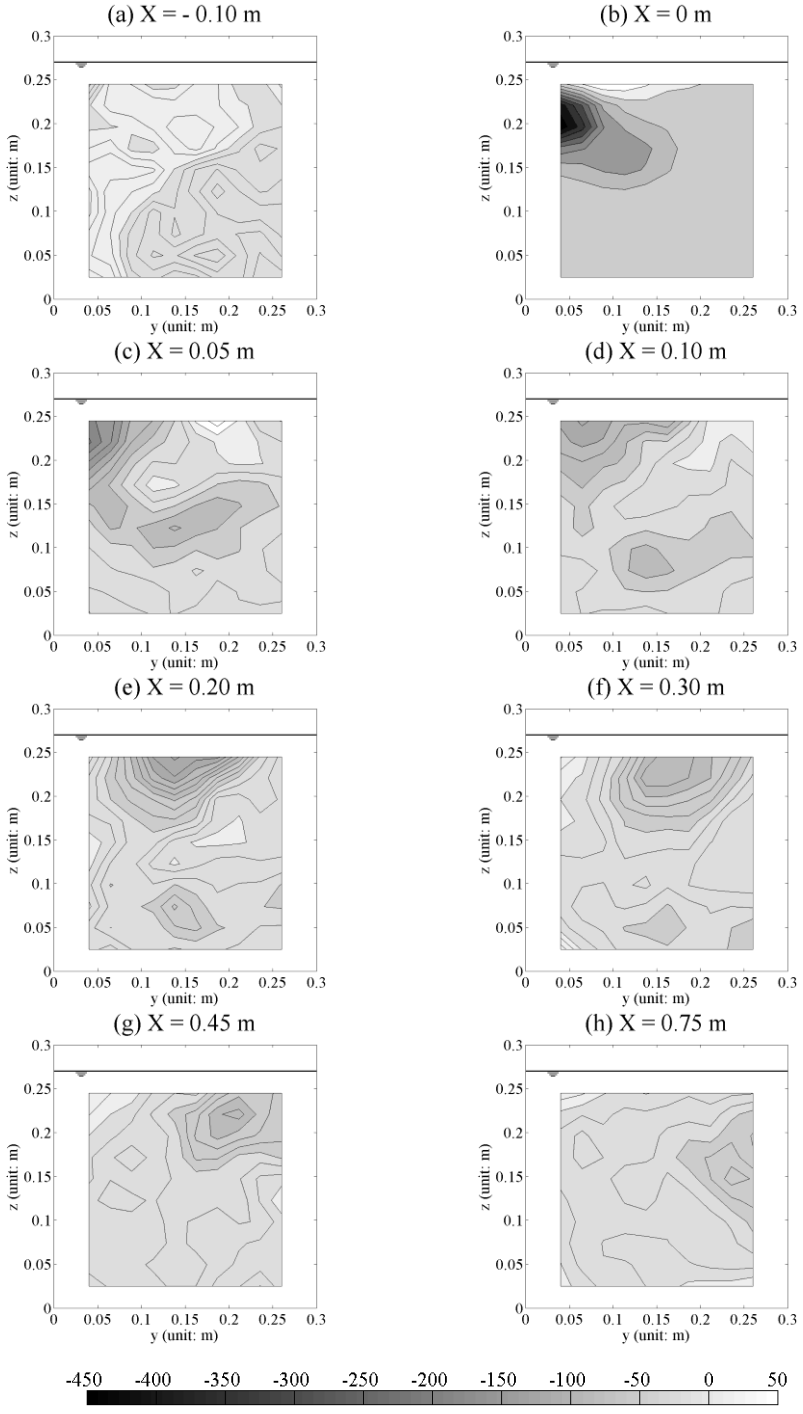

Figure A.87 (AR302) Vorticity contours

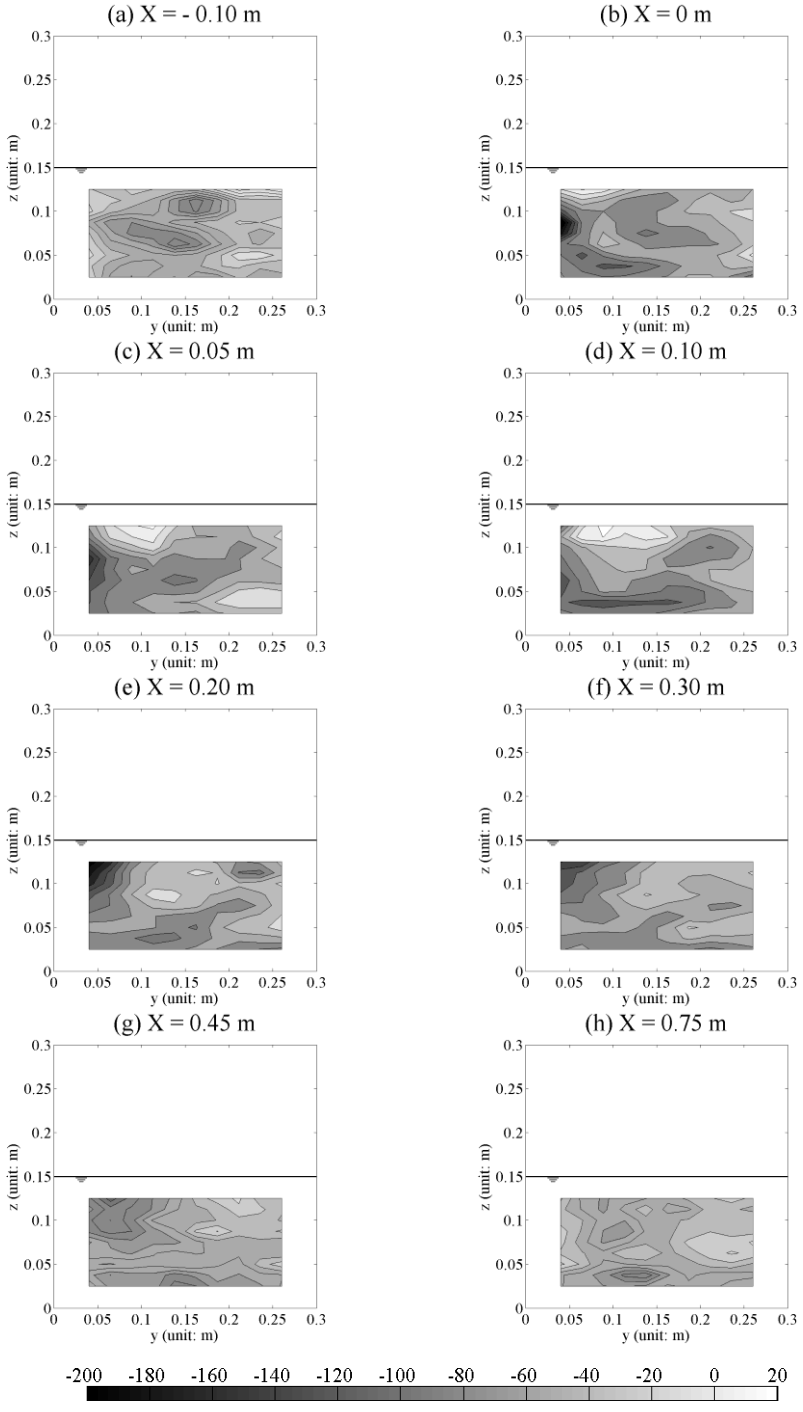

Figure 4.88 (AR103) Vorticity contours

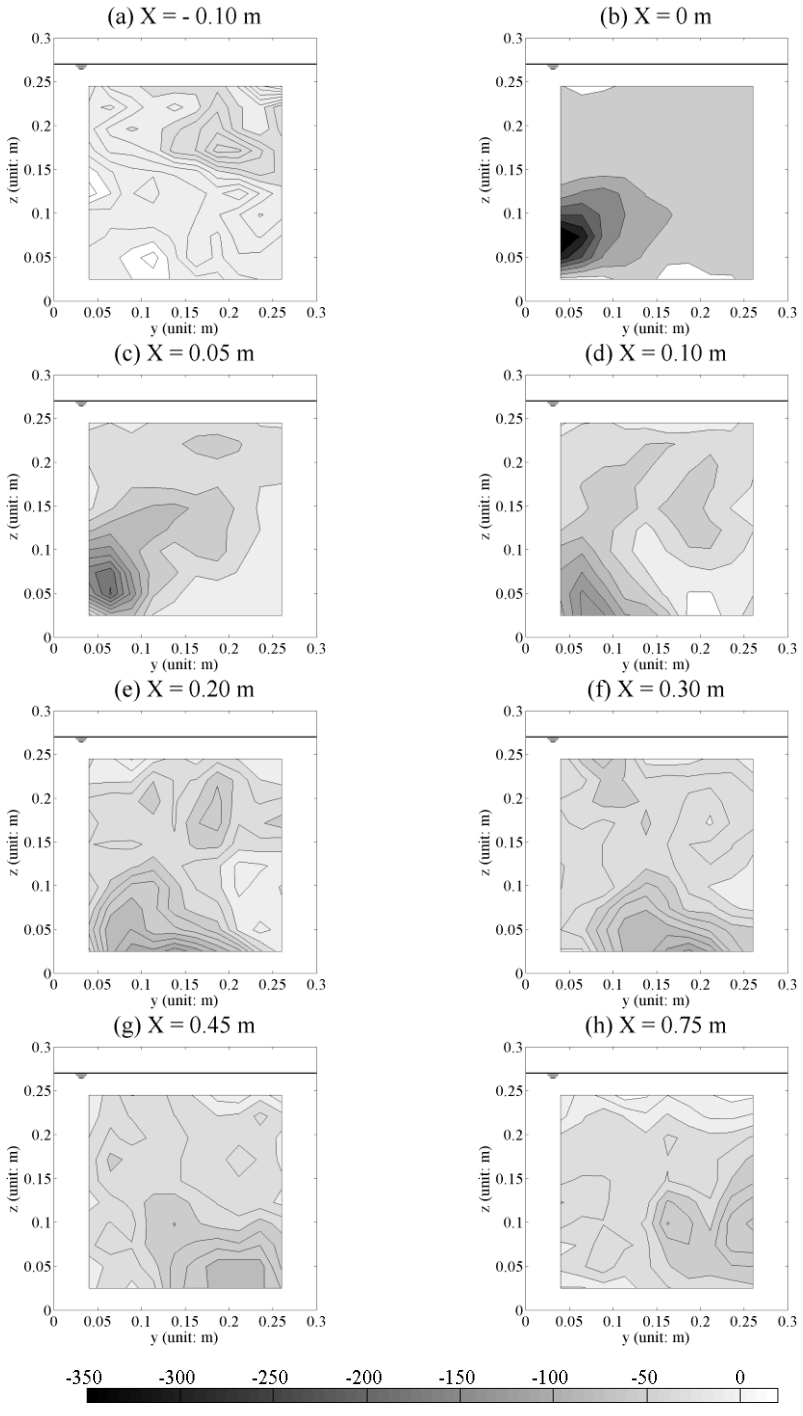

Figure 4.89 (AR303) Vorticity contours

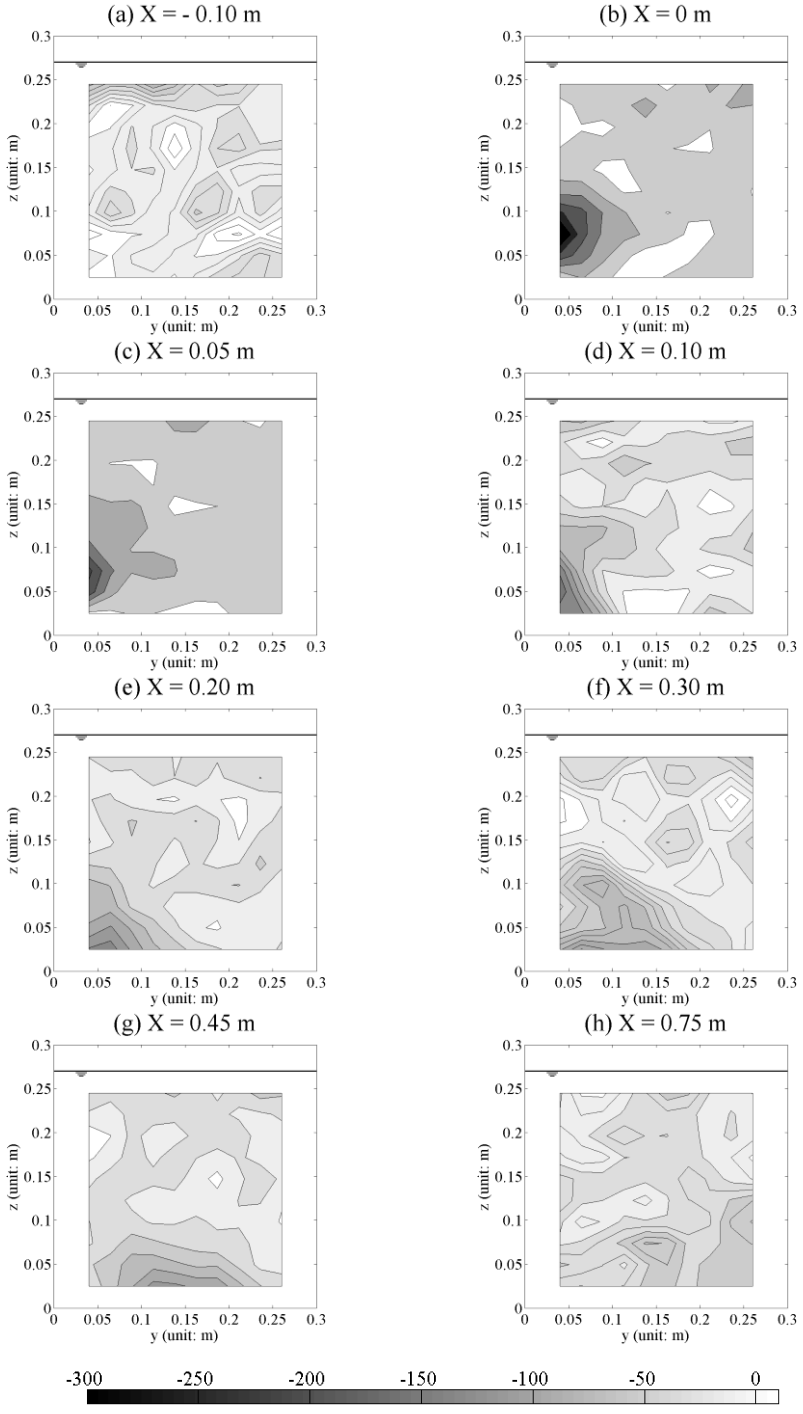

Figure A.90 (AR304) Vorticity contours

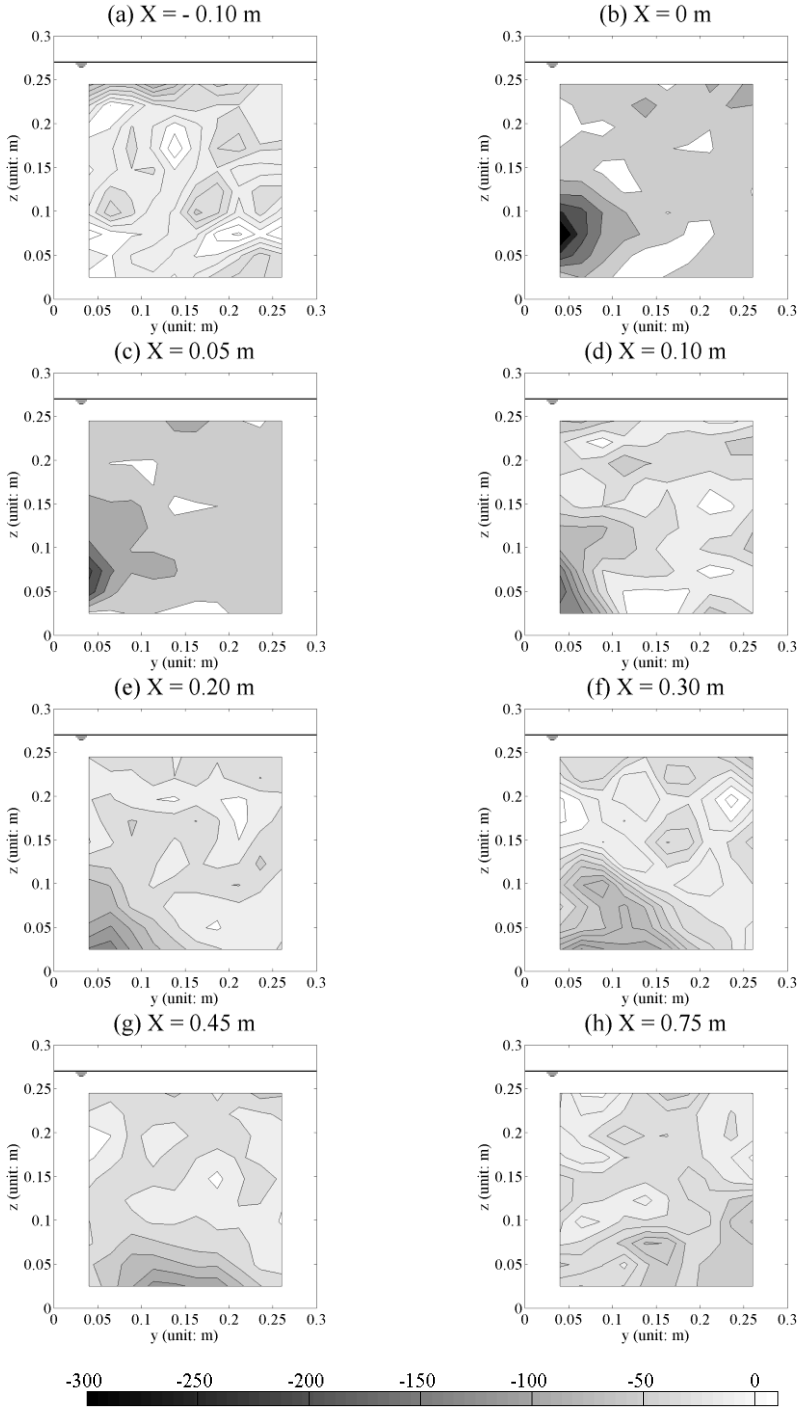

Figure A.91 (AR305) Vorticity contours

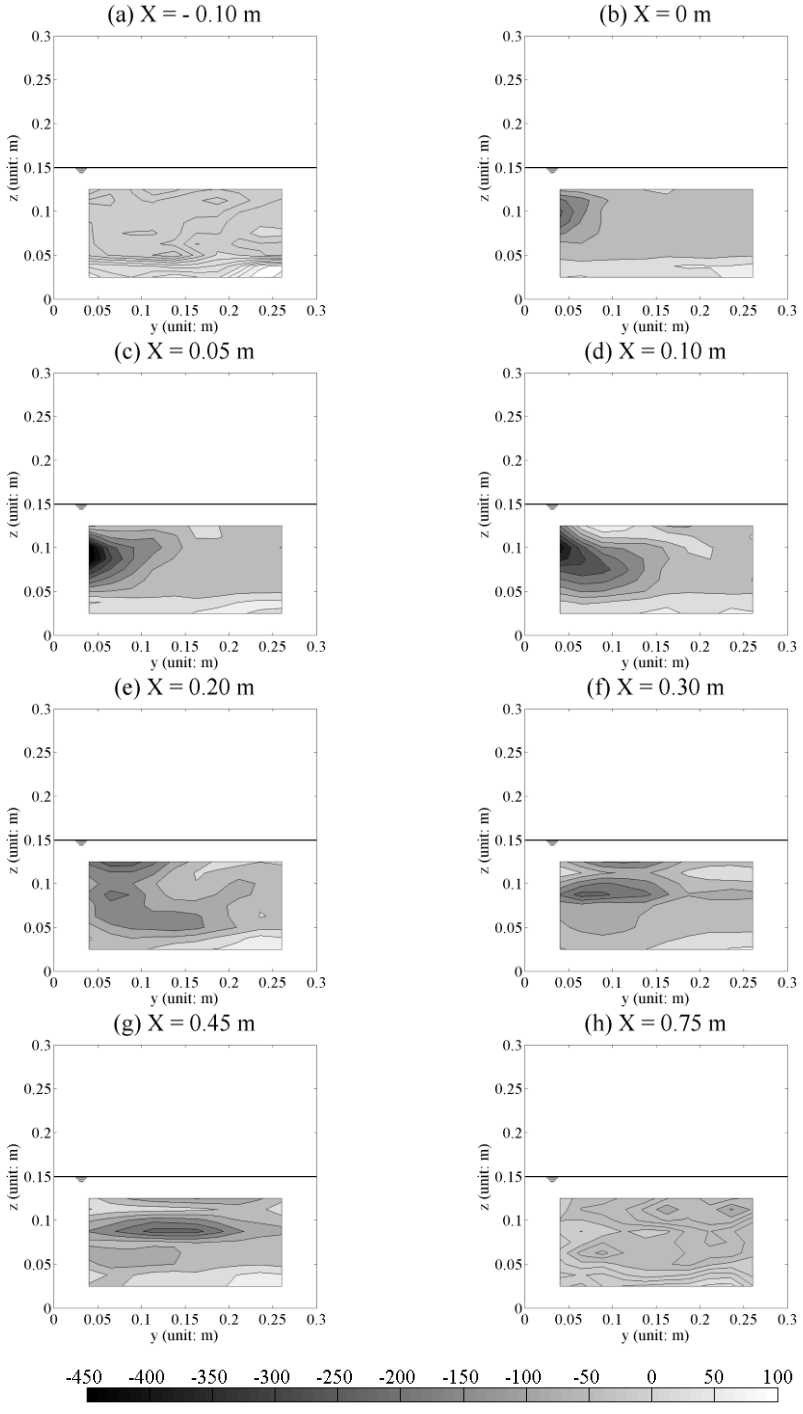

Figure A.92 (AM101) Vorticity contours

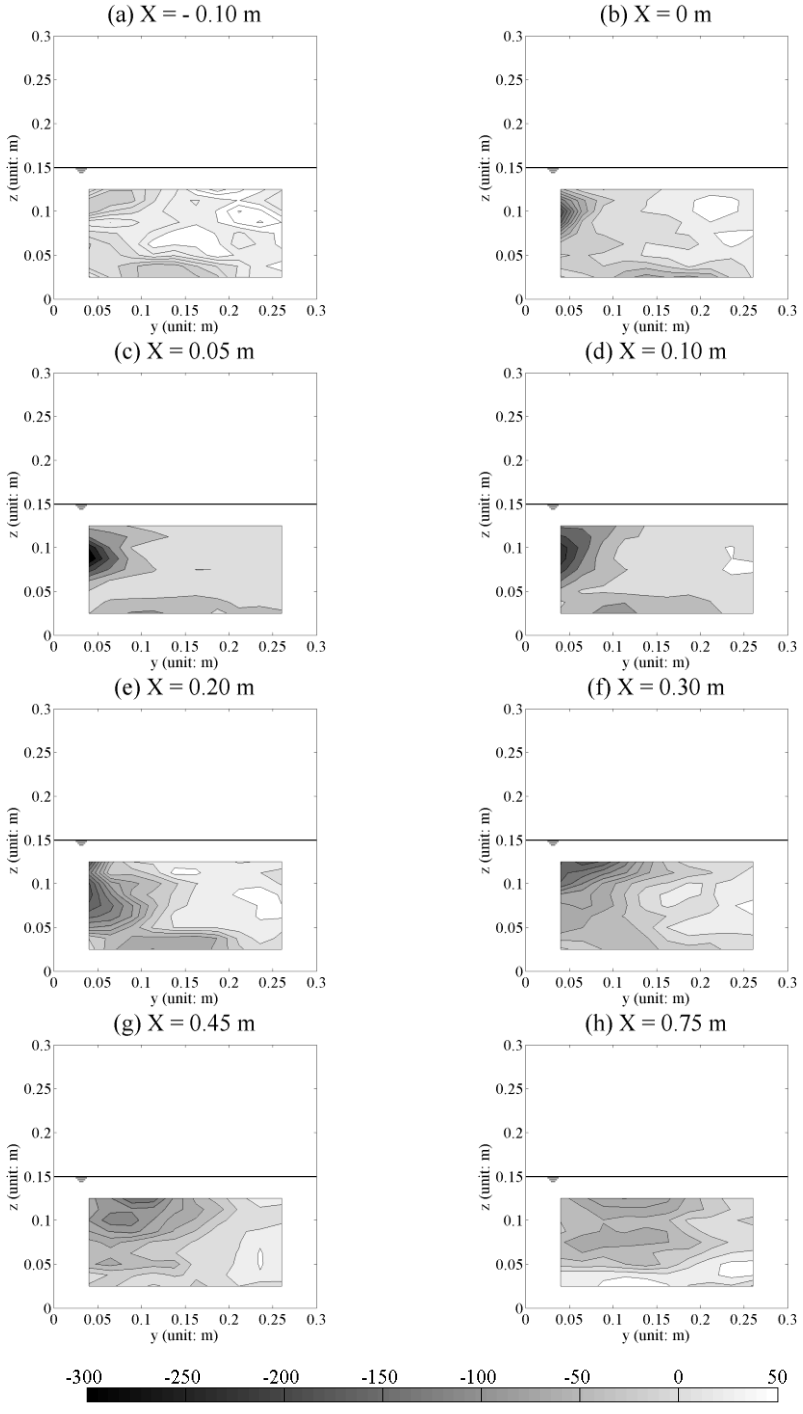

Figure A.93 (AM102) Vorticity contours

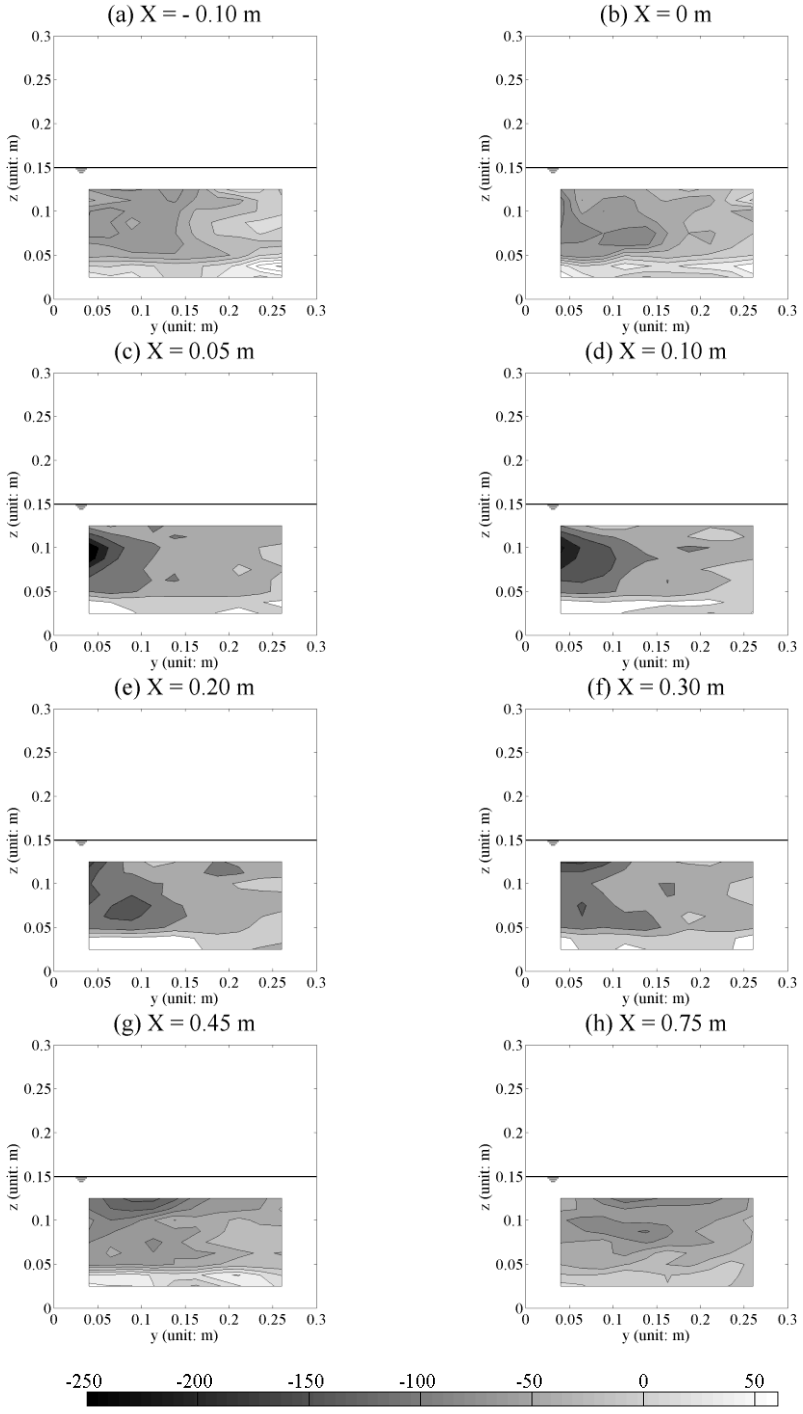

Figure A.94 (AM103) Vorticity contours

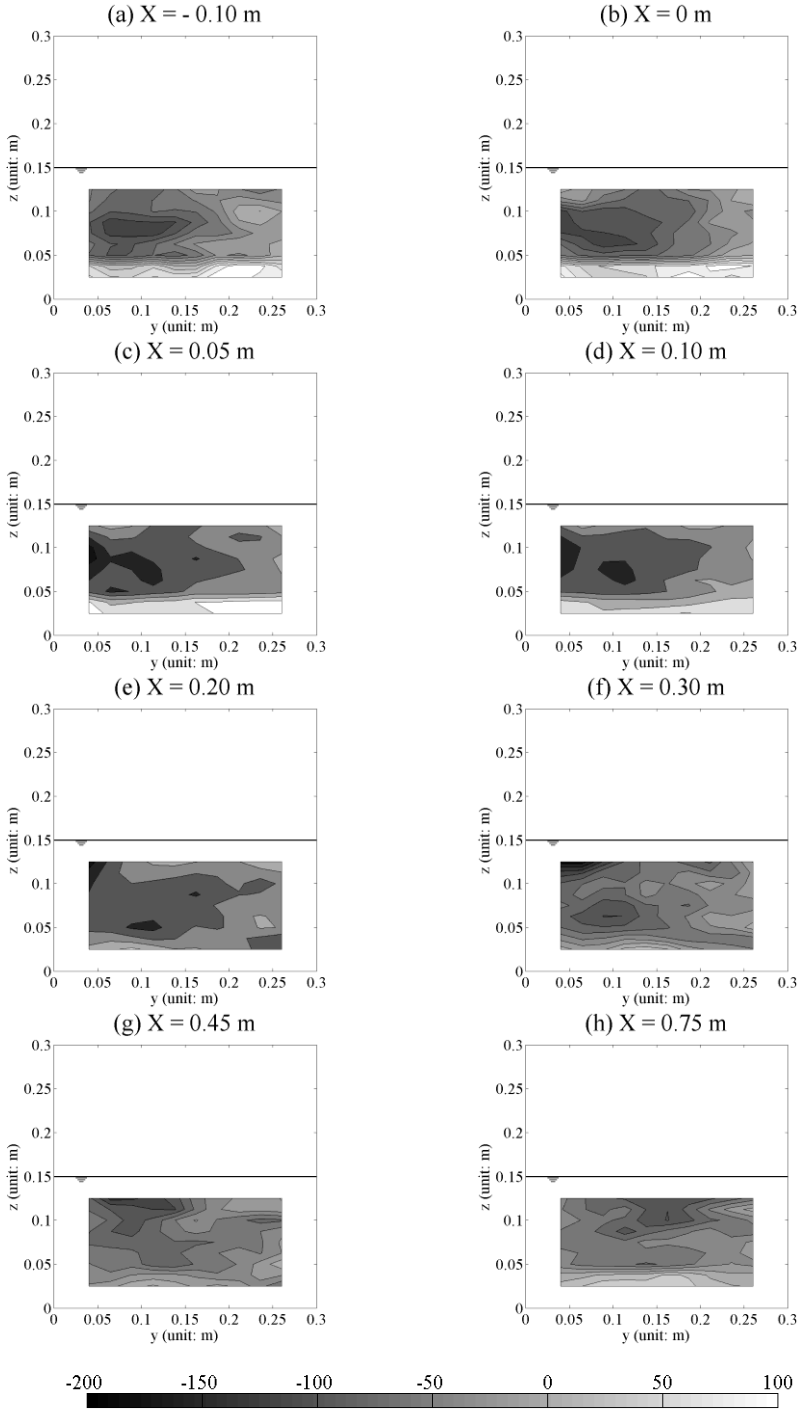

Figure A.95 (AM104) Vorticity contours

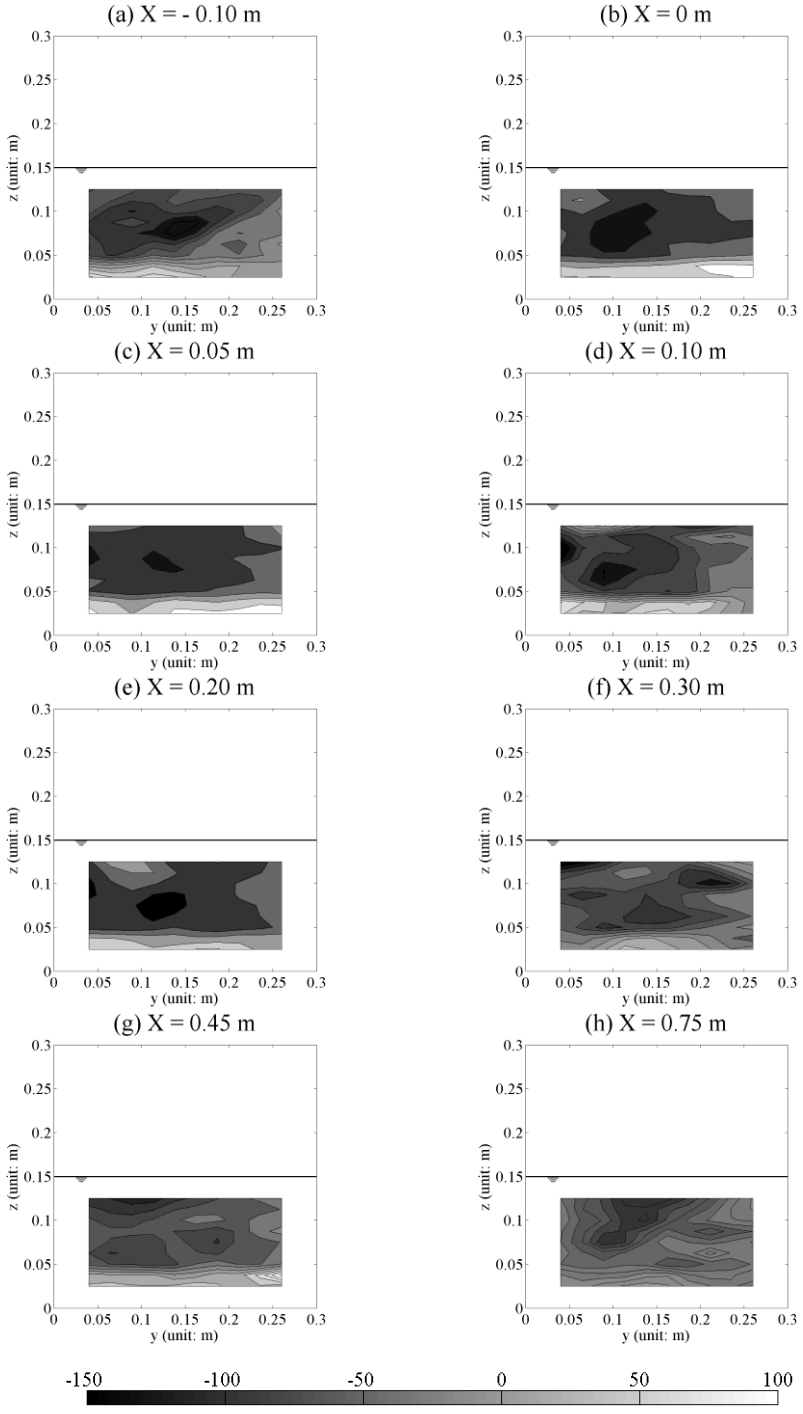

Figure A.96 (AM105) Vorticity contours

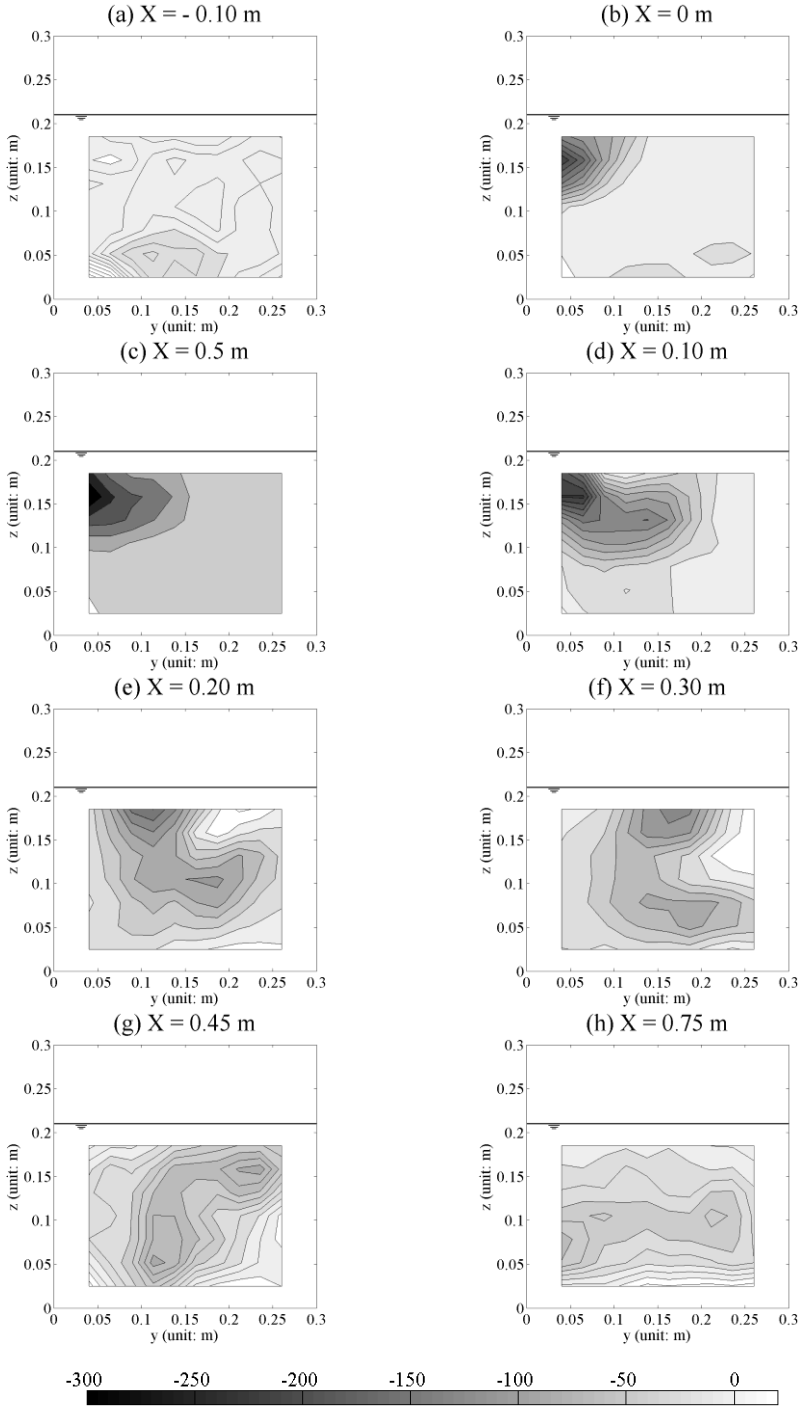

Figure A.97 (AM201) Vorticity contours

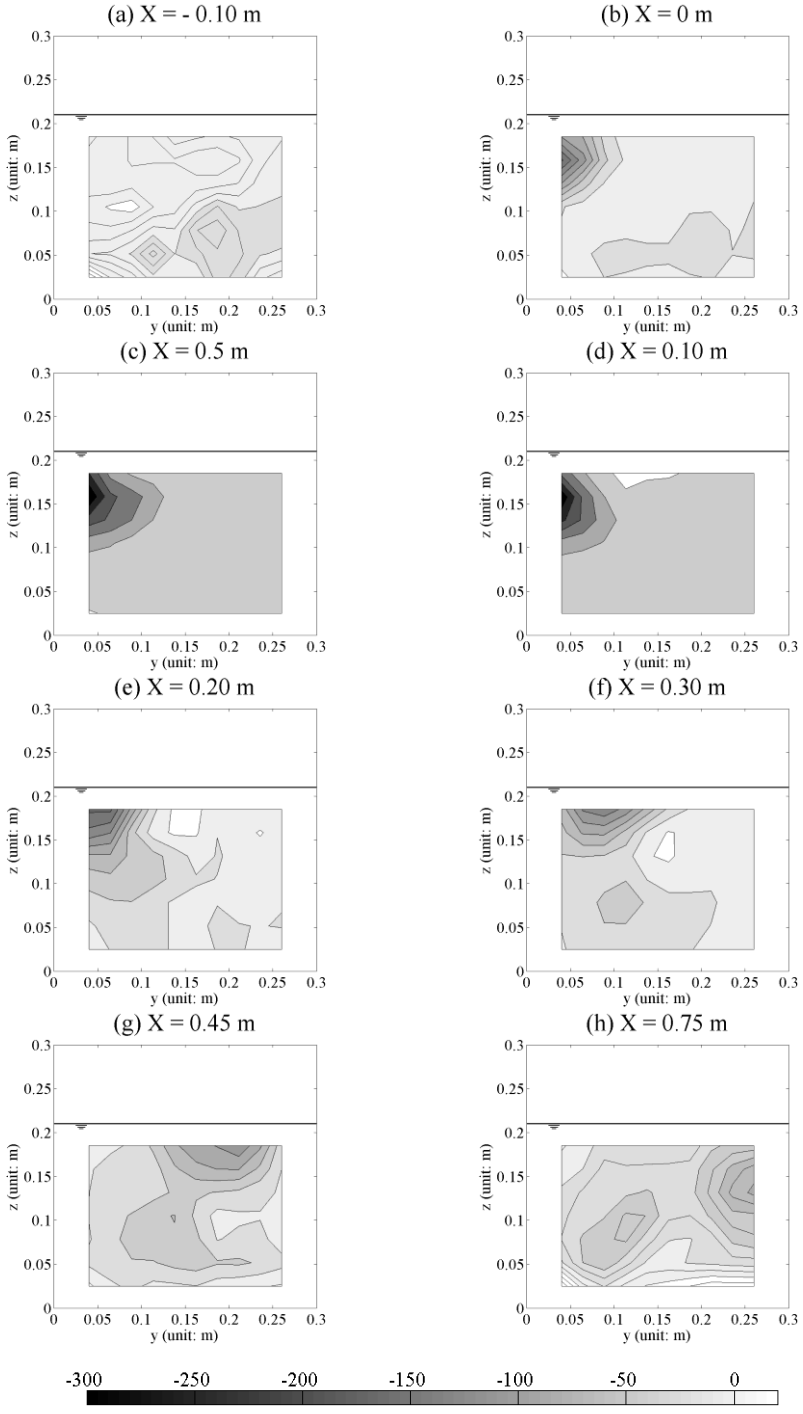

Figure A.98 (AM202) Vorticity contours

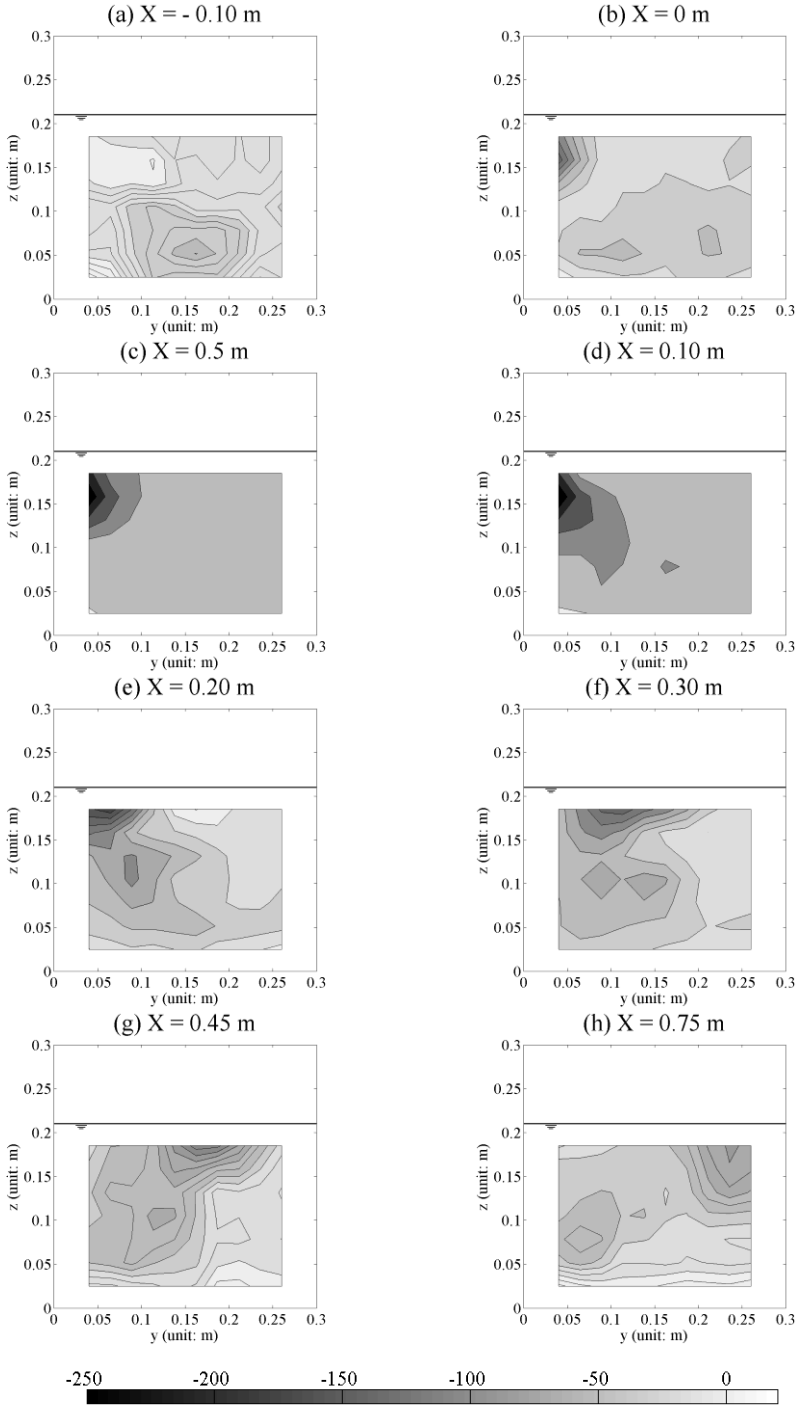

Figure 4.99 (AM203) Vorticity contours

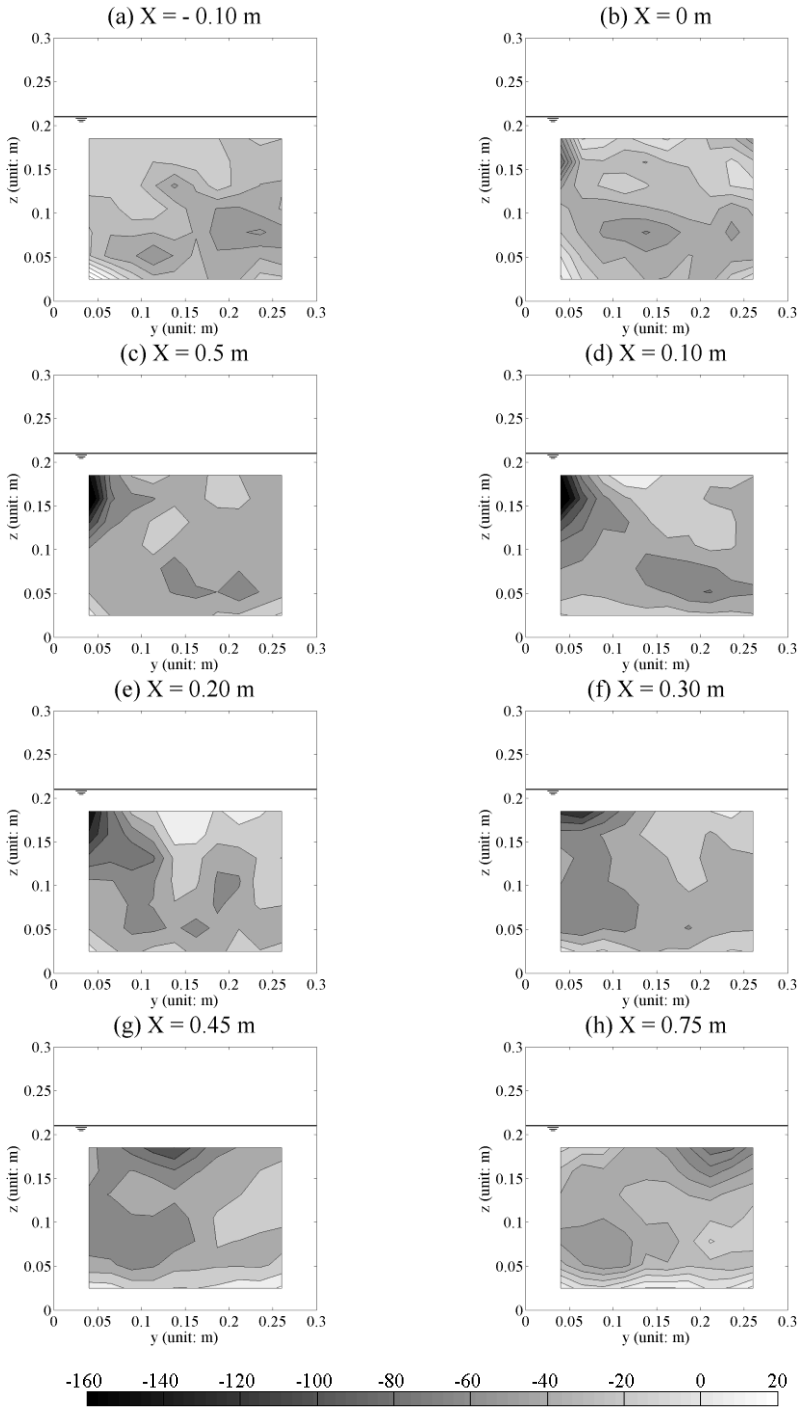

Figure A.100 (AM204) Vorticity contours

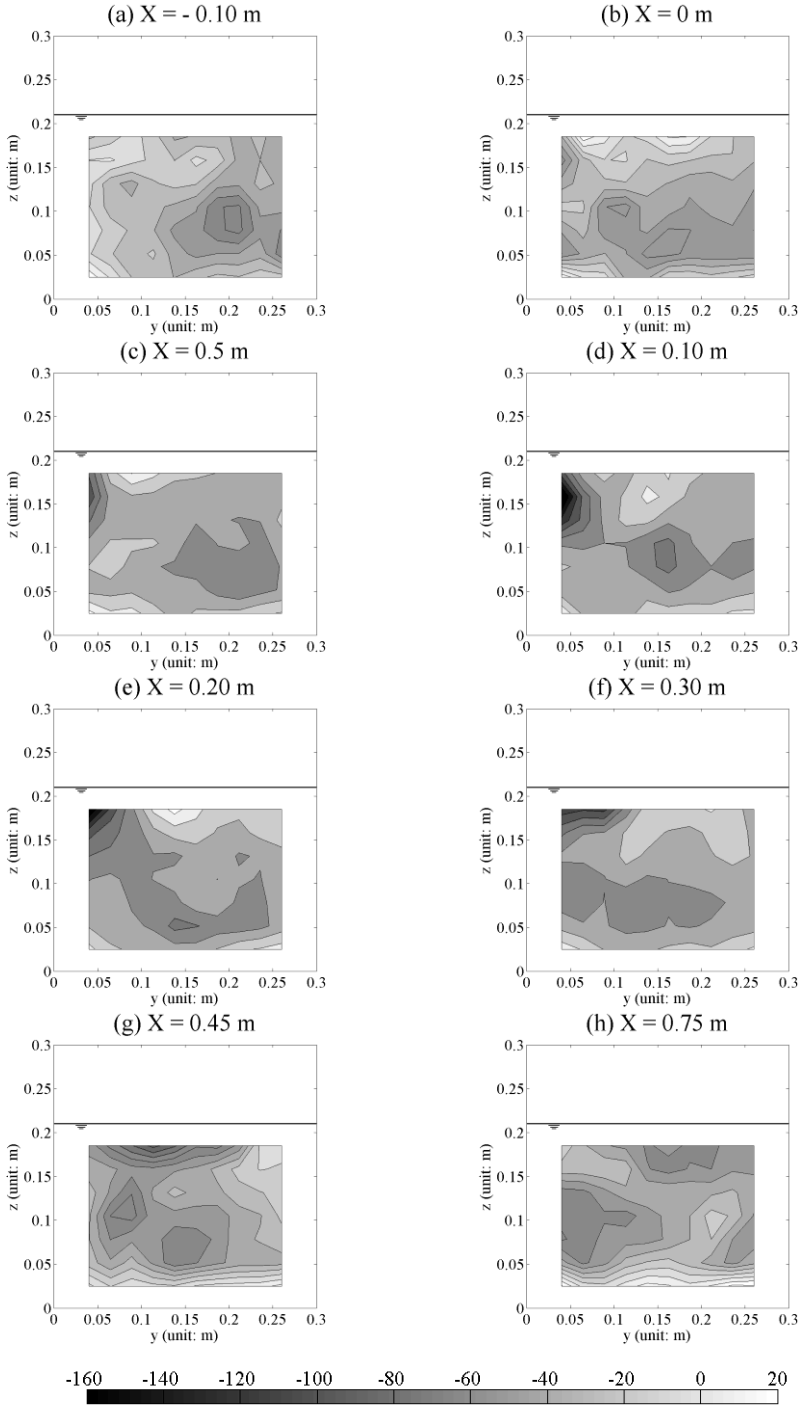

Figure A.101 (AM205) Vorticity contours

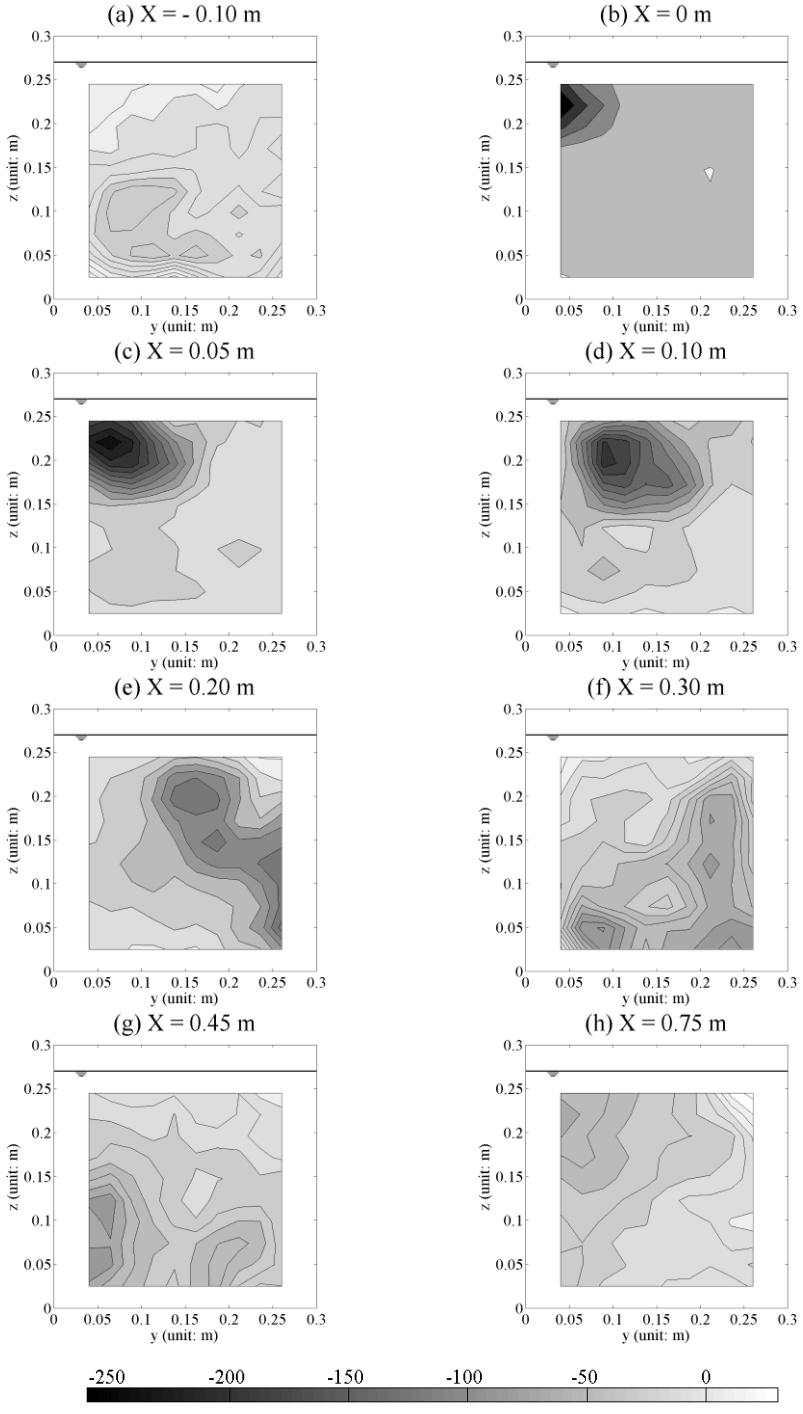

Figure A.102 (AM301) Vorticity contours

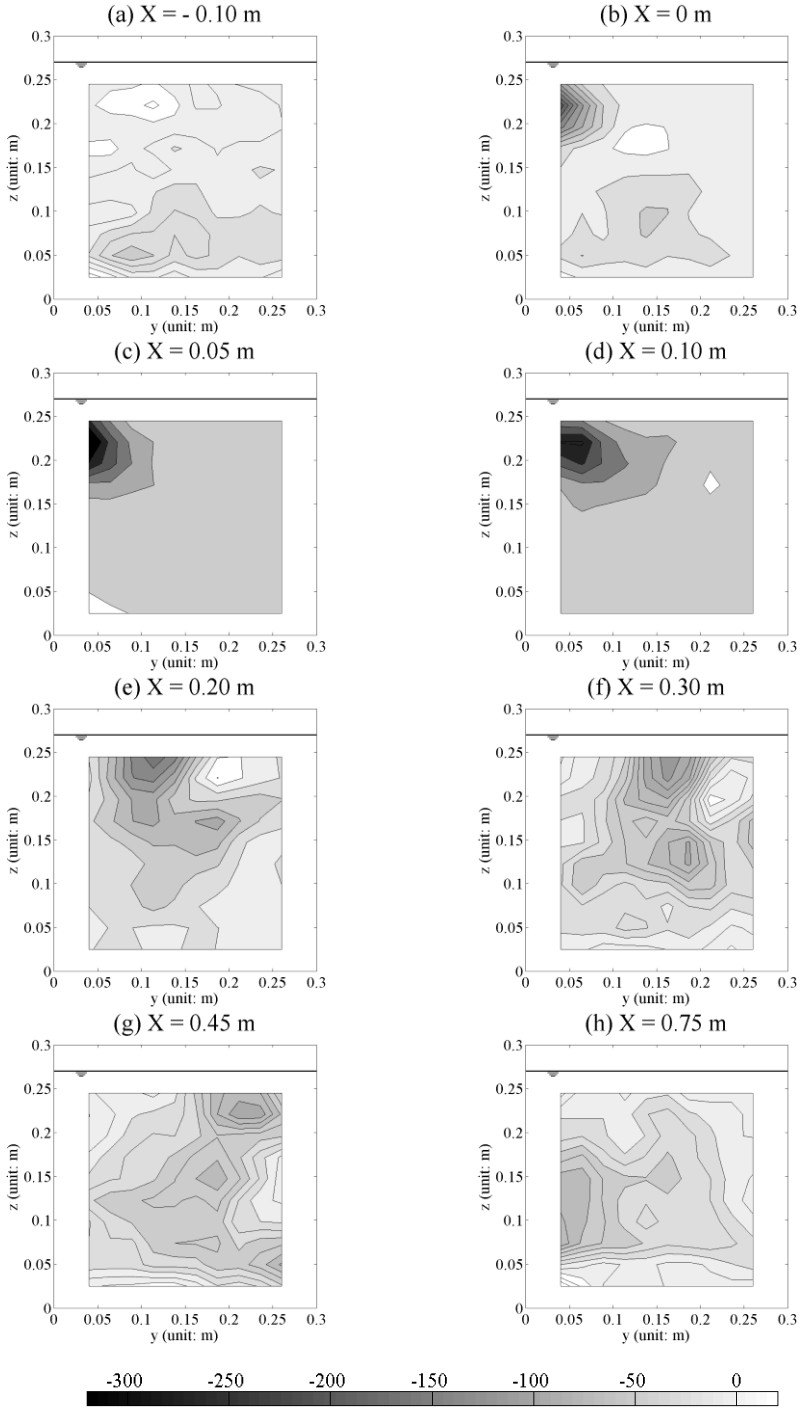

Figure A.103 (AM302) Vorticity contours

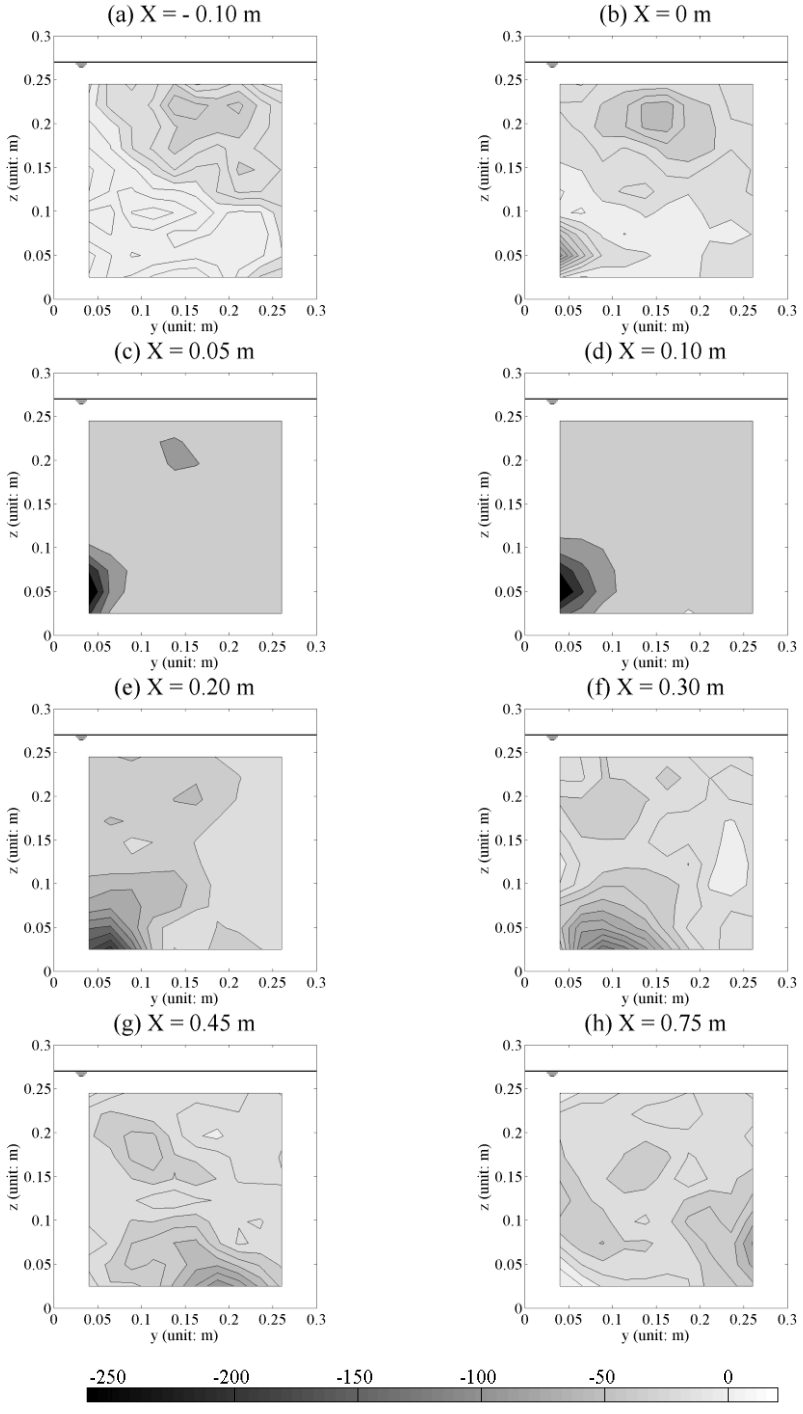

Figure A.104 (AM303) Vorticity contours

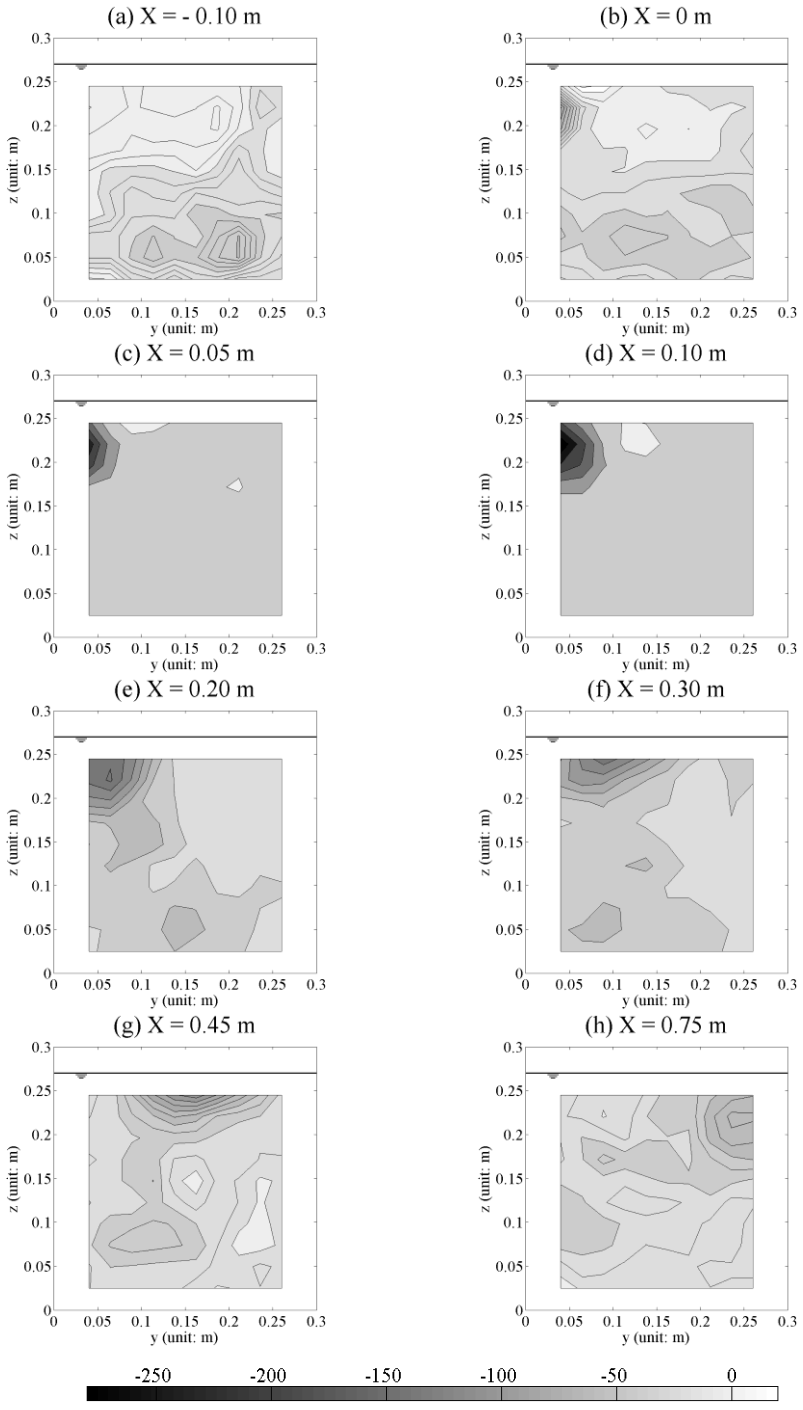

Figure A.105 (AM304) Vorticity contours

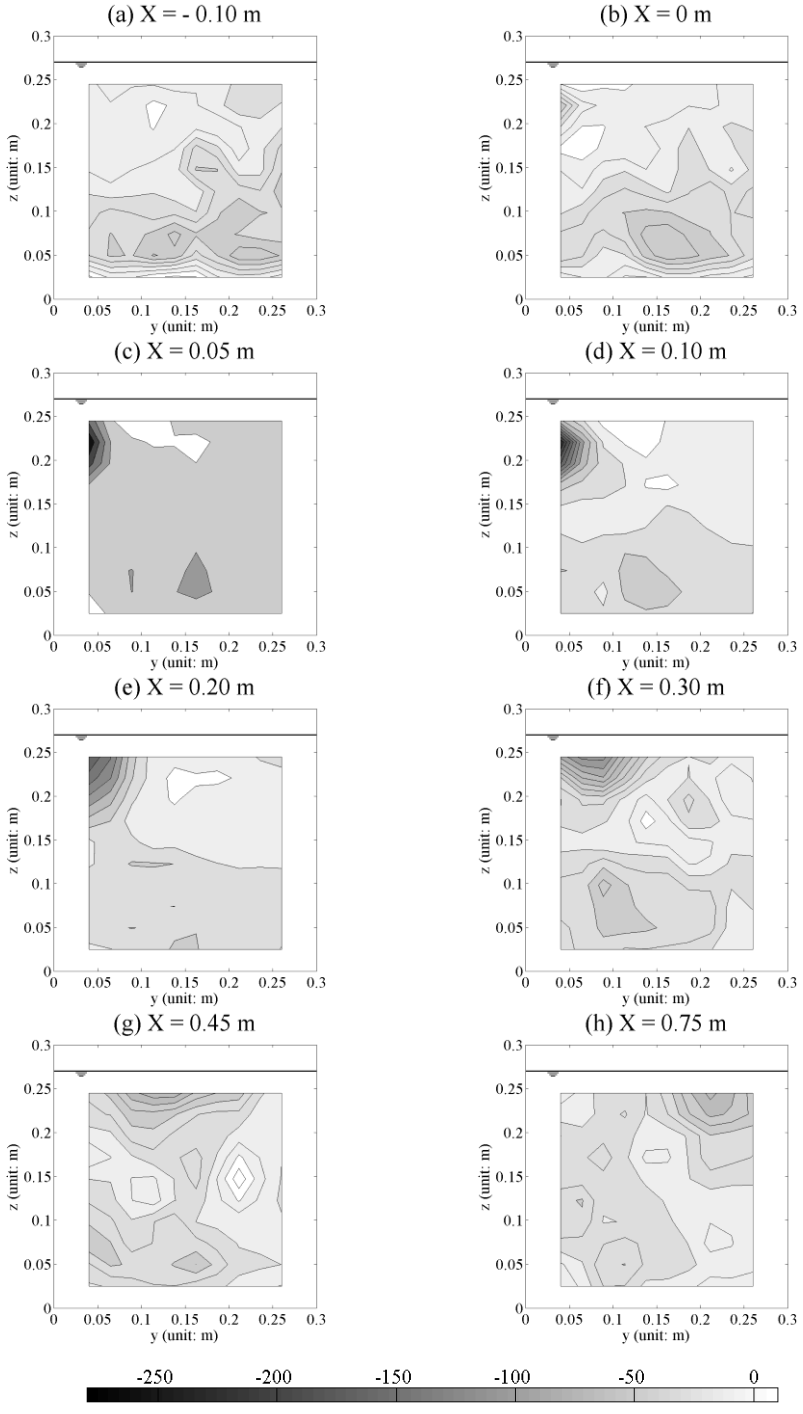

Figure A.106 (AM305) Vorticity contours

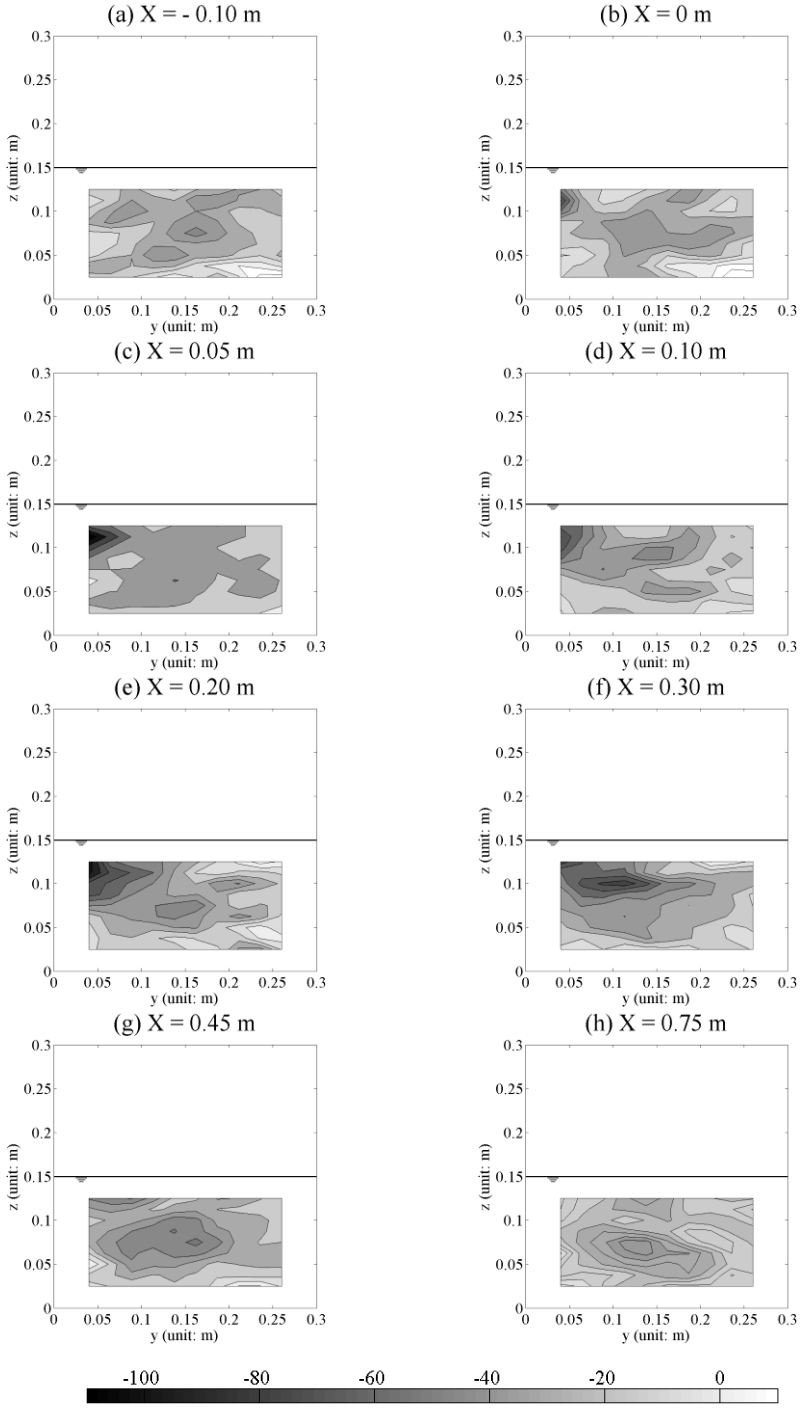

Figure A.107 (AS101) Vorticity contours

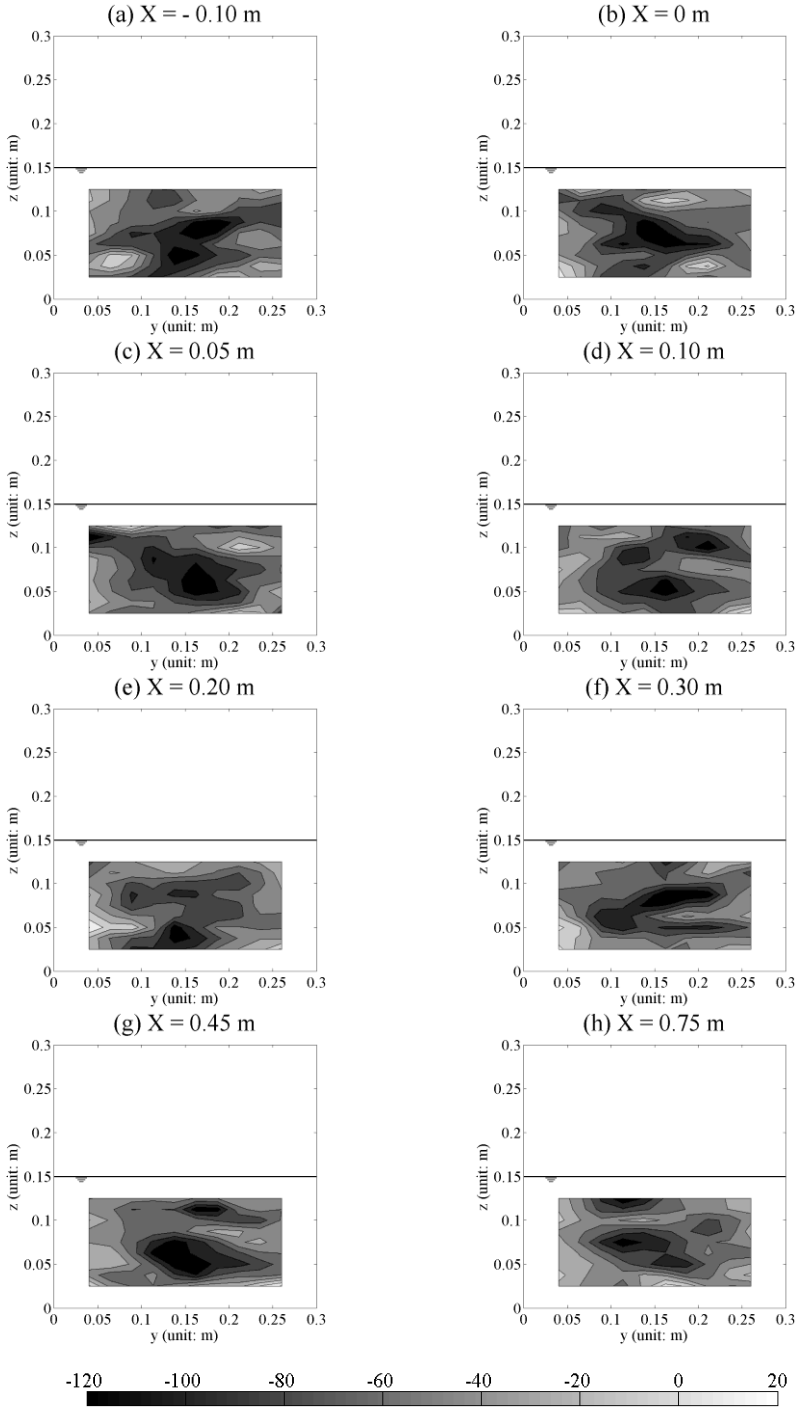

Figure A.108 (AS103) Vorticity contours

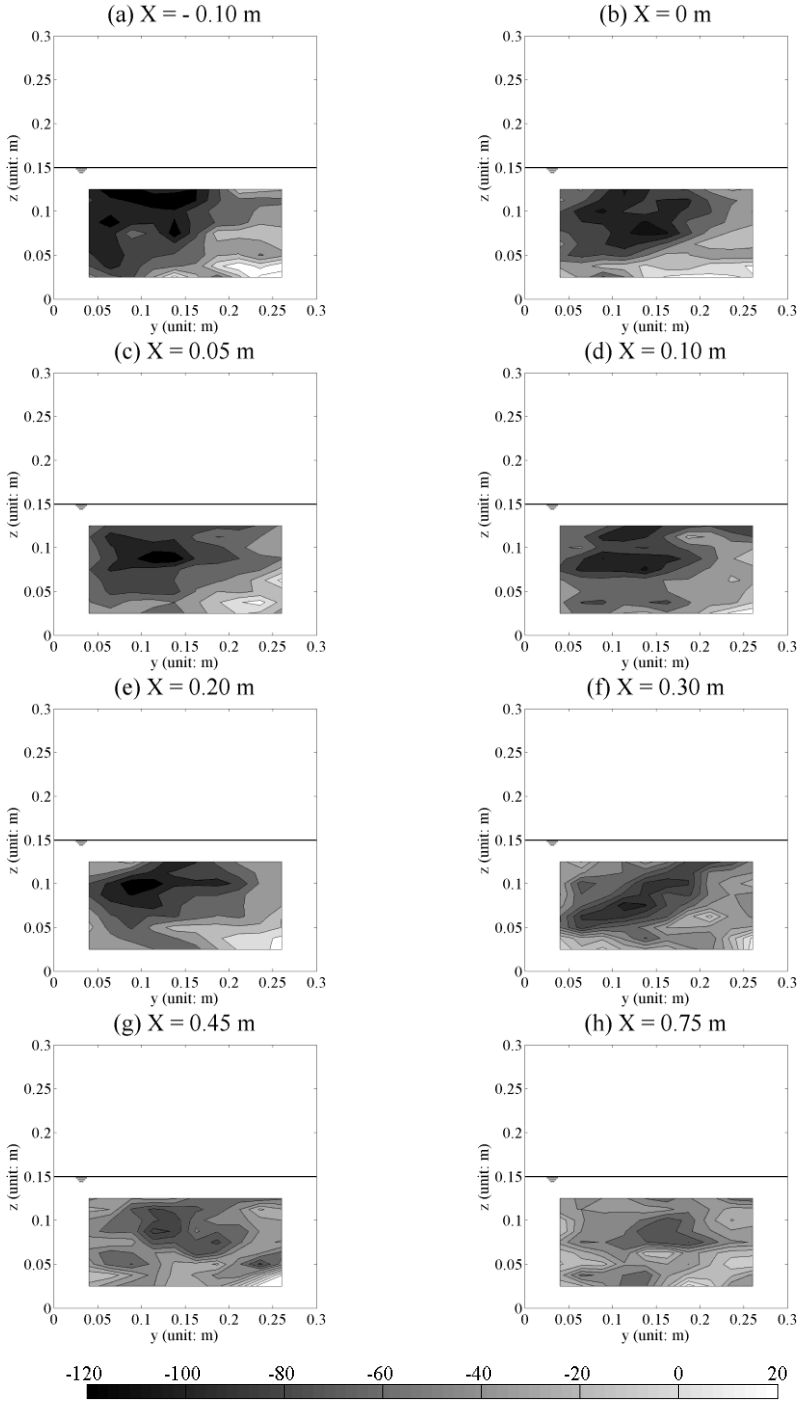

Figure A.109 (AS105) Vorticity contours

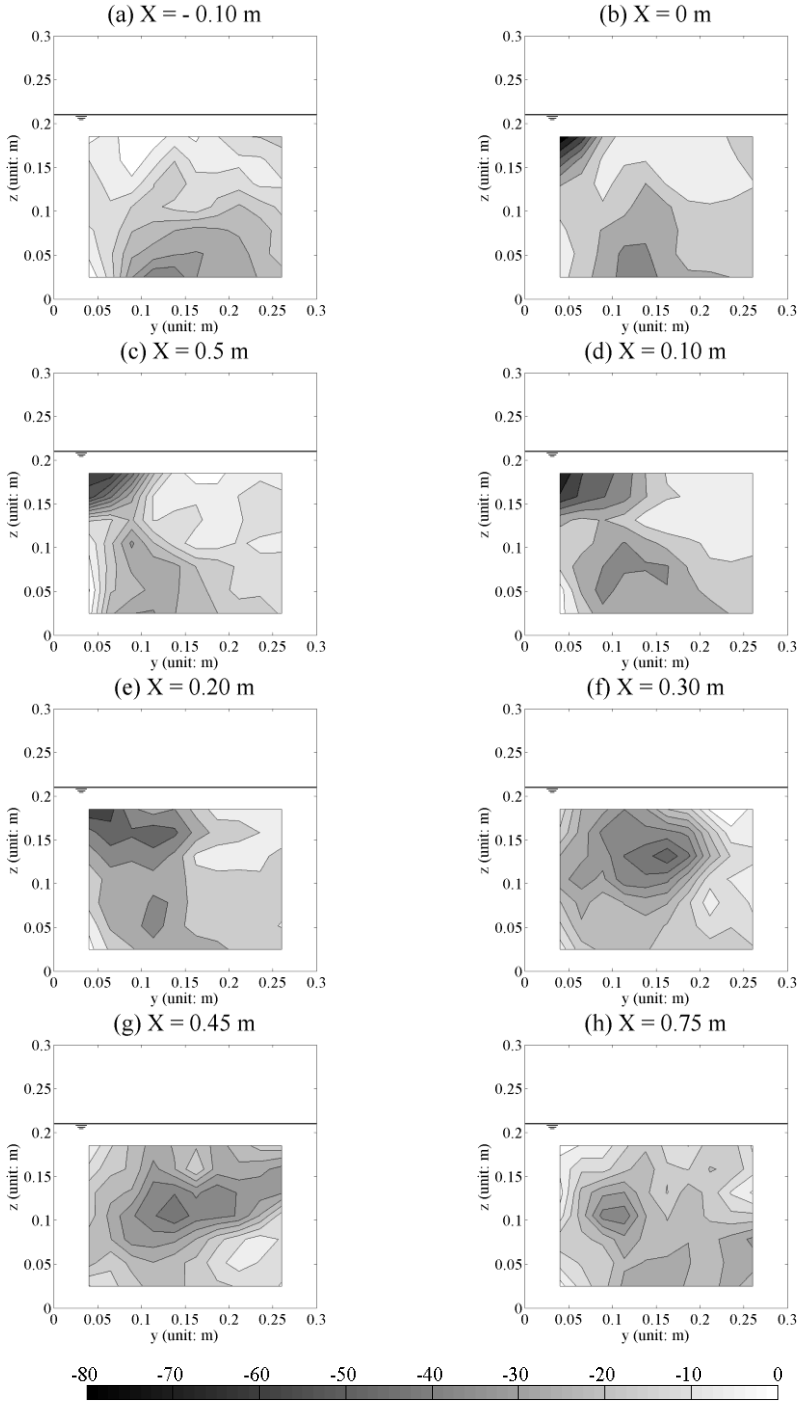

Figure A.110 (AS201) Vorticity contours

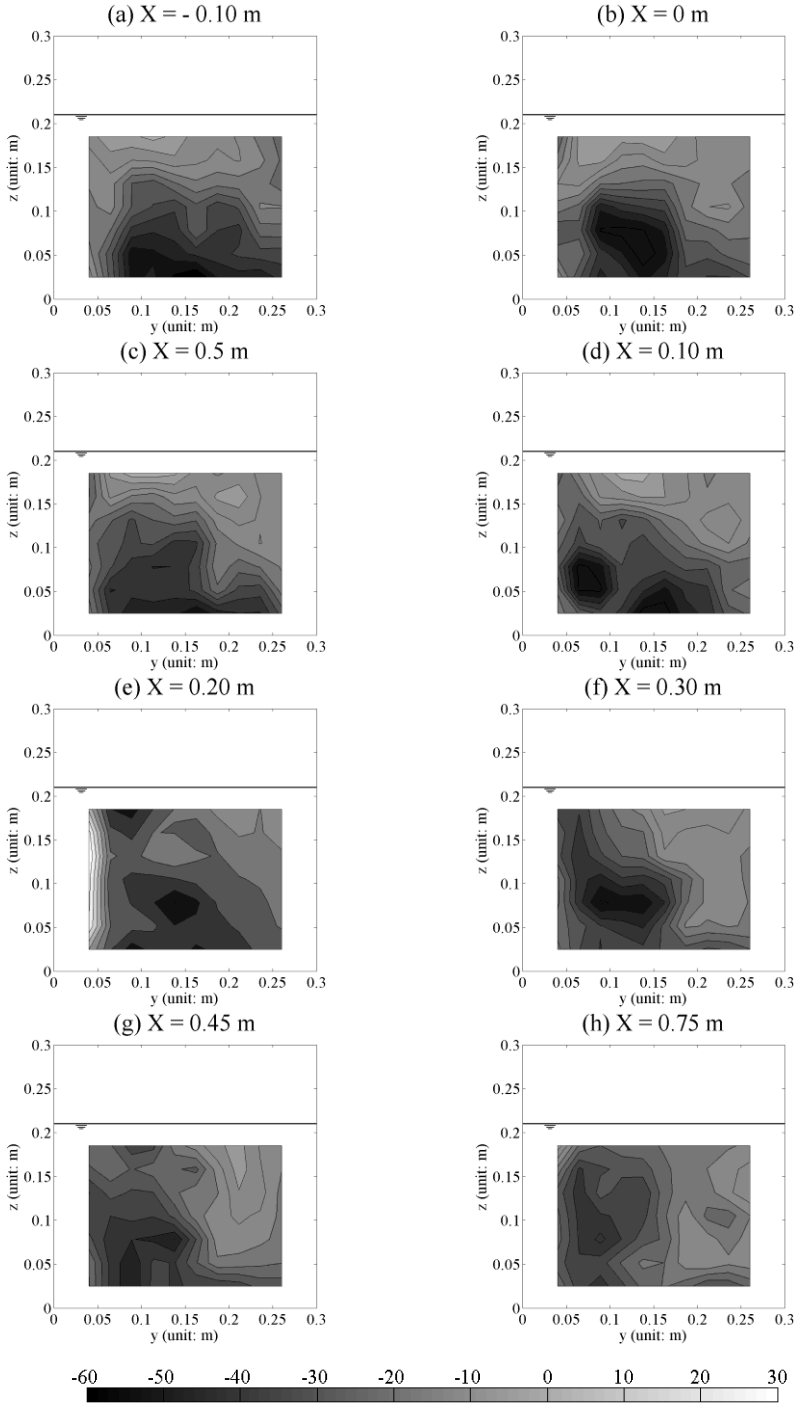

Figure A.111 (AS203) Vorticity contours

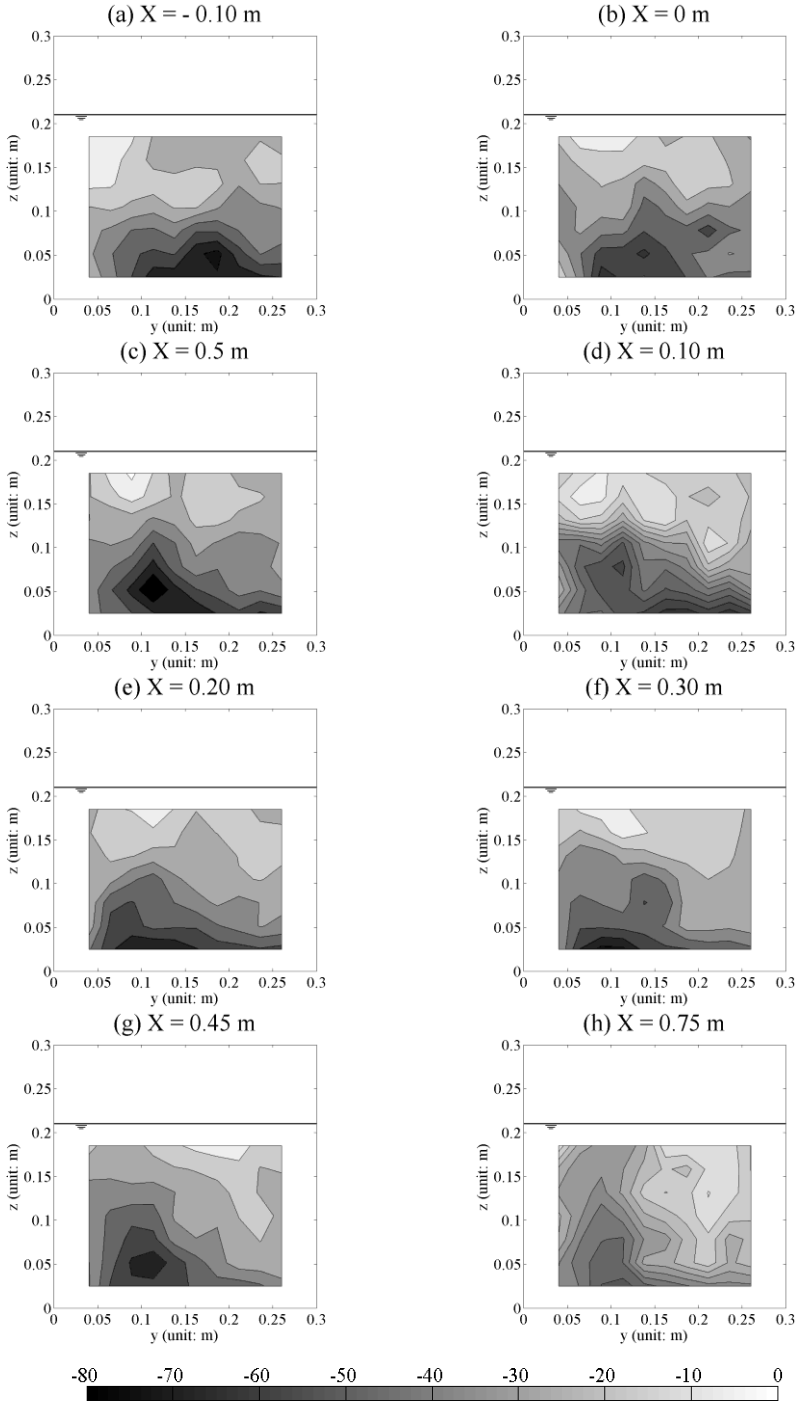

Figure A.112 (AS205) Vorticity contours

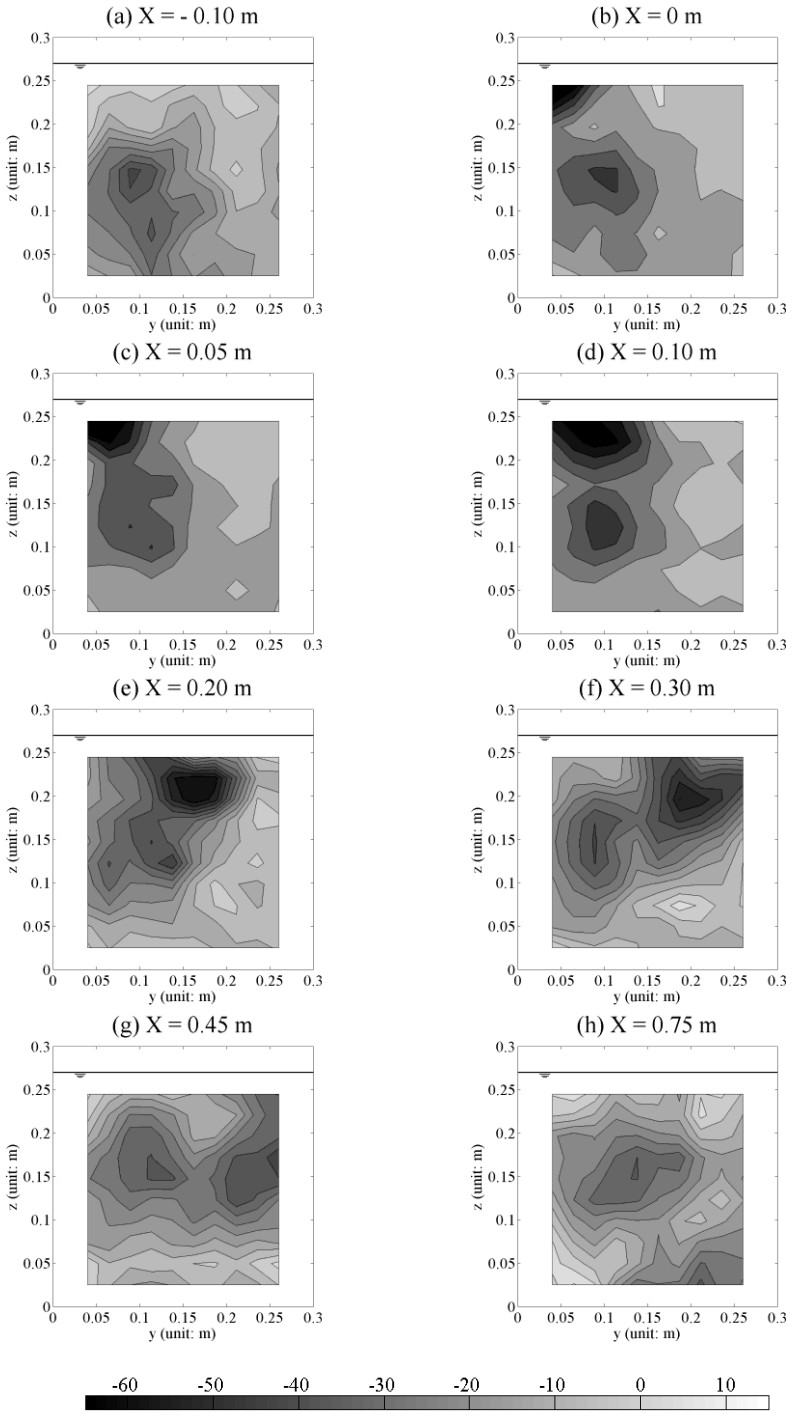

Figure A.113 (AS301) Vorticity contours

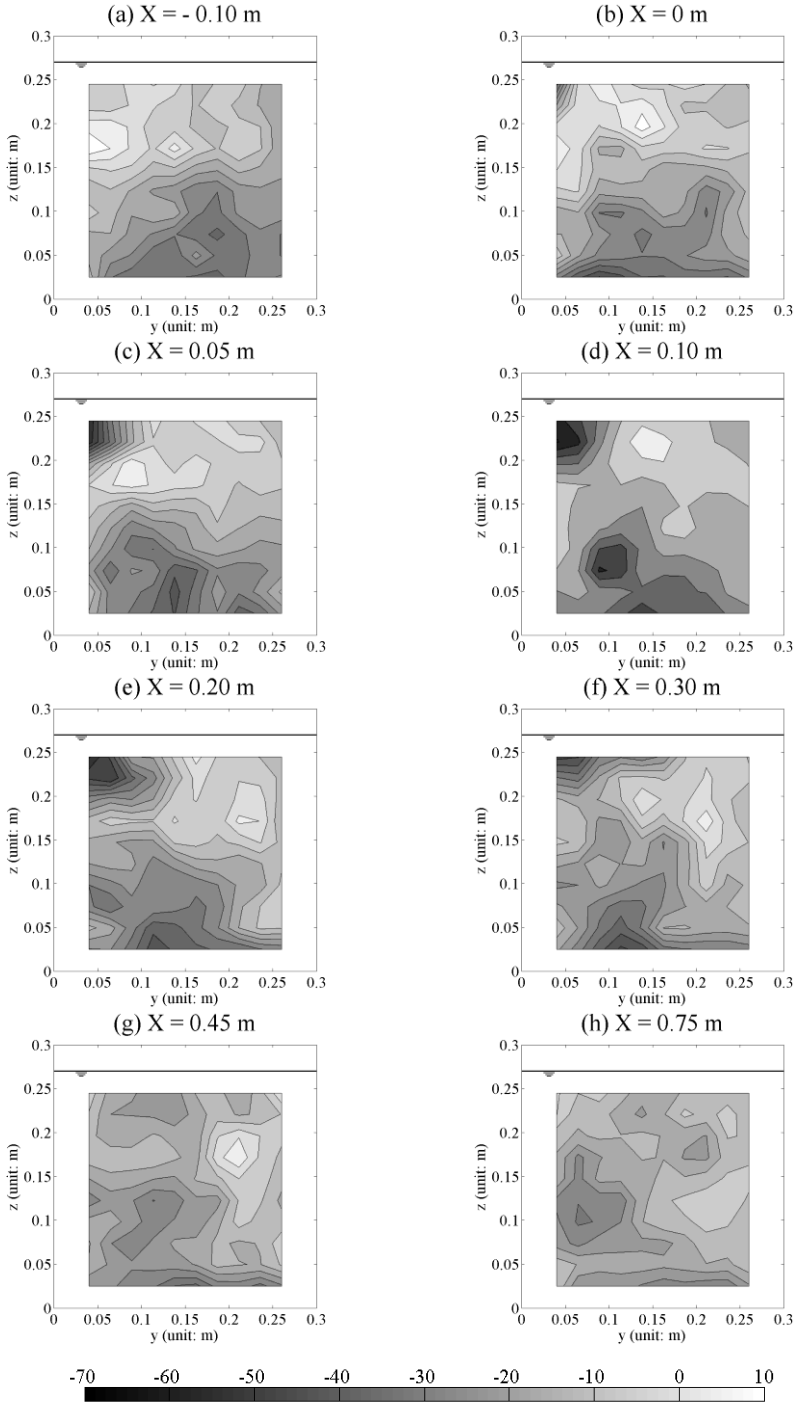

Figure A.114 (AS303) Vorticity contours

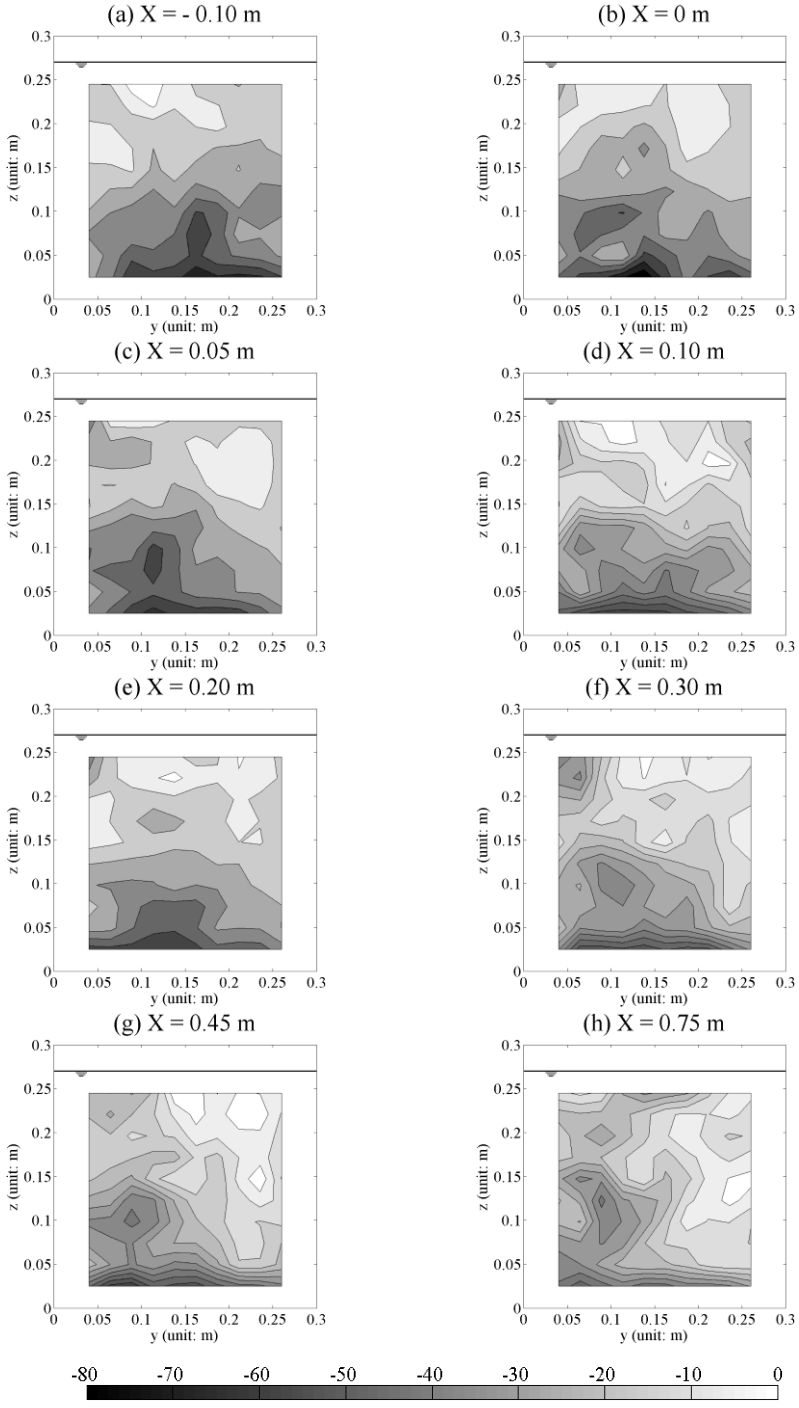

Figure A.115 (AS305) Vorticity contours

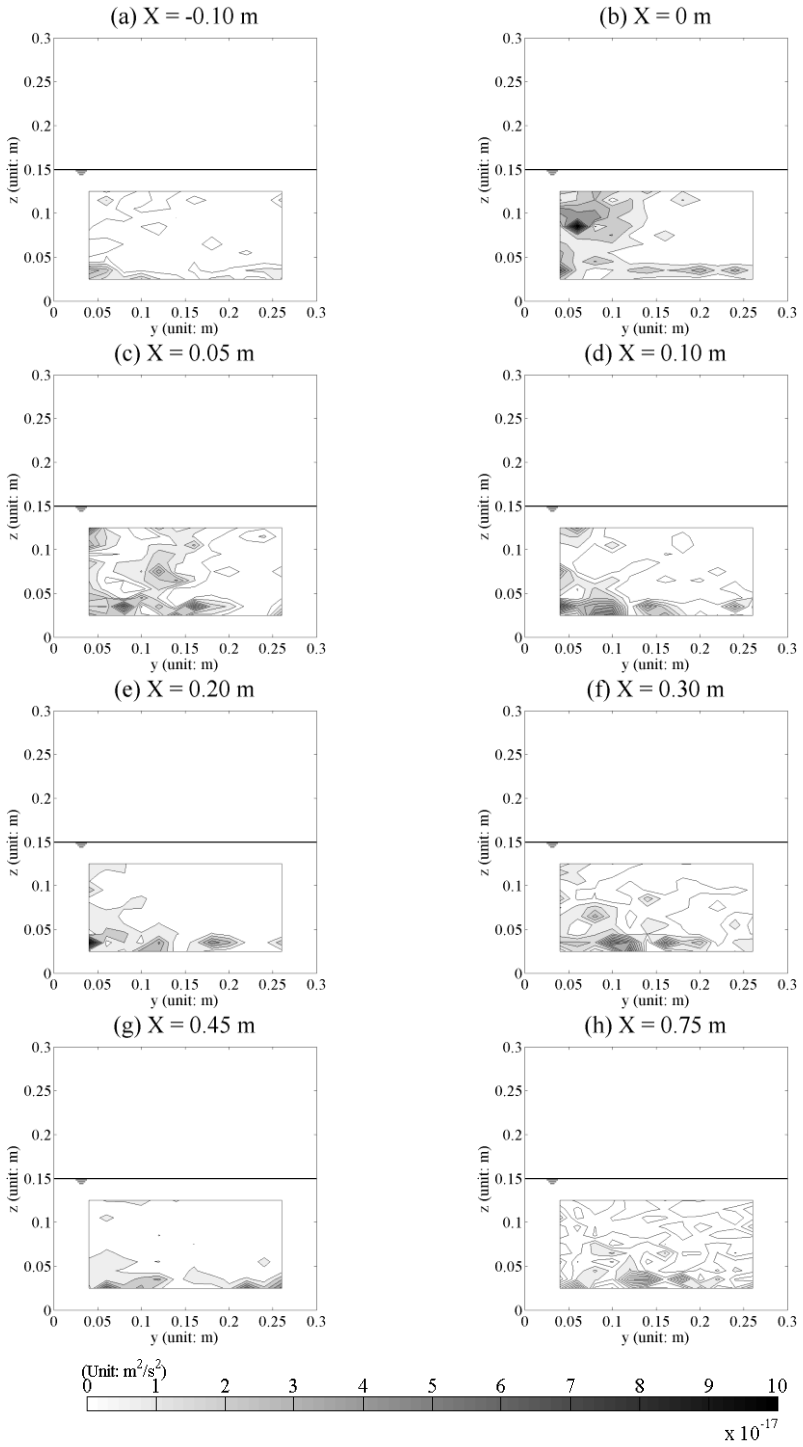

Figure A.116 (AR101) Turbulent Kinetic Energy contours

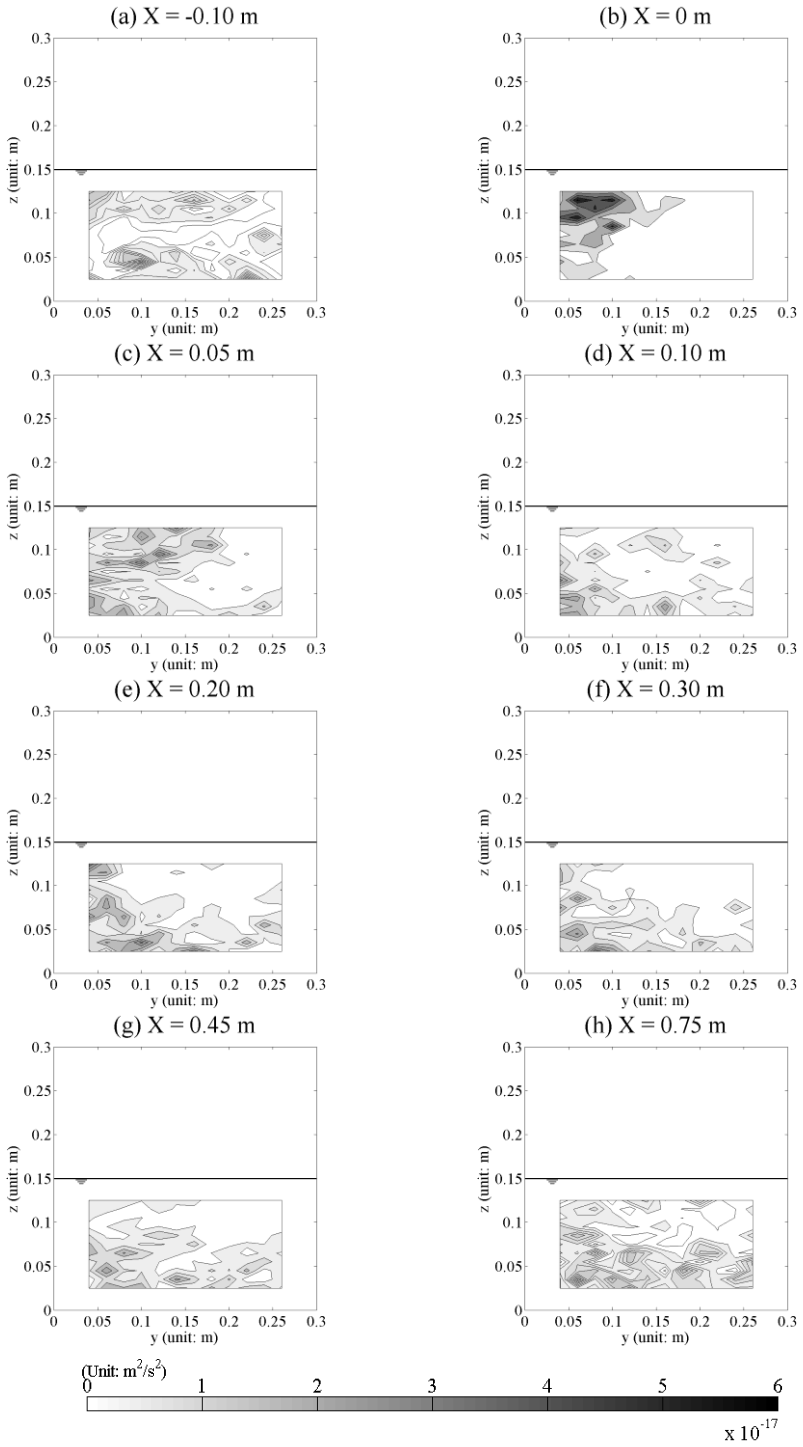

Figure A.117 (AR102) Turbulent Kinetic Energy contours

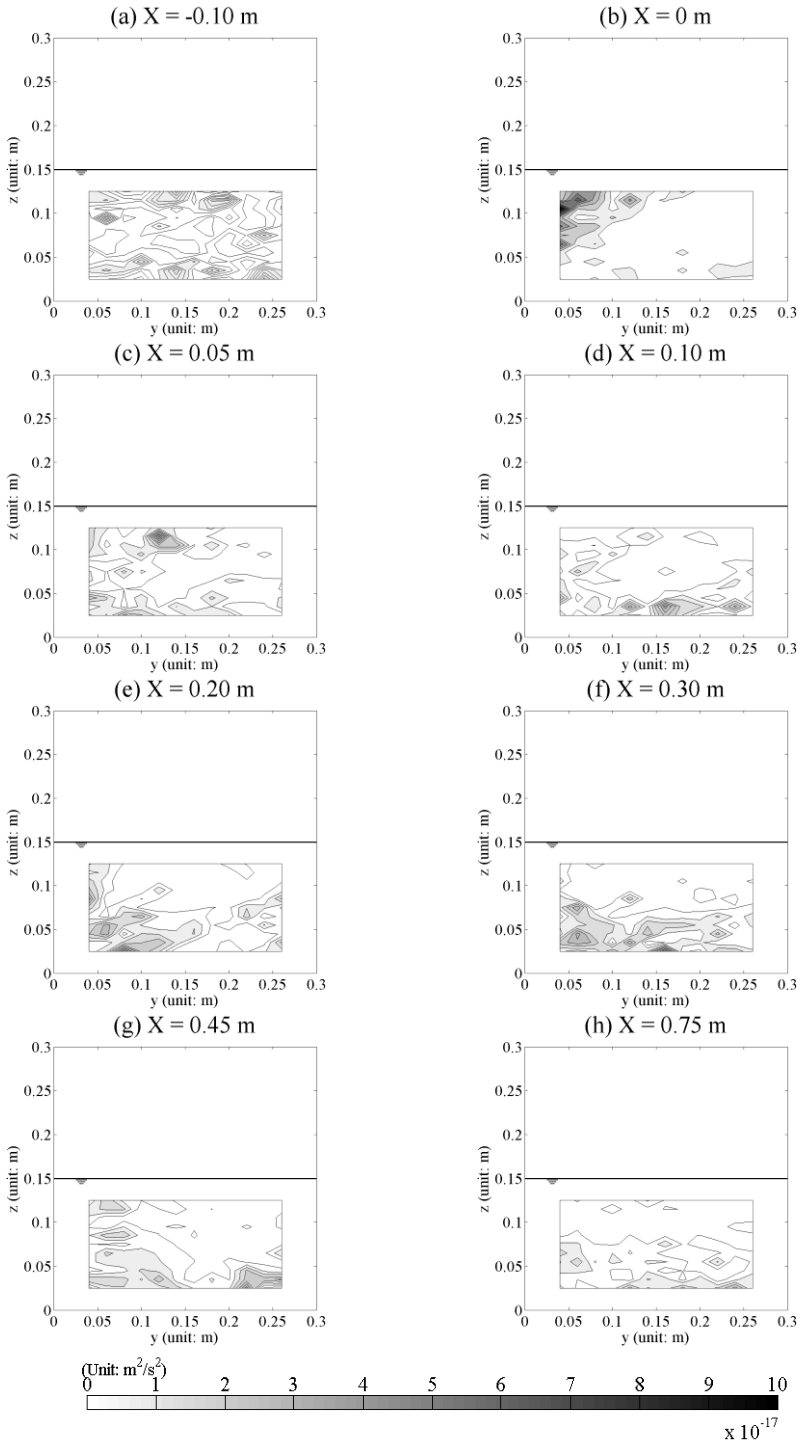

Figure A.118 (AR103) Turbulent Kinetic Energy contours

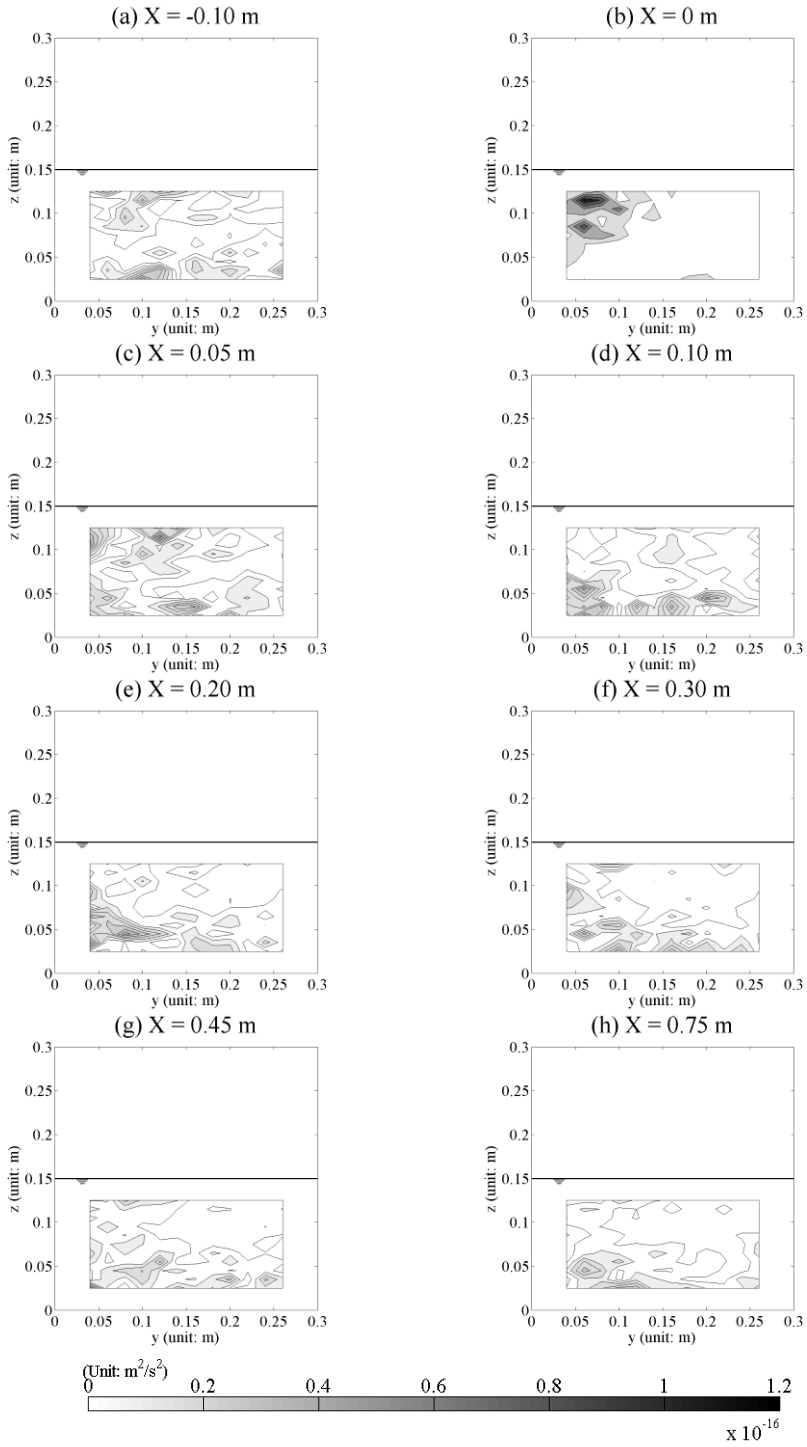

Figure A.119 (AR104) Turbulent Kinetic Energy contours

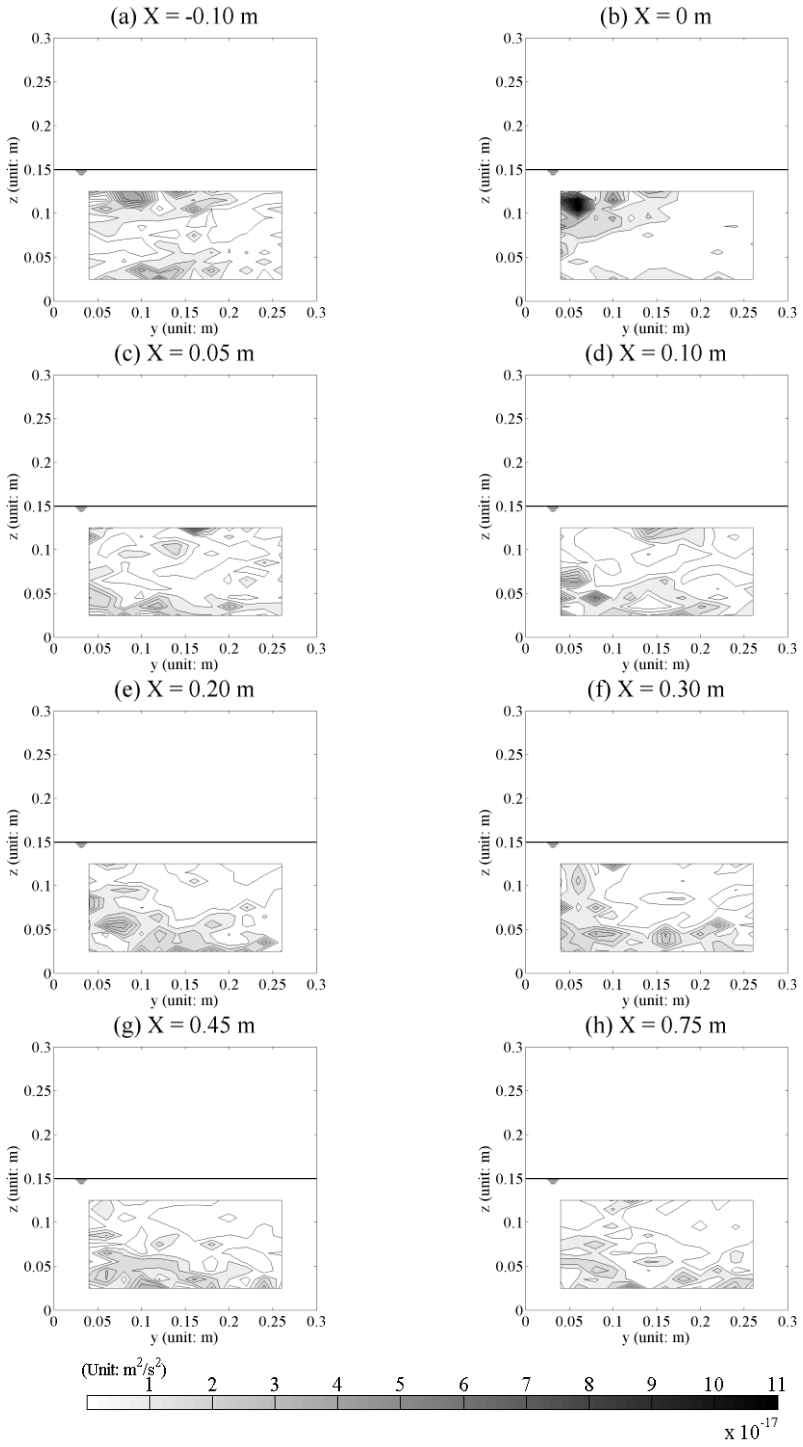

Figure A.120 (AR105) Turbulent Kinetic Energy contours

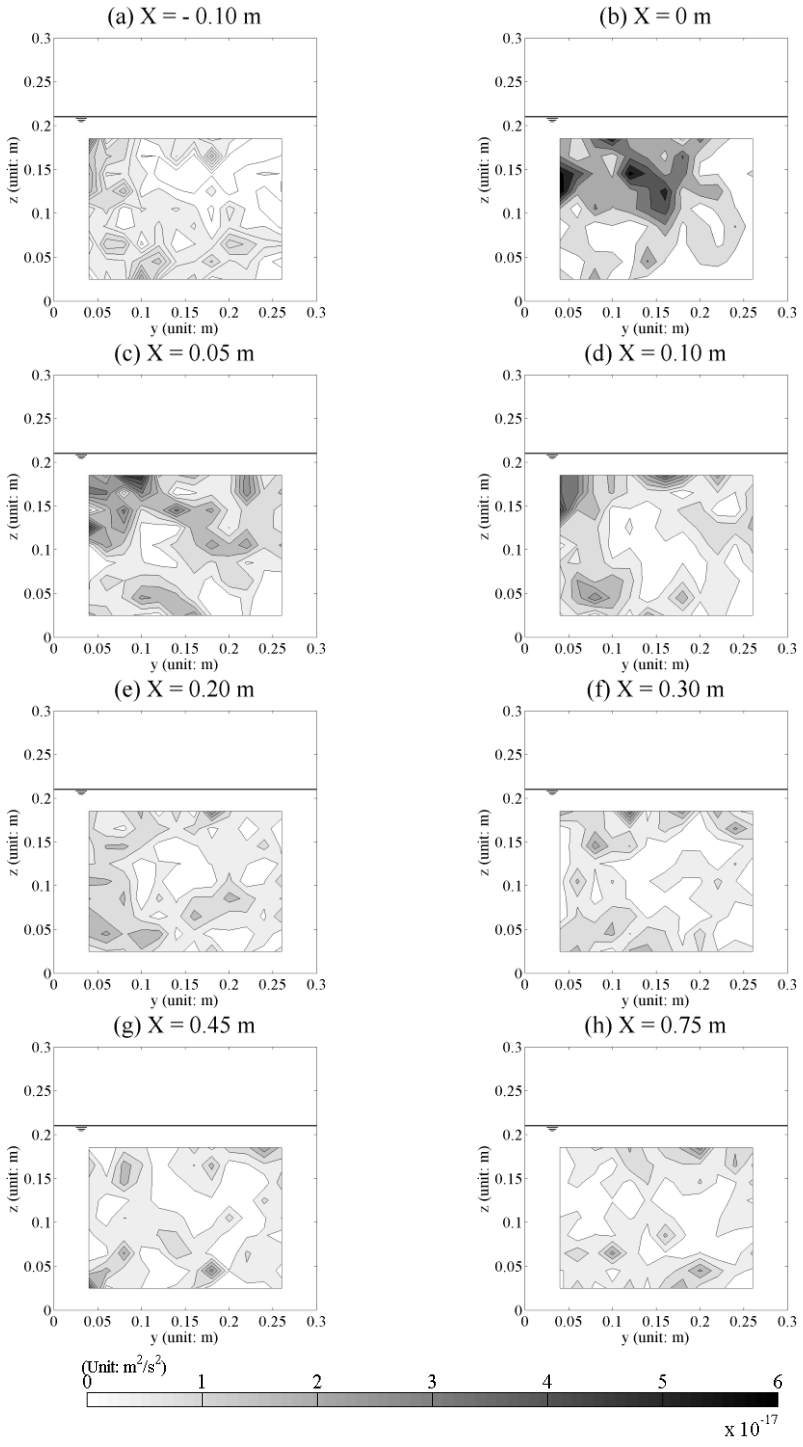

Figure A.121 (AR201) Turbulent Kinetic Energy contours

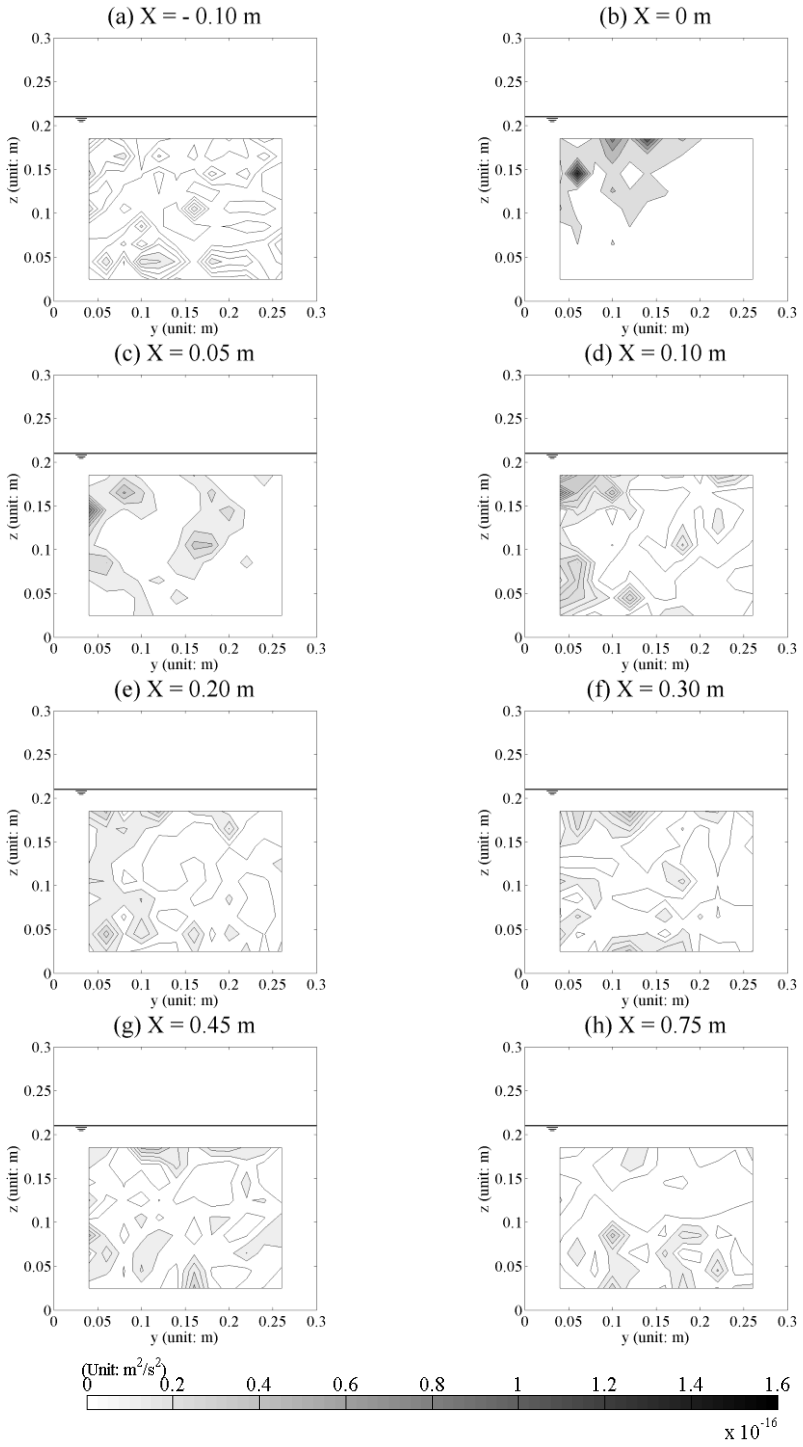

Figure A.122 (AR202) Turbulent Kinetic Energy contours

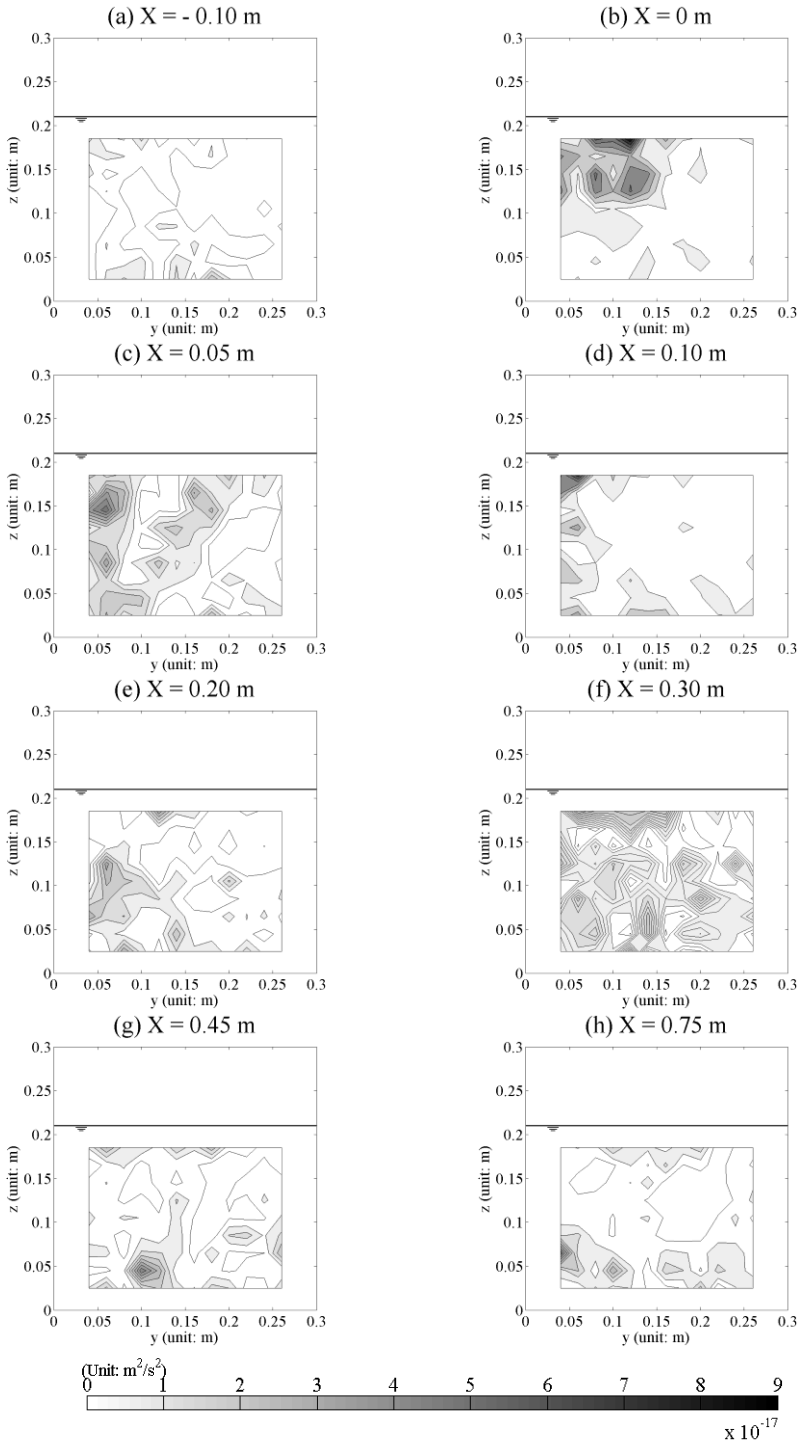

Figure A.123 (AR203) Turbulent Kinetic Energy contours

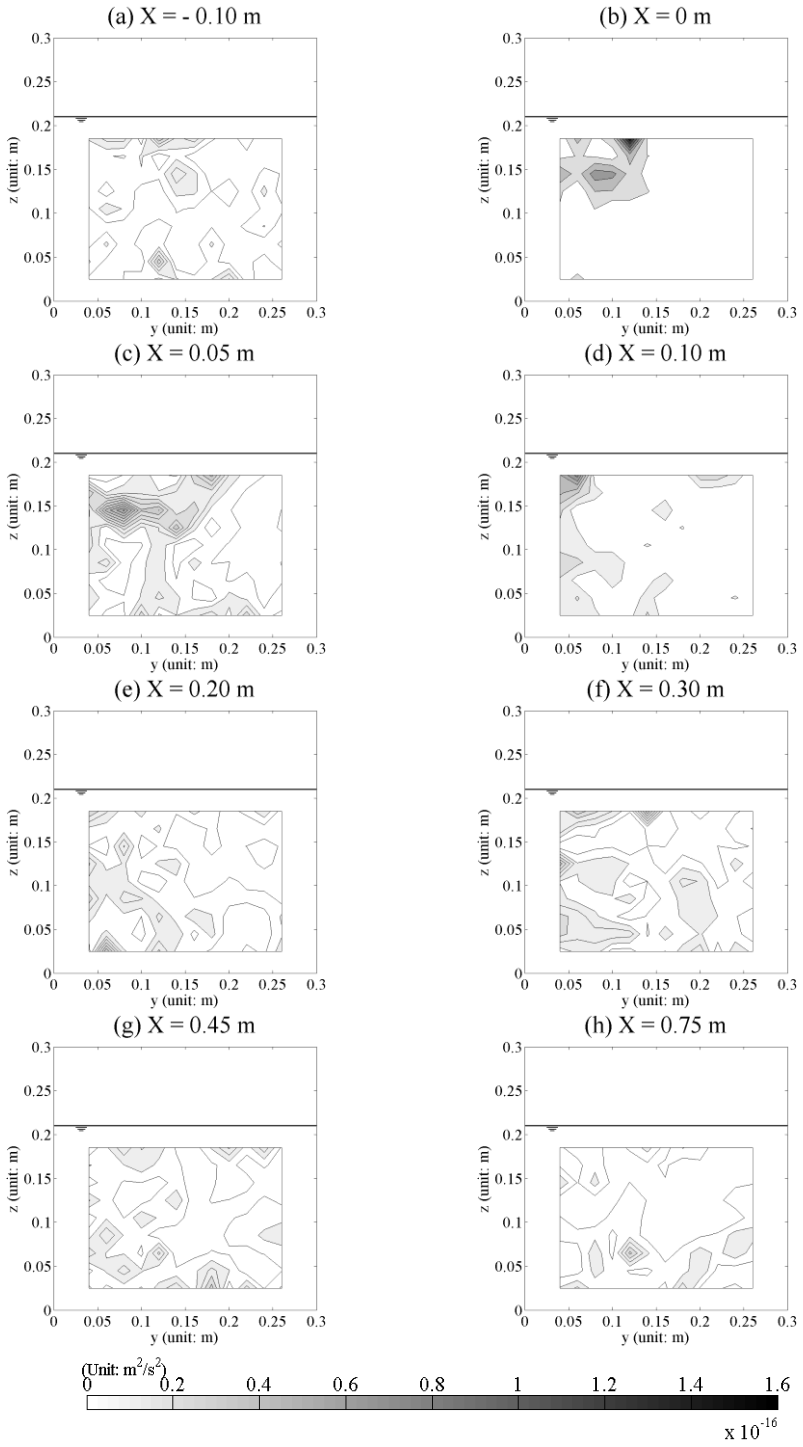

Figure A.124 (AR204) Turbulent Kinetic Energy contours

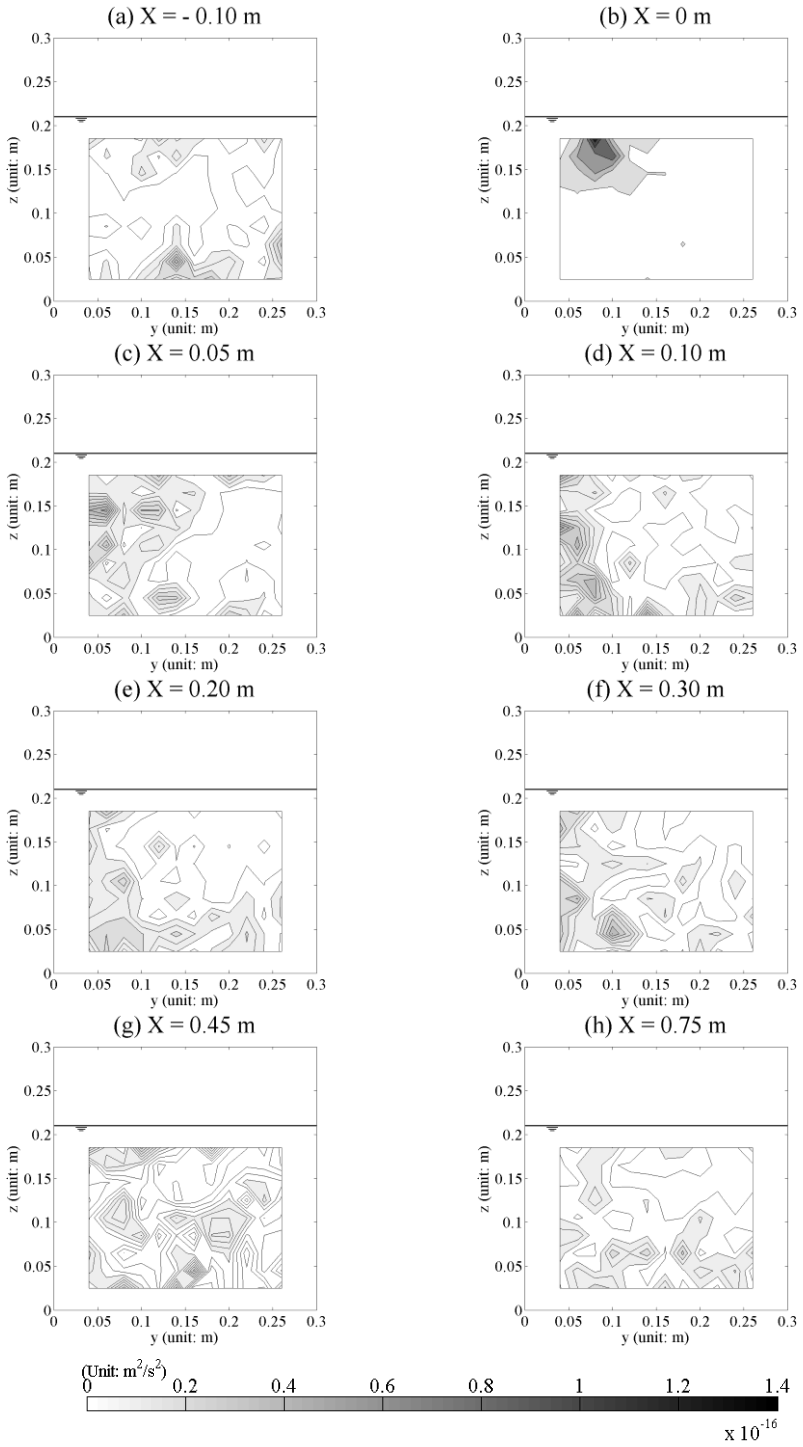

Figure A.125 (AR205) Turbulent Kinetic Energy contours

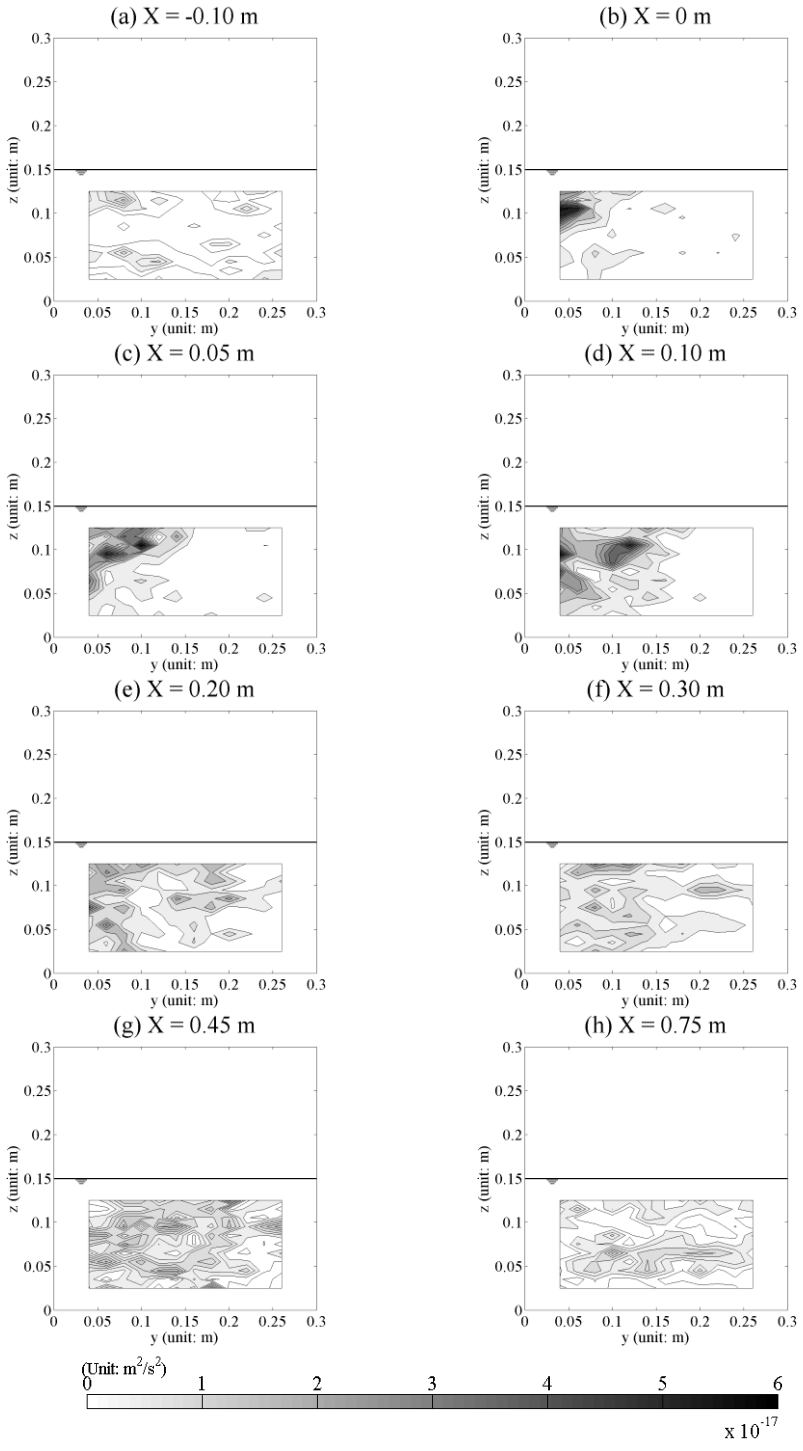

Figure A.126 (AM101) Turbulent Kinetic Energy contours

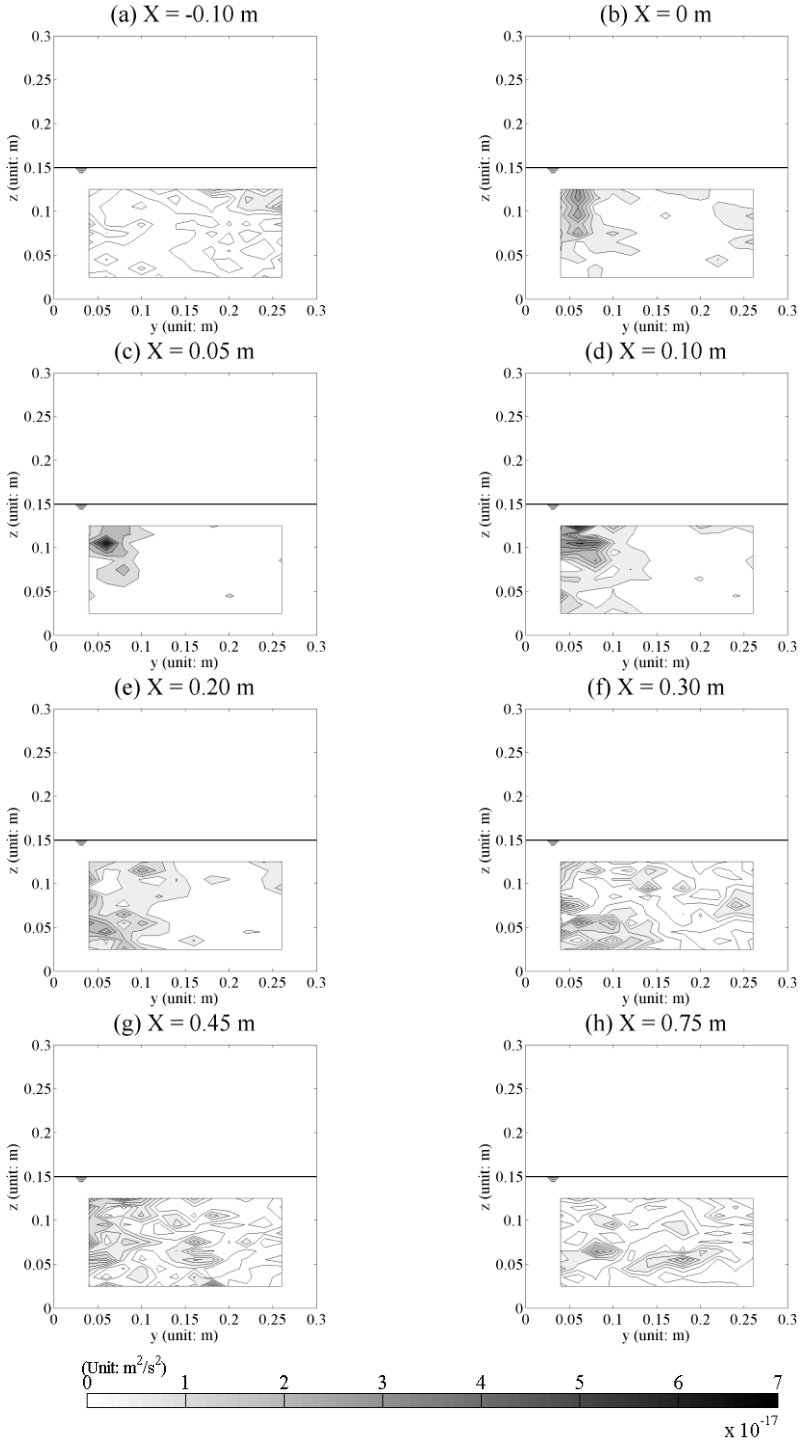

Figure A.127 (AM102) Turbulent Kinetic Energy contours

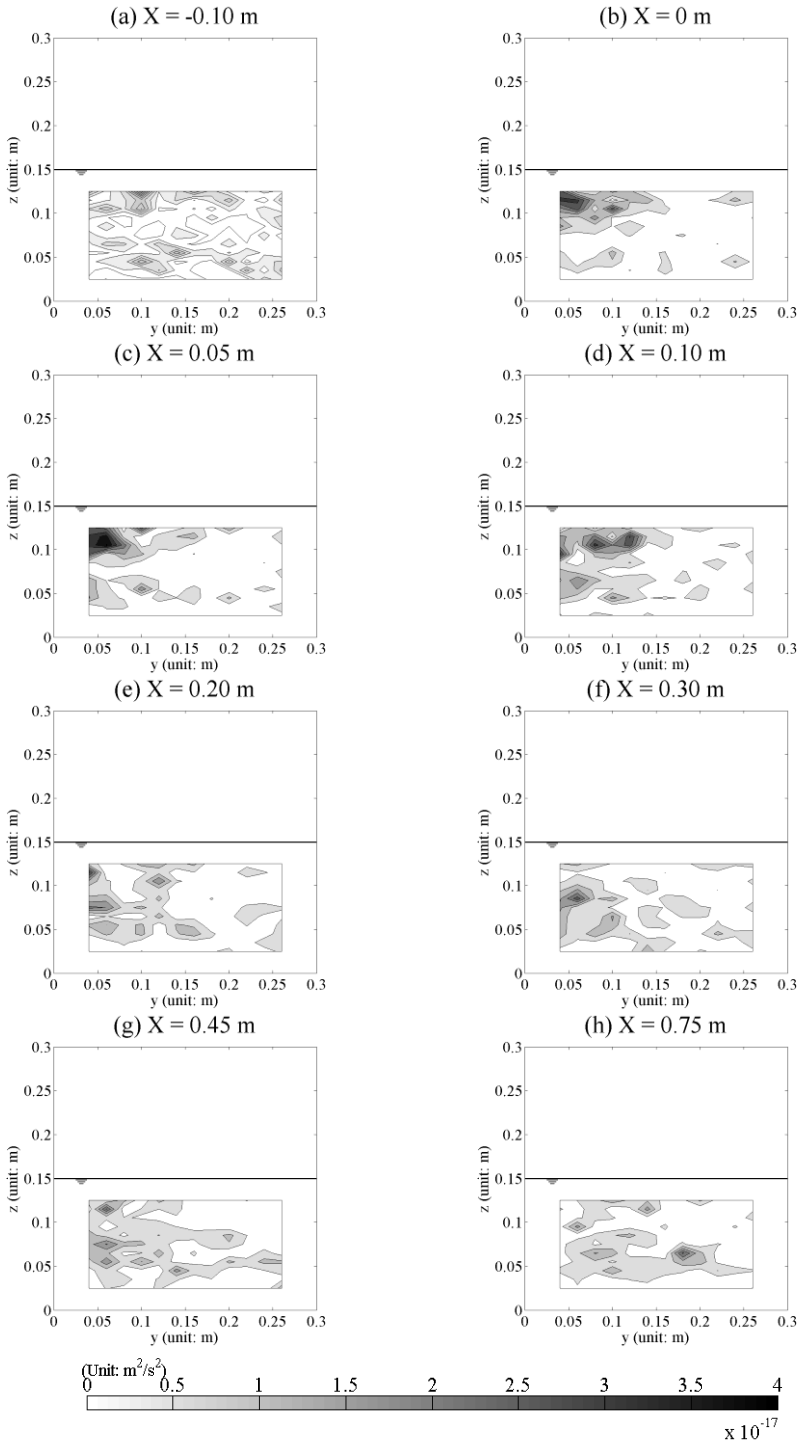

Figure A.128 (AM103) Turbulent Kinetic Energy contours

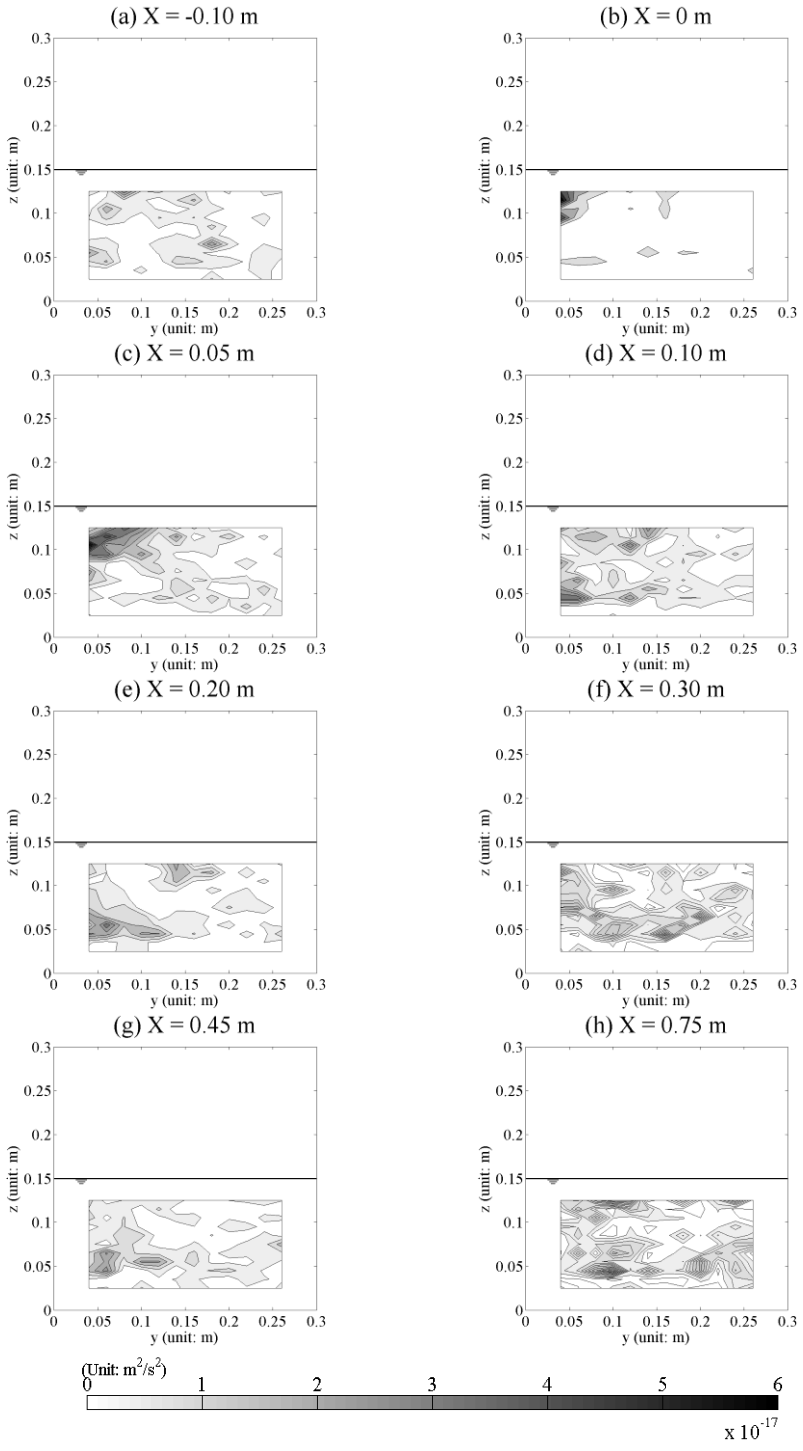

Figure A.129 (AM104) Turbulent Kinetic Energy contours

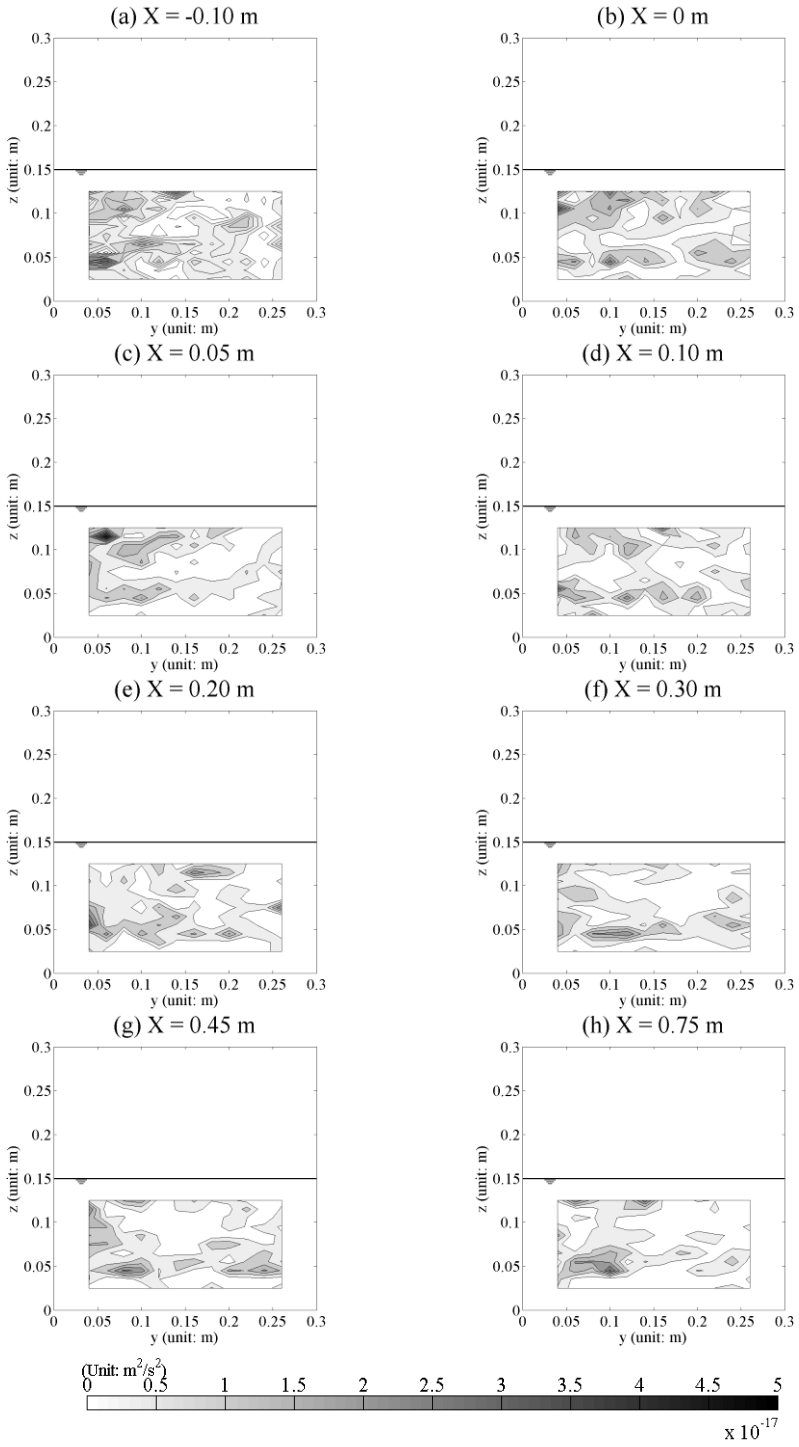

Figure A.130 (AM105) Turbulent Kinetic Energy contours

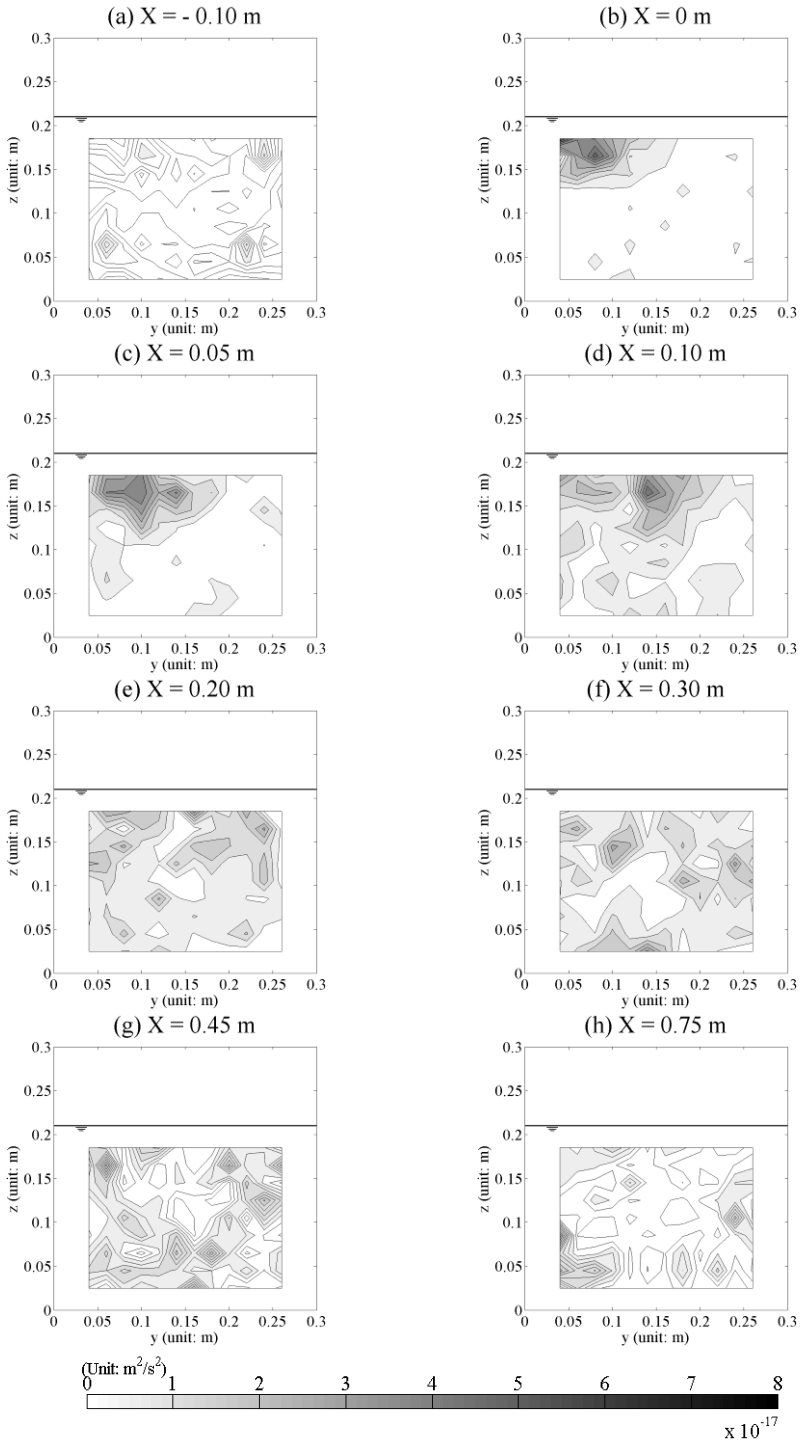

Figure A.131 (AM201) Turbulent Kinetic Energy contours

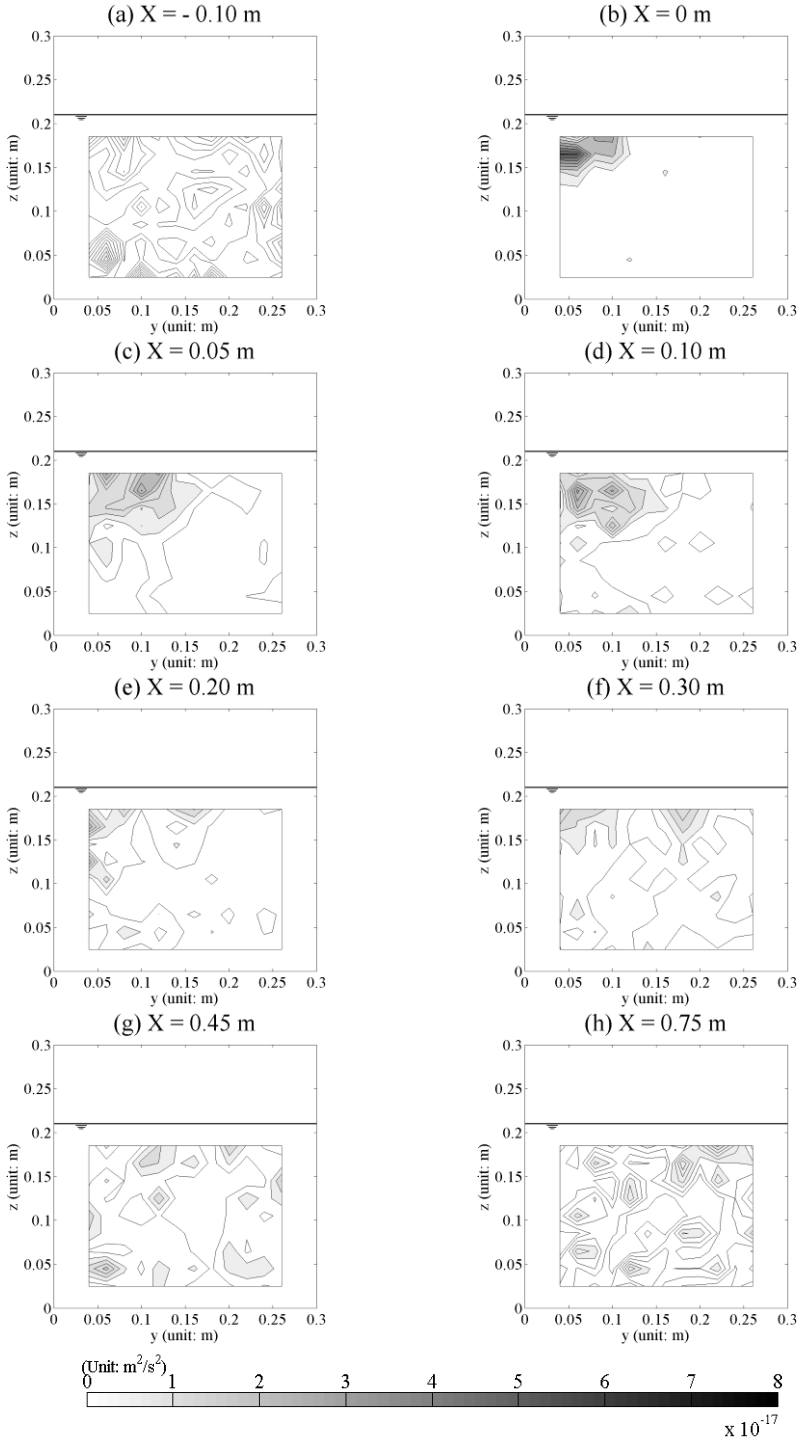

Figure A.132 (AM202) Turbulent Kinetic Energy contours

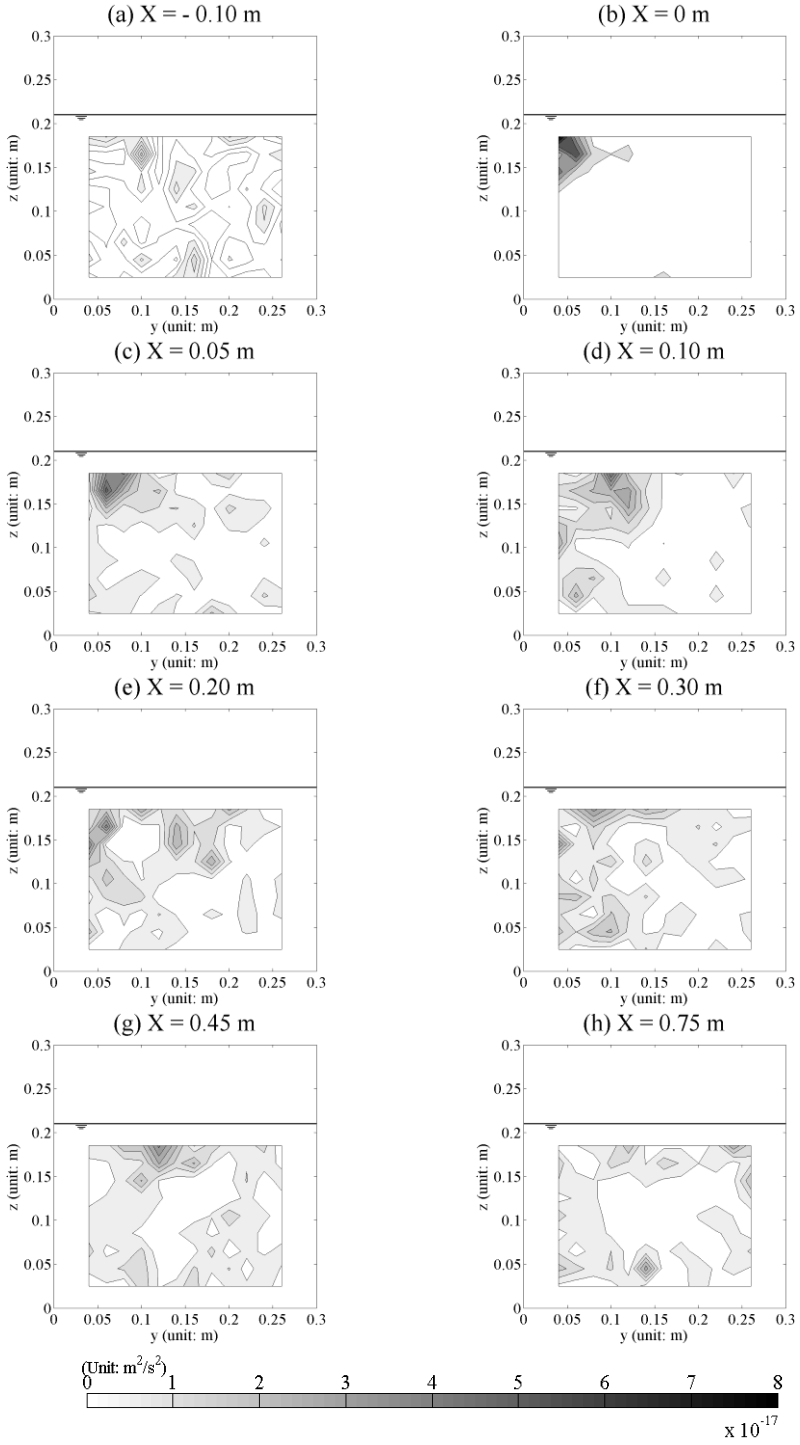

Figure A.133 (AM203) Turbulent Kinetic Energy contours

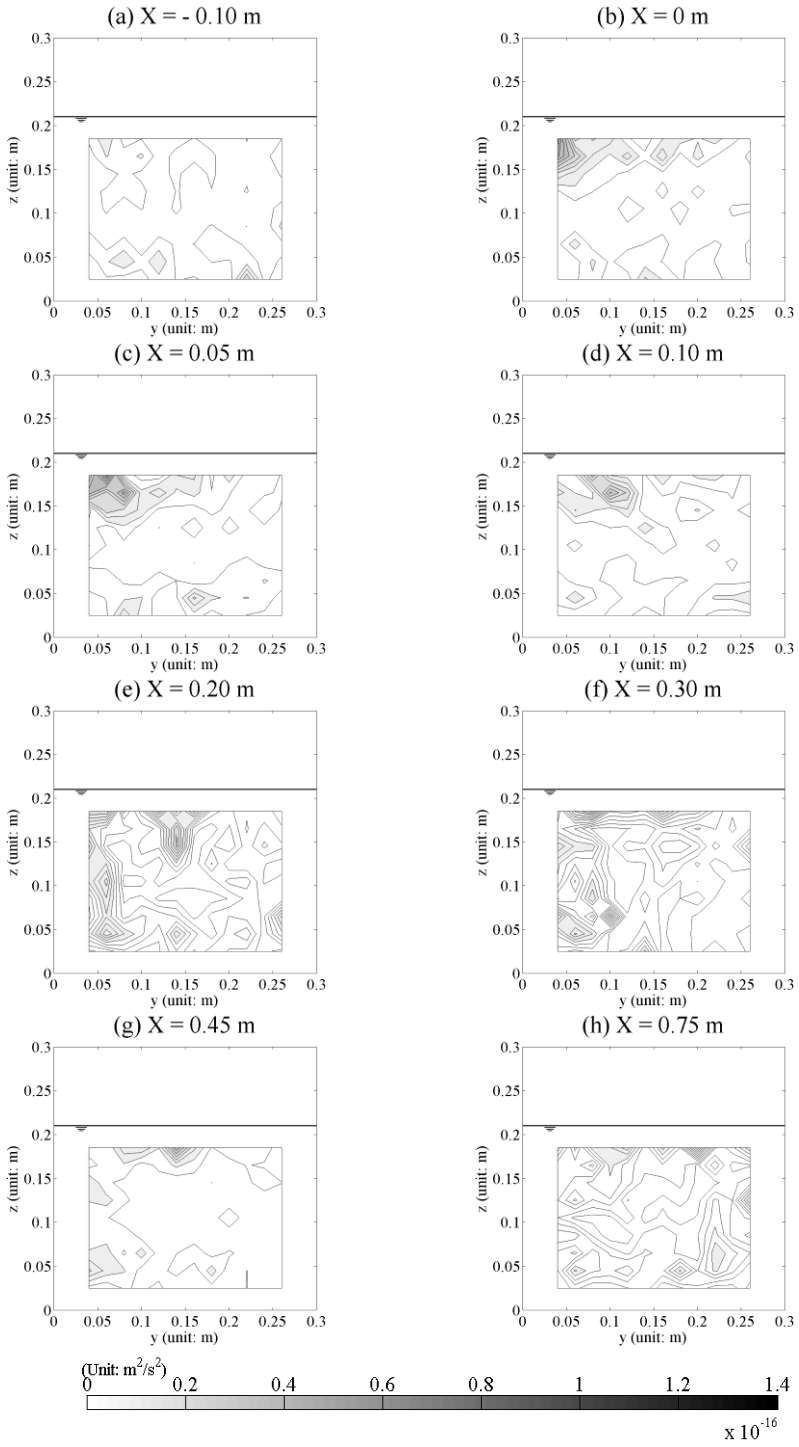

Figure A.134 (AM204) Turbulent Kinetic Energy contours

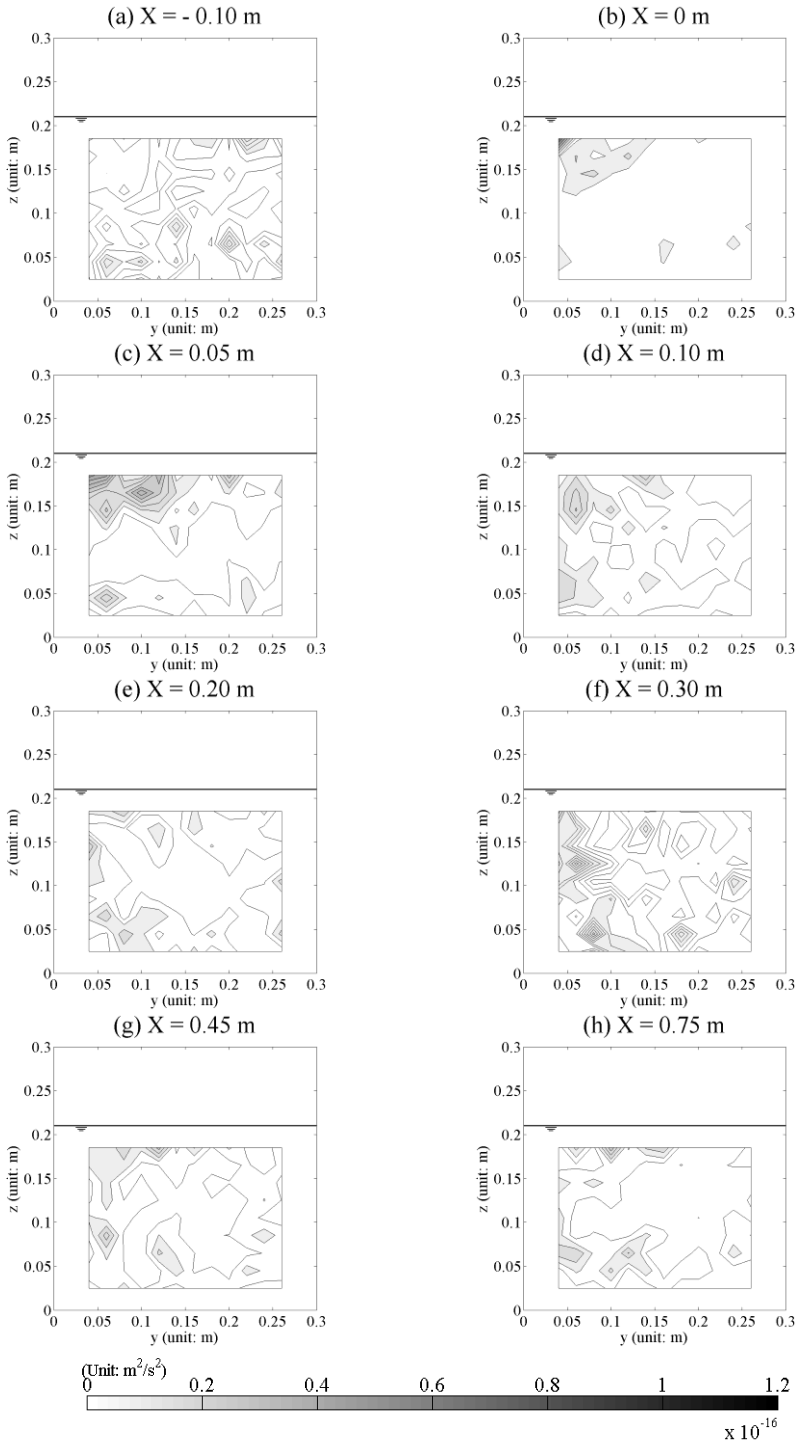

Figure A.135 (AM205) Turbulent Kinetic Energy contours

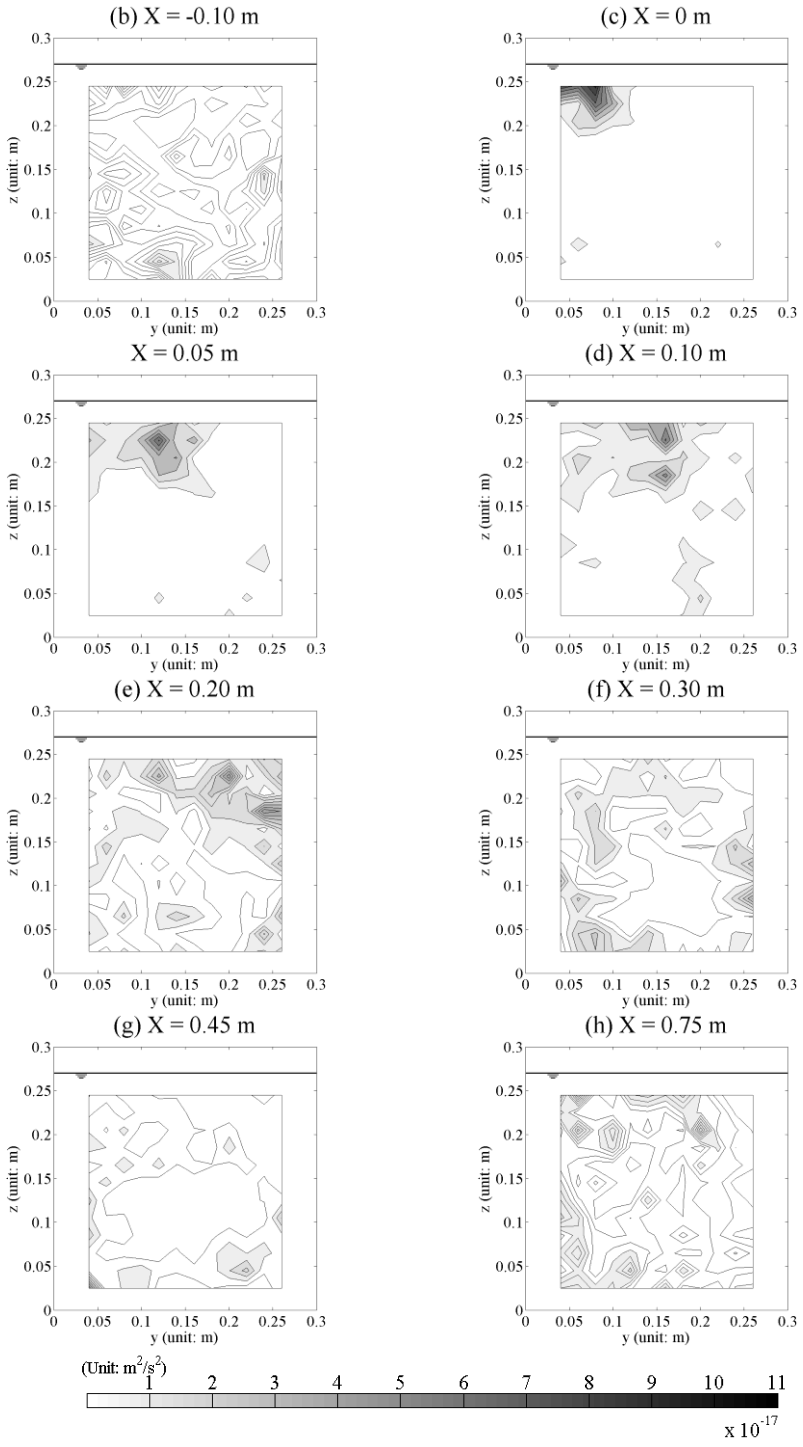

Figure A.136 (AM301) Turbulent Kinetic Energy contours

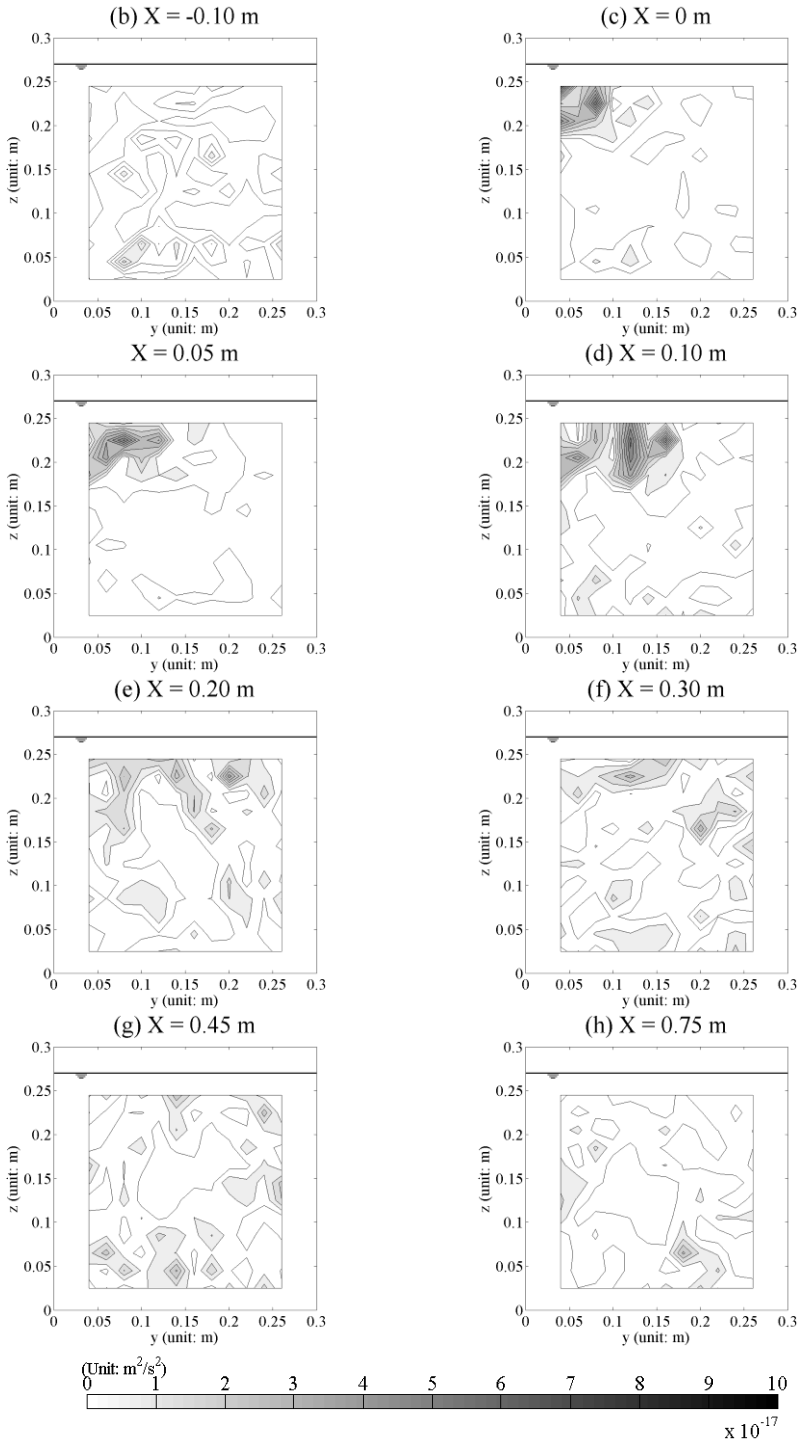

Figure A.137 (AM302) Turbulent Kinetic Energy contours

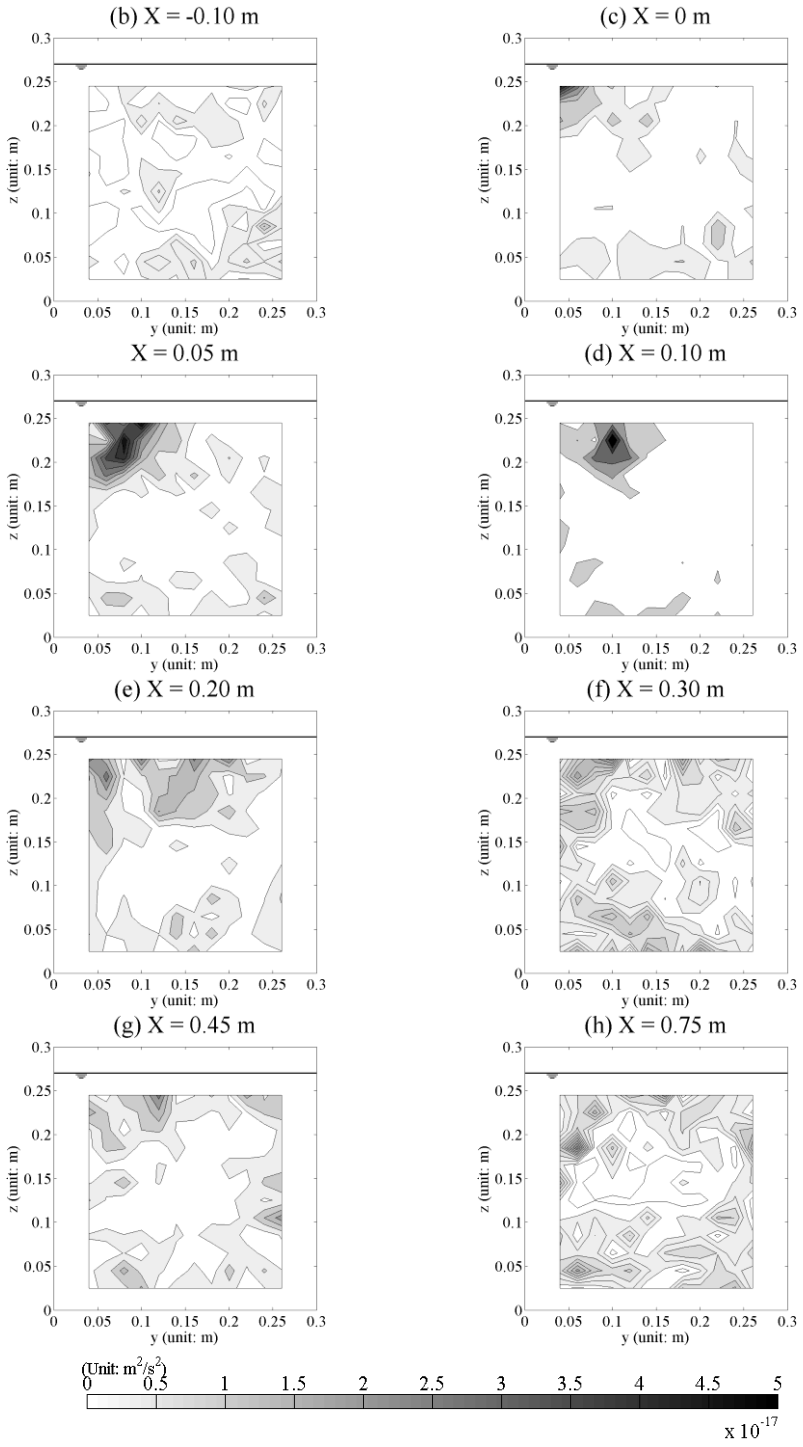

Figure A.138 (AM303) Turbulent Kinetic Energy contours

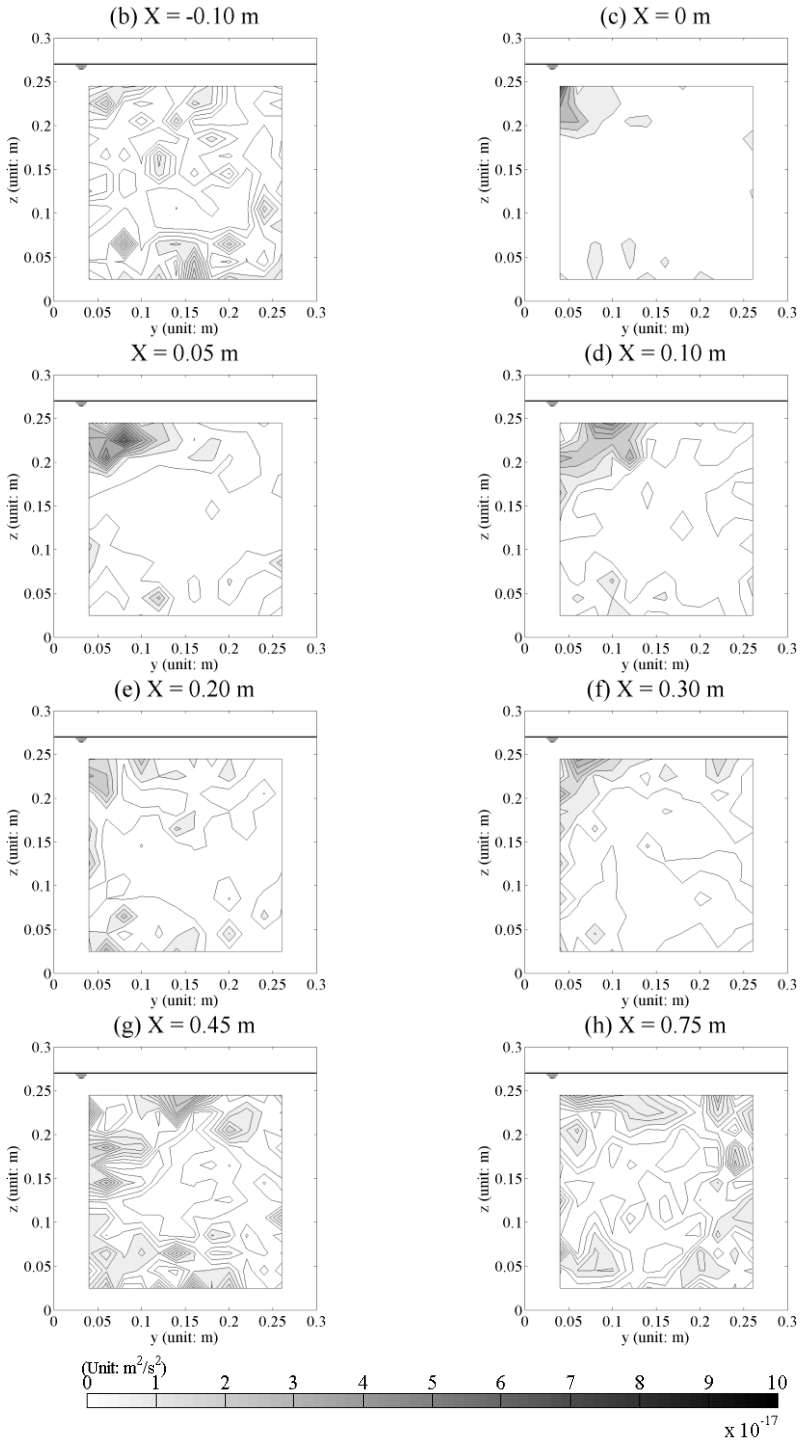

Figure A.139 (AM304) Turbulent Kinetic Energy contours

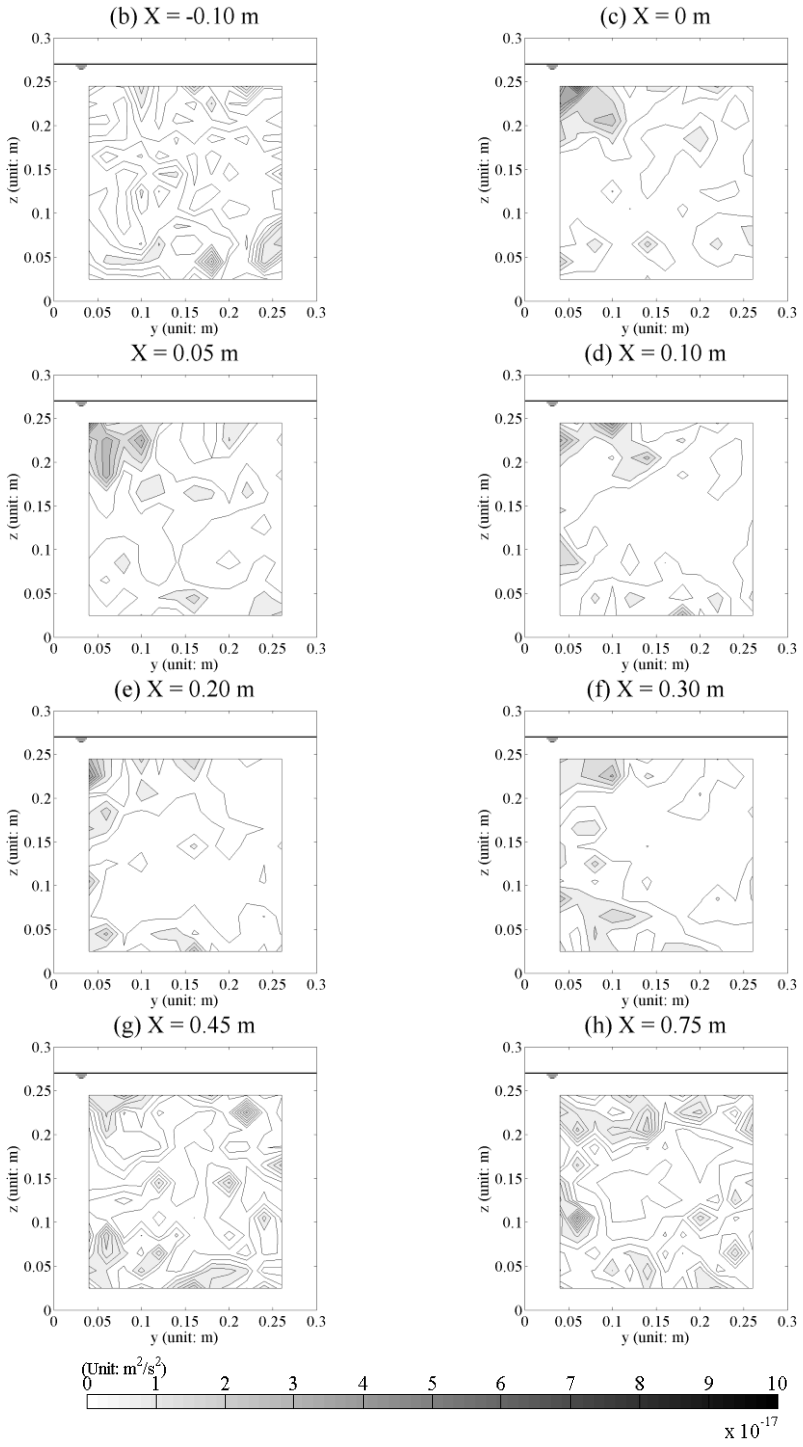

Figure A.140 (AM305) Turbulent Kinetic Energy contours

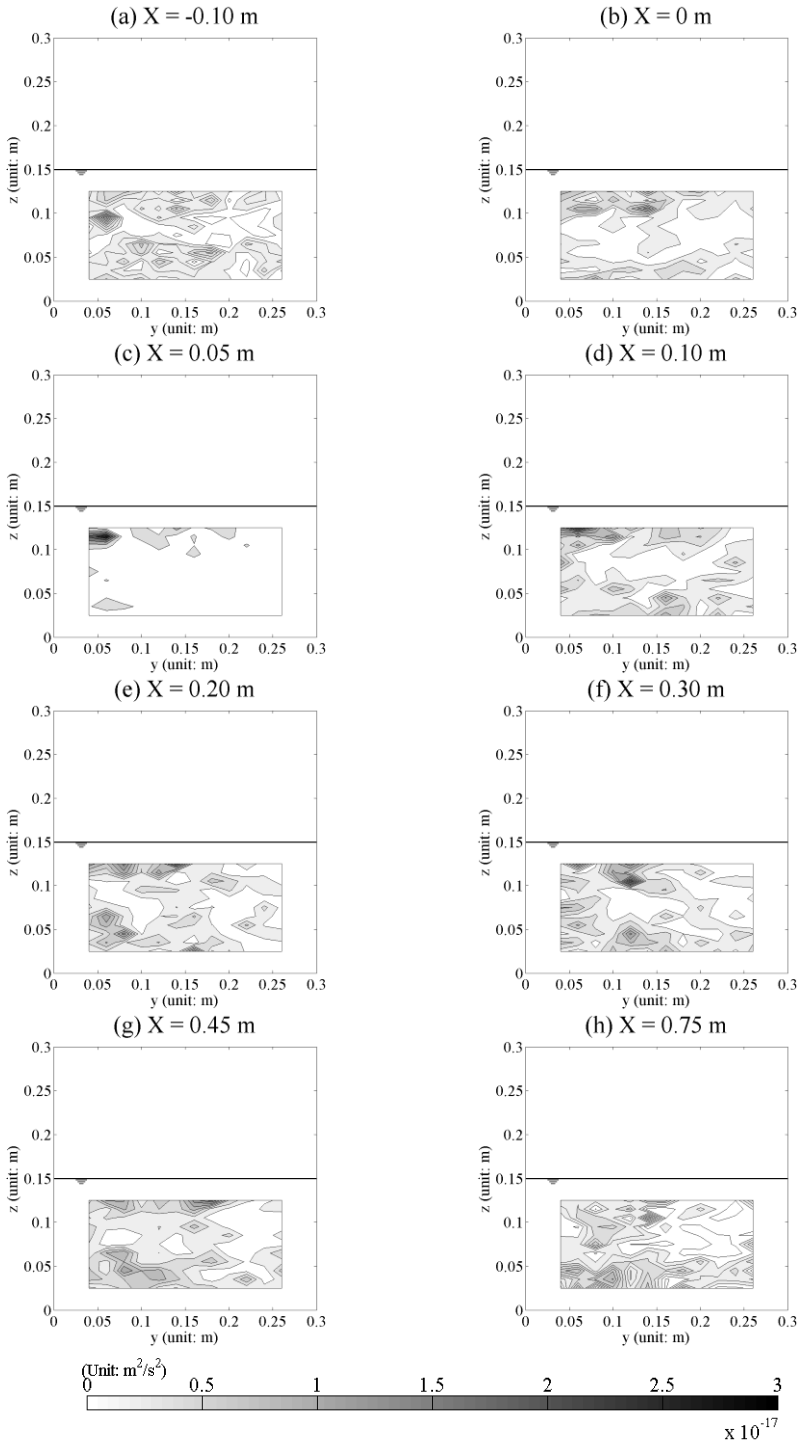

Figure A.141 (AS101) Turbulent Kinetic Energy contours

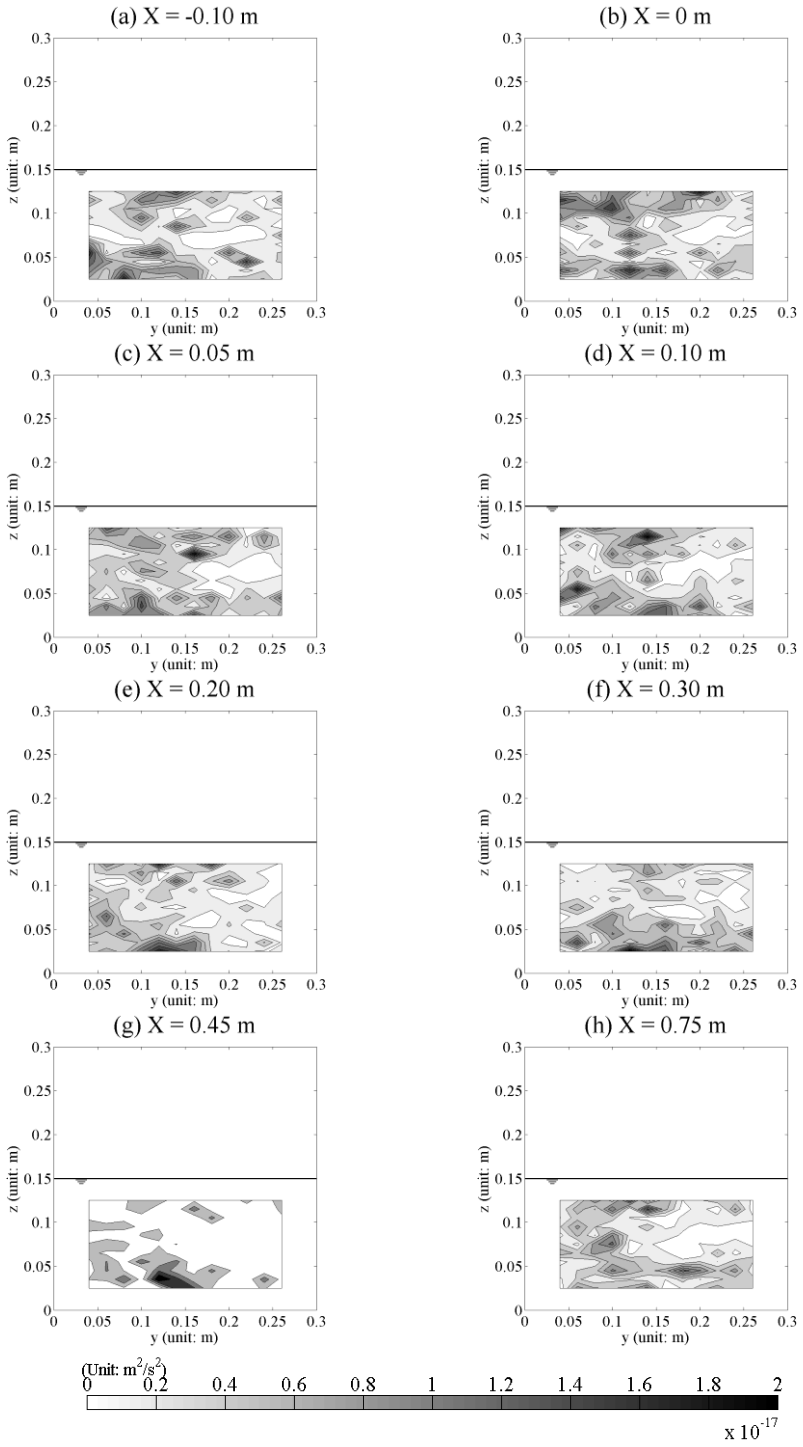

Figure A.142 (AS103) Turbulent Kinetic Energy contours

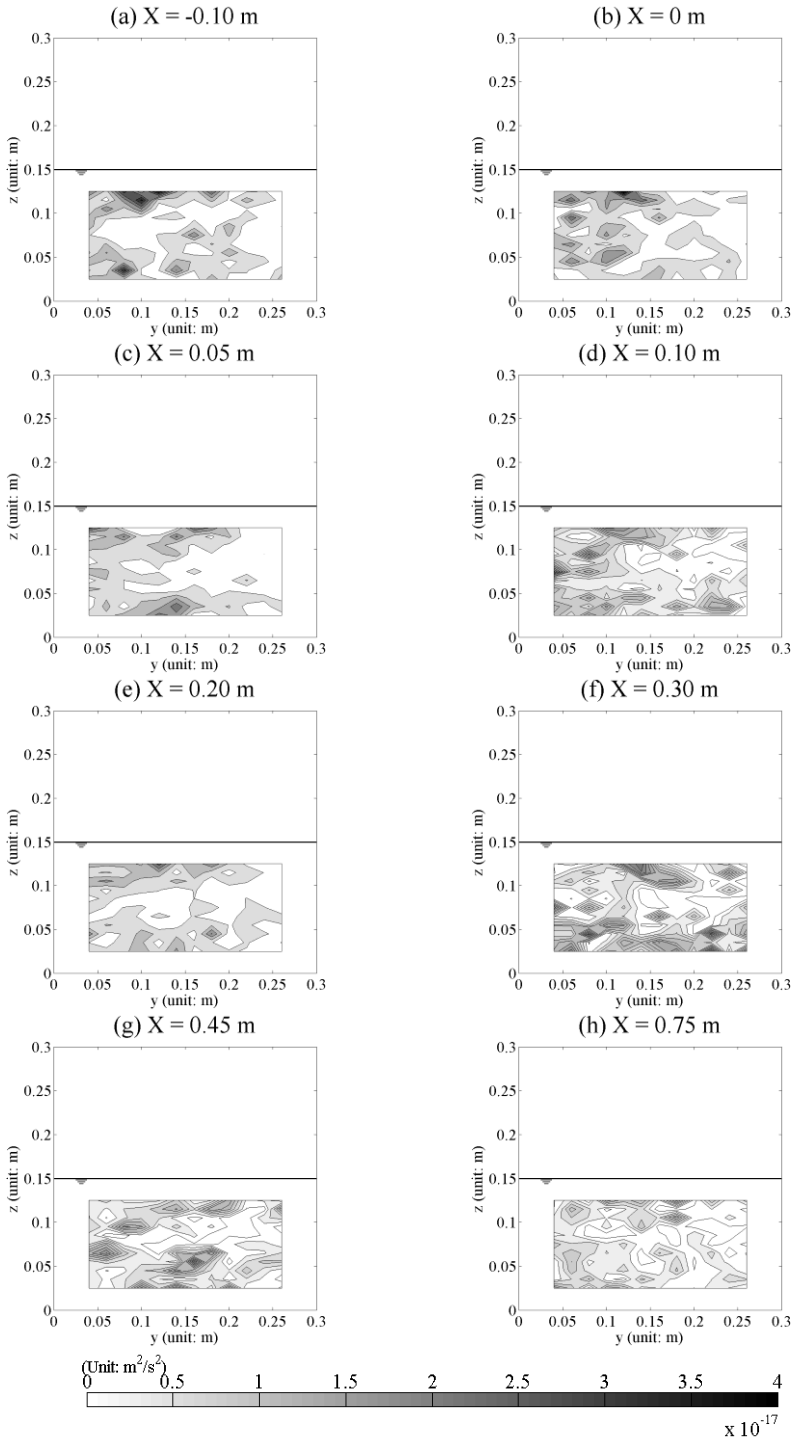

Figure A.143 (AS105) Turbulent Kinetic Energy contours

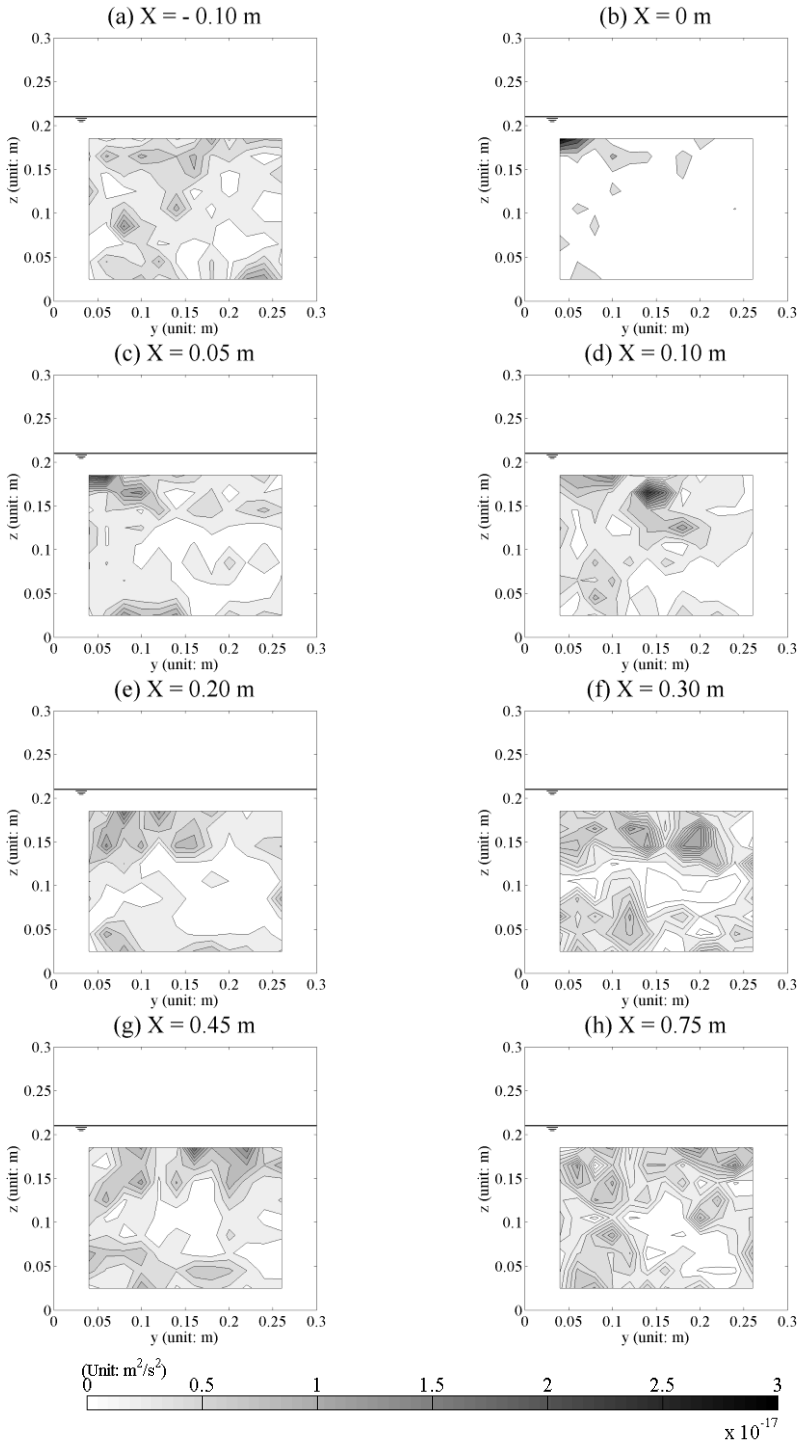

Figure A.144 (AS201) Turbulent Kinetic Energy contours

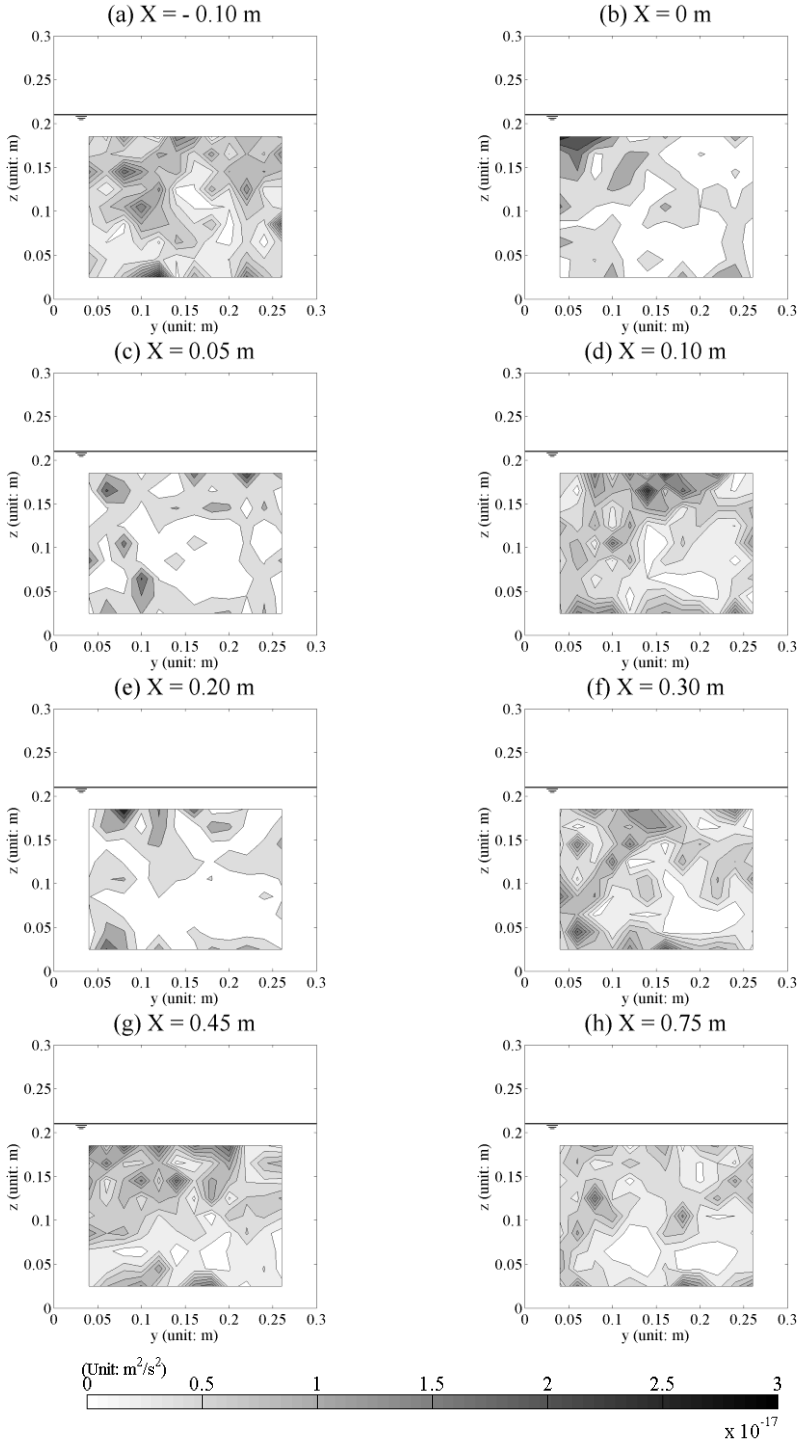

Figure A.145 (AS203) Turbulent Kinetic Energy contours

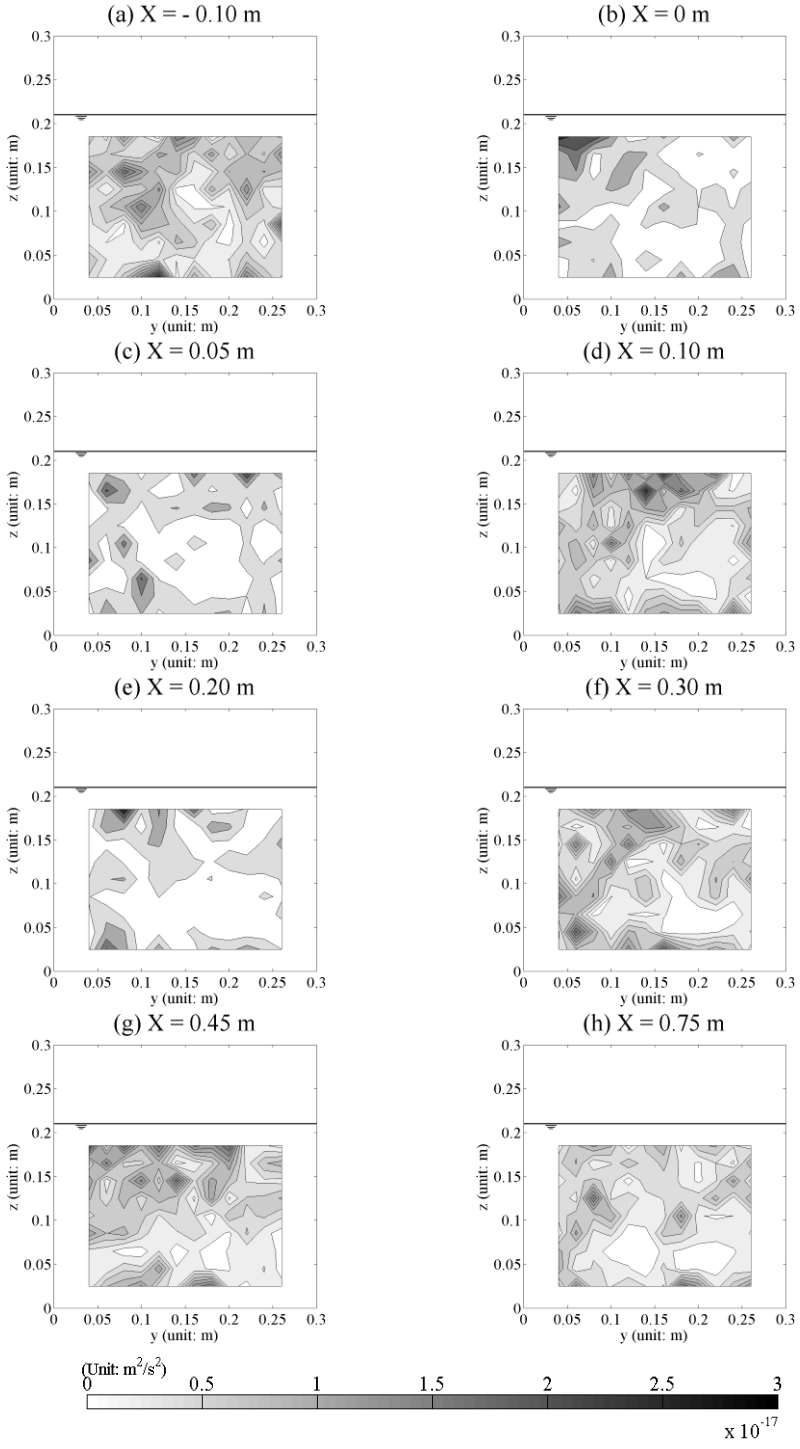

Figure A.146 (AS205) Turbulent Kinetic Energy contours

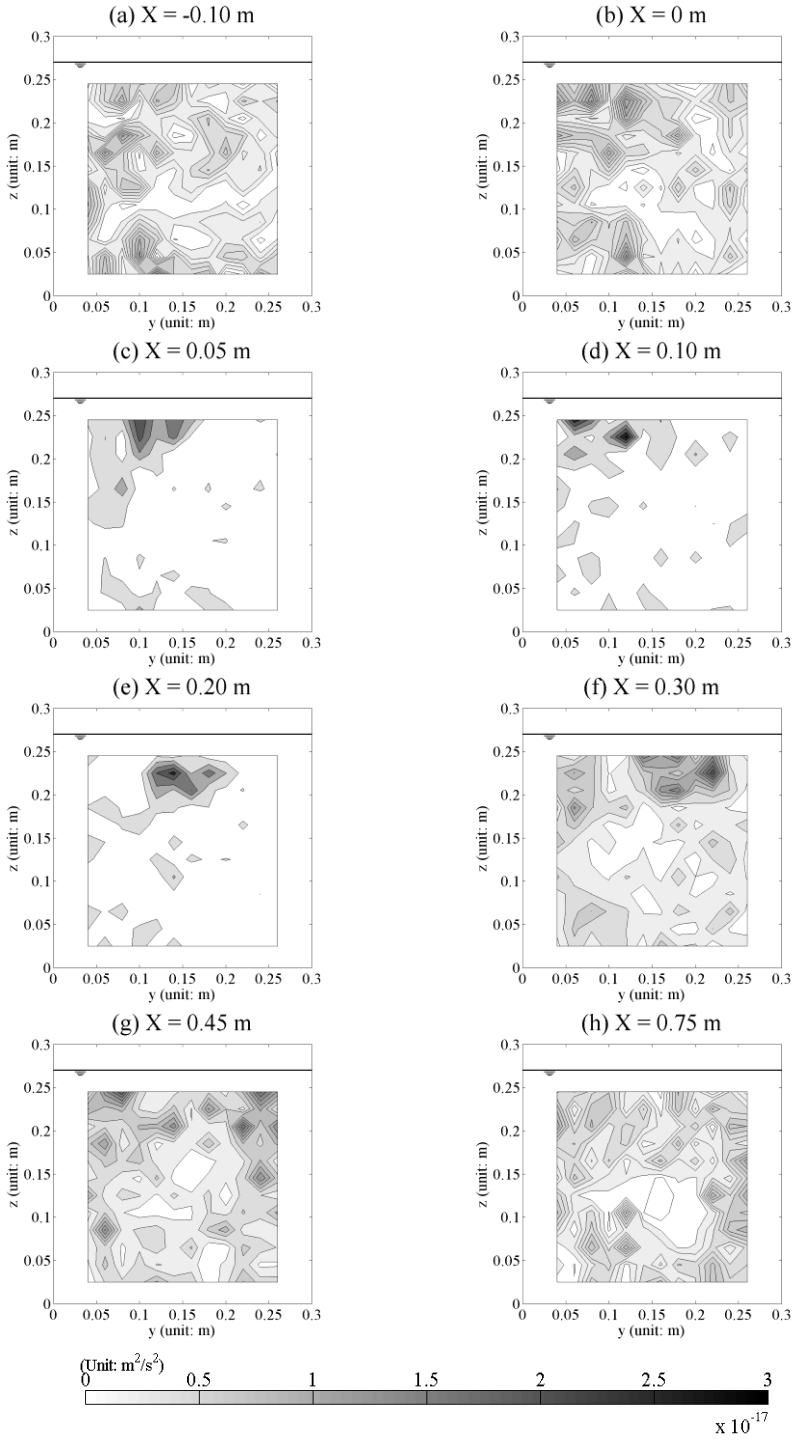

Figure A.147 (AS301) Turbulent Kinetic Energy contours

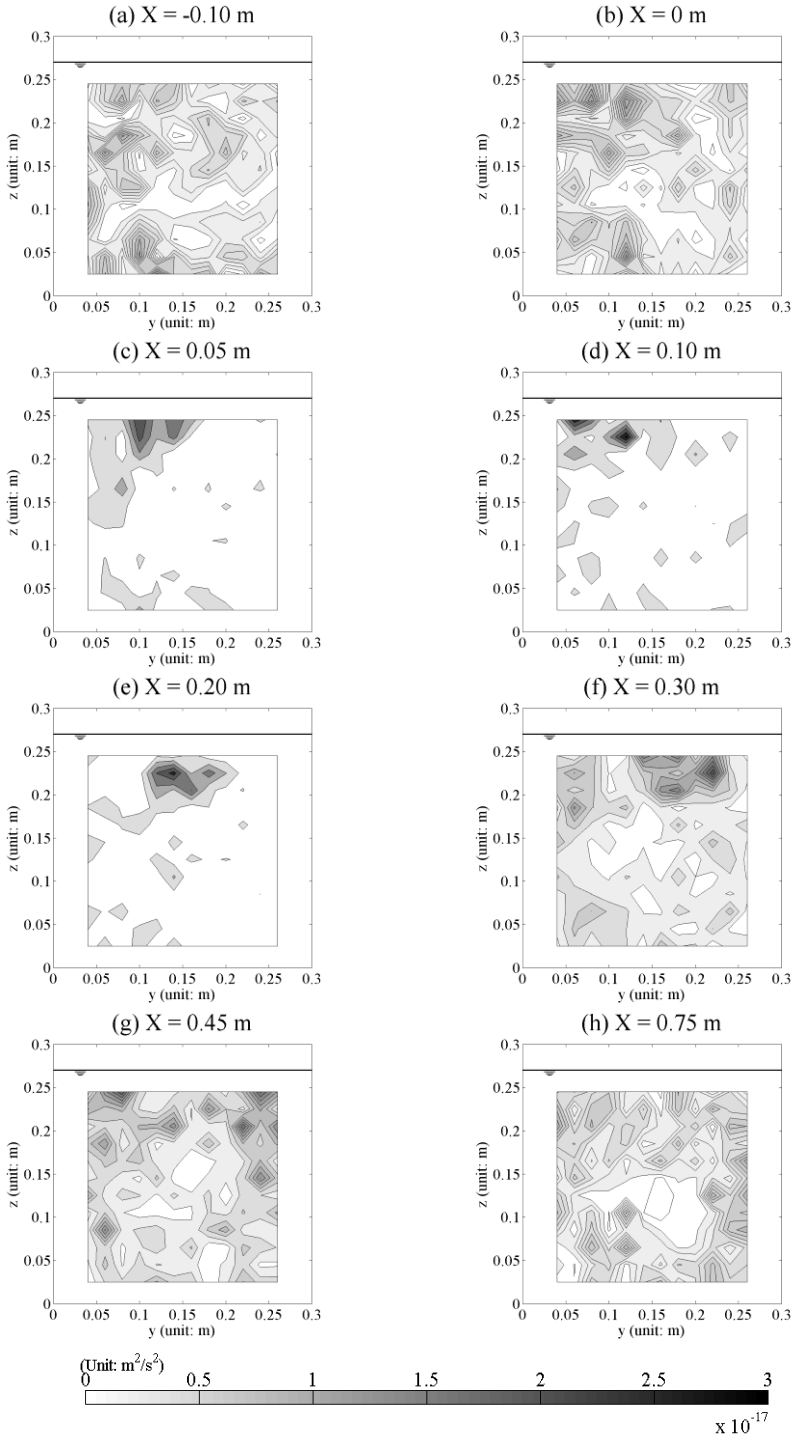

Figure A.148 (AS303) Turbulent Kinetic Energy contours

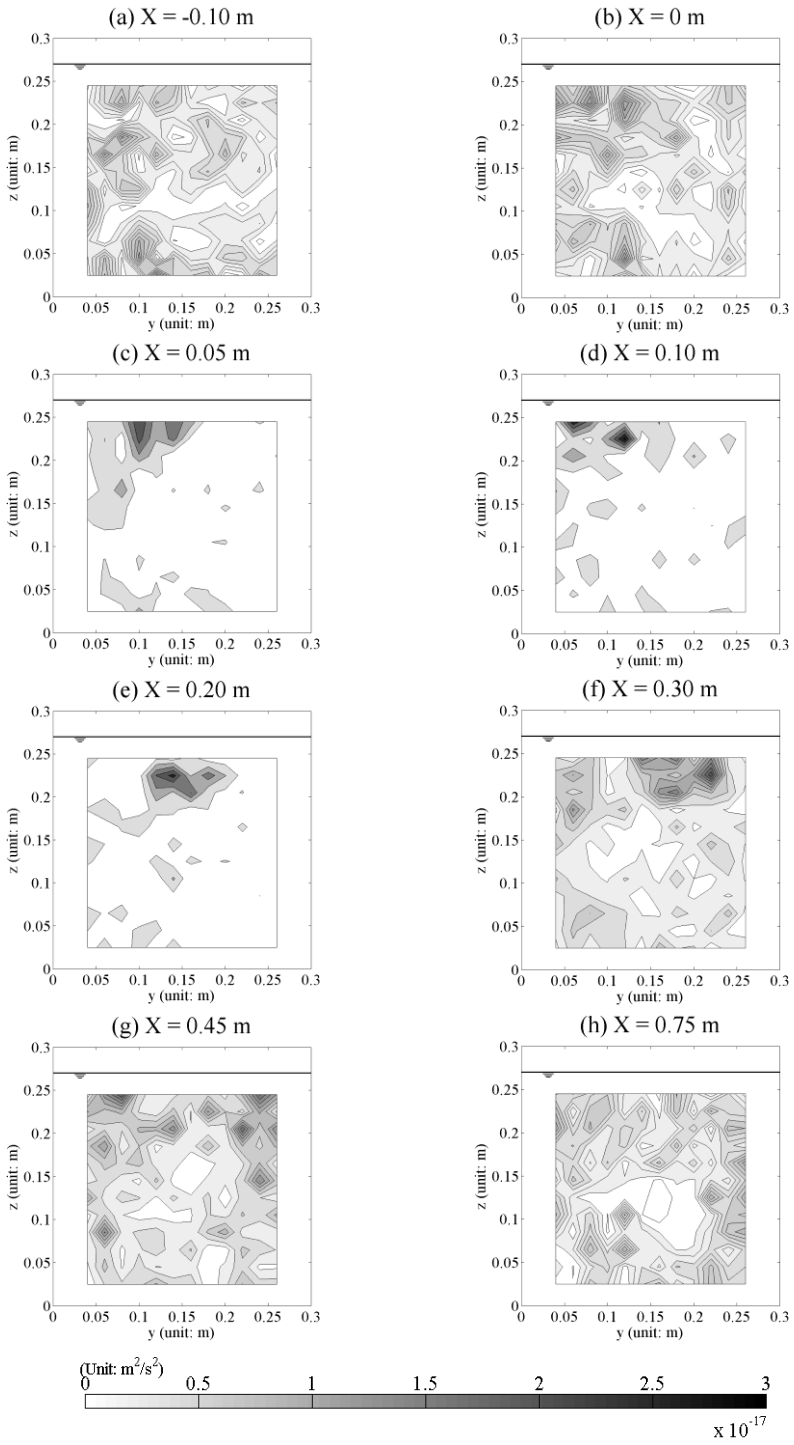

Figure A.149 (AS305) Turbulent Kinetic Energy contours

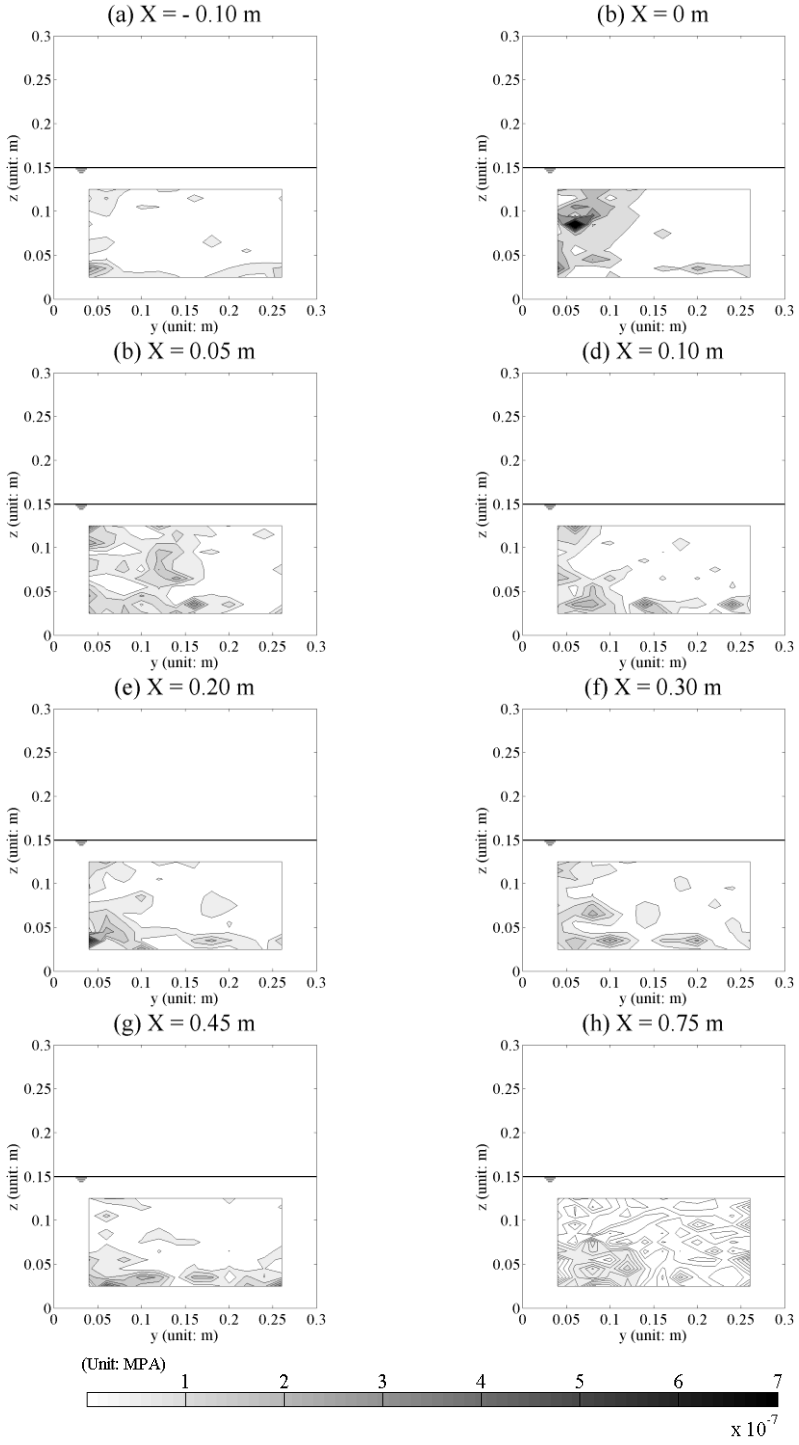

Figure A.150 (AR101) Reynolds shear stress contours

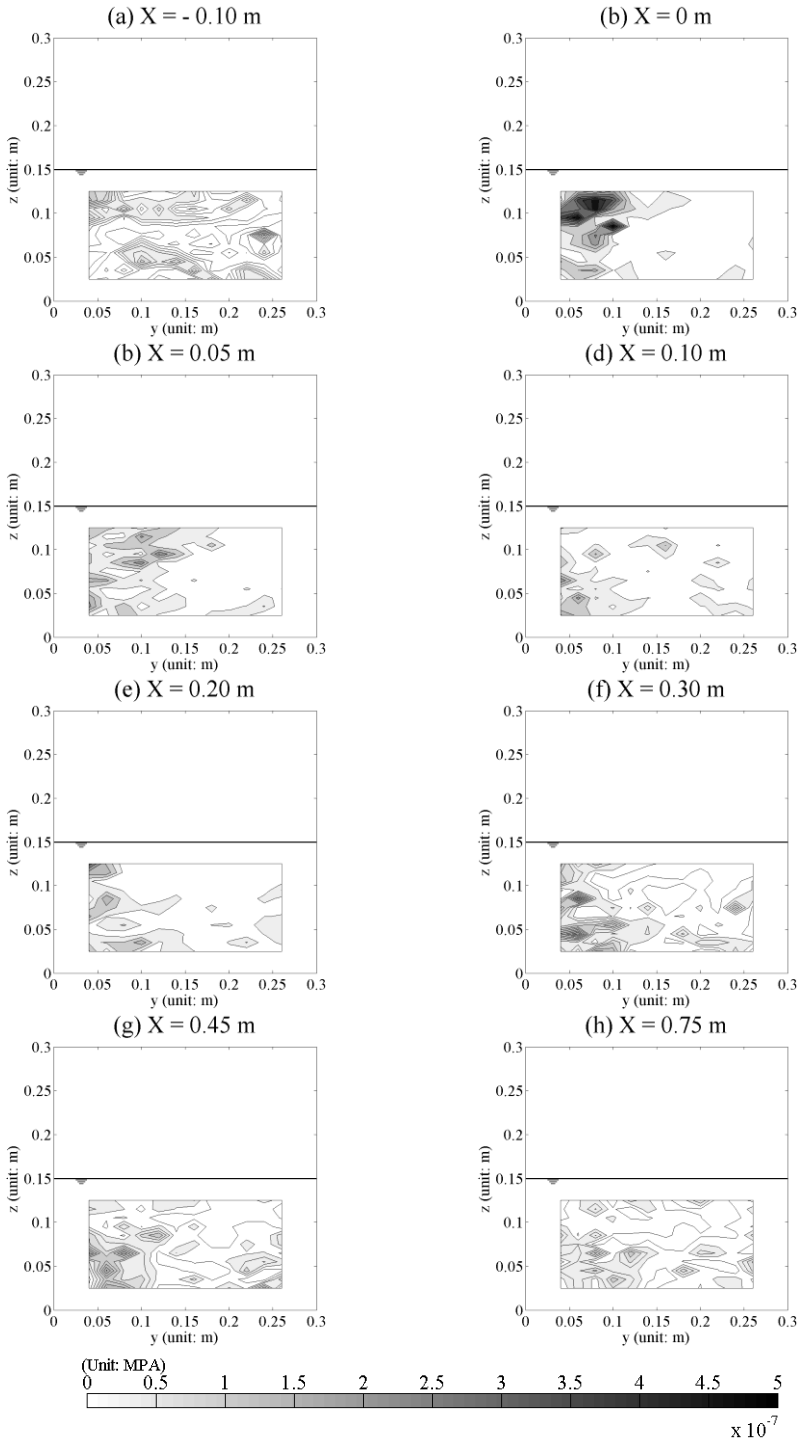

Figure A.151 (AR102) Reynolds shear stress contours

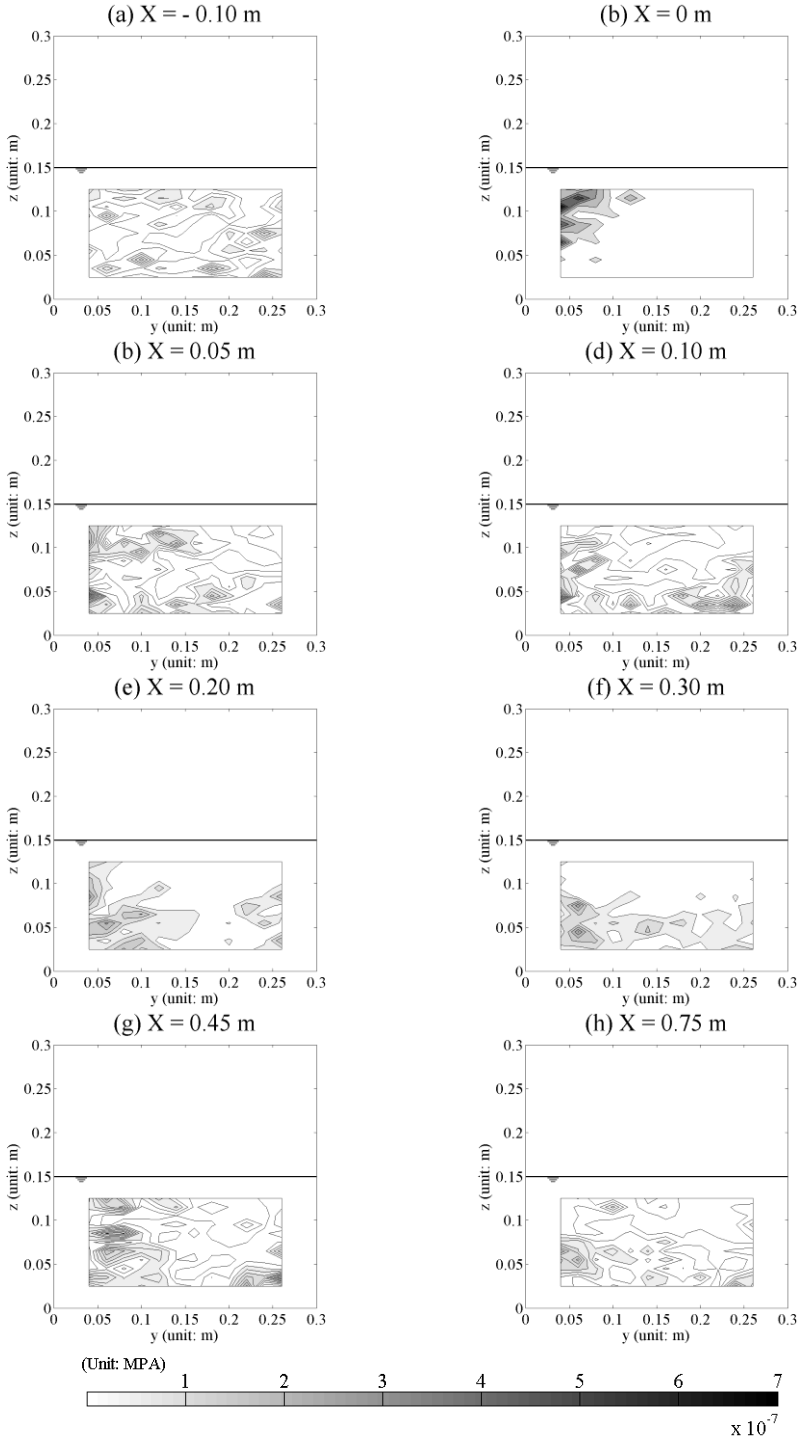

Figure A.152 (AR103) Reynolds shear stress contours

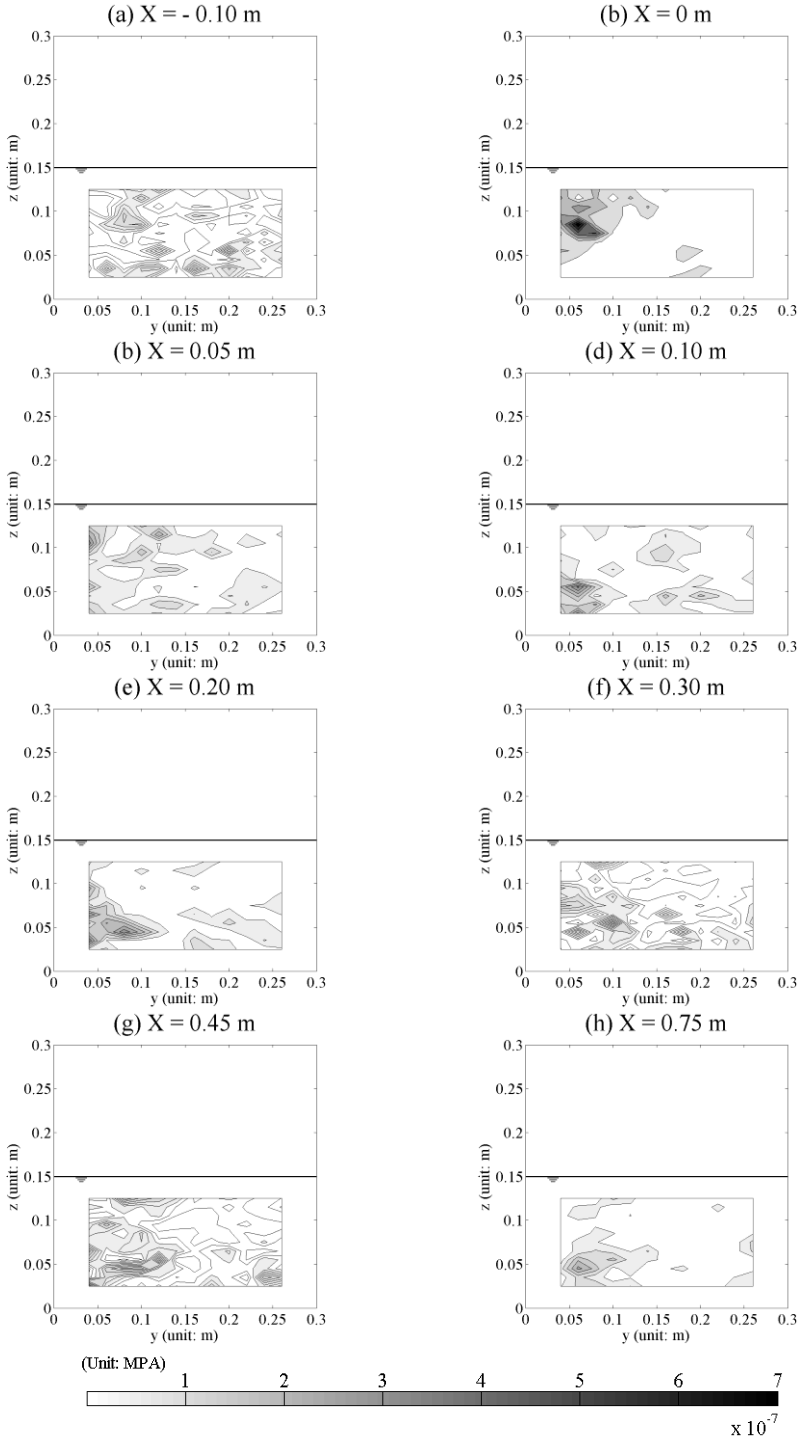

Figure A.153 (AR104) Reynolds shear stress contours

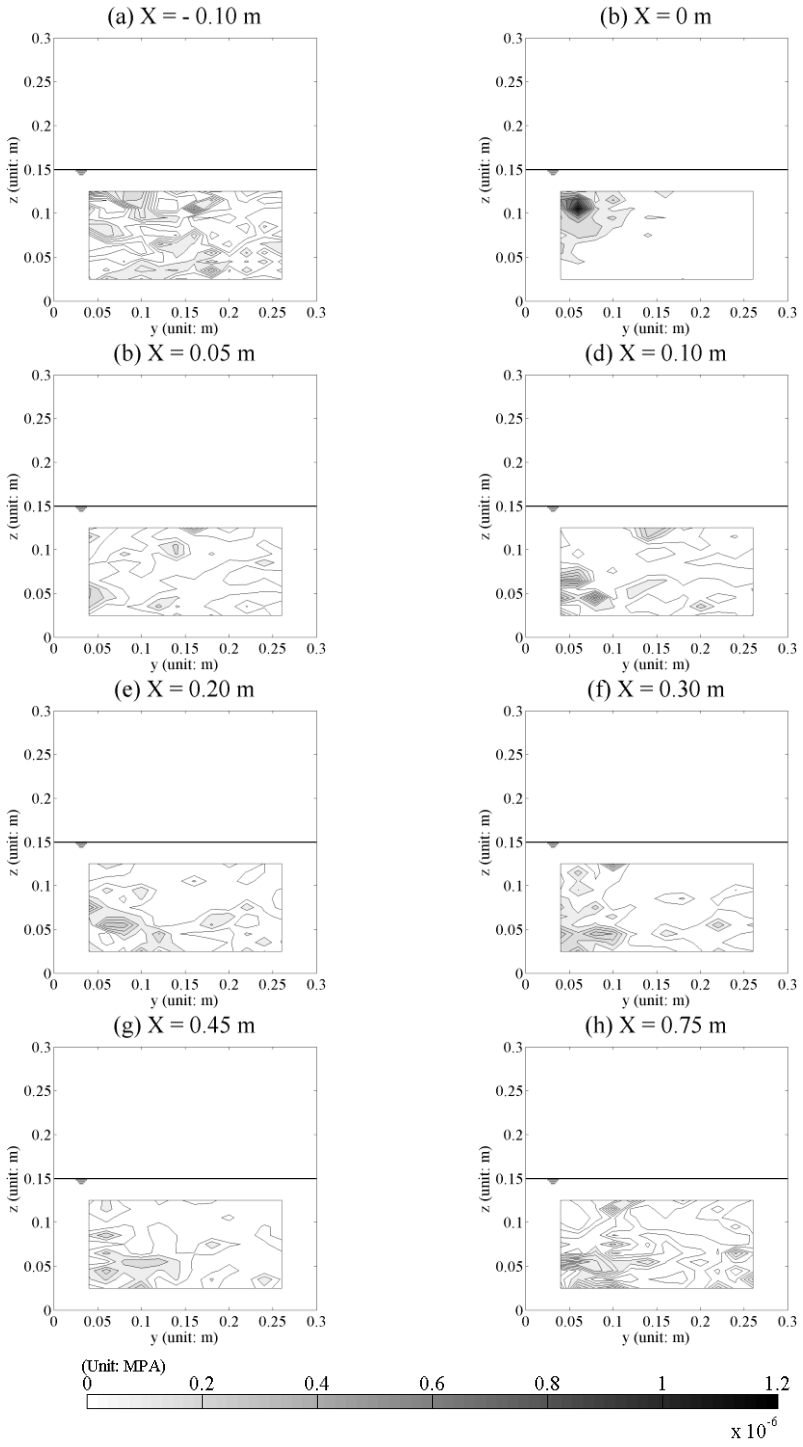

Figure A.154 (AR105) Reynolds shear stress contours

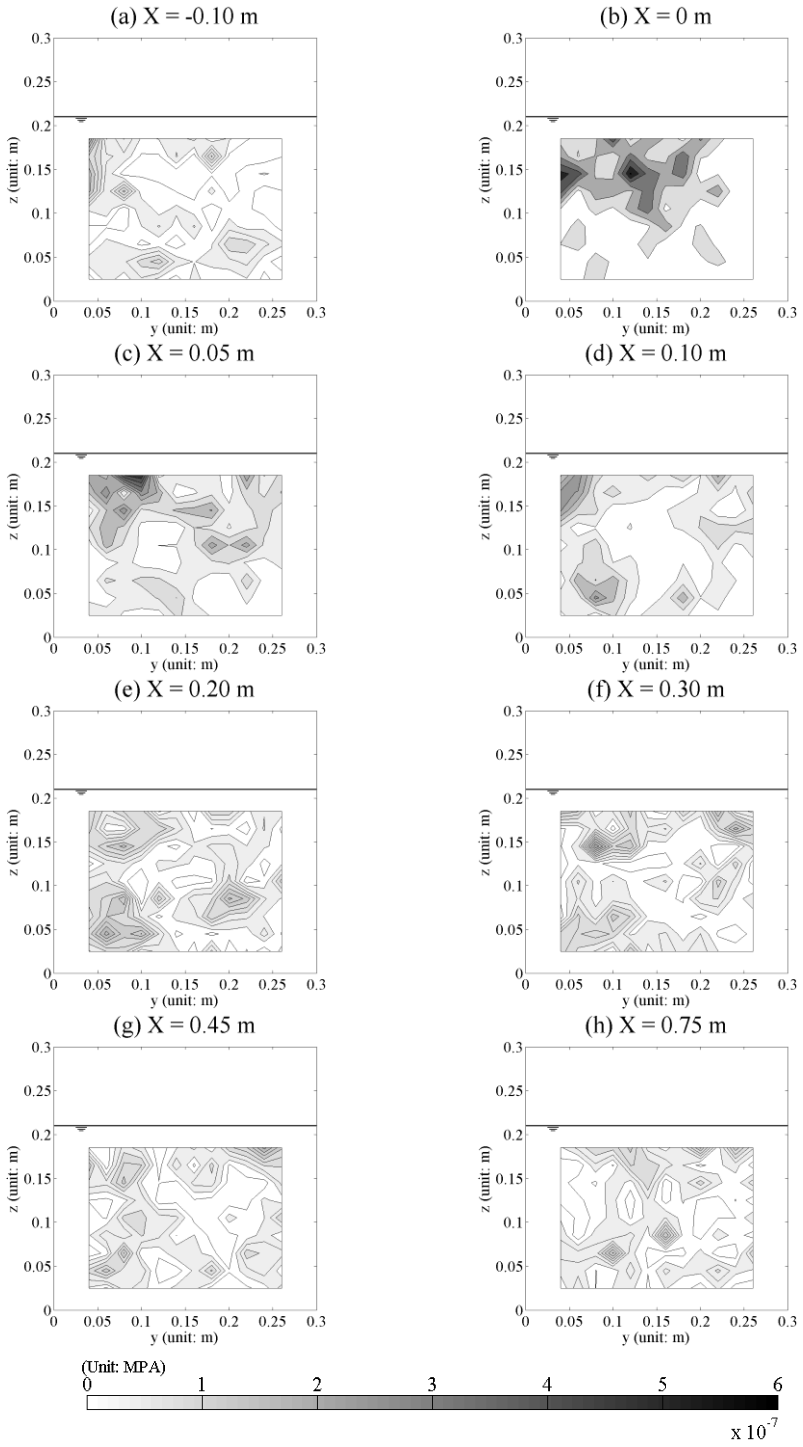

Figure A.155 (AR201) Reynolds shear stress contours

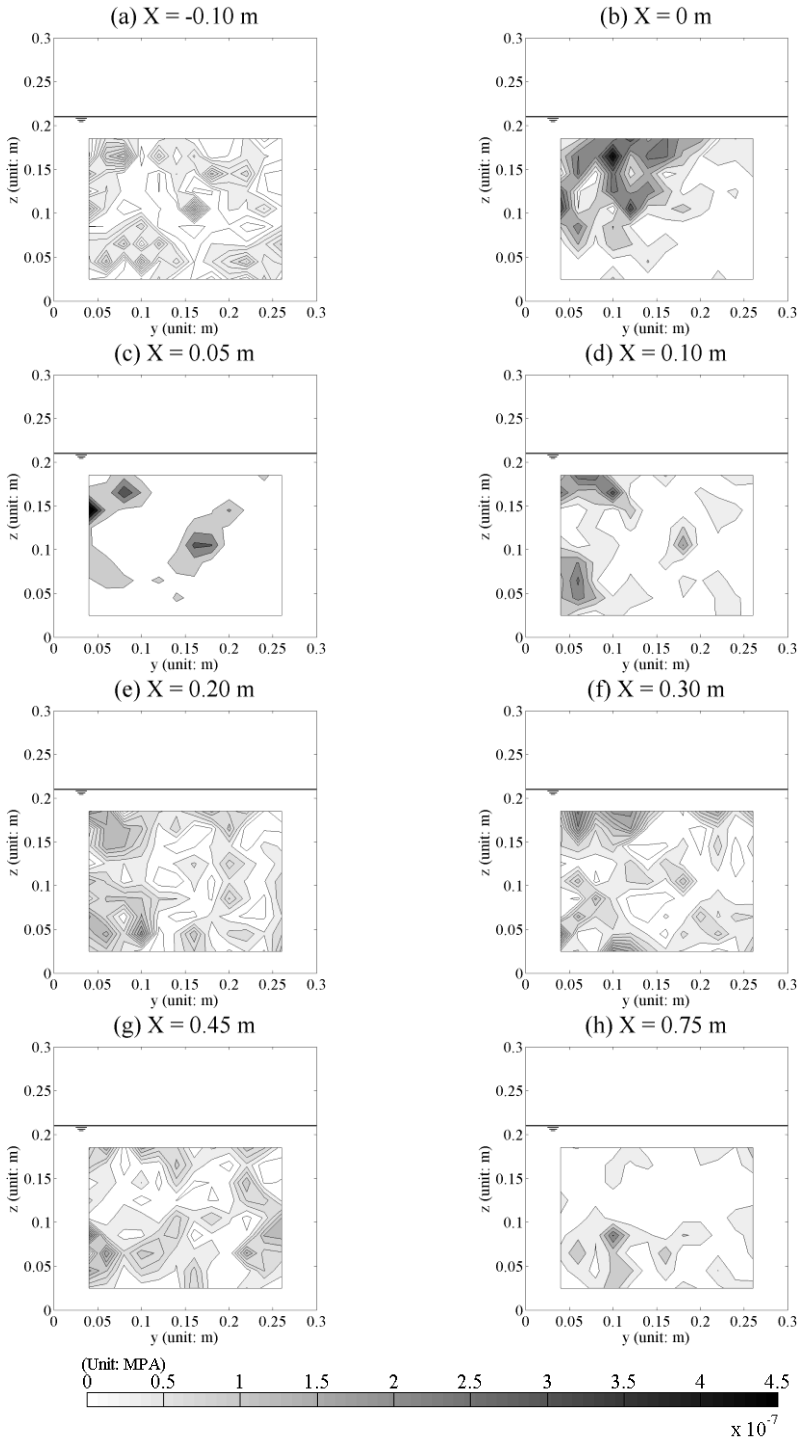

Figure A.156 (AR202) Reynolds shear stress contours

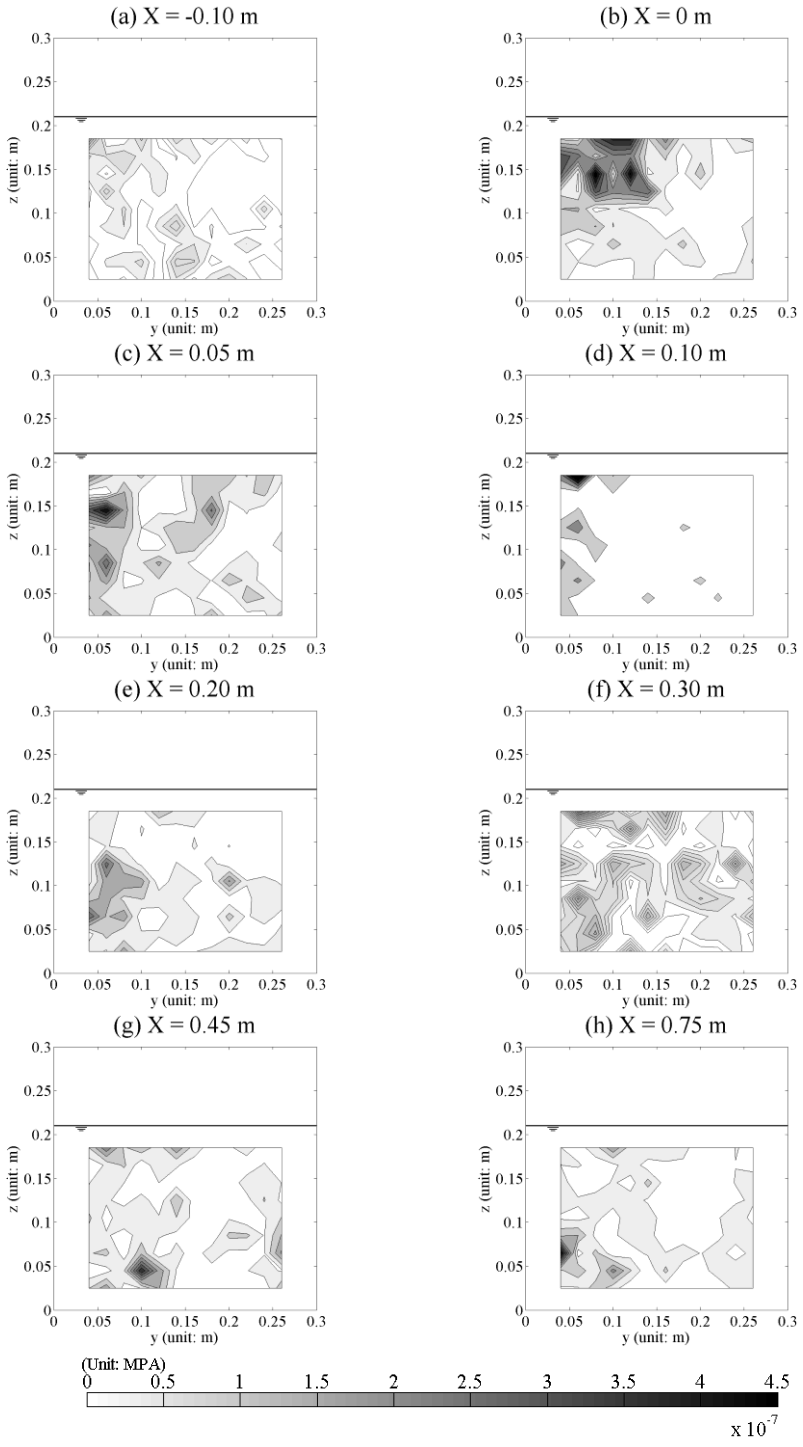

Figure A.157 (AR203) Reynolds shear stress contours

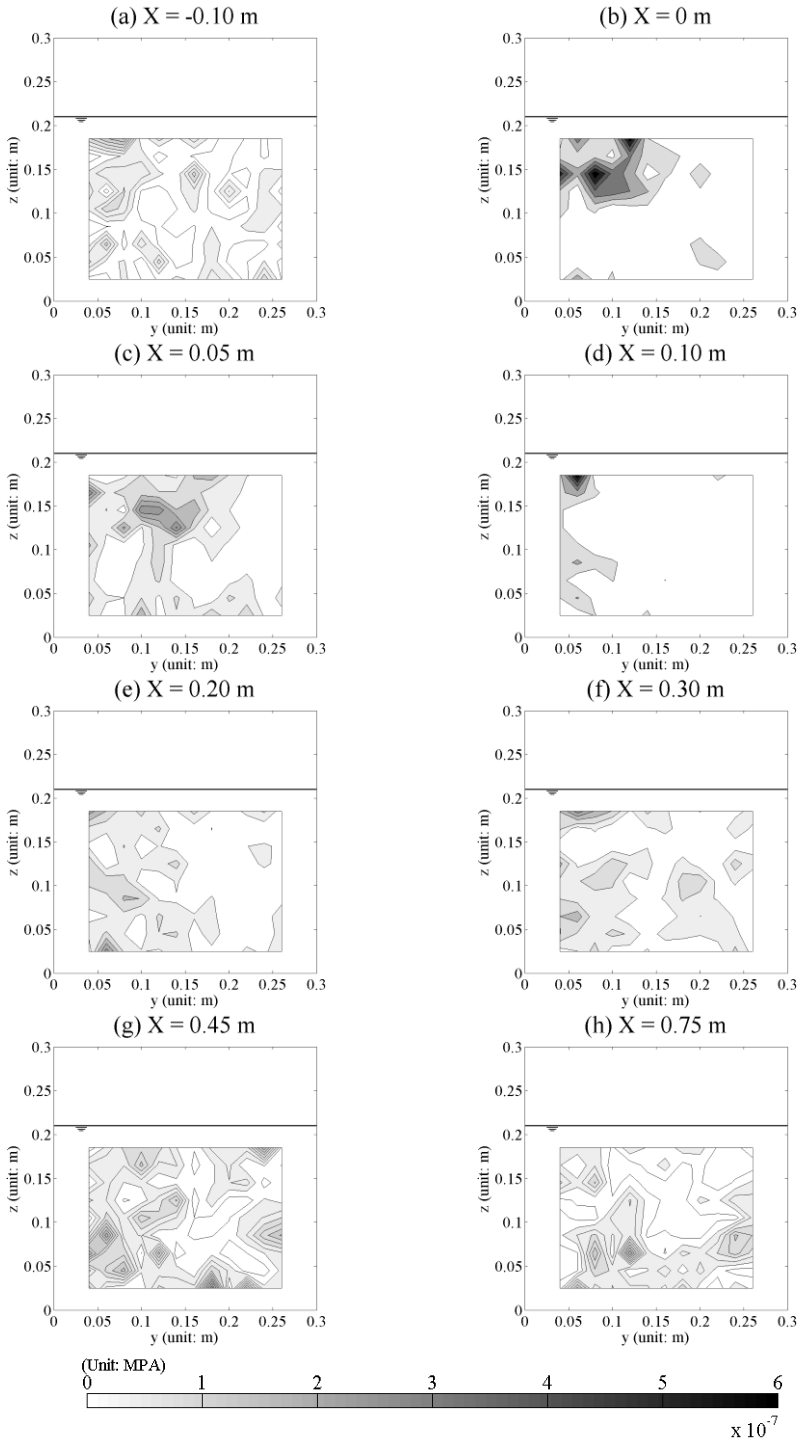

Figure A.158 (AR204) Reynolds shear stress contours

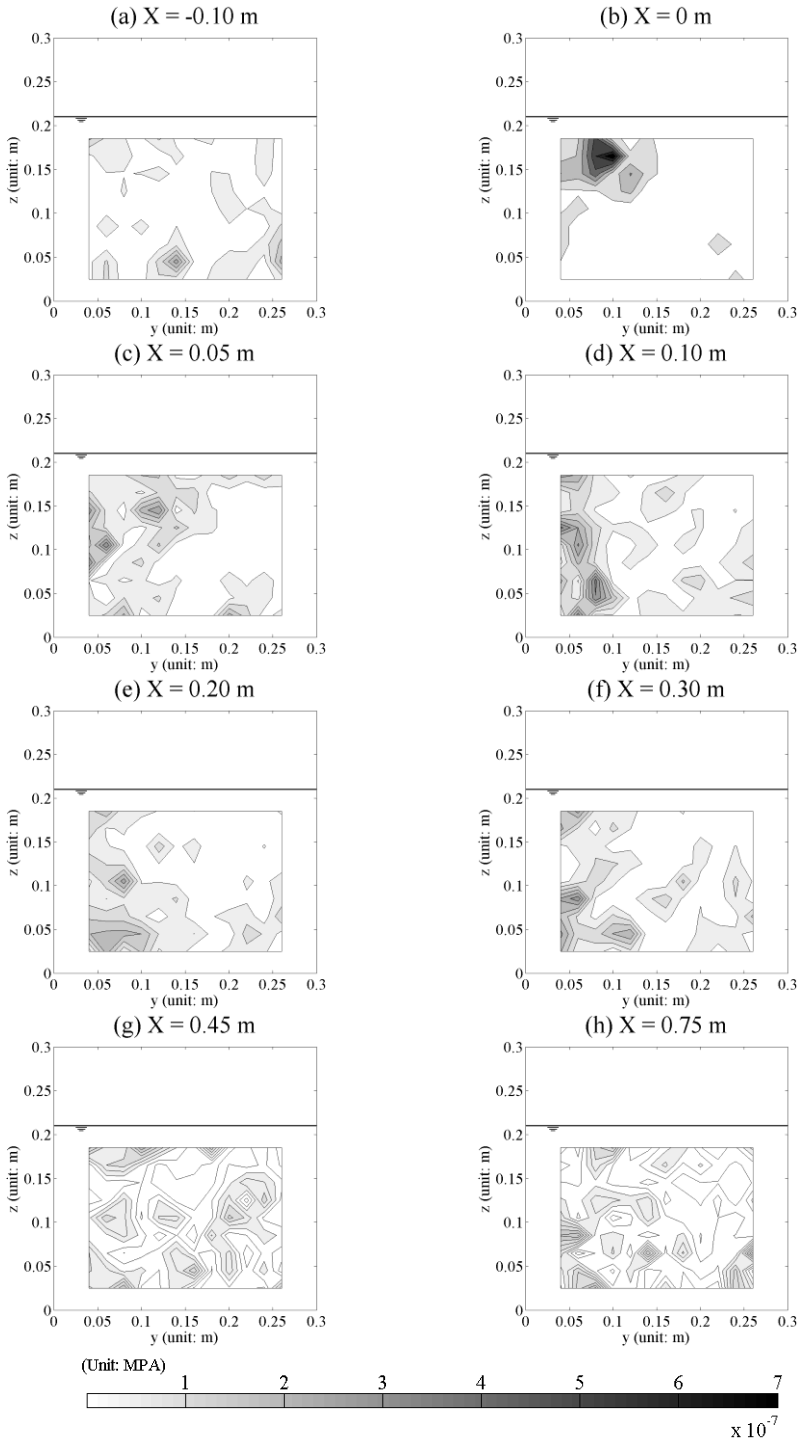

Figure A.159 (AR205) Reynolds shear stress contours

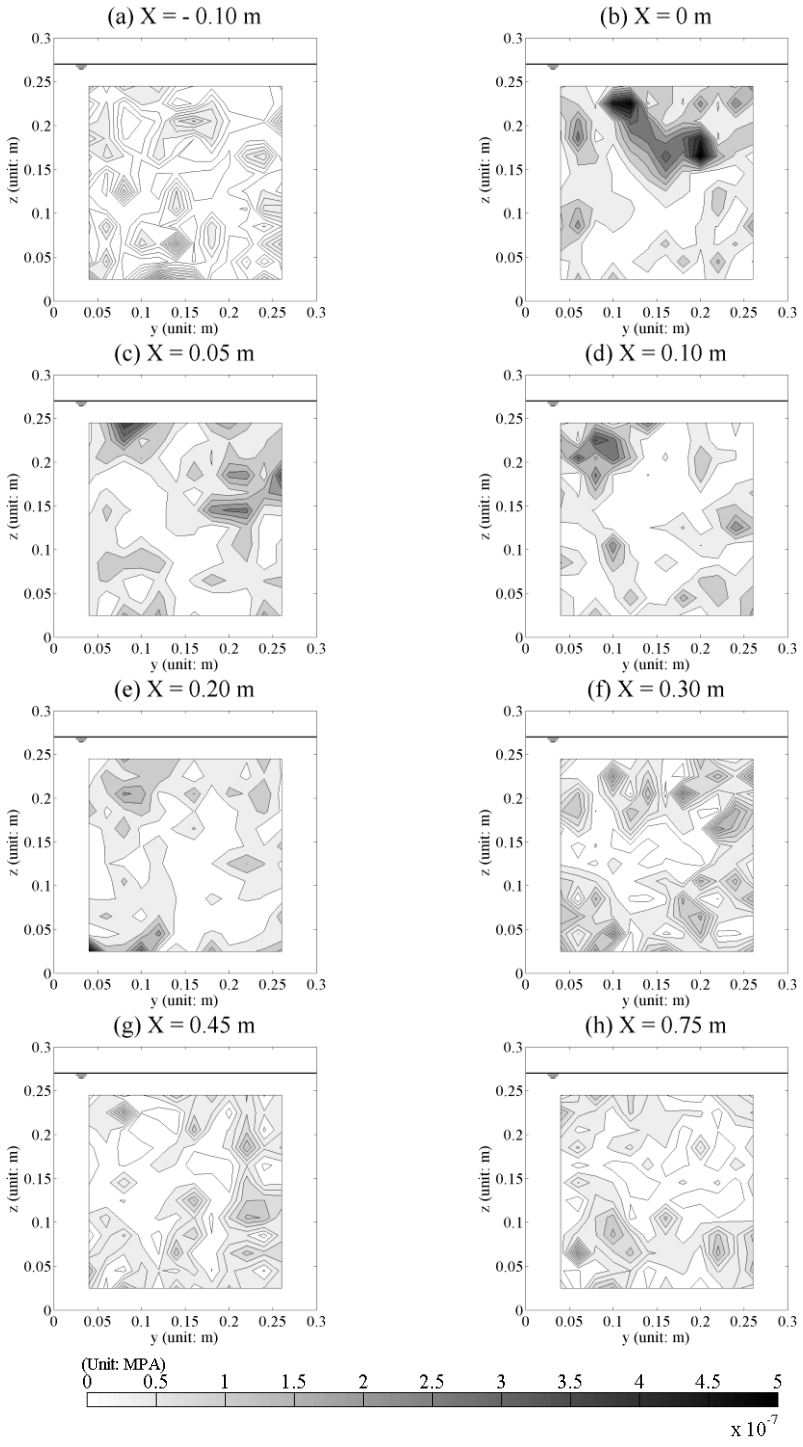

Figure A.160 (AR301) Reynolds shear stress contours

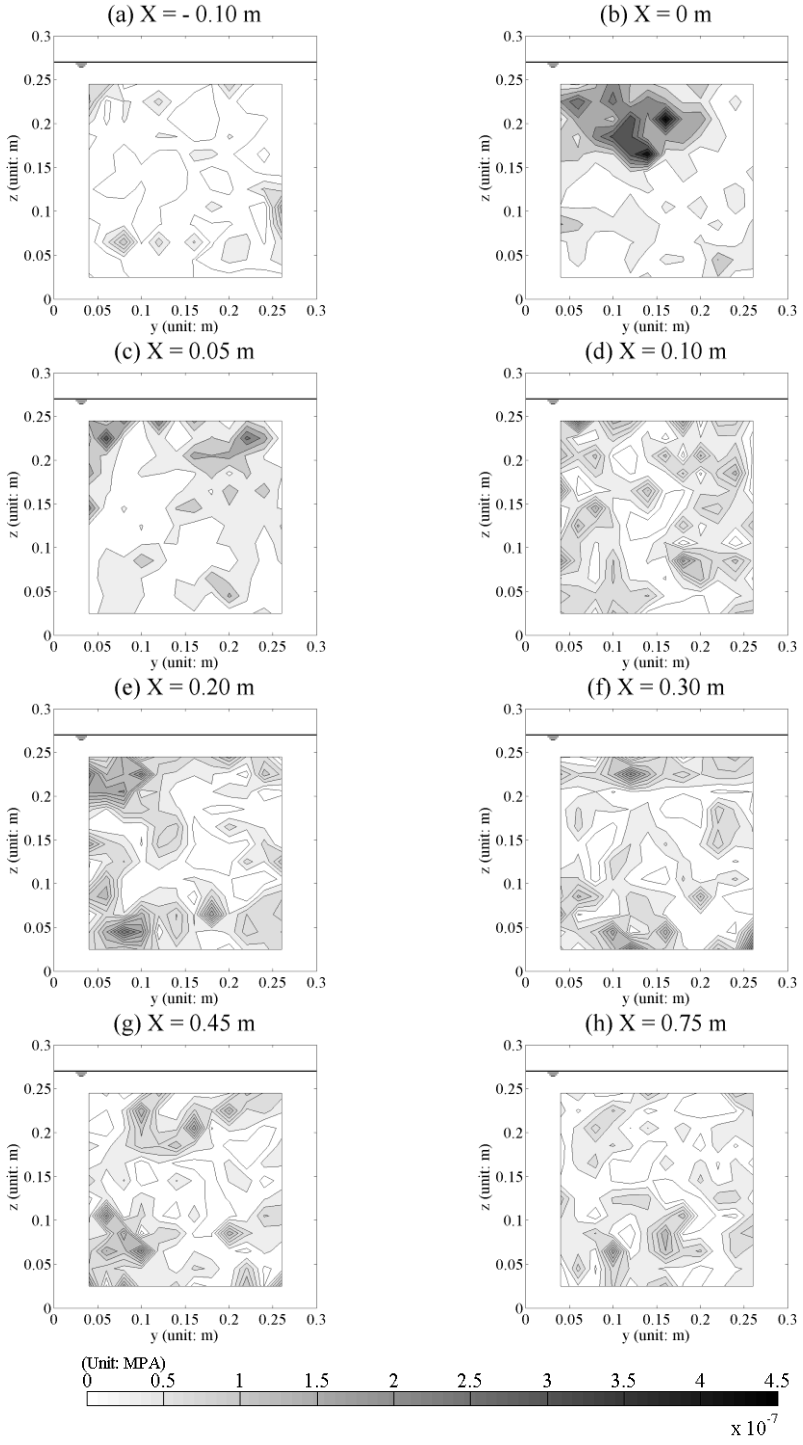

Figure A.161 (AR302) Reynolds shear stress contours

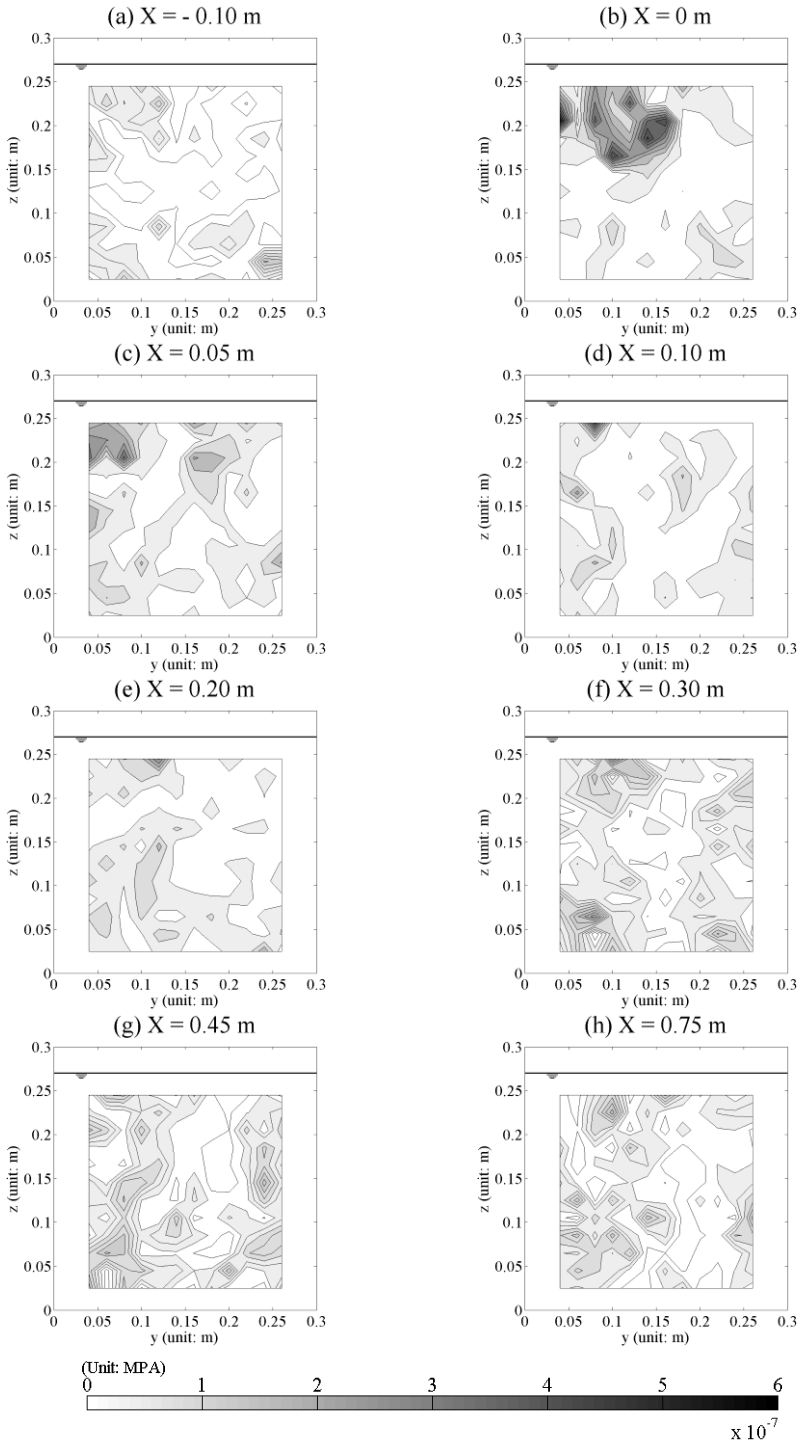

Figure A.162 (AR303) Reynolds shear stress contours

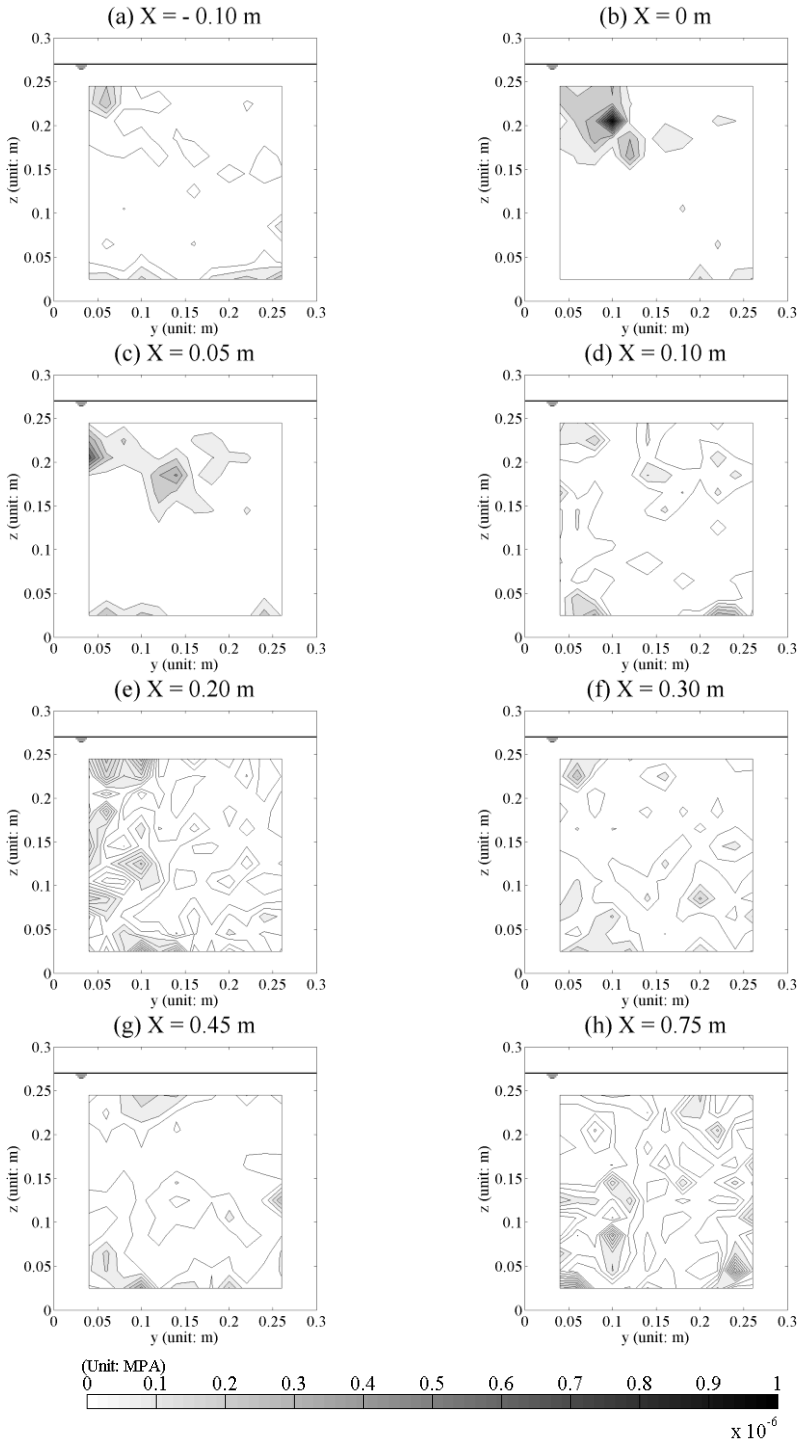

Figure A.163 (AR304) Reynolds shear stress contours

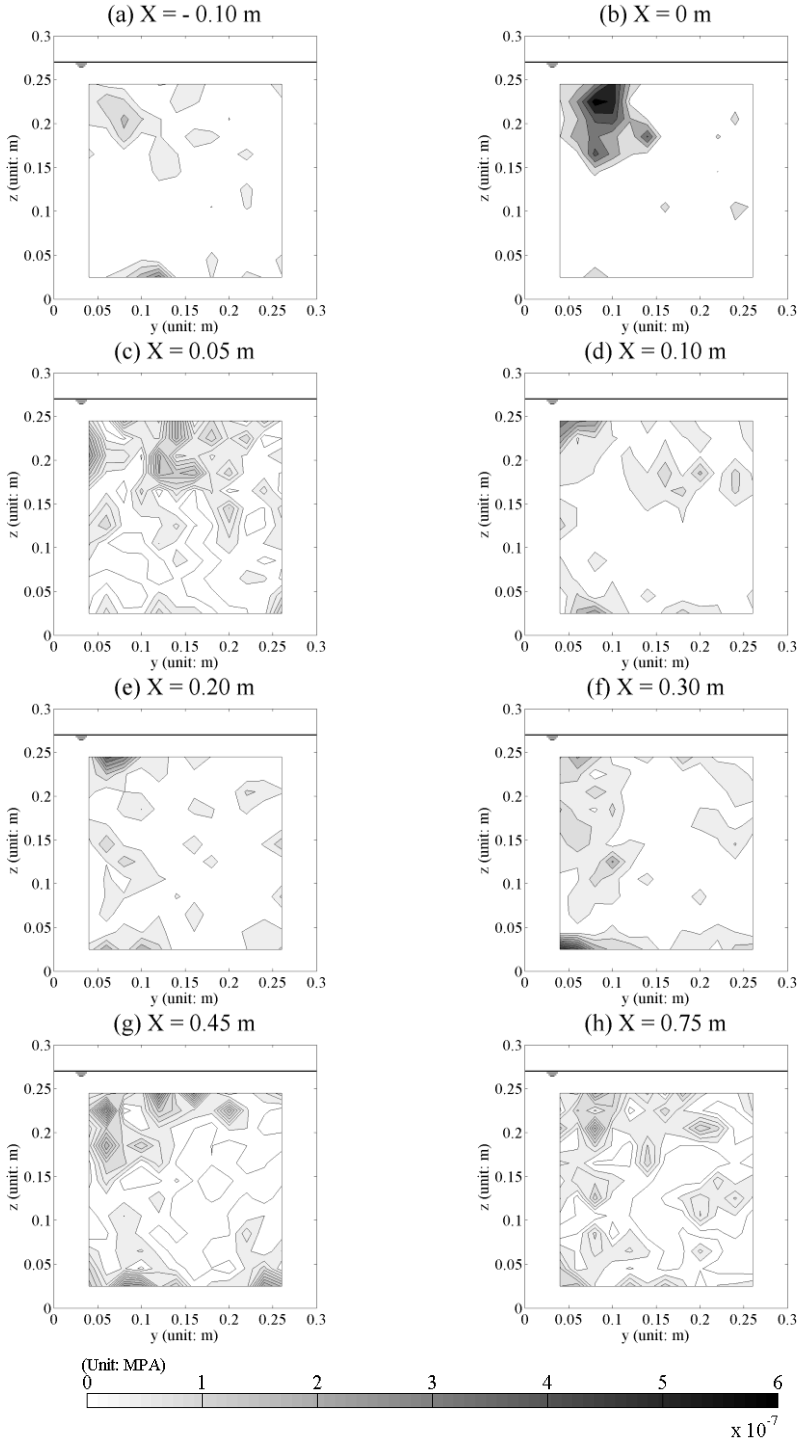

Figure A.164 (AR305) Reynolds shear stress contours

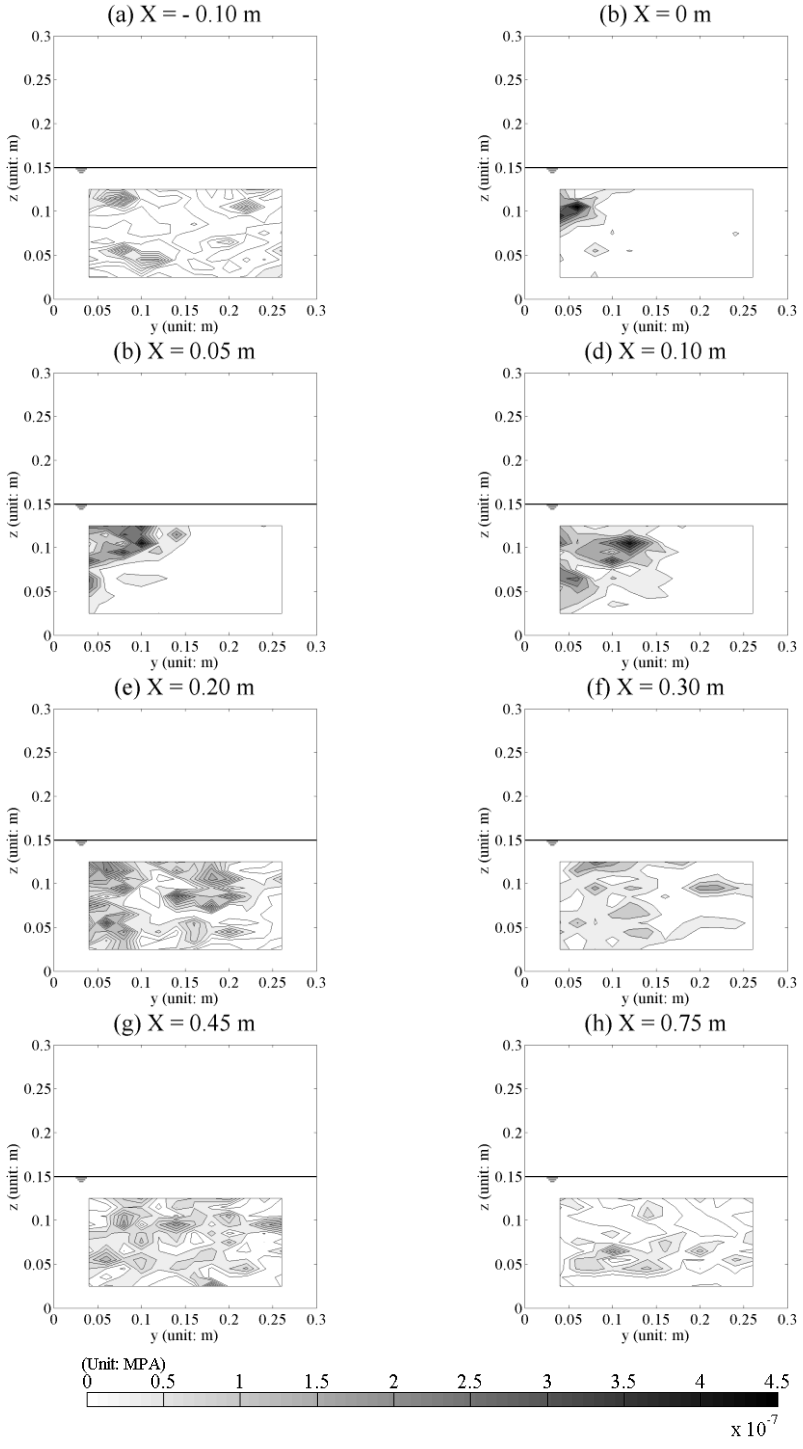

Figure A.165 (AM101) Reynolds shear stress contours

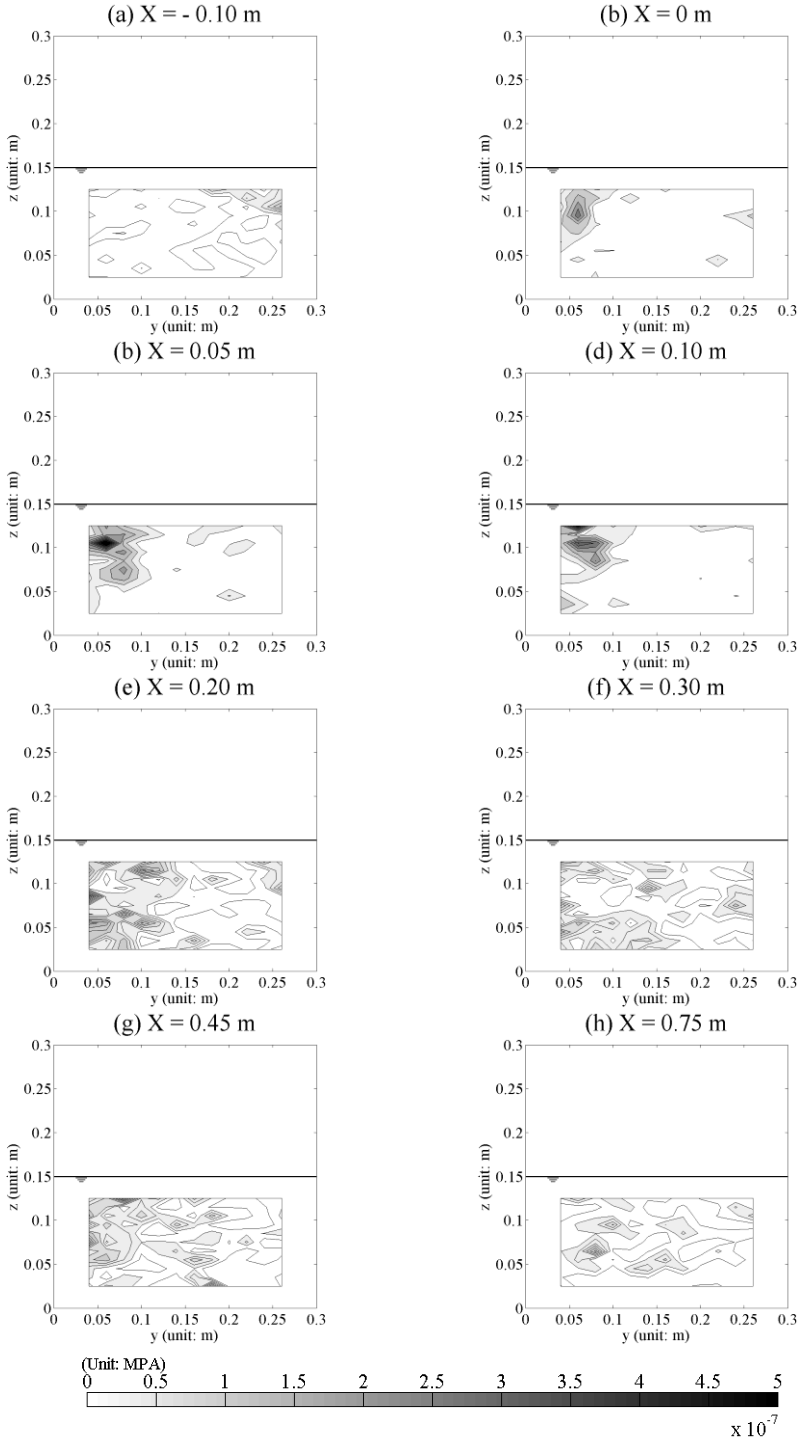

Figure A.166 (AM102) Reynolds shear stress contours

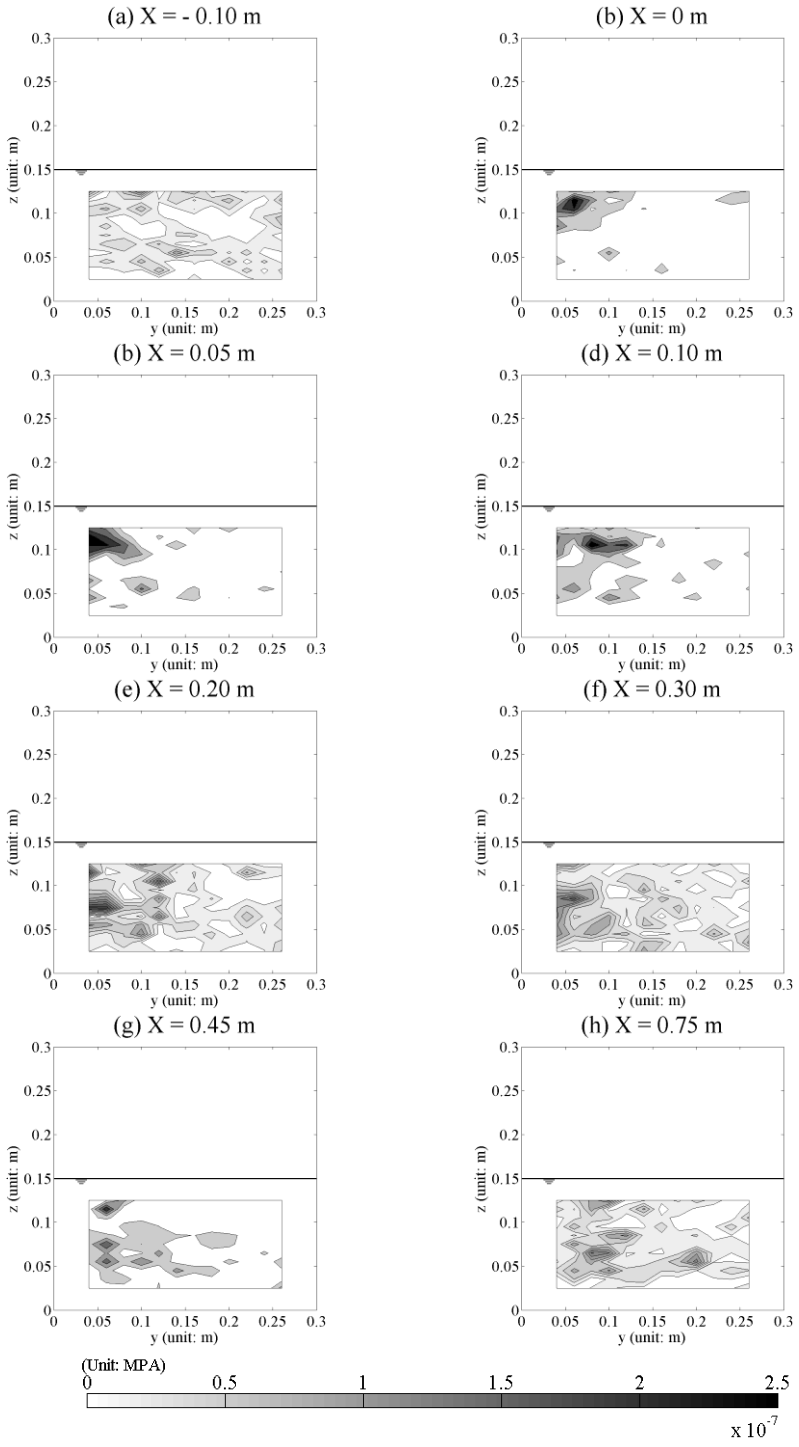

Figure A.167 (AM103) Reynolds shear stress contours

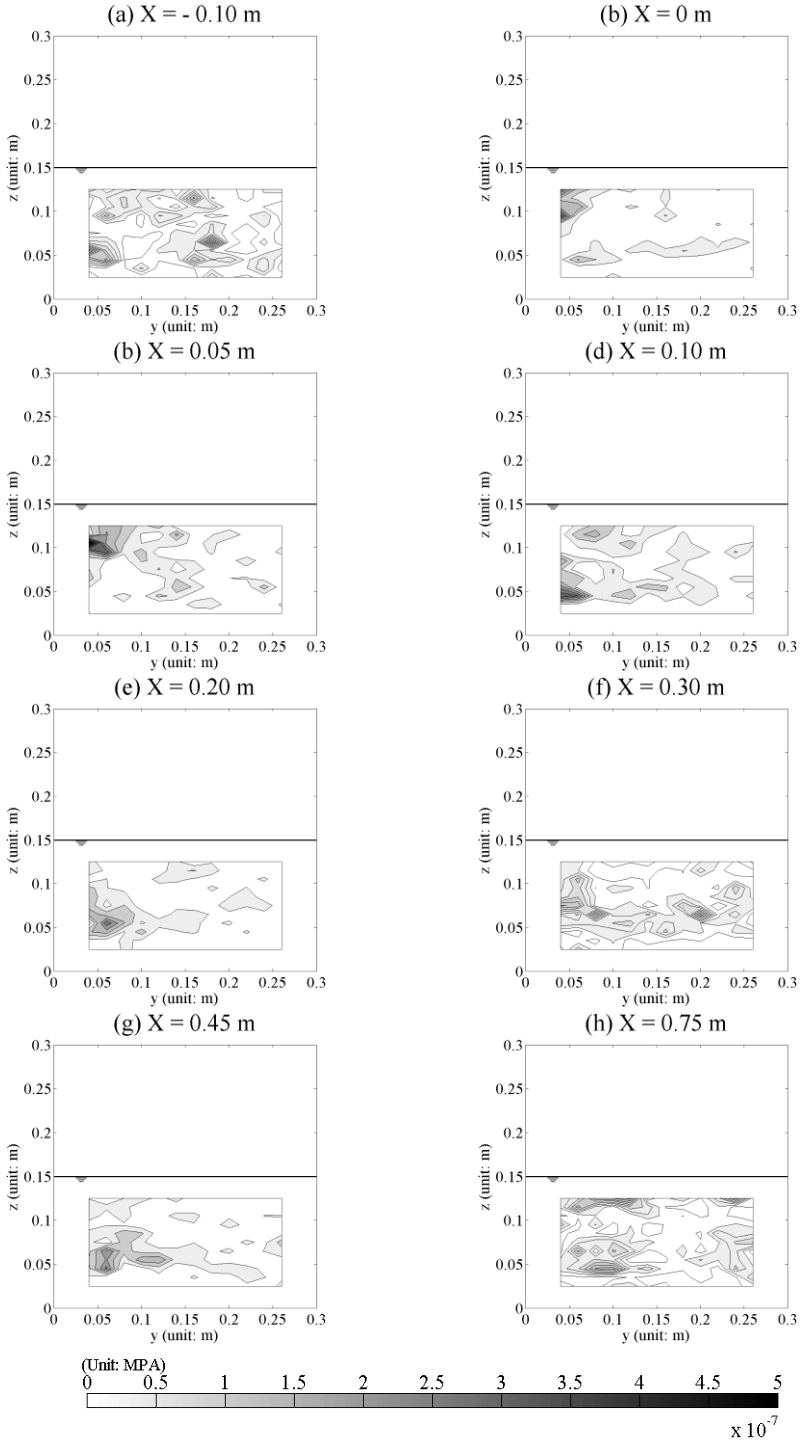

Figure A.168 (AM104) Reynolds shear stress contours

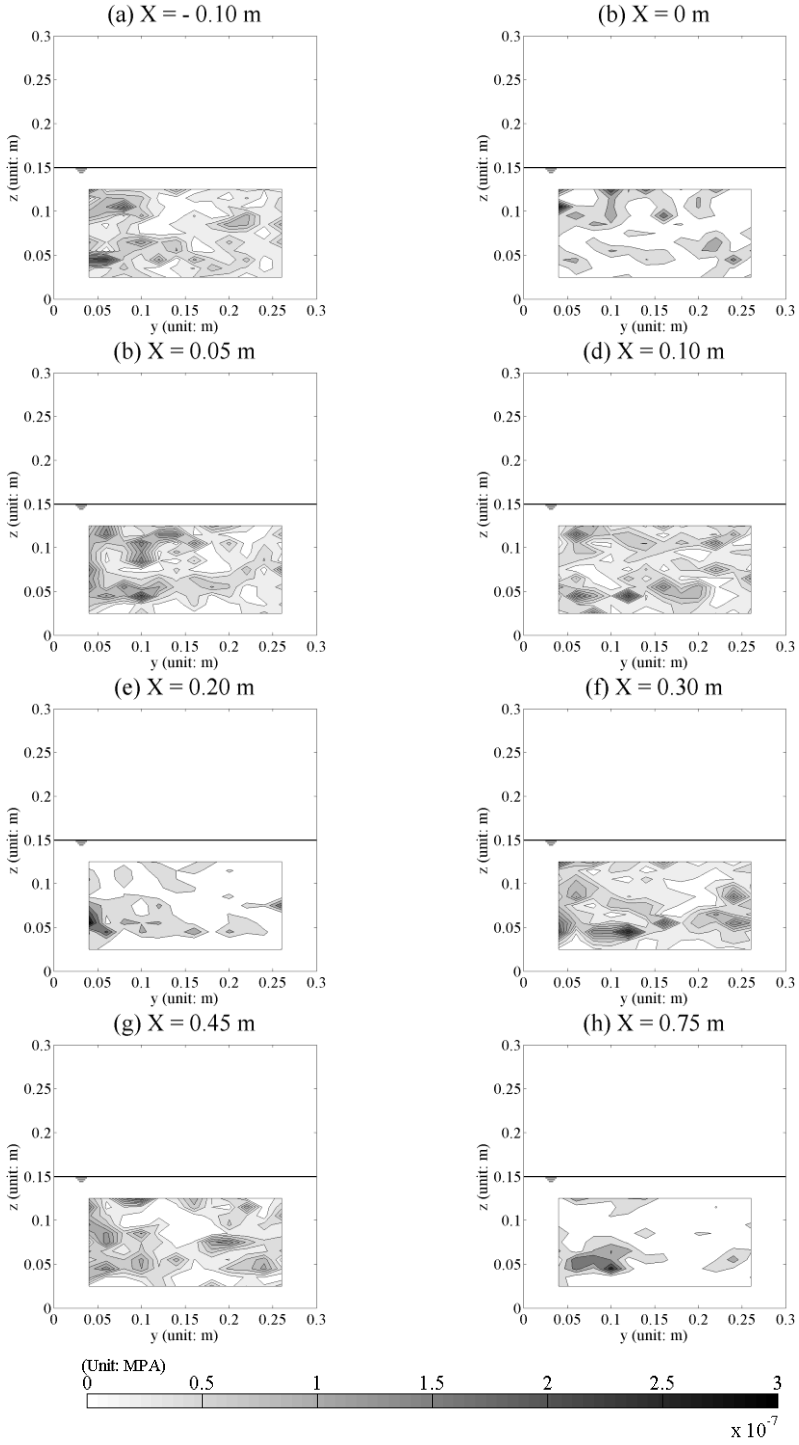

Figure A.169 (AM105) Reynolds shear stress contours

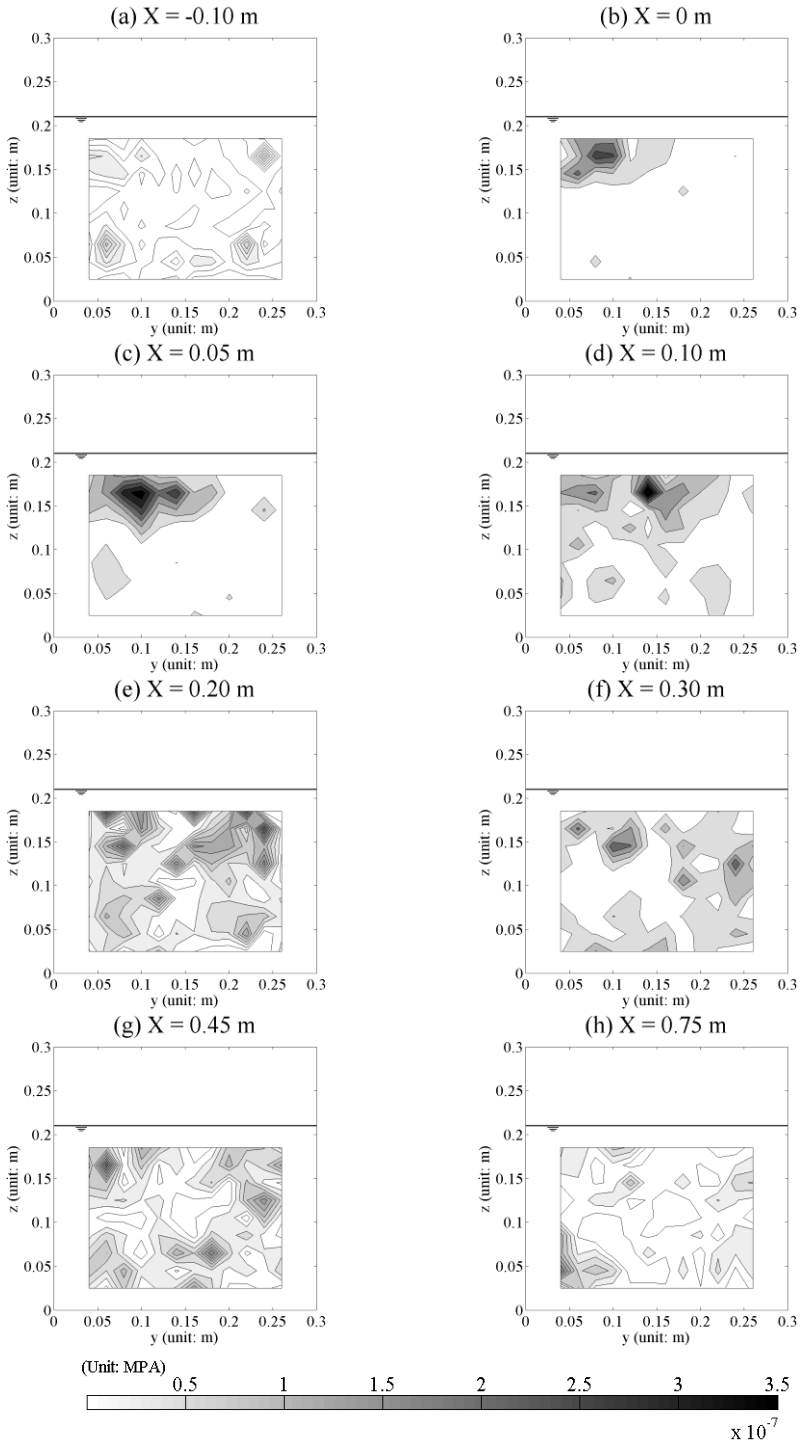

Figure A.170 (AM201) Reynolds shear stress contours

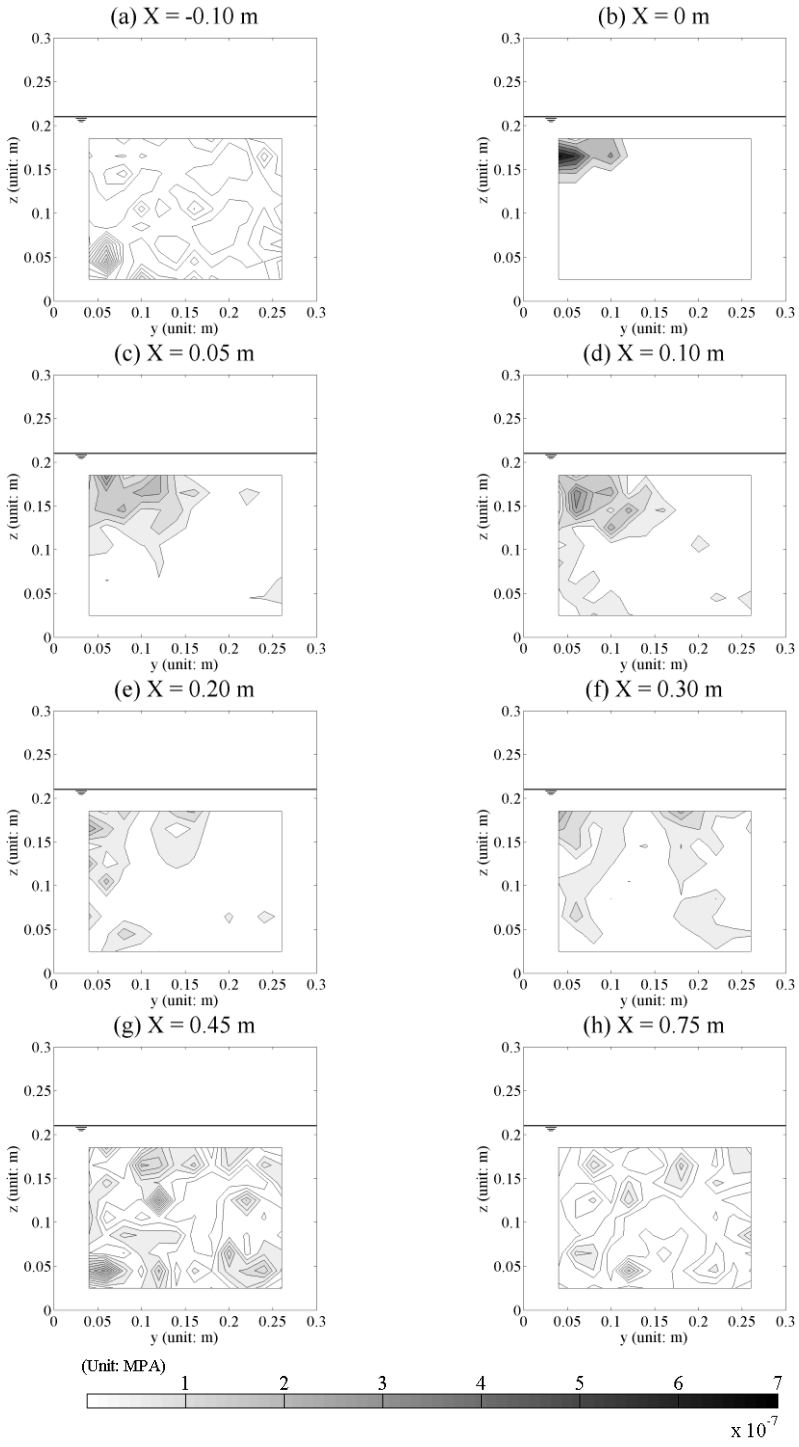

Figure A.171 (AM202) Reynolds shear stress contours

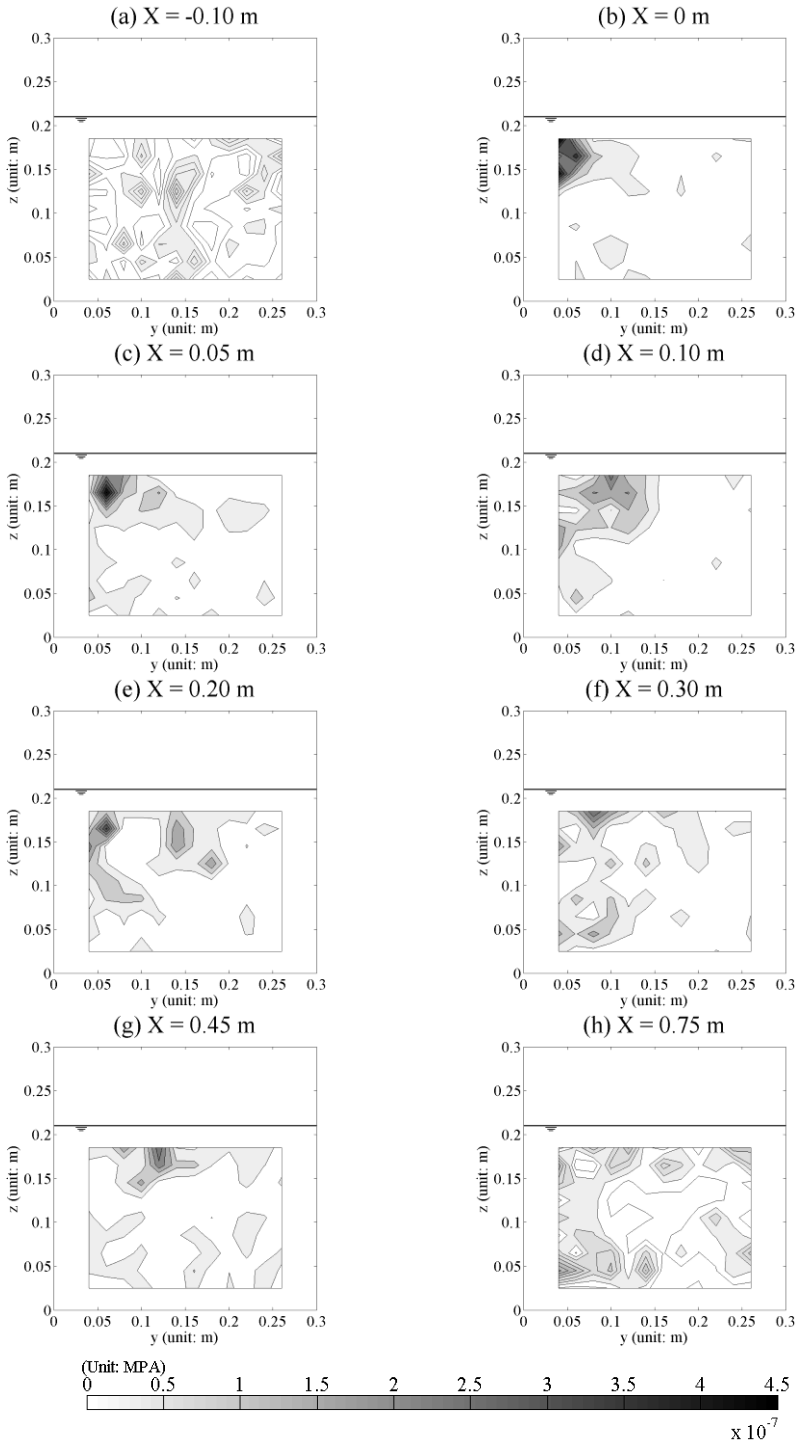

Figure A.172 (AM203) Reynolds shear stress contours

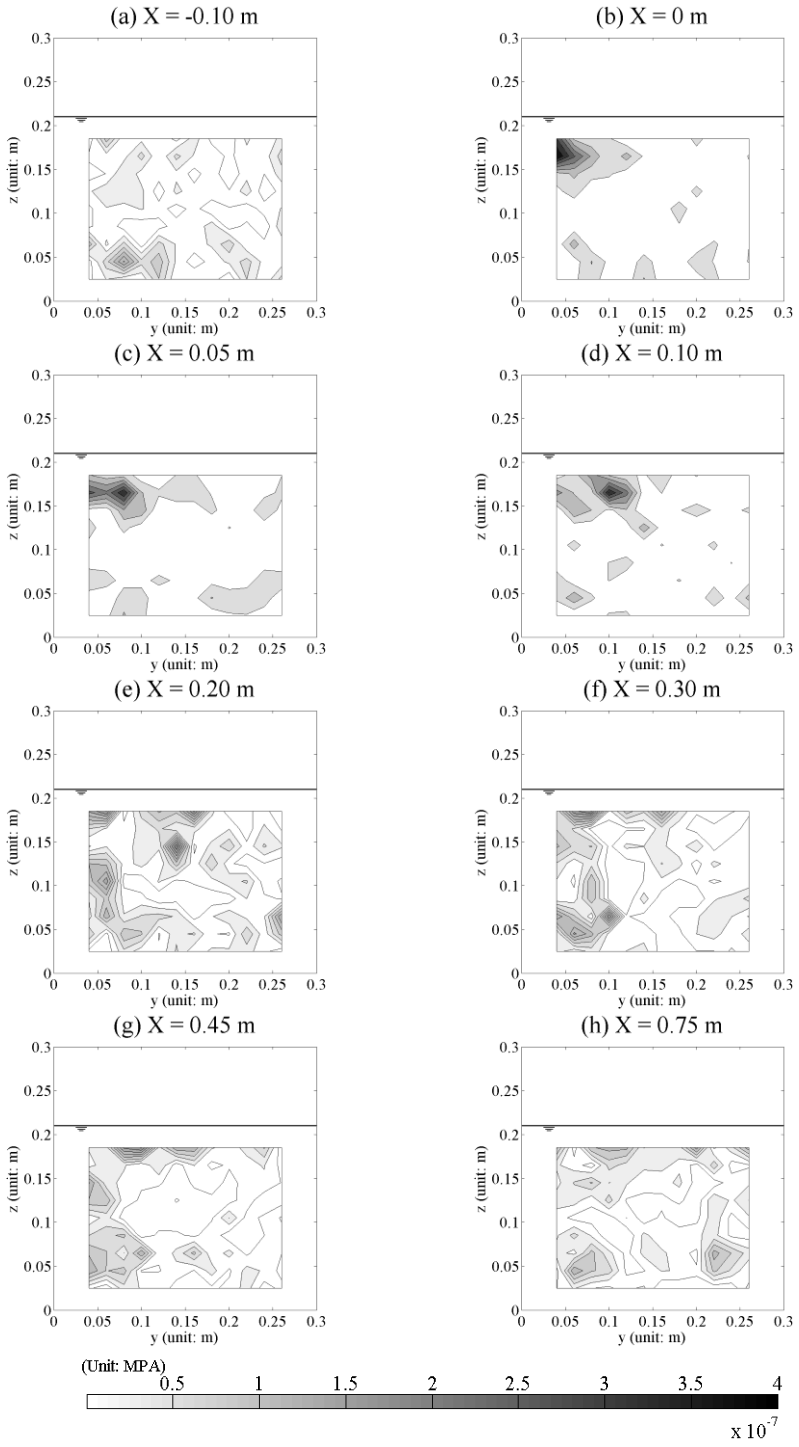

Figure A.173 (AM204) Reynolds shear stress contours

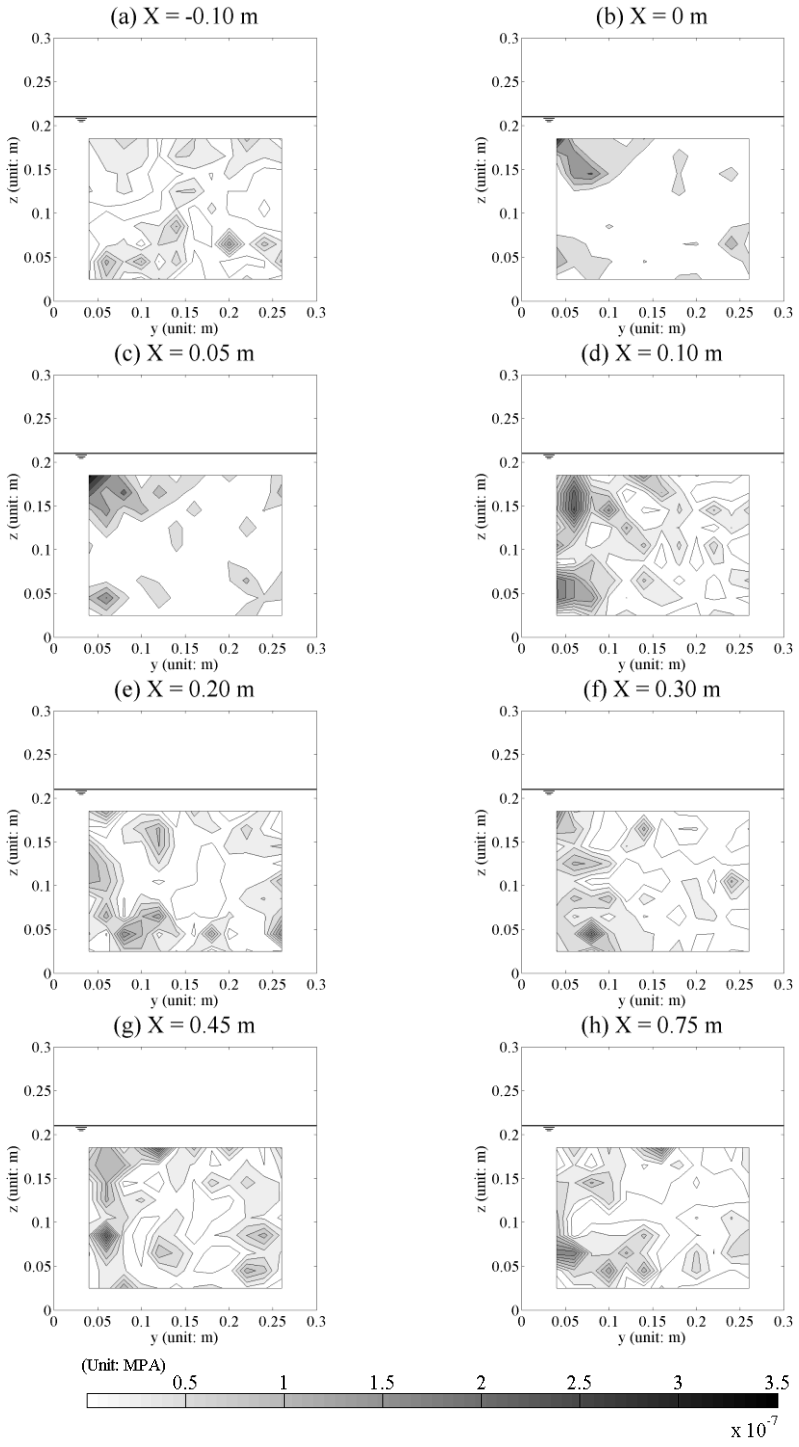

Figure A.174 (AM205) Reynolds shear stress contours

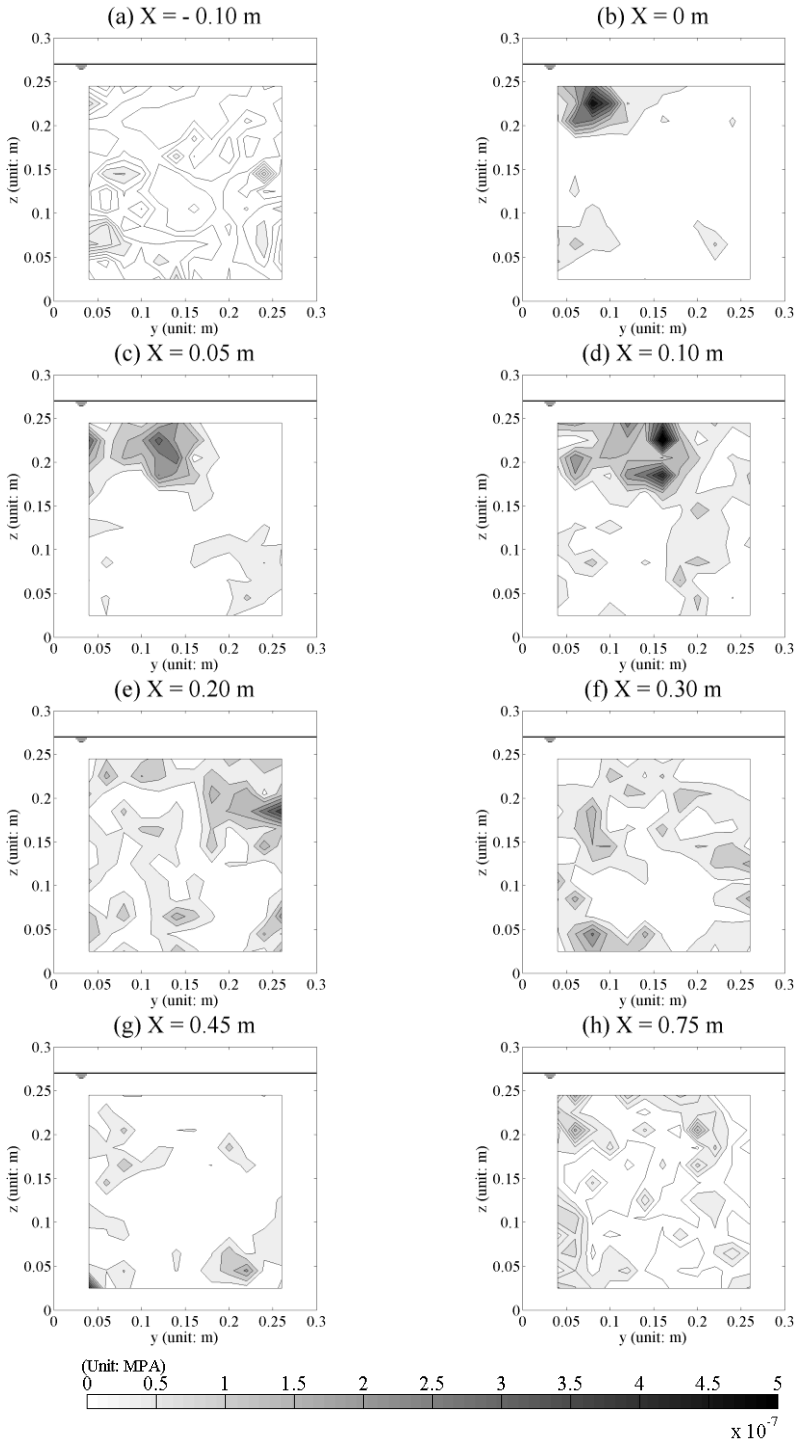

Figure A.175 (AM301) Reynolds shear stress contours

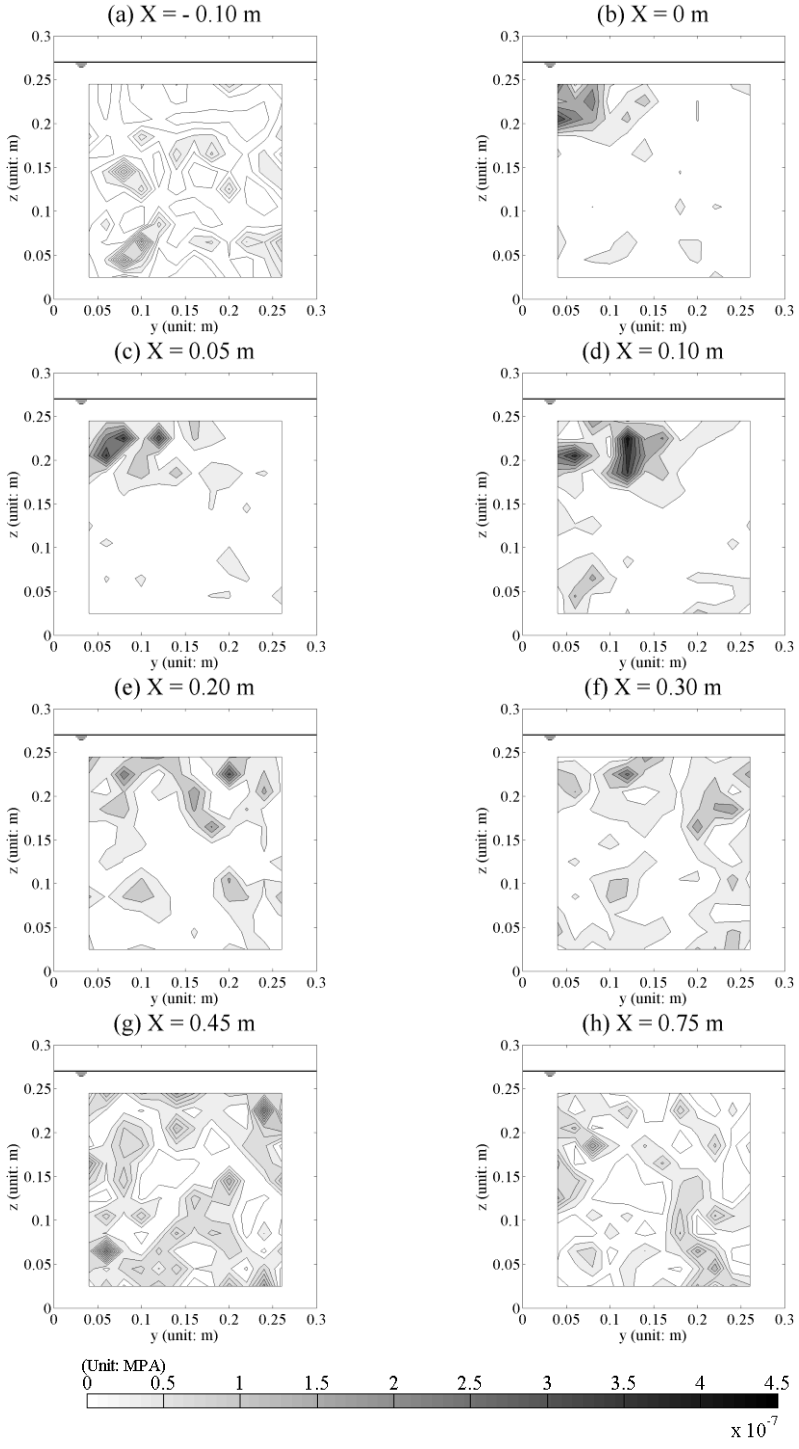

Figure A.176 (AM302) Reynolds shear stress contours

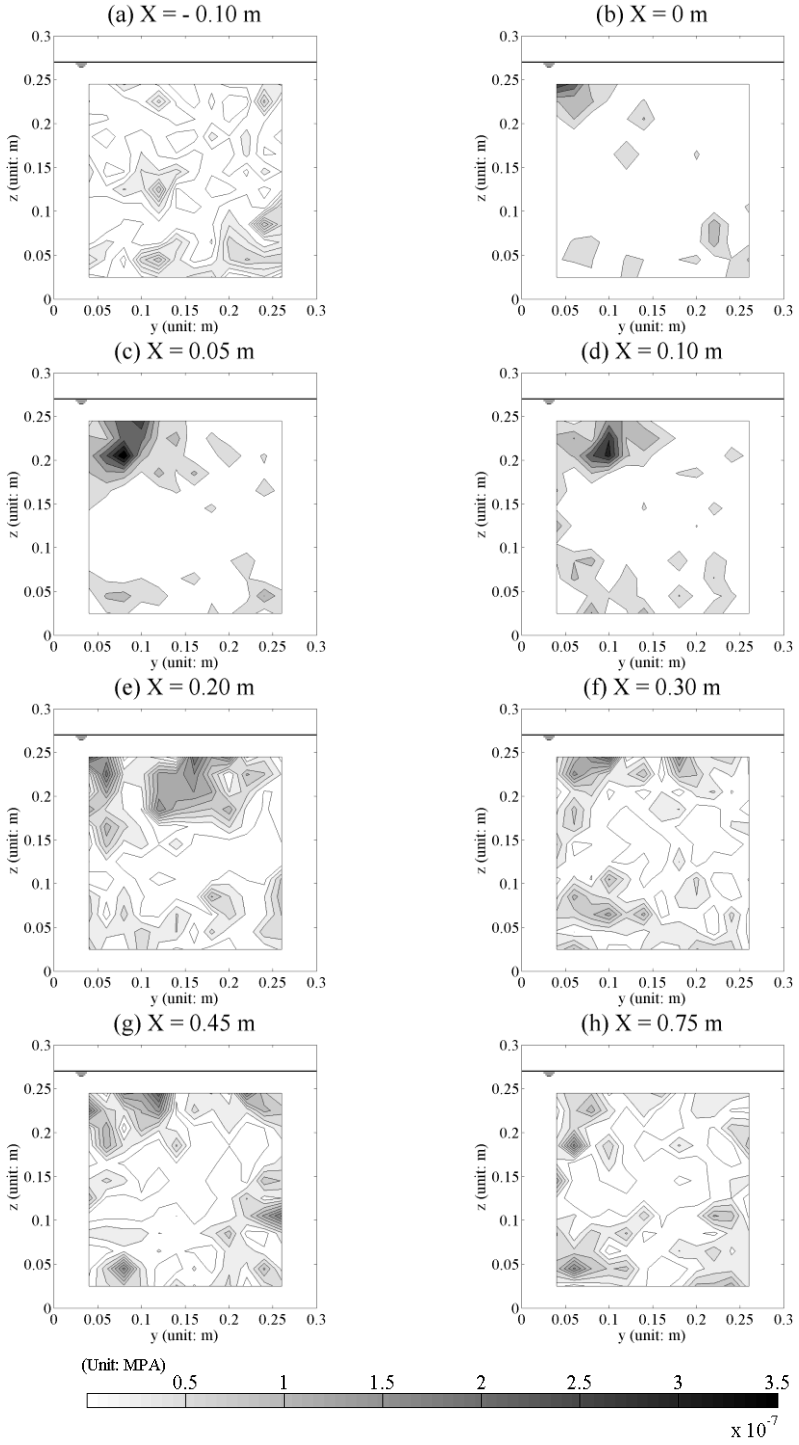

Figure A.177 (AM303) Reynolds shear stress contours

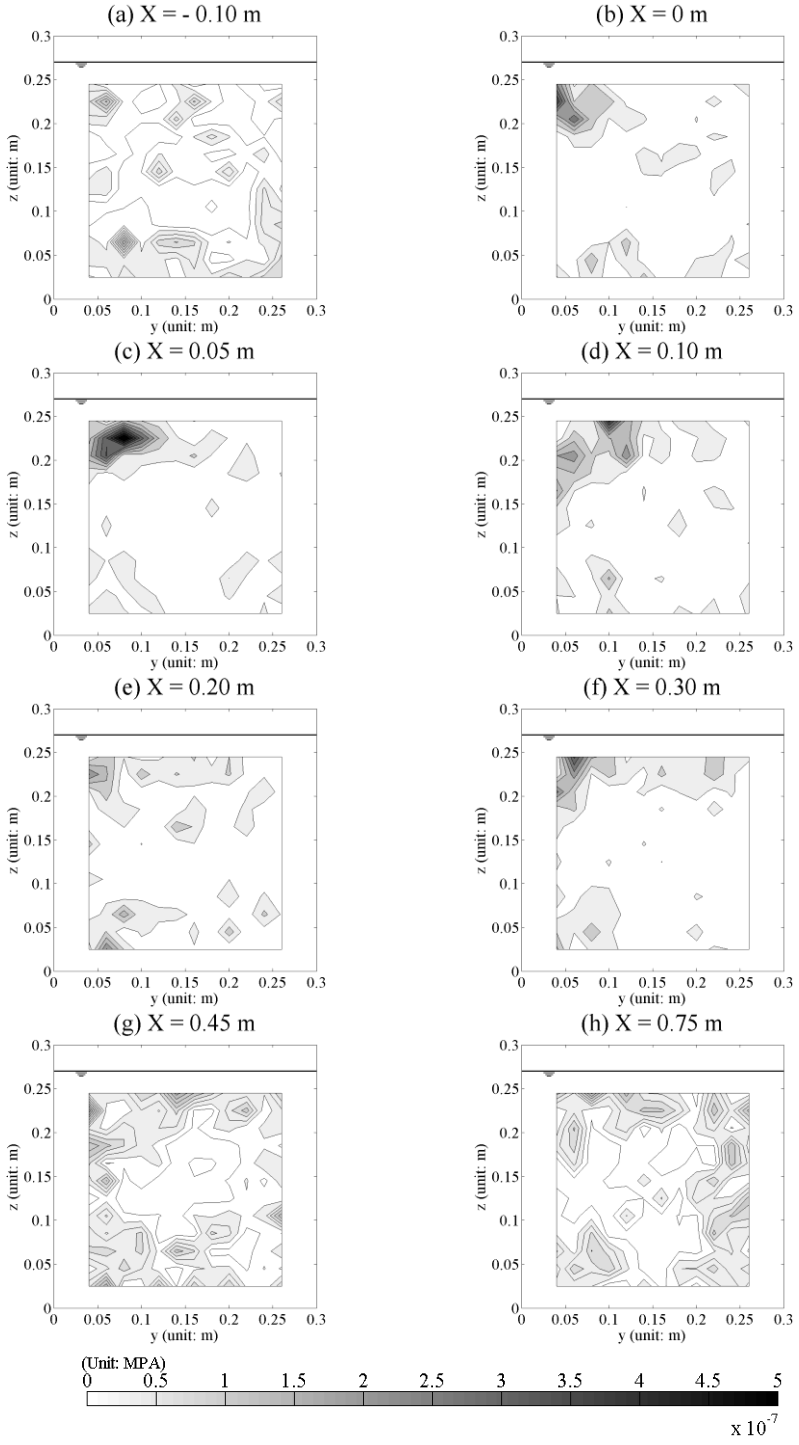

Figure A.178 (AM304) Reynolds shear stress contours

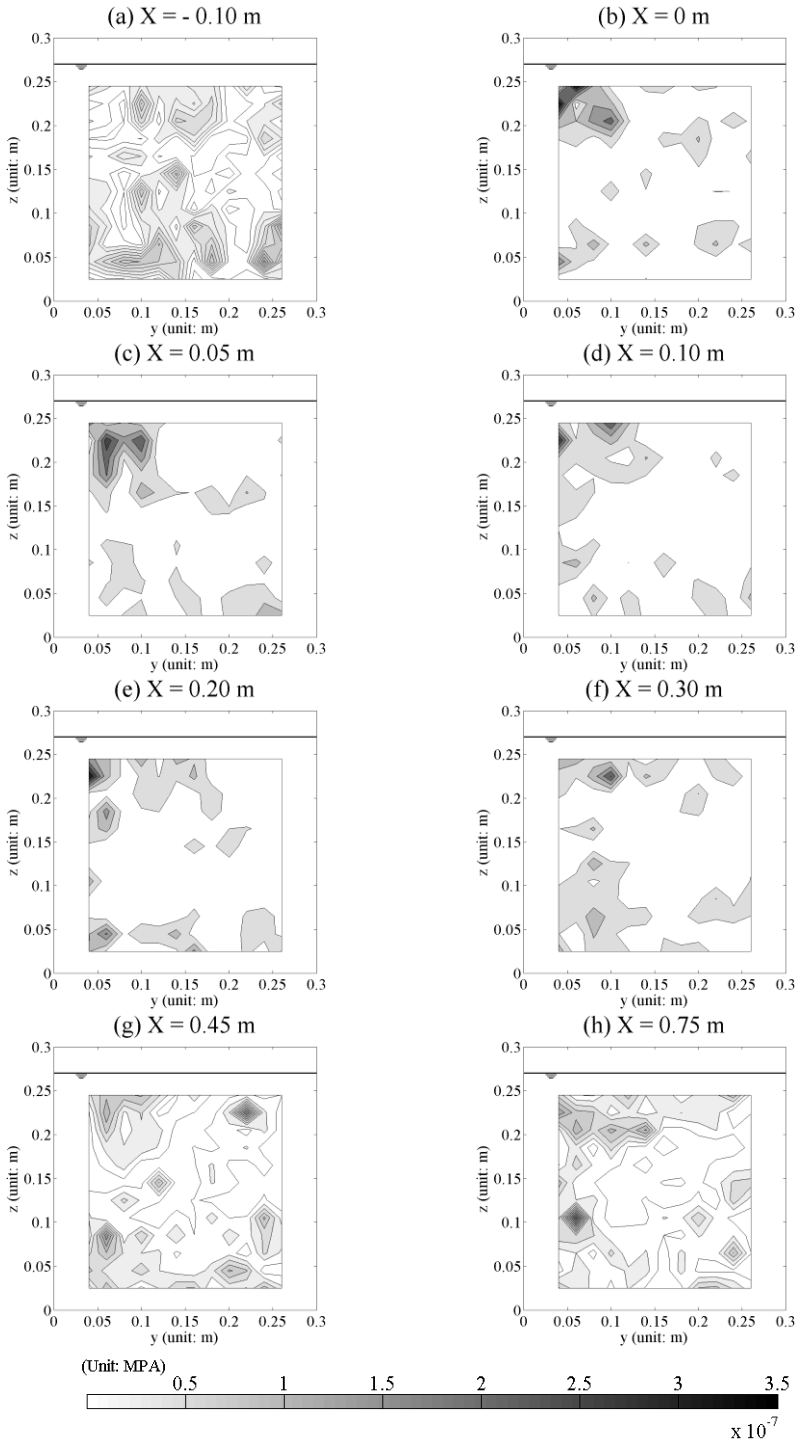

Figure A.179 (AM305) Reynolds shear stress contours

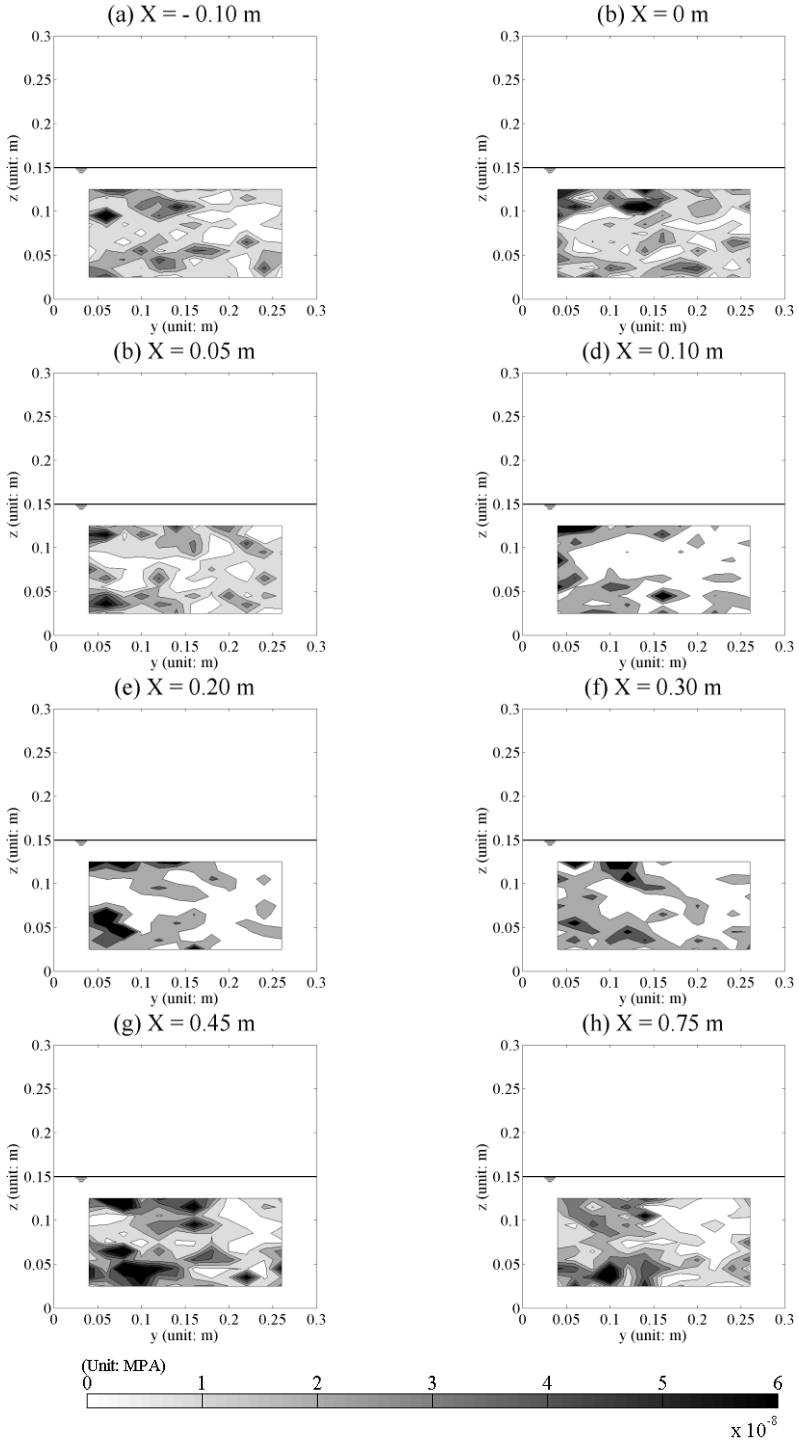

Figure A.180 (AS101) Reynolds shear stress contours

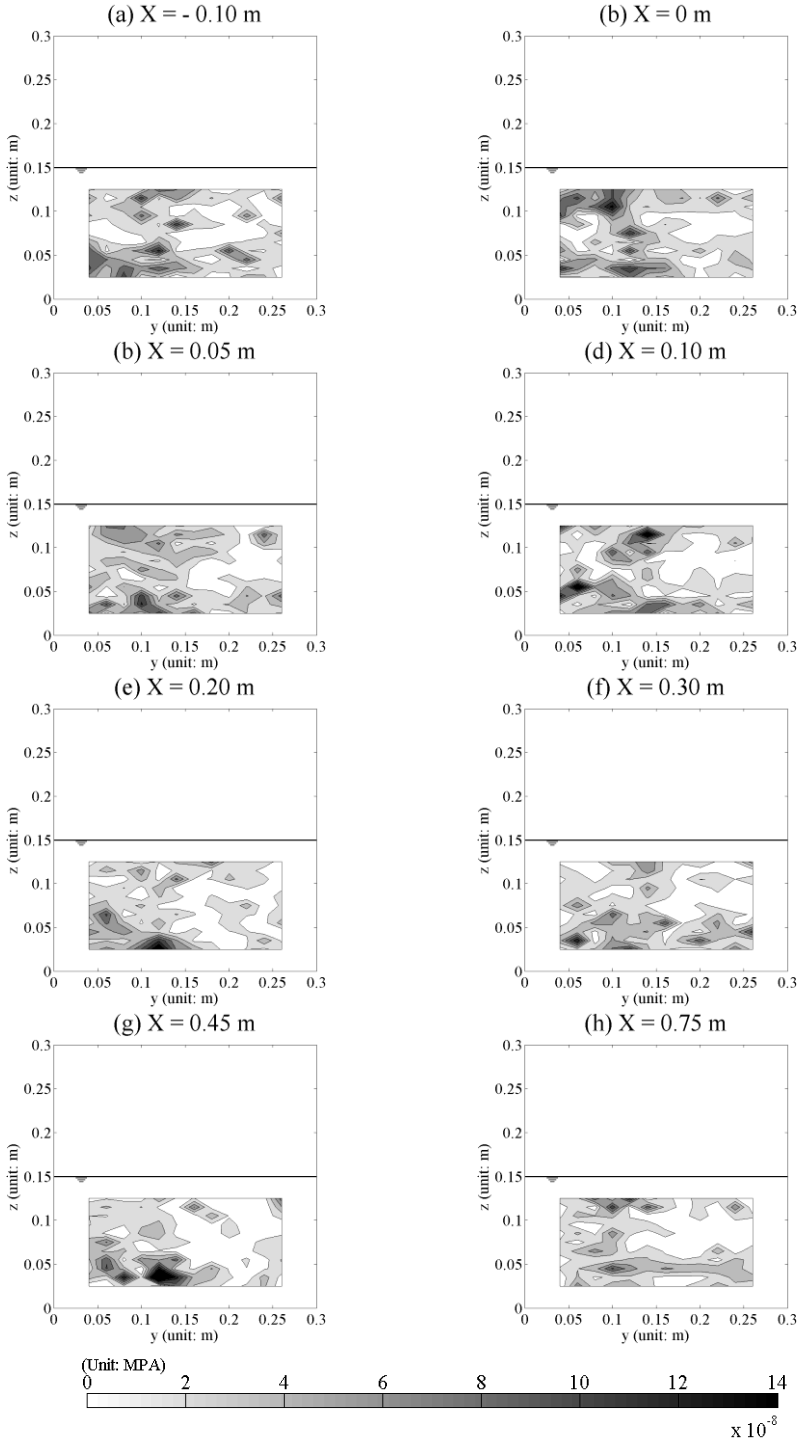

Figure A.181 (AS103) Reynolds shear stress contours

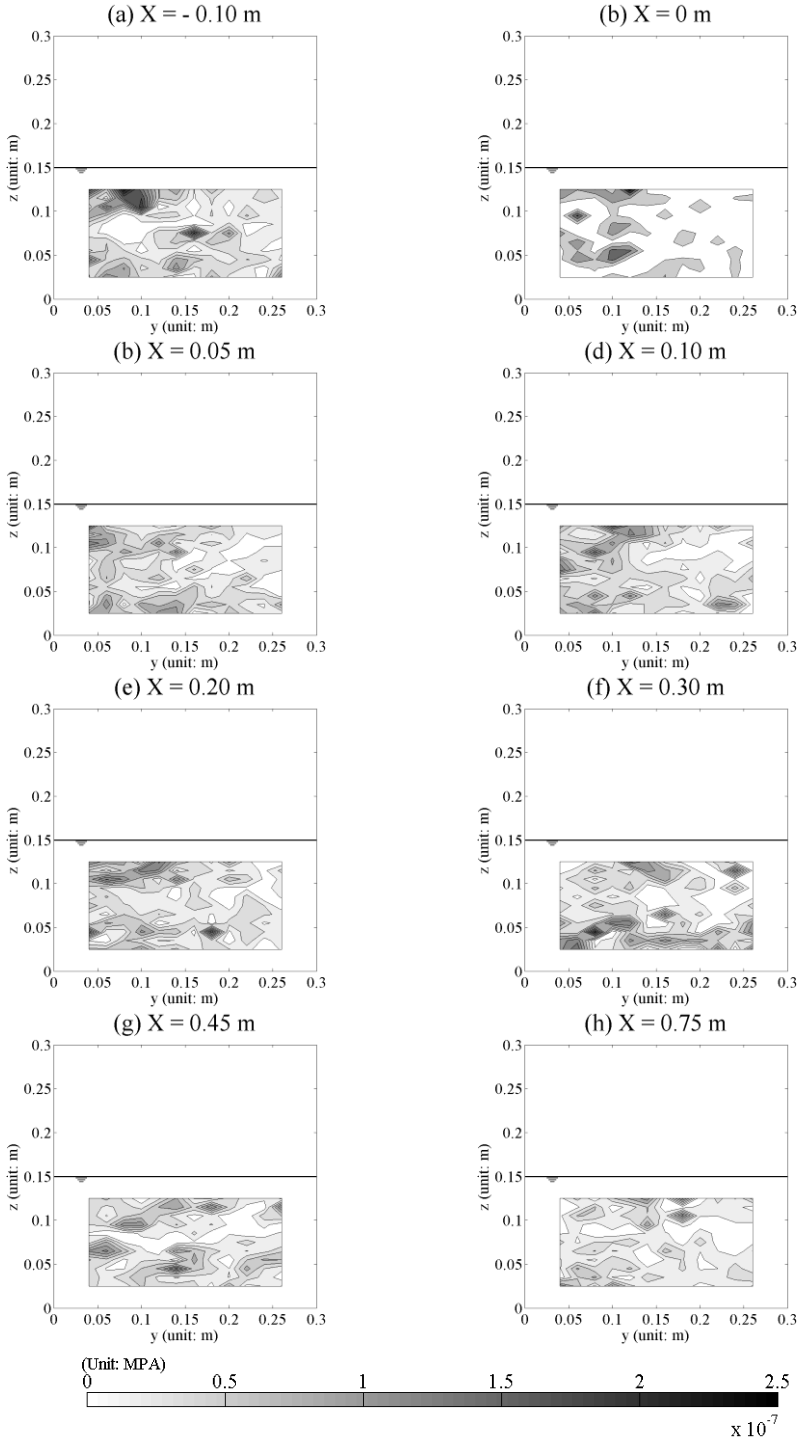

Figure A.182 (AS105) Reynolds shear stress contours

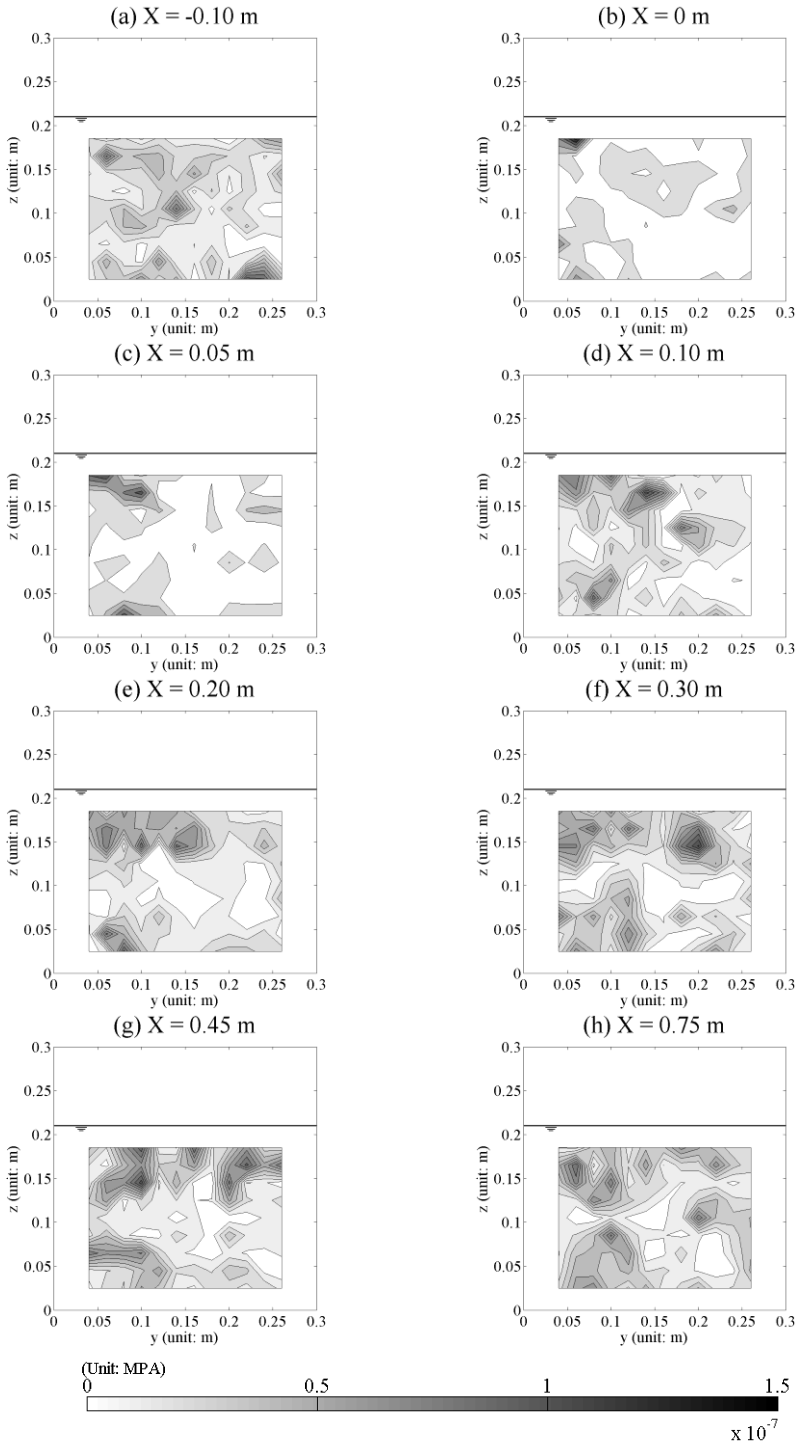

Figure A.183 (AS201) Reynolds shear stress contours

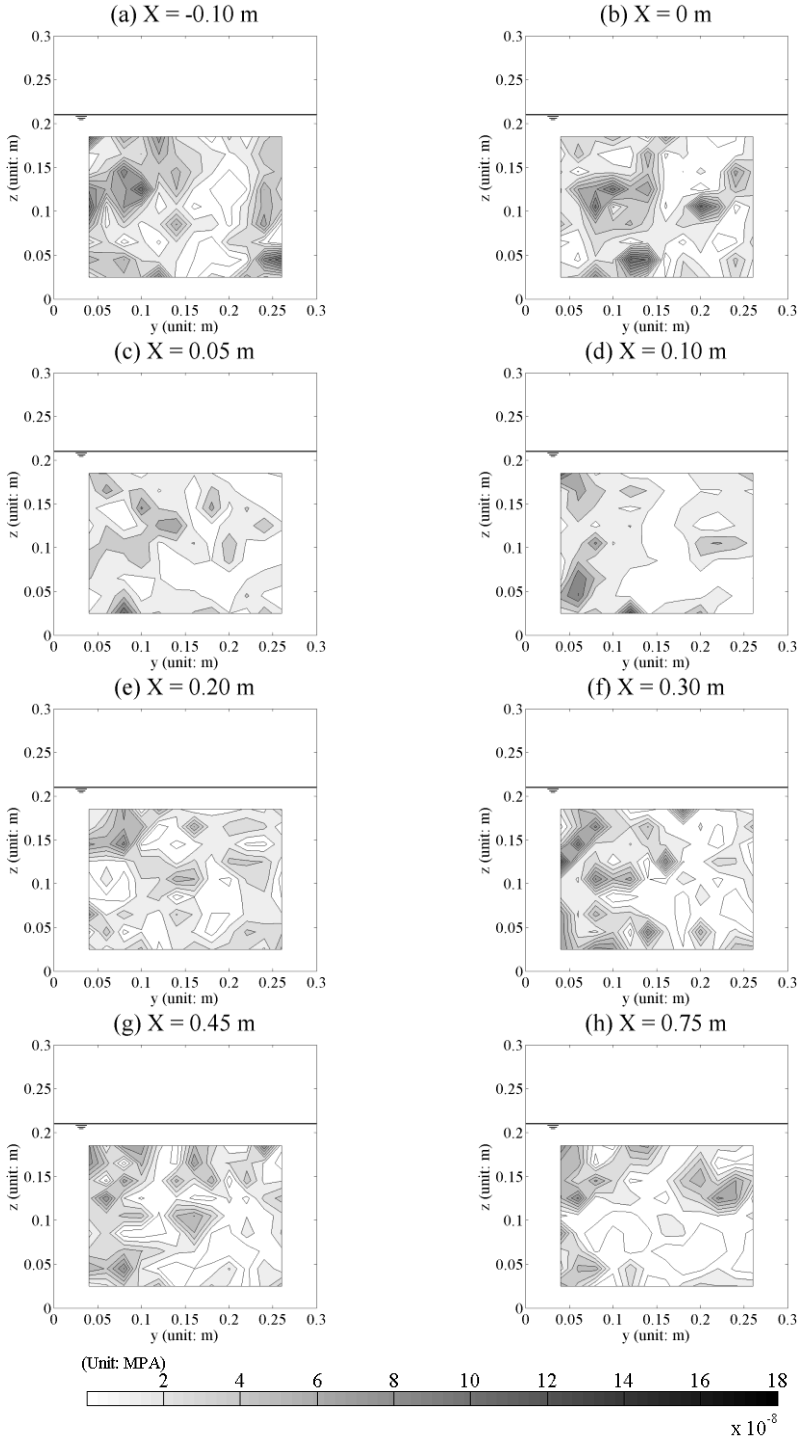

Figure A.184 (AS203) Reynolds shear stress contours

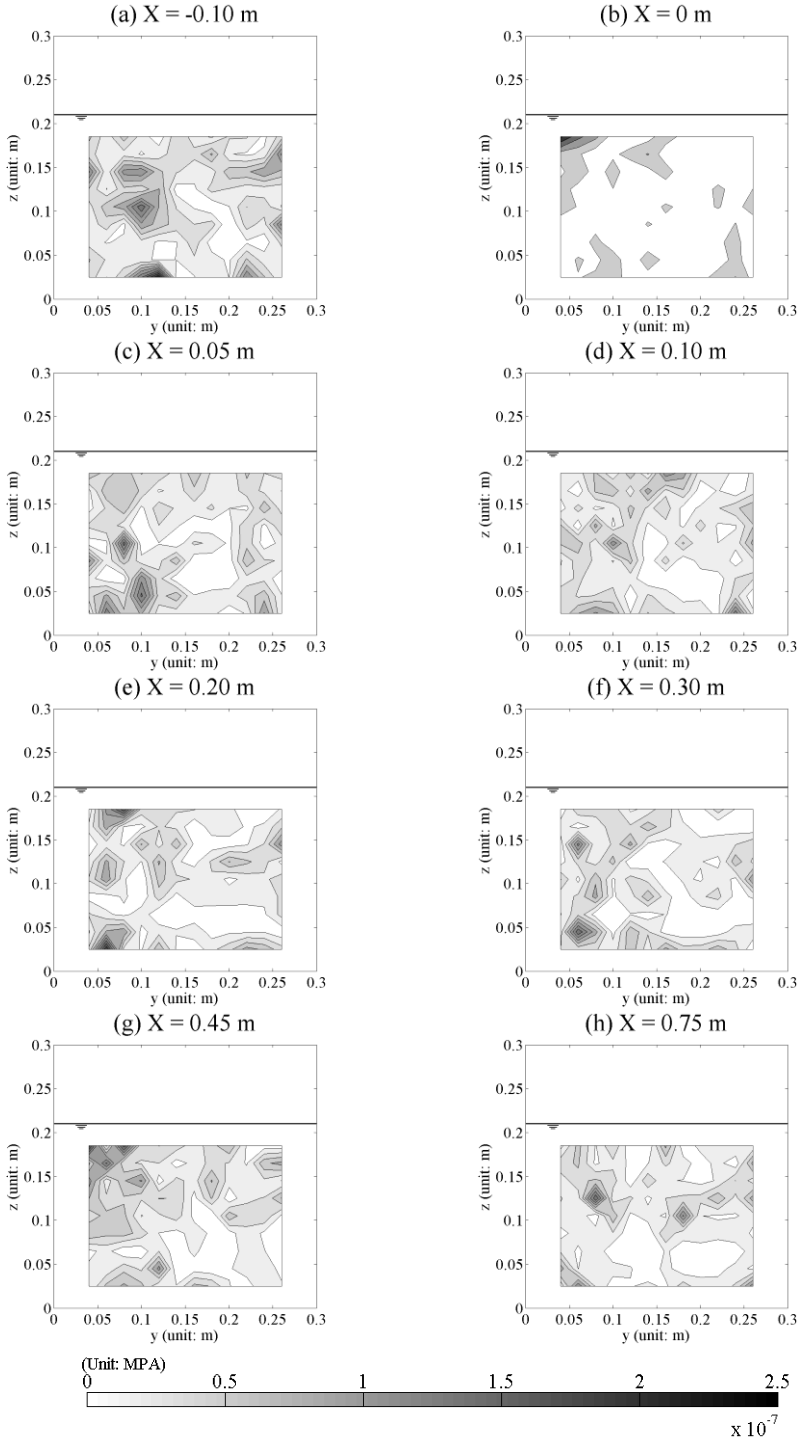

Figure A.185 (AS205) Reynolds shear stress contours

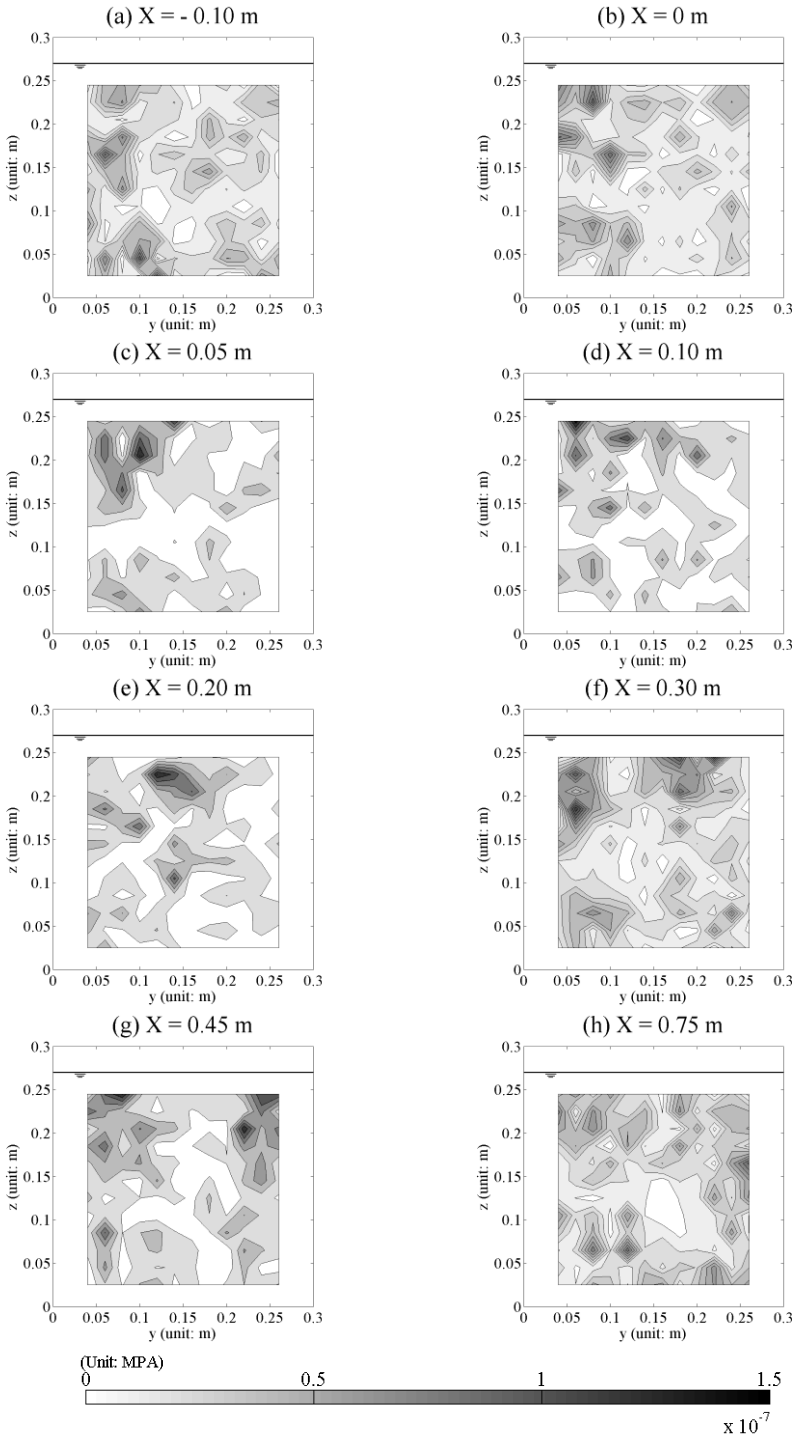

Figure A.186 (AS301) Reynolds shear stress contours

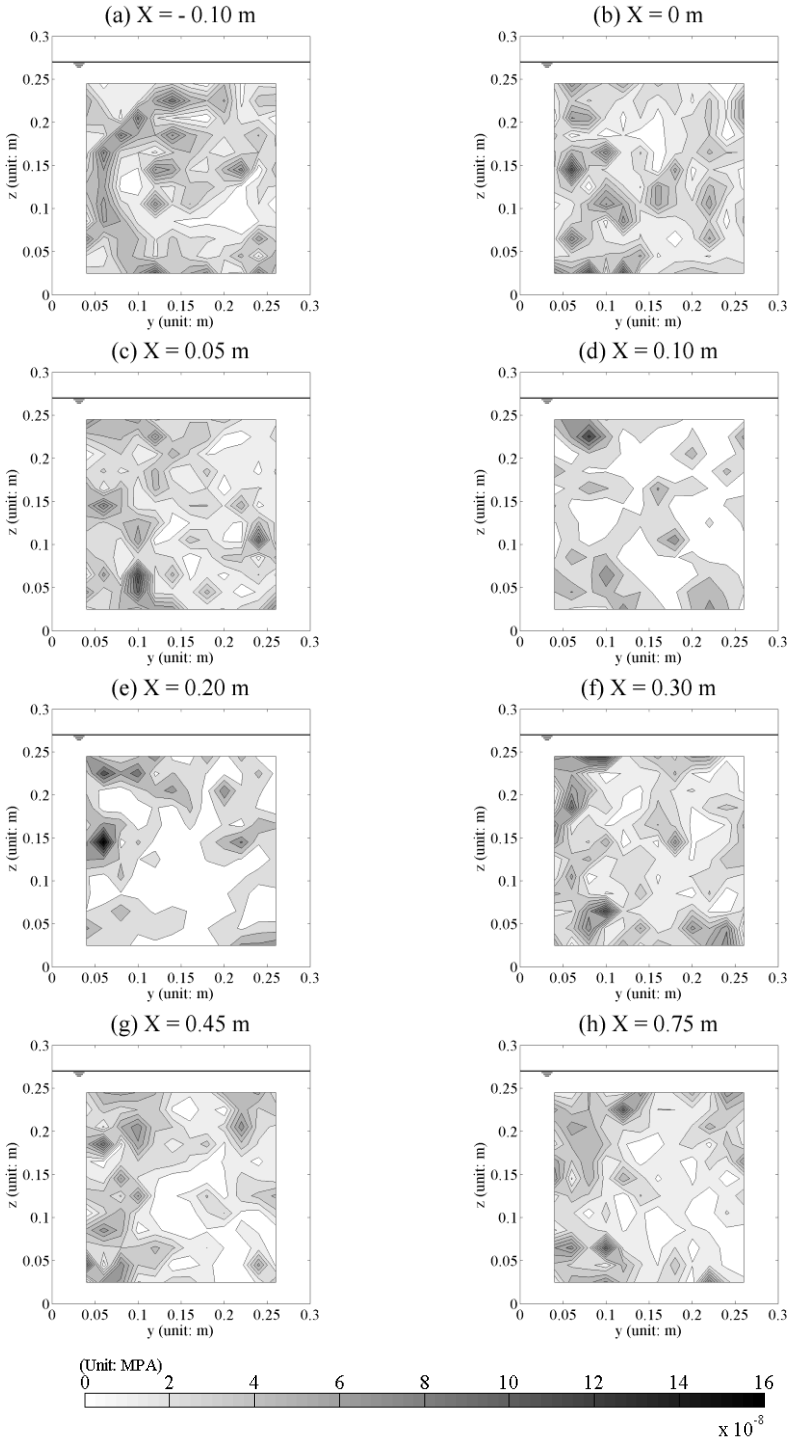

Figure A.187 (AS303) Reynolds shear stress contours

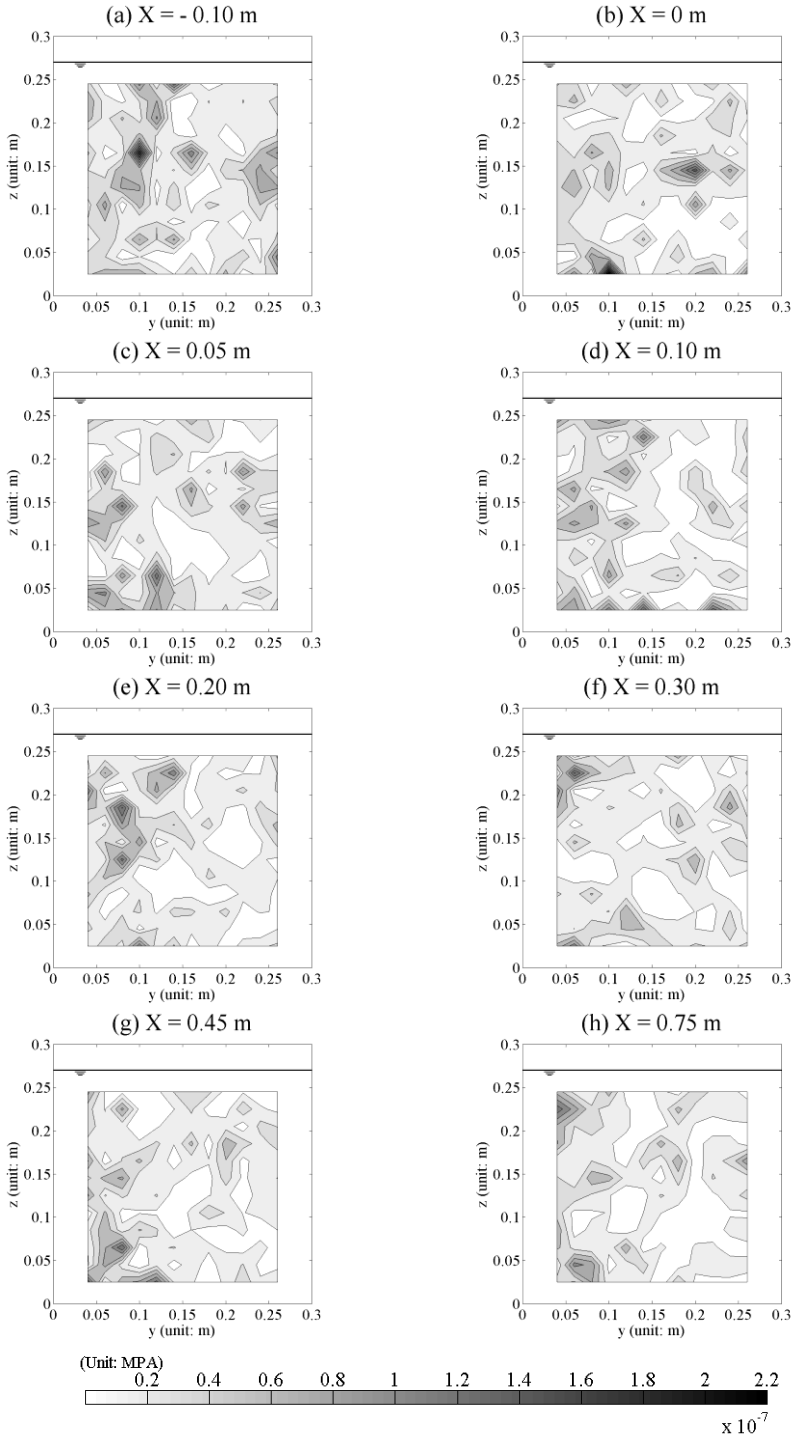

Figure A.188 (AS305) Reynolds shear stress contours

Appendix. 2. The Matlab Code

Appendix. 2.1 Averaging the instantaneous velocity data

After measuring the instantaneous velocities, the data was analyzed by the time averaging. Because the coordinates of the side looking micro-ADV are different to the down looking micro-ADV, the Matlab codes for the time averaging are also different. To import the data to the codes, the extention of the files is '*.Vu'. The commercial software, 'WinADV' was used to change the extention of the files.

1) The side looking micro-ADV

```
n = 2000     % sample number

dirName = 'd:\mathlab\x=-30\z=24.5~z=4.5'; %# folder path
files = dir( fullfile(dirName,'*.Vu') );   %# list all
*.Vu files
files = {files.name}';                    %'# file names

data = cell(numel(files),1);               %# store file
contents

for i=1:numel(files)
    fname = fullfile(dirName,files{i});     %# full path to
```

```
file
    data{i} = importdata(fname);       %# load file

    A{i} = (data{i}.data);

u{i} = A{i}(1:n, 6);
v{i} = A{i}(1:n, 5);
w{i} = A{i}(1:n, 4);

mean_u{i} = (linspace(mean(u{i}),mean(u{i}),n))';
mean_v{i} = (linspace(mean(v{i}),mean(v{i}),n))';
mean_w{i} = (linspace(mean(w{i}),mean(w{i}),n))';

fluc_u{i} = u{i}-mean_u{i};
fluc_v{i} = v{i}-mean_v{i};
fluc_w{i} = w{i}-mean_w{i};

mean_fluc_u{i} = mean(fluc_u{i});
mean_fluc_v{i} = mean(fluc_v{i});
mean_fluc_w{i} = mean(fluc_w{i});

b= [i]
output(b,4) = mean_u{i}(1,1);
output(b,5) = mean_v{i}(1,1);
output(b,6) = mean_w{i}(1,1);
output(b,7) = mean_fluc_u{i}(1,1);
output(b,8) = mean_fluc_v{i}(1,1);
output(b,9) = mean_fluc_w{i}(1,1);

end
```

```
X = -30; %# Y coordinates
Y = [4:2:26]; %# Y coordinates
Z = [24.5:-2:4.5]; %# Z coordinates
coordinate = zeros(132,3); %# Numbers of the measurement

coordinate(:,1)=X(:,:);

dum1 = length(Y);
dum2 = length(Z);

for j = 0: dum2-1
    for i = 1: dum1
        coordinate(j*dum1+i,2) = Y(i);
        coordinate(j*dum1+1:j*dum1+dum1,3) = Z(j+1);
    end
end

output(:,1:3)=coordinate(:,:);
```

2) The down looking micro-ADV

```
n = 3000     % sample number

dirName = 'd:\mathlab\x=-30\z=2.5'; ; %# folder path

files = dir( fullfile(dirName,'*.Vu') );   %# list all
*.Vu files
files = {files.name}';                    %'# file names
```

```
data = cell(numel(files),1);              %# store file
contents

for i=1:numel(files)
    fname = fullfile(dirName,files{i});     %# full path to
file
    data{i} = importdata(fname);        %# load file

    A{i} = (data{i}.data);

u{i} = A{i}(1:n, 4);
v{i} = A{i}(1:n, 5)*-1;
w{i} = A{i}(1:n, 6);

mean_u{i} = (linspace(mean(u{i}),mean(u{i}),n))';
mean_v{i} = (linspace(mean(v{i}),mean(v{i}),n))';
mean_w{i} = (linspace(mean(w{i}),mean(w{i}),n))';

fluc_u{i} = u{i}-mean_u{i};
fluc_v{i} = v{i}-mean_v{i};
fluc_w{i} = w{i}-mean_w{i};

mean_fluc_u{i} = mean(fluc_u{i});
mean_fluc_v{i} = mean(fluc_v{i});
mean_fluc_w{i} = mean(fluc_w{i});

b= [i]
output(b,4) = mean_u{i}(1,1);
output(b,5) = mean_v{i}(1,1);
output(b,6) = mean_w{i}(1,1);
output(b,7) = mean_fluc_u{i}(1,1);
```

```
output(b,8) = mean_fluc_v{i}(1,1);
output(b,9) = mean_fluc_w{i}(1,1);

end

X = -30; %# X coordinates
Y = [4:2:26]; %# Y coordinates
Z = 2.5; %# Z coordinates
coordinate = zeros(12,3); %# Numbers of the measurement

coordinate(:,1)=X(:,:);
coordinate(:,3)=Z(:,:);
coordinate(:,2)=Y(:,:);

output(:,1:3)=coordinate(:,:);
```

Appendix. 2.2 Plotting the time averaged velocities

Because the data of time averaged velocities is three dimension, the Matlab codes were used to plot the 2D flow fields, the vorticity contours, the turbulent kinetic energy contours and the Reynolds shear stress contours. There are the process of the calculation for the vorticity, the turbulent kinetic energy and the Reynolds shear stress in the codes.

1) u-v flow fields

```
A = xlsread('d:\mathlab\as203.xlsx'); %read the arranged
data sheet

dum1 = A(:,1:9);
dum2 = A(:,3);
a = find(dum2 == 18.5); %Selecting the Z coordinate
n = length(a);

for i = 1: n

    dum3(i,:) = dum1(a(i),:);

end

x=dum3(:,1)*0.01;
y=dum3(:,2)*0.01;
u=dum3(:,4)*0.01;
v=(dum3(:,5)*-1)*0.01;

h=figure;
quiver (x,y,u,v,'k');
axis equal
axis ([-1, 1.3, 0, 0.4])
set(gca,'YTick',[0 0.1 0.2 0.3 0.4])
set(gca, 'fontsize',20,'Fontname', 'times new roman');
xlabel('x (unit: m)');
ylabel('y (unit: m)');
```

```
h_xlabel = get(gca,'XLabel');
set(h_xlabel, 'FontName', 'Times New Roman');
set(h_xlabel,'FontSize',20);
h_ylabel = get(gca,'ylabel');
set(h_ylabel, 'fontsize',20);
set(h_ylabel, 'FontName', 'Times New Roman');
hold on

quiver(0.85,0.35,0.1,0,'color','k'); %k is black, r is
red
text(0.85,0.38,'0.1 m s^-^1','color','k')
set(0,'DefaultTextFontname', 'Times New Roman')
set(0,'DefaultTextFontSize', 20)

h_title= title('(a) u v vector field', 'color', 'k')
set(h_title,'Fontname', 'Times New Roman')
set(h_title,'FontSize', 30)

%Drawing the confluent channel

p1 = [0.3, -1];
p2 = [0.3, -0.1];
plot([p1(2),p2(2)],[p1(1),p2(1)],'Color','black','LineWid
th',1.5)

p3 = [0.3,0];
p4 = [0.3,1.8];
plot([p3(2),p4(2)],[p3(1),p4(1)],'Color','black','LineWid
th',1.5)

p5 = [0.4,-0.1];
```

```
p6 = [0.3, -0.1];
plot([p5(2),p6(2)],[p5(1),p6(1)],'Color','black','LineWid
th',1.5)

p7 = [0.4,0];
p8 = [0.3,0];
plot([p7(2),p8(2)],[p7(1),p8(1)],'Color','black','LineWid
th',1.5)

%Saving the results

set(gcf, 'Position', [100, 100, 2100, 400]);
saveas(h, 'as203_u_v_vector', 'fig');
saveas(h, 'as203_u_v_vector', 'png');
```

2) u contours

```
A = xlsread('d:\mathlab\ar305.xlsx'); %read the arranged
data sheet


dum1 = A(:,1:9);
dum2 = A(:,3);
a = find(dum2 == 24.5); %Selecting the Z coordinate
n = length(a);

for i = 1: n

    dum3(i,:) = dum1(a(i),:);
```

```
end

x=dum3(:,1)*0.01;
y=dum3(:,2)*0.01;
u=dum3(:,4)*0.01;
v=(dum3(:,5))*-1*0.01;

% Reshaping the data tables
x1 = reshape(x, 12, 19);
y1 = reshape(y, 12, 19);
u1 = reshape(u, 12, 19);

h=figure;
contourf(x1, y1, u1);
axis equal
% axis tight
axis ([-1, 1.3, 0, 0.4])
set(gca,'YTick',[0 0.1 0.2 0.3 0.4])
xlabel('x (unit: m)');
ylabel('y (unit: m)');
h_xlabel = get(gca,'XLabel');
set(h_xlabel, 'FontName', 'Times New Roman');
set(h_xlabel,'FontSize',20);
h_ylabel = get(gca,'ylabel');
set(h_ylabel, 'fontsize',20);
set(h_ylabel, 'FontName', 'Times New Roman');
hold on
colormap(gray)
colormap(flipud(colormap)) %Reversing the color bar
```

```
h_title= title('(b) u contour', 'color', 'k')
set(h_title,'Fontname', 'Times New Roman')
set(h_title,'FontSize', 30)

colorbar
set(gca, 'fontsize',20,'Fontname', 'times new roman');

text(1.3,0.43,'(Unit: m/s)','color','k');
set(0,'DefaultTextFontname', 'Times New Roman')
set(0,'DefaultTextFontSize', 20)

%Drawing the confluent channel

p1 = [0.3, -1];
p2 = [0.3, -0.1];
plot([p1(2),p2(2)],[p1(1),p2(1)],'Color','black','LineWid
th',1.5)

p3 = [0.3,0];
p4 = [0.3,1.6];
plot([p3(2),p4(2)],[p3(1),p4(1)],'Color','black','LineWid
th',1.5)

p5 = [0.4,-0.1];
p6 = [0.3, -0.1];
plot([p5(2),p6(2)],[p5(1),p6(1)],'Color','black','LineWid
th',1.5)

p7 = [0.4,0];
p8 = [0.3,0];
plot([p7(2),p8(2)],[p7(1),p8(1)],'Color','black','LineWid
```

```
th',1.5)

%Saving the results

set(gcf, 'Position', [100, 100, 2100, 400]);
saveas(h, 'ar305_u_contour', 'fig');
saveas(h, 'ar305_u_contour', 'png');
```

3) v-w flow fields

```
% Plotting the Secondary flow

A = xlsread('d:\mathlab\as105.xlsx'); %read the arranged
data sheet


dum1 = A(:,1:9);
dum2 = A(:,1);
a = find(dum2 == -30); %Selecting the X coordinate
n = length(a);

for i = 1: n

    dum3(i,:) = dum1(a(i),:);

end

y=abs(0.3-dum3(:,2)*0.01); %Revising the Y coordinate
z=dum3(:,3)*0.01;
v=(dum3(:,5))*0.01;
```

```
w=(dum3(:,6))*0.01;

h=figure;
quiver (y,z,v,w, 'k', 'linewidth', 1.3);
axis equal
axis ([0, 0.3, 0, 0.3])
set(gca,'fontsize',20, 'fontname', 'times new roman')
xlabel('y (unit: m)');
ylabel('z (unit: m)');
h_xlabel = get(gca,'XLabel');
set(h_xlabel, 'FontName', 'Times New Roman');
set(h_xlabel,'FontSize',20);
h_ylabel = get(gca,'ylabel');
set(h_ylabel, 'fontsize',20);
set(h_ylabel, 'FontName', 'Times New Roman');
set(gca,'YTick',[0 0.05 0.1 0.15 0.20 0.25 0.30])
set(gca,'XTick',[0 0.05 0.1 0.15 0.20 0.25 0.30])

hold on
h_title= title('X = - 0.3 m', 'color', 'k')
set(h_title,'Fontname', 'Times New Roman')
set(h_title,'FontSize', 30)

quiver(0.23,0.28,0.05,0,'color','k', 'linewidth', 1.3);
text(0.23,0.295,'0.05 m s^-^1','color','k')
set(0,'DefaultTextFontname', 'Times New Roman')
set(0,'DefaultTextFontSize', 20)

%Drawing the cross section of the free surface

p1 = [0.15, 0];
```

```
p2 = [0.15, 0.3];
plot([p1(2),p2(2)],[p1(1),p2(1)],'Color','black','LineWid
th',1.5)

p3 = [0.148, 0.025];
p4 = [0.148, 0.0375];
p6 = [0.146, 0.027];
p7 = [0.146, 0.0355];
p8 = [0.144, 0.029];
p9 = [0.144, 0.0335];
plot([p3(2),p4(2)],[p3(1),p4(1)],'Color','black','LineWid
th',1)
plot([p6(2),p7(2)],[p6(1),p7(1)],'Color','black','LineWid
th',1)
plot([p8(2),p9(2)],[p8(1),p9(1)],'Color','black','LineWid
th',1)

%Saving the results

saveas(h, 'x=-30', 'fig');
saveas(h, 'x=-30', 'png');
```

4) Vorticity contours

```
A = xlsread('d:\mathlab\as103.xlsx'); %read the arranged
data sheet


dum1 = A(:,1:9);
dum2 = A(:,1);
```

```
a = find(dum2 == -30); %Selecting the X coordinate
n = length(a);

for i = 1: n

    dum3(i,:) = dum1(a(i),:);

end

y=abs(0.3-dum3(:,2)*0.01); %Revising the Y coordinate
z=dum3(:,3)*0.01;

v=dum3(:,5);
w=dum3(:,6);

%Reshaping the data to calculate the vorticity

y1 = (reshape(y,12,11))';
z1 = (reshape(z,12,11))';
v1 = (reshape(v,12,11))';
w1 = (reshape(w,12,11))';

vorticity = vorticity(y1,z1,v1,w1,'circulation');
vorticity1=vorticity';

% Resetting the Y-Z coordinates

Y = [0.04:(0.22/9):0.26];
Z = [0.125:(-0.10/8):0.025];

dum1 = length(Y);
```

```
dum2 = length(Z);

for j = 0: dum2-1
    for i = 1: dum1
        coordinate(j*dum1+i,1) = Y(i);
        coordinate(j*dum1+1:j*dum1+dum1,2) = Z(j+1);
    end
end

y2 = reshape(abs(0.3-coordinate(:,1)), 10, 9);
z2 = reshape(coordinate(:,2), 10, 9);


h1 = figure;
contourf(y2, z2, vorticity1);
axis equal
% axis tight
axis ([0, 0.3, 0, 0.3])

caxis([-70 10])

set(gca, 'fontsize',20,'Fontname', 'times new roman');

colormap(gray)

xlabel('y (unit: m)');
ylabel('z (unit: m)');
h_xlabel = get(gca,'XLabel');
set(h_xlabel, 'FontName', 'Times New Roman');
set(h_xlabel,'FontSize',20);
h_ylabel = get(gca,'ylabel');
```

```
set(h_ylabel, 'fontsize',20);
set(h_ylabel, 'FontName', 'Times New Roman');
set(gca,'YTick',[0 0.05 0.1 0.15 0.20 0.25 0.30])
set(gca,'XTick',[0 0.05 0.1 0.15 0.20 0.25 0.30])
hold on

h_title= title('X = - 0.30 m', 'color', 'k')
set(h_title,'Fontname', 'Times New Roman')
set(h_title,'FontSize', 30)


%Drawing the cross section of the free surface

p1 = [0.15, 0];
p2 = [0.15, 0.3];
plot([p1(2),p2(2)],[p1(1),p2(1)],'Color','black','LineWid
th',1.5)

p1 = [0.15, 0];
p2 = [0.15, 0.3];
plot([p1(2),p2(2)],[p1(1),p2(1)],'Color','black','LineWid
th',1.5)

p3 = [0.148, 0.025];
p4 = [0.148, 0.0375];
p6 = [0.146, 0.027];
p7 = [0.146, 0.0355];
p8 = [0.144, 0.029];
p9 = [0.144, 0.0335];
plot([p3(2),p4(2)],[p3(1),p4(1)],'Color','black','LineWid
th',1)
```

```
plot([p6(2),p7(2)],[p6(1),p7(1)],'Color','black','LineWid
th',1)
plot([p8(2),p9(2)],[p8(1),p9(1)],'Color','black','LineWid
th',1)


%Saving the results

saveas(h1, 'x=-30', 'fig');
saveas(h1, 'x=-30', 'png');
```

5) Turbulent kinetic Energy contours

```
A = xlsread('d:\mathlab\as105.xlsx'); %read the arranged
data sheet

dum1 = A(:,1:9);
dum2 = A(:,1);
a = find(dum2 == -30); %Selecting the X coordinate
n = length(a);

for i = 1: n

    dum3(i,:) = dum1(a(i),:);

end

y=abs(0.3-dum3(:,2)*0.01); %Revising the Y coordinate
z=dum3(:,3)*0.01;
fluc_u=sqrt(abs(dum3(:,7))*0.01);
```

```
fluc_v=sqrt(abs(dum3(:,8))*0.01);
fluc_w=sqrt(abs(dum3(:,9))*0.01);
tke=0.5*(fluc_v.^2+fluc_w.^2);

y1 = reshape(y, 12, 11);
z1 = reshape(z, 12, 11);
tke1 = reshape(tke, 12, 11);

h1 = figure;
contourf(y1, z1, tke1);
axis equal
axis ([0, 0.3, 0, 0.3])
set(gca,'fontsize',20, 'fontname', 'times new roman')
xlabel('y (unit: m)');
ylabel('z (unit: m)');
h_xlabel = get(gca,'XLabel');
set(h_xlabel, 'FontName', 'Times New Roman');
set(h_xlabel,'FontSize',20);
h_ylabel = get(gca,'ylabel');
set(h_ylabel, 'fontsize',20);
set(h_ylabel, 'FontName', 'Times New Roman');
set(gca,'YTick',[0 0.05 0.1 0.15 0.20 0.25 0.30])
set(gca,'XTick',[0 0.05 0.1 0.15 0.20 0.25 0.30])

caxis([0 4*10^-17])

set(gca, 'fontsize',20,'Fontname', 'times new roman');

colormap(gray)
colormap(flipud(colormap)) %Reversing the color bar
xlabel('y (unit: m)');
```

```
ylabel('z (unit: m)');
hold on

h_title= title('X = -0.30 m', 'color', 'k')
set(h_title,'Fontname', 'Times New Roman')
set(h_title,'FontSize', 30)

%Drawing the cross section of the free surface

p1 = [0.15, 0];
p2 = [0.15, 0.3];
plot([p1(2),p2(2)],[p1(1),p2(1)],'Color','black','LineWid
th',1.5)

p1 = [0.15, 0];
p2 = [0.15, 0.3];
plot([p1(2),p2(2)],[p1(1),p2(1)],'Color','black','LineWid
th',1.5)

p3 = [0.148, 0.025];
p4 = [0.148, 0.0375];
p6 = [0.146, 0.027];
p7 = [0.146, 0.0355];
p8 = [0.144, 0.029];
p9 = [0.144, 0.0335];
plot([p3(2),p4(2)],[p3(1),p4(1)],'Color','black','LineWid
th',1)
plot([p6(2),p7(2)],[p6(1),p7(1)],'Color','black','LineWid
th',1)
plot([p8(2),p9(2)],[p8(1),p9(1)],'Color','black','LineWid
th',1)
```

```
%Saving the results

saveas(h1, 'x=-30', 'fig');
saveas(h1, 'x=-30', 'png');
```

6) Reynolds shear stress contours

```
A = xlsread('d:\mathlab\as105.xlsx'); %read the arranged
data sheet

dum1 = A(:,1:9);
dum2 = A(:,1);
a = find(dum2 == 0); %Selecting the X coordinate
n = length(a);

for i = 1: n

    dum3(i,:) = dum1(a(i),:);

end

y=abs(0.3-dum3(:,2)*0.01); %Revising the Y coordinate
z=dum3(:,3)*0.01;
fluc_u=sqrt(abs(dum3(:,7))*0.01);
fluc_v=sqrt(abs(dum3(:,8))*0.01);
fluc_w=sqrt(abs(dum3(:,9))*0.01);
R_S=9800.*fluc_v(:,:).*fluc_w(:,:)*10^6;

y1 = reshape(y, 12, 11);
z1 = reshape(z, 12, 11);
```

```
R_S1 = reshape(R_S, 12, 11);

h1 = figure;
contourf(y1, z1, R_S1);
axis equal
% axis tight
axis ([0, 0.3, 0, 0.3])

caxis([0 2.5*10^-7])

set(gca, 'fontsize',20,'Fontname', 'times new roman');

colormap(gray)
colormap(flipud(colormap)) %Reversing the color bar
xlabel('y (unit: m)');
ylabel('z (unit: m)');
h_xlabel = get(gca,'XLabel');
set(h_xlabel, 'FontName', 'Times New Roman');
set(h_xlabel,'FontSize',20);
h_ylabel = get(gca,'ylabel');
set(h_ylabel, 'fontsize',20);
set(h_ylabel, 'FontName', 'Times New Roman');
set(gca,'YTick',[0 0.05 0.1 0.15 0.20 0.25 0.30])
set(gca,'XTick',[0 0.05 0.1 0.15 0.20 0.25 0.30])
hold on


h_title= title('(b) X = 0 m', 'color', 'k')
set(h_title,'Fontname', 'Times New Roman')
set(h_title,'FontSize', 30)
```

```
%Drawing the confluent channel
p1 = [0.15, 0];
p2 = [0.15, 0.3];
plot([p1(2),p2(2)],[p1(1),p2(1)],'Color','black','LineWid
th',1.5)

p1 = [0.15, 0];
p2 = [0.15, 0.3];
plot([p1(2),p2(2)],[p1(1),p2(1)],'Color','black','LineWid
th',1.5)

p3 = [0.148, 0.025];
p4 = [0.148, 0.0375];
p6 = [0.146, 0.027];
p7 = [0.146, 0.0355];
p8 = [0.144, 0.029];
p9 = [0.144, 0.0335];
plot([p3(2),p4(2)],[p3(1),p4(1)],'Color','black','LineWid
th',1)
plot([p6(2),p7(2)],[p6(1),p7(1)],'Color','black','LineWid
th',1)
plot([p8(2),p9(2)],[p8(1),p9(1)],'Color','black','LineWid
th',1)

%Saving the results

saveas(h1, 'x=0', 'fig');
saveas(h1, 'x=0', 'png');
```